6. SITE 690[1]

Shipboard Scientific Party[2]

HOLE 690A

Date occupied: 19 January 1987, 1704 local time

Date departed: 20 January 1987, 0315 local time

Time on hole: 10 hr, 11 min

Position: 65°9.629′S; 1°12.296′E

Bottom felt (rig floor: m, drill pipe): 2925

Distance between rig floor and sea level (m): 11

Water depth (drill-pipe measurement from sea level, m): 2914

Penetration (m): 9.86

Number of cores: 1

Total length of cored section (m): 7.7

Total core recovered (m): 9.86

Core recovery (%): 128

Oldest sediment cored:
Depth sub-bottom (m): 9.86
Nature: diatom ooze
Age: middle Pliocene
Measured velocity (km/s): 1.583

HOLE 690B

Date occupied: 20 January 1987, 0315 local time

Date departed: 21 January 1987, 0700 local time

Time on hole: 27 hr, 45 min

Position: 65°9.629′S; 1°12.296′E

Bottom felt (rig floor: m, drill pipe): 2925

Distance between rig floor and sea level (m): 11

Water depth (drill-pipe measurement from sea level, m): 2914

Penetration (m): 213.4

Number of cores: 25

Total length of cored section (m): 213.4

Total core recovered (m): 214.59

Core recovery (%): 100

Oldest sediment cored:
Depth sub-bottom (m): 213.4
Nature: mud-bearing nannofossil ooze
Age: late Paleocene
Measured velocity (km/s): 1.652

HOLE 690C

Date occupied: 21 January 1987, 0700 local time

Date departed: 23 January 1987, 2130 local time

Time on hole: 62 hr, 30 min

Position: 65°9.621′S; 1°12.285′E

Bottom felt (rig floor: m, drill pipe): 2925

Distance between rig floor and sea level (m): 11

Water depth (drill-pipe measurement from sea level, m): 2914

Penetration (m): 321.2

Number of cores: 24

Total length of cored section (m): 200.6

Total core recovered (m): 185.6

Core recovery (%): 88

Oldest sediment cored:
Depth sub-bottom (m): 317.0
Nature: muddy chalk
Age: early Maestrichtian to late Campanian
Measured velocity (km/s): 1.973

Basement rocks:
Depth sub-bottom (m): 321.2
Nature: amygdaloidal pyroxene-olivine alkali basalt
Measured velocity (km/s):

Principal results: Site 690, on the southwestern flank of Maud Rise, is the deeper of two sites on Maud Rise that form part of a depth transect for studies of vertical-water-mass stratification and biogenic sedimentation during the late Mesozoic and Cenozoic around Antarctica. Objectives are similar to those at Site 689. Three holes were drilled: Hole 690A consists of a single advanced piston corer (APC) core to 9.86 m below seafloor (mbsf); Hole 690B consists of 25 APC cores to 213.4 mbsf. Hole 690C consists of 9 APC cores to 83.6 mbsf, a washed interval from 83.6 mbsf to 204.2 mbsf, and 14 extended core barrel (XCB) cores from 204.2 to 321.2 mbsf. The lower 1.71 m of the cored sequence is basement consisting of amygdaloidal pyroxene-olivine alkali basalt. Sediments immediately overlying basement are most likely late Campanian in age. The quality of the cores is generally excellent with marked disturbance only in the uppermost cores in each hole.

Drilling at Site 690 sampled 317.0 m of almost pure siliceous and calcareous oozes in the upper half of the sequence and mixed calcareous ooze/chalk and terrigenous sediments in the lower half. Minor cherts occur in the basal sediments. The sequence has fewer hiatuses and better preservation of microfossils than Site 689. A major hiatus spans the middle-upper Eocene and part of the lower Oligocene. Preliminary magnetostratigraphy indicates the presence of another hiatus in the middle Oligocene. The uppermost Miocene and the upper Pliocene/lower-middle Quaternary hiatuses are present, as at Site 689.

Site 690 provides a fine biostratigraphic section that reinforces and adds to the biostratigraphy of Site 689. Site 690 provides a superb Paleogene calcareous biostratigraphic sequence that is reasonably complete except for the middle Eocene to lower Oligocene and part of the middle Oligocene. The middle Eocene to lower Oligocene is preserved in Site 689, whereas the middle Oligocene hiatus is present at both sites. Therefore, together the two sites seem to provide a complete Paleogene sequence except for an undefined interval in the middle Oligocene. Sedimentation across the Paleocene/Eocene boundary was continuous at Site 690, unlike at Site 689. Sedimentation across the K/T boundary was also continuous at Site 690, and the boundary is associated with a clay that appears to be of volcanogenic origin, as at Site 689.

[1] Barker, P. F., Kennett, J. P., et al., 1988. *Proc. ODP, Init. Repts.*, 113: College Station, TX (Ocean Drilling Program).

[2] Shipboard Scientific Party is as given in the list of Participants preceding the contents.

Apart from a thin (2.1 m) uppermost layer of foraminiferal ooze of Quaternary age, the upper part of the sequence (late Miocene and Pliocene age) is represented entirely by biosiliceous ooze, followed by a sequence of interbedded diatom and calcareous nannofossil oozes of late Miocene to latest Oligocene age. This in turn is underlain by an interval of foraminifer-bearing nannofossil ooze of early Eocene and late Oligocene age. Beneath is a nannofossil ooze mixed with terrigenous sediments of latest Campanian/earliest Maestrichtian to early Eocene age, and the lowest part has an even stronger terrigenous component mixed with calcareous nannofossil ooze.

Five units have been recognized: Unit I extends from the seafloor to 24.4 mbsf, is of late Miocene to Quaternary age, and is composed of an upper 2.2 m of foraminiferal ooze and a lower 22.2 m of diatom ooze with varying amounts of other biosiliceous components. Unit II extends from 24.4 to 92.9 mbsf and consists of a wide variety of pure and mixed biogenic siliceous and biogenic calcareous oozes of late Miocene to early Oligocene age. Unit III extends from 92.9 to 137.8 mbsf and consists of foraminiferal nannofossil oozes of early Oligocene and early Eocene age. Unit IV extends from 137.8 to 281.1 mbsf, and consists of nannofossil ooze-chalk with varying amounts of terrigenous sediments (quartz, clay, mica) of late Maestrichtian to early Eocene age. Unit V extends from 281.1 m to 317.0 mbsf, is of late Campanian(?) to early Maestrichtian age, and is dominated by terrigenous components, volcanic glass, and carbonate ooze-chalk. Dominant sediments are muddy chalk, calcareous mudstone, and nannofossil-bearing mudstone. Unit V is directly underlain by basaltic basement (Unit VI).

As at Site 689, the sediment sequence and biotic changes reflect a sequential cooling of the Antarctic water mass, with biosiliceous facies progressively replacing carbonates during the late Cenozoic. Siliceous sedimentation began during the early Oligocene, a major increase in siliceous sedimentation occurred at the beginning of the Neogene, and exclusively siliceous sedimentation commenced in the late Miocene. The rate of sediment accumulation was low throughout the sequence and seems to decrease upward slightly in contrast to Site 689, which shows an upward increase in rates of sedimentation.

During the Late Cretaceous, terrigenous sediments (fine-grained quartz, clay, and mica) were a very important component, and continued to be so at various intervals during the Paleocene and early Eocene. The prominence of this terrigenous component and its virtual absence in Site 689 is the major difference between the two sites. This clay is likely to be eolian material initially derived from East Antarctica and then winnowed by bottom currents away from the crest of Maud Rise and deposited in the flank area of Site 690. East Antarctica was a rich source of fine-grained terrigenous sediments for Maud Rise during the Late Cretaceous to early Eocene.

BACKGROUND AND OBJECTIVES

Site 690 is located on the southwestern flank of Maud Rise in the eastern Weddell Sea (Fig. 1) in a water depth of 2914 m. The site is 116 km southwest of Site 689, located at shallower depth (2080 m) near the crest of Maud Rise. With Site 689, Site 690 forms part of a depth transect for studies of vertical water-mass stratification during the latest Mesozoic and Cenozoic around Antarctica. Site 690 was selected to obtain a high quality (APC-XCB), continuously cored sequence through the late Mesozoic and Cenozoic in the area of the present Antarctic water mass. Being so close to Site 689, the site lies beneath the same present-day water mass: no major oceanographic boundary separates the sites now, nor may have at any time in the past.

The multichannel seismic reflection profile acquired during site survey for Site 690 (Fig. 2) is similar to that at Site 689 and indicates the presence of a relatively thin (0.35 s two-way traveltime) sequence of acoustically layered to partly transparent sediments inferred to be pelagic oozes. The regional tectonic setting is the same as at Site 689, but the sediment sequence is about 50 m thinner at Site 690.

Given the similarities between the two sites, we expected that Site 690 would provide data that would corroborate, in many respects, observations made at Site 689. For instance, planktonic microfossil zonations developed for Site 689 should apply also at Site 690. We expected to see a similar broad-scale evolution of the biogenic sediment facies in the two sites, reflecting the development of water masses and their associated planktonic biota during the Cenozoic, and to observe a similar ice-rafted detrital record. Both siliceous and calcareous microfossil groups were expected to occur at Site 690, as at Site 689, providing an additional opportunity to study their biostratigraphic relations and to calibrate with the magnetostratigraphy. Since hiatuses occur in the sedimentary sequence at Site 689, drilling at Site 690 would provide an opportunity to sample missing parts of the record.

The greater water depth at Site 690 would almost certainly have caused greater dissolution of the calcareous sedimentary component, especially during the Neogene when the calcareous component was much diminished compared with the Paleogene, and the calcareous microfossil assemblages sampled at Site 689 showed the effects of dissolution. We expected that deposition at Site 690 would have been close to the foraminiferal and calcareous nannofossil lysoclines during the Neogene but above the calcium carbonate compensation depth (CCD). Before Site 690 was drilled, it was considered that the thinner sequence at this location and water depth might have been the result of dissolution of a fraction of the calcium carbonate. The complete dominance of carbonate sediments in the Paleogene and Upper Cretaceous at Site 689 suggested that this part of the record should be similar in Site 690, providing an excellent calcareous microfossil record.

Drilling at Site 690 was also expected to provide the first opportunity to better understand the development of Antarctic intermediate water masses during the Cenozoic by comparing the benthic foraminiferal assemblages and the benthic oxygen and carbon isotopic records at Sites 690 and 689. For instance, we were interested in determining whether any changes occurred in the vertical oxygen isotopic temperature gradient at the latitudes of Sites 690 and 689 during the Paleogene, when the initial stages of glacial development are inferred to have been occurring. For example, did changes in the vertical temperature gradient occur at the Eocene/Oligocene boundary when the oceanic thermohaline circulation commenced as a result of major Antarctic sea-ice development, as has been suggested by Shackleton and Kennett (1975)? Were there further changes during the middle Oligocene (30 Ma) when the first ice sheets may have accumulated (Miller and Fairbanks, 1985; Murphy and Kennett, 1986)? It is very likely that by the early Neogene, the Antarctic surface water mass had become sufficiently cold that little temperature difference remained between surface and bottom waters.

The depth transect was also intended to provide an opportunity to examine changes in benthic foraminiferal assemblages within intermediate water masses during the Cenozoic. Benthic foraminifers are valuable tracers of changes in bottom-water characteristics through time (Douglas and Woodruff, 1981). They either migrate, evolve, or become extinct in response to bottom-water changes. The cores in the Weddell Sea depth transect are expected to allow benthic foraminiferal changes to be evaluated within a framework of paleodepths and stable isotopic paleotemperatures.

If the presumed middle Cretaceous (Cenomanian?) basement age for Maud Rise is correct, then basement at Site 689 is likely to have been subaerial for about 10 m.y. after formation. The greater present depth of Site 690, under similar assumptions, would indicate an initial basement depth just below sea level, so that a continuous depositional record was a possibility.

The drilling plan for Site 690 was to core two APC holes to refusal and to core continuously with XCB the remainder of one hole to basement.

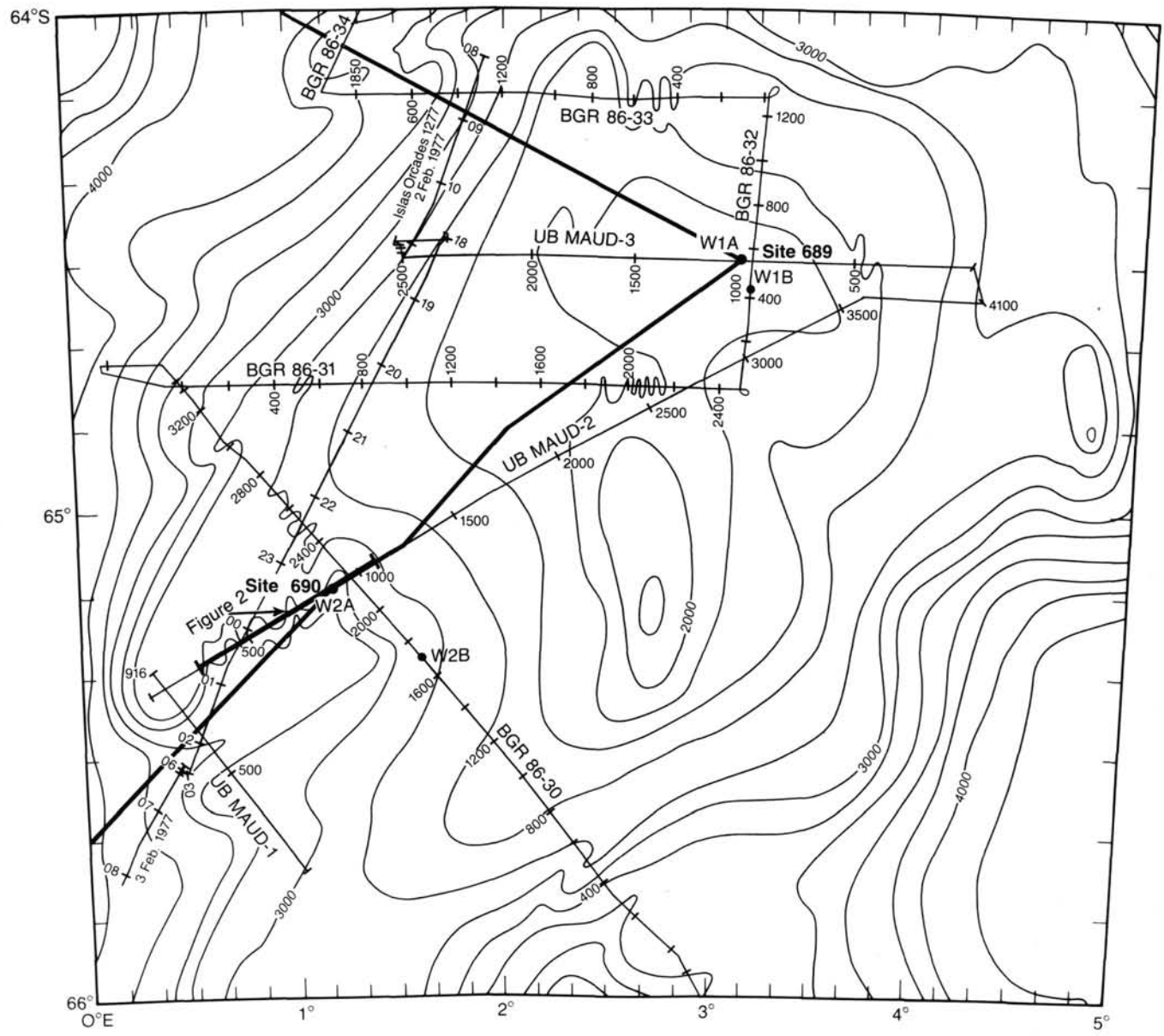

Figure 1. Location map showing positions of Sites 689 and 690 on Maud Rise. Bathymetric contours in meters. Smoothed approach and departure, Site 690. Also position of Norwegian (NARE 85) seismic reflection profile (UB Maud 2). SOM = South Orkney microcontinent.

OPERATIONS

Site 690

On the first pass over Site 690, a floating marker was dropped and the ship continued for 10 min. The ship then turned on a reciprocal heading and ran 0.4 km past the marker-buoy where the beacon (3.5 kHz) was launched at 1700 hr, 19 January. The ship returned to the site by 1850 hr and lowered the thrusters. The *Maersk Master* carried out an ice reconnaissance and found only one iceberg, which was 25 km away.

Hole 690A

The same bottom hole assembly (BHA) and bit used for Site 689 were deployed, except for the drilling jars. The precision depth recorder (PDR) indicated a water depth of 2931.3 m dual elevator stool (DES), and the first APC was shot with the bit at 2924 m. A full 9.86-m core was obtained (Table 1) indicating loss of the mud line and hence a second attempt was required forming Hole 690B.

Hole 690B

For the second shot, the bit was positioned 6 m higher at 2918 m and a 2.12-m-long core was recovered. This established the depth from the rig floor to the seafloor at Hole 690B to be 2925.4 m. The first core should therefore have contained the mud line, and its absence may have been caused by ship heave.

Eighteen APC cores were taken to 166.6 mbsf with 100% recovery (Table 1). The piston did not extend completely on the nineteenth core. Normally this would be sufficient reason to change to the XCB assembly, but the K/T boundary was expected to be encountered. Use of the APC was thus continued, even at the risk of its loss. Cores 113-690B-19H to -24H were taken to 204.2 mbsf with only partial piston extension. The bit was advanced only the amount that the piston stroked for each core. Recovery was quite high but there was much liner collapse.

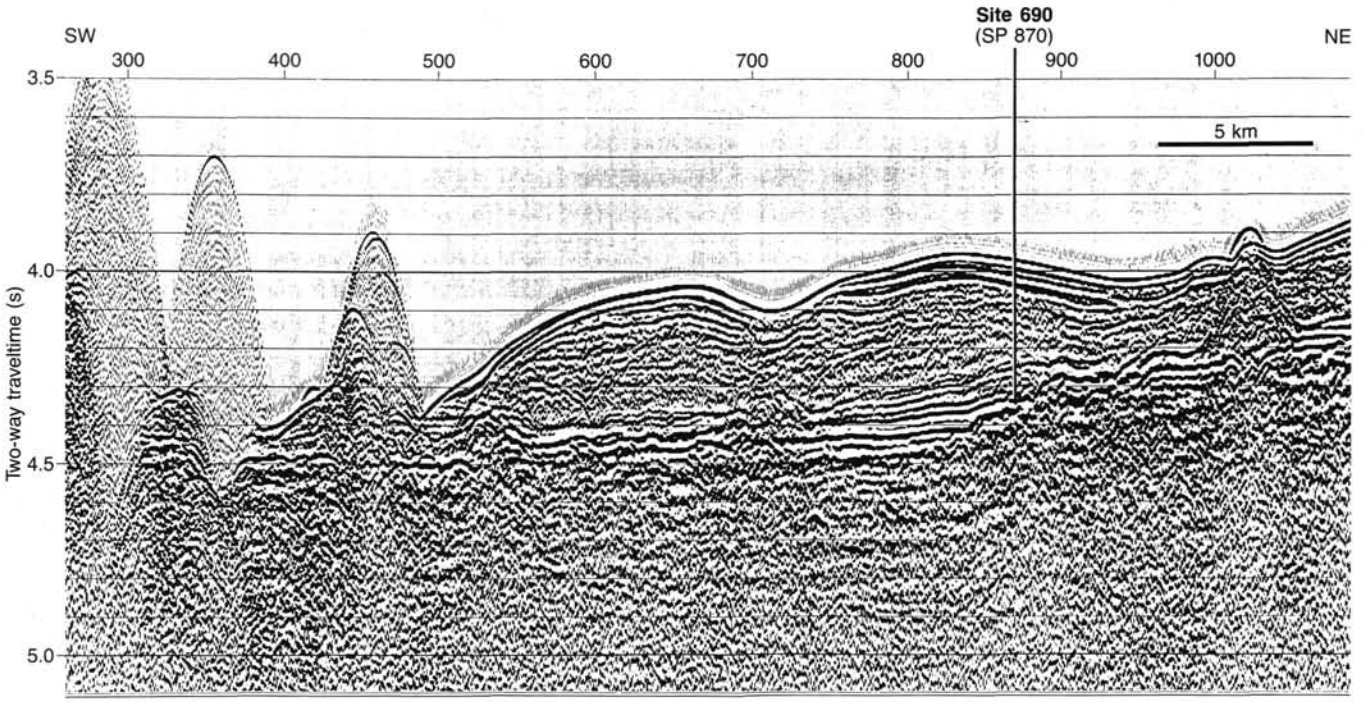

Figure 2. Norwegian (NARE 85) seismic reflection profile (UB Maud 2) showing position of Site 690. Located in Figure 1.

Core 113-690B-25H was unusual in that the barrel stroked a full 9.4 m and pulled loose with only 25,000 lb overpull. Surface monitors indicated that in this attempt to core below Core 25H, the core barrel made a full stroke. This barrel, however, could not be freed with 100,000 lb overpull. While attempting to rotate the bit over the barrel, the bottom end of the inner polished rod failed and the assembly was lost.

Hole 690C

The drill pipe was pulled clear of the seafloor, and the ship was moved 16 m in a direction of 240°. This hole, by default, was now to be the APC/XCB hole of Site 690. The mud-line shot was taken with the bit at 2933 m. This would provide an overlap of 4 m in relation to Hole 690B. A core length of 6.5 m was required to match the mud-line depth of Hole 690B, but 8.37 was cored (Table 1), although the top meter of material was unconsolidated and flowed out of the core liner when brought on deck. The core was recorded as "cored 6.1 and recovered 8.35." Therefore the mud line is the same depth for Holes 690B and 690C.

Nine APC cores were taken to a depth of 83.6 mbsf. Heat-flow measurements were taken in conjunction with Cores 113-690C-3H, -6H, and -9H. Recovery was 100%. Following this, the sequence was washed from 83.6 to 204.2 mbsf, and an XCB wash core obtained (113-690C-10W). Cores 113-690C-11X to -16X were taken routinely with rotating times of about 12 min each. Cores 113-690C-17X and -18X required 55 and 70 min, respectively. Recovered sediments did not seem to be harder and did not contain chert. It is not known why the two cores cut so slowly, but a balled-up bit is suspected. Cores 113-690C-19X and -20X were drilled in 26 and 13 min, respectively.

The bottom of Core 113-690C-22X, at 319.7 mbsf, contained a small amount of ground-up black material which appeared to be basalt. The same soft formation XCB cutter was run on Core 113-690C-23X and only 0.5 m was made in 30 min. The core contained 0.58 m of basalt and the cutter was worn about ½ in. A final basalt core of 1.1 m length was cut in 1 hr using an Acker Amalgamated diamond XCB shoe. The hole was abandoned and filled with seawater at a depth of 321.6 mbsf.

Departure

The drill pipe and BHA were recovered. Ice and weather were never a problem at Site 690. As the ship left the site, the geophysical gear was streamed. The ship made a large-radius turn passing back over the location. Full speed ahead for Site 691 (W4/A) was ordered at 2310 hr, 23 January.

LITHOSTRATIGRAPHY

The sedimentary sequence drilled at Site 690 is of mixed pelagic and terrigenous origin. The sediments recovered have been divided into five lithostratigraphic units (Table 2, Fig. 3), based upon composition as determined from smear slide data (Fig. 4), plus a sixth, Unit VI, basement. Unit boundary locations are based on lithologic changes in Hole 690B for the upper 213 m and changes in Hole 690C for boundary locations below 213 mbsf. Below a calcareous veneer, the siliceous components (diatoms, radiolarians, and silicoflagellates) decrease with increasing depth and are rarely observed below 92.9 mbsf (Sample 113-690B-11H-3, 82 cm; Core 113-690C-10W). The calcareous component (foraminifers, nannofossils, and calcispheres) is dominant from approximately 43.8 mbsf (Sample 113-690B-6H-3; 42.7 mbsf, Section 113-690C-5H-6) until basement is reached at 317.0 mbsf (Sample 113-690C-22X, CC, 30 cm). Terrigenous and volcanic detritus become significant components around 137.8 mbsf (Core 113-690B-16H).

Lithostratigraphic Unit I, 24.4 m thick, is composed of biogenic ooze. It can be divided into two subunits: Subunit Ia, 2.4 m thick, of Quaternary age, consists of foraminiferal ooze. Subunit Ib, 22.0 m thick, is composed of biogenic siliceous ooze, ranging in age from Miocene to Pleistocene. Unit II, 68.5 m thick, is dominated by a mixture of biogenic siliceous and calcareous oozes of Miocene to early Oligocene age. This unit can be further divided; Subunit IIA, 29.0 m thick, of Miocene to late Oligocene age shows a decrease in siliceous biogenic components with depth. Subunit IIB, 39.5 m thick, of late Oli-

Table 1. Coring summary, Site 690.

Core no.	Date (Jan. 1987)	Time	Depths (mbsf)	Cored (m)	Recovered (m)	Recovery (%)
113-690A-						
1H	20	0315	0.0–7.7	7.7	9.86	128.0
				7.7	9.86	
113-690B-						
1H	20	0445	0.0–2.1	2.1	2.12	101.0
2H	20	0600	2.1–11.7	9.6	9.94	103.0
3H	20	0715	11.7–21.4	9.7	10.00	103.1
4H	20	0815	21.4–31.1	9.7	9.02	93.0
5H	20	0915	31.1–40.8	9.7	9.67	99.7
6H	20	1015	40.8–50.4	9.6	9.69	101.0
7H	20	1145	50.4–60.1	9.7	9.77	101.0
8H	20	1300	60.1–69.8	9.7	9.86	101.0
9H	20	1400	69.8–79.4	9.6	9.74	101.0
10H	20	1500	79.4–89.1	9.7	10.03	103.4
11H	20	1600	89.1–98.8	9.7	9.96	102.0
12H	20	1700	98.8–108.5	9.7	9.82	101.0
13H	20	1830	108.5–118.5	10.0	9.80	98.0
14H	20	1930	118.5–128.1	9.6	9.85	102.0
15H	20	2015	128.1–137.8	9.7	9.85	101.0
16H	20	2115	137.8–147.5	9.7	9.85	101.0
17H	20	2215	147.5–157.2	9.7	9.82	101.0
18H	20	2315	157.2–166.9	9.7	9.45	97.4
19H	21	0030	166.9–174.3	7.4	7.41	100.0
20H	21	0130	174.3–180.3	6.0	5.98	99.6
21H	21	0245	180.3–185.2	4.9	4.90	100.0
22H	21	0400	185.2–191.2	6.0	5.95	99.1
23H	21	0500	191.2–198.2	7.0	6.94	99.1
24H	21	0600	198.2–204.2	6.0	5.77	96.1
25H	21	0700	204.2–213.4	9.2	9.40	102.0
				213.4	214.59	
113-690C-						
1H	21	1315	0.0–6.1	6.1	8.35	137.0
2H	21	1415	6.1–15.8	9.7	10.06	103.7
3H	21	1515	15.8–25.5	9.7	9.82	101.0
4H	21	1645	25.5–35.2	9.7	9.59	98.8
5H	21	1815	35.2–44.9	9.7	9.89	102.0
6H	21	1930	44.9–54.6	9.7	10.10	104.1
7H	21	2030	54.6–64.3	9.7	9.70	100.0
8H	21	2130	64.3–74.0	9.7	9.86	101.0
9H	21	2245	74.0–83.6	9.6	10.21	106.3
10W	22	0400	83.6–204.2	N.A.	N.A.	7.0
11X	22	0630	204.2–213.9	9.7	5.53	57.0
12X	22	0830	213.9–223.6	9.7	4.16	42.9
13X	22	1100	223.6–233.2	9.6	8.98	93.5
14X	22	1315	233.2–242.9	9.7	7.79	80.3
15X	22	1500	242.9–252.5	9.6	9.65	100.0
16X	22	1545	252.5–261.8	9.3	5.73	61.6
17X	22	1930	261.8–271.4	9.6	5.03	52.4
18X	22	2200	271.4–281.1	9.7	6.97	71.8
19X	23	0100	281.1–290.8	9.7	9.61	99.1
20X	23	0300	290.8–300.4	9.6	9.83	102.0
21X	23	0515	300.4–310.1	9.7	7.72	79.6
22X	23	0745	310.1–319.7	9.6	6.90	71.9
23X	23	1000	319.7–320.2	0.5	0.58	110.0
24X	23	1300	320.2–321.2	1.0	1.13	113.0
				200.6	177.2	

gocene to early Oligocene age, is dominated by calcareous nannofossil oozes, but contains local diatomaceous horizons. Unit III, 44.9 m thick, consists of foraminiferal nannofossil oozes of early Oligocene to early Eocene/late Paleocene age. Unit IV, 143.3 m thick, is dominated by nannofossil ooze and is distinguished by the presence of terrigenous material. It can be divided into three subunits. Subunit IVA, 39.5 m thick, of late Paleocene age, contains more than 20% terrigenous material (quartz, clay, and mica). Subunit IVB, 75.2 m thick, of late Paleocene to Maestrichtian age, contains less than 10% terrigenous material and Subunit IVC, 28.6 m thick, of Maestrichtian age, contains an increasing amount of terrigenous material and a decreasing amount of nannofossil chalk/ooze. Unit V, 35.9 m thick, of Maestrichtian to Maestrichtian/Campanian age, is distinguished by nannofossil chalk/ooze no longer being the dominant component and by the high percentage of terrigenous sediment and volcanic glass. Unit V is directly underlain by basaltic basement (Unit VI).

In addition to the dominant lithologies, the sequence contains volcanic glass. Although some of the glass may occur as distinct layers, these layers are commonly altered to clay, so their origin cannot be ascertained. The glass component increases toward basement and is most abundant in the 20 m overlying basement.

Ice-rafted dropstones are even more rare in Site 690 than they are at Site 689. At Site 689 they were observed in sediments as old as late Oligocene. The oldest dropstones at Site 690 are in Miocene sediments, and as at Site 689, they tend to occur in the darker layers.

Sediments of Site 690, are generally only slightly to moderately disturbed by the drilling process. Soupy structures occur in the uppermost cores of each hole. Additional sediment disturbance is common at the top of each APC core and as drilling biscuits in the interlayered ooze and chalk sequences.

Unit I (Depth 0–24.4 mbsf; Age upper Miocene/lower Pliocene to Quaternary)

Section 113-690A-1H; depth 0.0–7.7 mbsf; thickness 7.7 m; lower Pliocene to upper Pliocene.

Section 113-690B-1H through Section 113-690B-4H-2; depth 0–24.4 mbsf; thickness 24.4 m; upper Miocene/lower Pliocene to Quaternary.

Section 113-690C-1H through Section 113-690C-3H-6; depth 0.0–24.8 mbsf; thickness 24.8 m; upper Miocene/lower Pliocene to Quaternary.

Unit I is characterized by two distinct biogenic oozes, a foraminiferal ooze and a diatom ooze. Each ooze constitutes a different subunit. The boundary between the subunits is gradational and occurs in the upper 2–5 m.

Subunit IA (Depth 0–2.4 mbsf)

Section 113-690A-1H through Sample 113-690A-1H-3, 10 cm; depth 0–3.1 mbsf; thickness 3.1 m; Pleistocene.

Section 113-690B-1H through Sample 113-690B-2H-1, 30 cm; depth 0–2.4 mbsf; thickness 2.4 m; Pleistocene.

Section 113-690C-1H through Sample 113-690C-1H-3, 130 cm; depth 0–4.3 mbsf; thickness 4.3 m; Pleistocene.

The sediments of Subunit IA are light yellowish brown (2.5Y 6/3), pale yellow (2.5Y 7/3), and light gray (10YR 7/1) foraminiferal ooze, and very pale brown (10YR 7/3) and light gray (10YR 7/2) diatom-bearing foraminiferal ooze. A thin transition interval of light gray (10YR 7/2) diatom foraminiferal ooze occurs at the boundary between Subunits IA and IB (Fig. 5). Glacial dropstones are present and are as large as 10 mm.

Bioturbation is absent to minor. In part, this may result from coring disturbance because this interval is commonly soupy to moderately disturbed. Near the base of this subunit bioturbation is more distinct, and specific bioturbation features such as halo burrows, vertical burrows, and Planolites are observed.

Subunit IB (Depth 2.4–24.4 mbsf)

Sample 113-690A-1H-3, 10 cm, through Section 113-690A-1H, CC; depth 3.1–7.7 mbsf; thickness 4.6 m; Pliocene.

Sample 113-690B-2H-1, 30 cm, through Section 113-690B-4H-2; depth 2.4–24.4 mbsf; thickness 22.0 m; upper Miocene/lower Pliocene to Pliocene.

Table 2. Lithostratigraphic units, Site 690. Unit boundaries are based on Hole 690B in the upper 213 m and on Hole 690C below 213 mbsf.

Unit	Dominant lithology	Interval (mbsf)	Thickness (m)	Age
I				
IA	Foraminiferal ooze	0–2.4	2.4	Quaternary
IB	Diatom ooze	2.4–24.4	22.0	Miocene to Pliocene
II				
IIA	Diatom-bearing nannofossil ooze	24.4–53.4	29.0	Oligocene to Miocene
IIB	Nannofossil ooze, with diatom-rich layers	53.4–92.9	39.5	Oligocene
III				
	Foraminifer-bearing nannofossil ooze	92.9–137.8	44.9	Eocene to Paleocene
IV				
IVA	Mud-bearing nannofossil ooze	137.8–177.3	39.5	Paleocene
IVB	Nannofossil ooze (chalk)	177.3–252.5	75.2	Maestrichtian to Paleocene
IVC	Foraminifer-bearing muddy nannofossil ooze (chalk)	252.5–281.1	28.6	Maestrichtian
V				
	Muddy chalk, calcareous mudstone	281.1–317.0	36	Campanian/Maestrichtian to Maestrichtian

Sample 113-690C-1H-3, 130 cm, through Section 113-690C-3H-6; depth 4.3–24.8 mbsf; thickness 20.5 m; upper Miocene/lower Pliocene to Pliocene.

Subunit IB contains two dominant lithologies, diatom ooze and radiolarian-bearing diatom ooze. Both occur in a wide variety of colors. No one color appears to be dominant in the diatom ooze, and the colors include very white (10YR 8/0), white (10YR 8/2), very pale brown (10YR 7/4), light yellowish brown (10YR 6/4), light gray (2.5Y 7/1, 2.5Y 7/2), pale yellow (2.5Y 6/4), and light olive gray (2.5Y 6/4). There are two dominant colors in the radiolarian-bearing ooze, very pale brown (10YR 7/3, 10YR 7/4) and light gray (10YR 7/2). Additional colors include white (10YR 8/2), light brownish gray (10YR 6/2), light yellowish brown (10YR 6/3, 2.5Y 6/3), grayish brown (10YR 5/2), pale yellow (2.5Y 7/3), and light olive brown (2.5Y 6/4). In addition to the major lithologies, three minor lithologies are present: a primarily white (10YR 8/2) and light gray (2.5Y 7/2) silicoflagellate-bearing diatom ooze, silicoflagellate- and radiolarian-bearing diatom ooze, and silicoflagellate-diatom ooze.

An apparent color cyclicity is observed (Fig. 6). The cycles contain distinct dark to light brown gradational color changes, and range from less than 50 cm to over 7 m in length. The longest cycle occurs in Sample 113-690B-2H-1, 30 cm, to Sample 113-690B-2H-6, 58 cm. Superimposed on this major color cycle are smaller symmetric color changes. No identifiable compositional differences are observed in smear slides from the different color areas.

Bioturbation in Subunit IB is primarily minor to moderate with local areas where it is strong. Only a few sections show clearly definable bioturbation structures, mostly of the halo burrow, vertical burrow, and Planolites type. The contrast between the darker background and the white mottles commonly gives the core a calico appearance (Fig. 6).

Glacial marine dropstones occur in Cores 113-690A-1H, 113-690B-2H, and 113-690B-3H, and 113-690C-2H (Fig. 6) and 113-690C-3H. They are more common in the darker layers and represent the only source of coarse (sand size or greater) terrigenous detrital input. Smaller pieces of ice-rafted detritus are probably represented by the fine sand and silt-sized "accessory" minerals identifiable in smear slides (Fig. 4). No dropstones are observed in Units II–V.

Unit II (Depth 24.4–92.9 mbsf; Age lower Oligocene to upper Miocene/lower Pliocene)

Section 113-690B-4H-3 through Sample 113-690B-11H-3, 80 cm; depth 24.8–92.9 mbsf; thickness 68.5 m; lower Oligocene to upper Miocene/lower Pliocene.

Section 113-690C-3H-7 through Core 113-690C-9H, depth 24.8–83.6 mbsf; thickness 58.8 m; lower Oligocene to upper Miocene/lower Pliocene.

Unit II is characterized by a wide variety of pure and mixed biogenic siliceous and biogenic calcareous oozes, and is divided into two subunits. The boundary between Unit I and Unit II is marked by both a decrease in diatoms and an increase in the fluctuations in the abundance of the different biogenic groups.

Subunit IIA (Depth 24.4–53.4 mbsf)

Section 113-690B-4H-3 through Section 113-690B-7H-2; depth 24.4–53.4 mbsf; thickness 29.0 m; upper Oligocene to Miocene/lower Pliocene.

Section 113-690C-3H-7 through Section 113-690C-7H-1; depth 24.8–56.1 mbsf; thickness 31.3 m; Oligocene to upper Miocene/lower Pliocene.

Nine different classes of sediment are identified in Subunit IIA. However, diatom-bearing nannofossil ooze is clearly dominant, accounting for approximately 50% of the sediments. Its primary colors are, in order of descending abundance: light gray (10YR 7/1, 10YR 7/2), white (10YR 8/0, 10YR 8/1, 10YR 8/2, 2.5Y 8/0), and light brownish gray (10YR 6/2). The second most abundant lithology is diatom ooze, which is primarily white (10YR 8/0, 10YR 8/1, 10YR 8/2), light yellowish brown (2.5Y 6/4), and olive brown (2.5Y 4/4).

Secondary sediment types include olive brown (2.5Y 4/4) mud-bearing diatom ooze, muddy diatom ooze, and mud- and radiolarian-bearing diatom ooze; light brownish gray (10YR 6/2) and grayish brown (10YR 5/2) nannofossil-bearing diatom ooze; gradational from white (10YR 8/0) to brown (10YR 5/3) nannofossil diatom ooze; and white (2.5Y 8/0) and light gray (10YR 7/2) diatom nannofossil ooze.

There are larger color contrasts in Subunit IIA than in Unit I. Overall the cyclicity appears to be less, with each color dominating for a longer period of time. Bioturbation ranges from

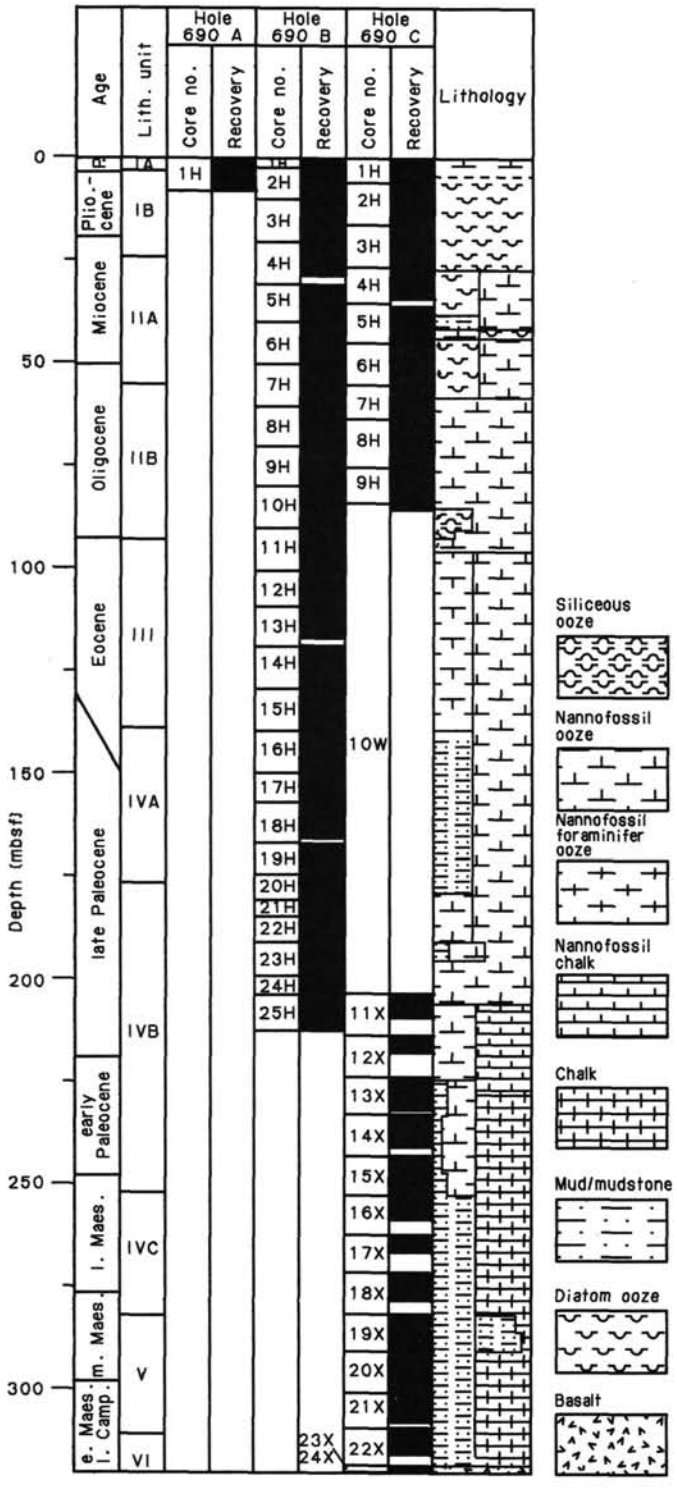

Figure 3. Lithostratigraphic summary of Site 690, Maud Rise.

minor to strong. It is difficult to observe in the white layers, tends to be minor to moderate in the dark layers, and is most prominent near color transitions and in the lighter colored intervals. Identifiable types of bioturbation include Planolites, Zoophycos, vertical burrows, and halo burrows.

Subunit IIB (Depth 53.4–92.9 mbsf)

Section 113-690B-7H-3 through Sample 113-690B-11H-3, 80 cm; depth 53.4–92.9 mbsf; thickness 39.5 m; Oligocene.

Section 113-690C-7H-2 through Section 113-690C-9H, CC; depth 56.1–83.6 mbsf; thickness 27.5 m; Oligocene.

The sediments of Subunit IIB are characterized by large fluctuations in abundance of diatoms and nannofossils. Radiolarians decrease to insignificant numbers. Foraminifers become an additional, but still minor sediment component in the lower section. Quartz and clay are also minor components in this Subunit.

The major lithology of Subunit IIB is light gray (10YR 7/2, 2.5Y 7/2) nannofossil ooze. Additional colors include, in order of decreasing abundance, light brownish gray (10YR 6/3, 10YR 6/4), white (10YR 8/0-8/2, 2.5Y 8/2), very pale brown (10YR 7/3), light yellowish brown (2.5Y 6/4), and pale brown (10YR 6/3). Secondary lithologies include light gray (2.5Y 7/2, 10YR 7/2) and light brownish gray (2.5Y 6/2) diatom-bearing nannofossil ooze; white (2.5Y 8/1) foraminifer- and radiolarian-bearing nannofossil ooze; light gray (2.5Y 7/2) radiolarian-bearing nannofossil ooze, radiolarian- and foraminifer-bearing nannofossil ooze, diatom- and radiolarian-bearing nannofossil ooze, and siliceous nannofossil ooze; and light yellowish brown (2.5Y 6/4) siliceous nannofossil ooze.

Overall, this is a light-colored unit. However, many gradual, subtle, and possibly cyclic color changes were observed on the scale of about 30–130 cm. Bioturbation is absent to moderate. Identifiable types include Zoophycos, Planolites, and halo burrows. As with Subunit IIA, bioturbation is best observed adjacent to color contacts.

Unit III (Depth 92.9–137.8 mbsf; Age lower middle Eocene to upper Paleocene)

Sample 113-690B-11H-3, 80 cm, through Core 113-690B-15H; depth 92.9–137.8 mbsf; thickness 44.9 m; lower middle Eocene to upper Paleocene.

Lithostratigraphic Unit III is composed almost exclusively of calcareous biogenic sediment. It is dominated by a white (10YR 8/0, 10YR 8/2) and very pale brown (10YR 8/3) foraminifer-bearing nannofossil ooze. Two other major lithologies are present, a dominantly white (7.5YR 8/0, 10YR 8/1) nannofossil ooze, and a white (10YR 8/2) and very pale brown (10YR 8/3) foraminiferal nannofossil ooze. Toward the base of the unit, the colors become slightly more pinkish (7.5YR 8/2) and even reddish yellow (7.5YR 7/6).

The boundary between lithostratigraphic Units II and III occurs at an erosional contact in Core 113-690B-11H-3, 80 cm (Fig. 7). Coincident with the erosion is a slight color change from white (2.5Y 8/2) below to very white (2.5Y 8/0) above. Overall color changes are very slight in this lithologic unit.

Bioturbation is generally minor and commonly absent. However, in a few areas it is moderate to strong. Identifiable types include Planolites, Zoophycos, Chondrites, halo burrows, and vertical burrows. In addition to the limited bioturbation structures, a 3–4-cm-deep scour is observed at 106.8 mbsf (Sample 113-690B-12H-6, 46 cm; Fig. 8). The scour is also a color boundary with white (10YR 8/2) overlying very pale brown (10YR 8/3). Rounded and subrounded fragments of the eroded sediment occur as much as 20 cm above the scour, decreasing in size upward.

Unit IV (Depth 137.8–281.1 mbsf; Age Maestrichtian to upper Paleocene)

Core 113-690B-16H through Core 113-690B-25H; depth 137.8–213.4 mbsf; thickness 75.6 m; upper Paleocene.

Core 113-690C-11X through Core 113-690C-18X; depth 204.2–281.1 mbsf; thickness 76.9 m; Maestrichtian to upper Paleocene.

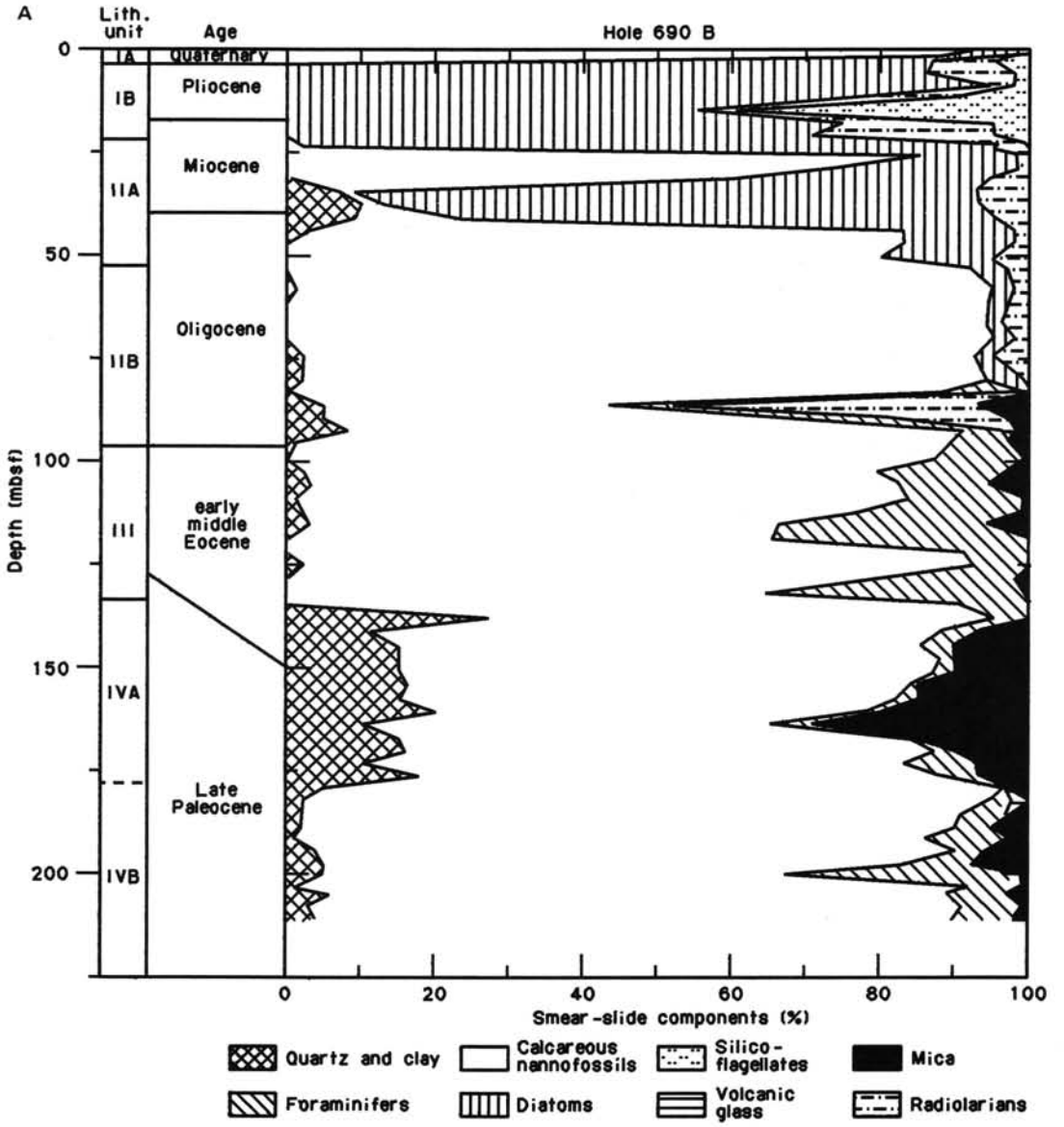

Figure 4. Sediment composition at Site 690, Maud Rise, from shipboard smear slide data. A. Hole 690B. B. Hole 690C.

Sediments of Unit IV are dominated by nannofossils with widely varying amounts of terrigenous sediment, and, with a few minor exceptions, fairly constant abundances of foraminifers. On the basis of variations in these components, Unit IV can be divided into three subunits.

Subunit IVA (Depth 137.8–177.3 mbsf)

Core 113-690B-16H through Section 113-690B-20H-2; depth 137.8–177.3 mbsf; thickness 39.5 m; upper Paleocene.

Subunit IVA, although dominated by nannofossil ooze, contains at least 15% terrigenous material, including a significant but highly variable component of mica. The small mica flakes twinkle on the surface of the split core. The quartz and clay fraction remains fairly constant.

The major lithologies of this subunit are mud-bearing nannofossil ooze and silty nannofossil ooze. Minor lithologies include clay-bearing nannofossil ooze, muddy nannofossil ooze, mud- and foraminifer-bearing nannofossil ooze, and silt-bearing nannofossil ooze. Colors in this subunit show an overall change from reddish-yellow colors at the top, to whites and grays in the middle, and browns near the base. The colors include reddish yellow (5YR 7/6, 5YR 6/6), pinkish reddish yellow (5YR 7/5), pink (5YR 7/4, 7.5YR 8/4, 7.5YR 7/4), very pale brown (10YR 7/3), white (10YR 8/1), light yellowish brown (10YR 5/4), pale brown (10YR 6/3), yellowish brown (10YR 5/4), and brown (7.5YR 5/4). Over a large part of the core the color changes are cyclic and gradual.

Bioturbation is present throughout most of the section in minor to moderate amounts. Specific types include Chondrites, Zoophycos, Planolites, and vertical burrows. One vertical burrow (113-690B-17H-3) is at least 83 cm long.

Subunit IVB (Depth 177.3–252.5 mbsf)

Section 113-690B-20H-3 through Core 113-690B-25H; depth 177.3–213.4 mbsf; thickness 36.1 m; upper Paleocene.

Core 113-690C-11X through Core 113-690C-15X; depth 204.2–252.5 mbsf; thickness 48.3 m; Maestrichtian to Paleocene.

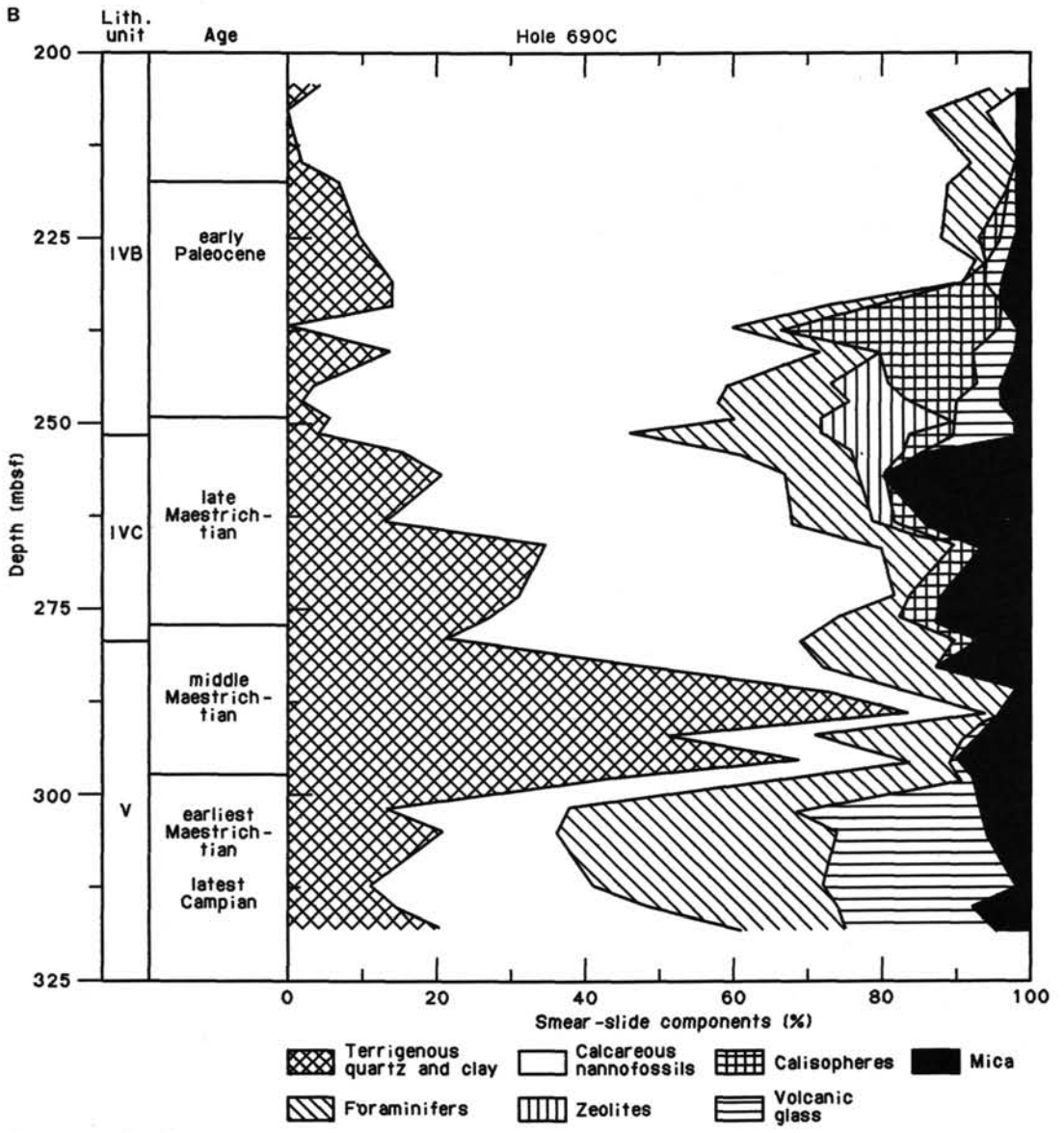

Figure 4 (continued).

Combined thickness is 75.2 m.

Subunit IVB is dominated by nannofossil ooze, with minor amounts of quartz, clay, mica, and foraminifers. Its upper boundary (with Subunit IVA) is defined by a decrease in terrigenous material and mica. Its base is defined by the reverse, an increase in mica and terrigenous material. In addition to the change in composition, sediments in this unit undergo a diagenetic change, and chalk becomes dominant over ooze near 242.9 mbsf (Core 113-690C-15X). The dominant lithologies are pinkish white (7.5YR 8/3, 7.5YR 8/2) and white (5YR 8/1) nannofossil ooze, mud-bearing nannofossil ooze, and foraminifer- and mud-bearing nannofossil chalk. Additional lithologies include foraminifer-bearing nannofossil ooze, foraminiferal nannofossil ooze, clayey nannofossil ooze, foraminiferal nannofossil chalk, and mud-bearing chalk. Additional colors include brownish yellow (10YR 6/6), strong brown (10YR 5/6), reddish yellow (7.5YR 6/6), light brown (7.5 YR 7/3), pink (7.5YR 7/4) and pinkish gray (7.5YR 7/2). The color changes are commonly gradational and cyclic. The variation in colors in this subunit is the most distinctive of this site. Based on a particularly vivid color change observed at Sample 113-690B-25H-2, 0–27 cm (Fig. 9) and the lack of that particular interval at Hole 690C, we suspect that the two holes do not contain an area of overlap.

A thin, light gray (10YR 7/1) bioturbated ash layer occurs at 227.7 mbsf (Sample 113-690C-13X-3, 116–118 cm; Fig. 10). It is similar to an ash layer that was observed at 211.4 mbsf (Sample 113-689B-23X-4, 66–80 cm) at Site 689. The two layers may be correlated (see Fig. 8 in "Site 689" chapter, this volume).

Bioturbation is minor to strong throughout the subunit. Specific types of bioturbation include Planolites, Zoophycos, Chondrites, and vertical burrows. It is common to see overlying white and gray sediments, displaced downward into the pinker layers.

Included in this subunit is a continuous K/T boundary sequence. It occurs between 247.4 and 248.9 mbsf (Section 113-690C-15X-4). Within this strongly bioturbated interval, there is a color change from very pale brown (10YR 7/4) at the top to white (10YR 8/2) below. The change occurs over a gradational boundary between 40 and 55 cm. Although it is suspected that

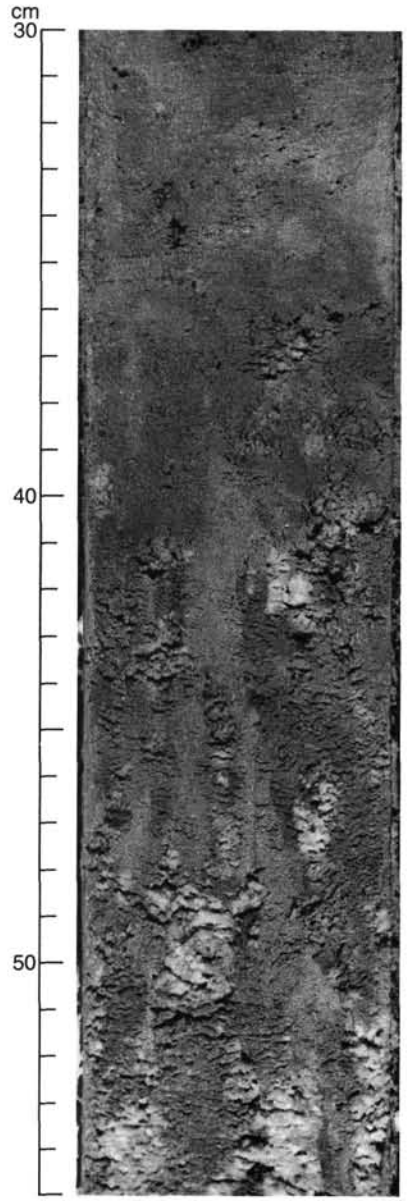

Figure 5. Gradual transition between foraminiferal ooze of Subunit IA and diatom ooze of Subunit IB. The diatom ooze separates on the cut surface and is mottled.

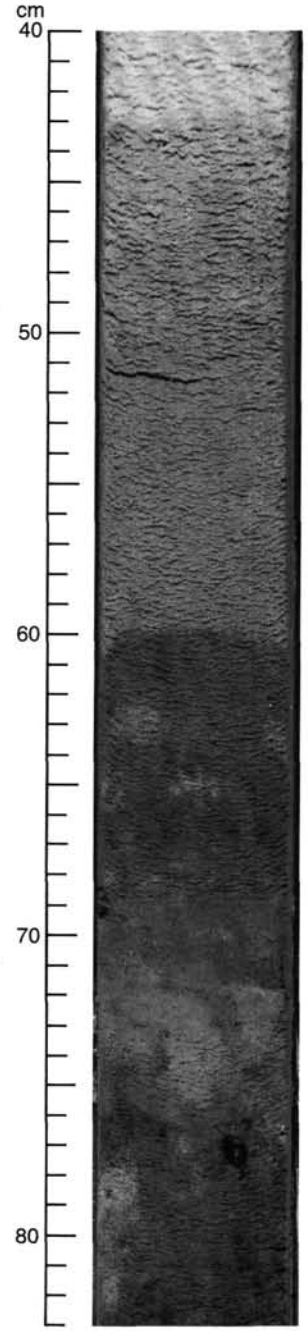

Figure 6. Distinct color changes in Sample 113-690C-2H-3, 40–83 cm, from very white (10YR 8/0) at the top (40–43 cm), white (2.5Y 8/2) from 43–60.5 cm, and mottled light yellowish brown (2.5Y 6/3) from 60.5 m to the base. A 10-mm dropstone occurs at 77 cm.

the color change is associated with a volcanic layer, volcanic glass is rare in smear slides from this interval, and any glass that may have been present has been altered to clay minerals.

Subunit IVC (Depth 252.5–282.6 mbsf)

Core 113-690C-16X through Core 113-690C-18X; depth 252.5–281.1 mbsf; thickness 28.6 m; Maestrichtian.

Sediments of Subunit IVC consist of dominantly white (10YR 8/0, 10YR 8/1, 10YR 8/2, 5Y 8/1, 5Y 8/2), light gray (10YR 7/2) and very pale brown (10YR 7/3) foraminifer-bearing muddy nannofossil ooze and chalk, and muddy nannofossil ooze and chalk. Additional colors include light olive gray (5Y 6/2), pale green (5G 7/2), light greenish gray (5GY 7/1), and light brown (2.5Y 6/2). In general, the ooze intervals, which may be an artifact of coring, are lighter than the chalk intervals.

Within the chalk, many sedimentary structures were observed, including layers with orientations that range from vertical to horizontal, folded layers, microfaults, possible incipient stylolites, and bioturbation structures. The origin of these structures, however, is not straightforward. For example, some of the apparent layers may be primary (bedding) or secondary (bioturbation). In addition, some of the folded and sheared layers (Figs. 11A, -B) may be primary or they may be induced by drilling.

Unit V (Depth 281.1–317.0 mbsf; Age Campanian(?) to Maestrichtian)

Core 113-690C-18X through Sample 113-690C-22X, CC, 30 cm; depth 282.6–317.0 mbsf; thickness 35.9 m; upper Campanian/lower Maestrichtian.

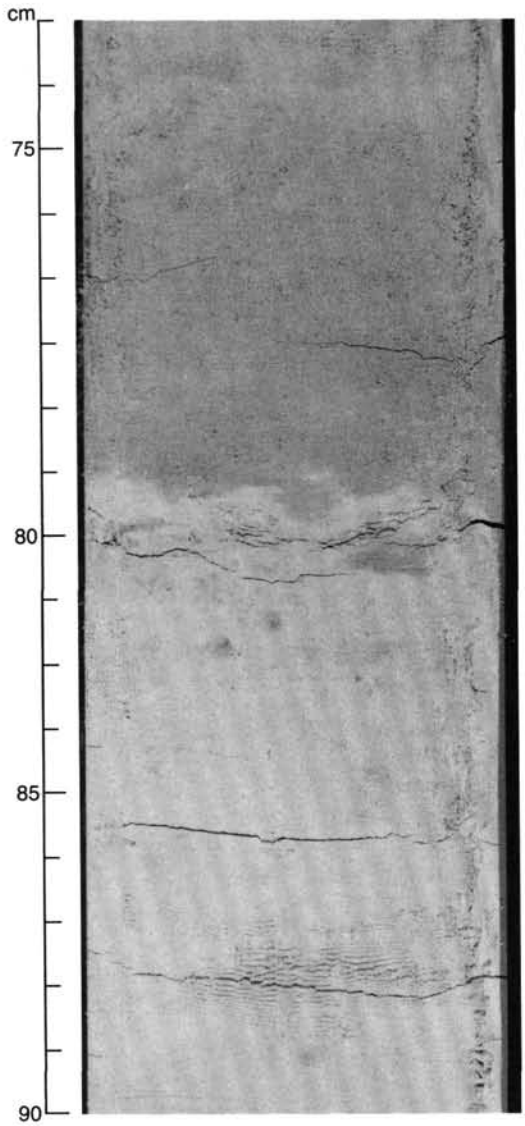

Figure 7. Erosional contact within a nannofossil ooze marking the boundary between lithologic Units II and III, from Sample 113-690B-11H-3, 73–90 cm. The upper sediment is white (2.5Y 8/2) and the lower sediment is very white (2.5Y 8/0).

The boundary between Units IV and V is drawn at the point where the nannofossil component is no longer dominant. In addition, there is a large increase in volcanic glass within the section beginning at about 300 mbsf (Core 113-690C-21X). The lower boundary of Unit V has a sharp contact with basalt. This occurs at 317.0 mbsf in Sample 113-690C-22X-CC, 30 cm.

Sediments of Unit V consist of three major lithologies: light gray (10YR 7/2, 2.5Y 7/2, 2.5Y 7/1) and very pale brown (10YR 7/3) clayey chalk, greenish gray (5GY 5/1) and light olive gray (5Y 6/2) calcareous claystone, and light gray (5Y 7/2, 7.5YR 7/0) and greenish gray (5GY 6/1) calcareous claystone. Colors in addition to those listed above are observed in the muddy chalk and include white (10YR 8/1), yellowish brown (10YR 5/4), light brownish gray (2.5Y 6/2), and gray (5Y6/1).

Two minor lithologies are present in this unit. In Sample 113-690C-22X-3, 128–131 cm, at 314 mbsf, a light greenish ash layer occurs. Pale brown (10YR 6/3) and yellowish brown (10YR 5/4) chert fragments and layers were observed between Samples 113-690C-22X-1, 32–39 cm, (310.42–310.49 mbsf) and 138–150 cm (311.48–311.6 mbsf), 113-690C-22X-2, 91 cm (312.5 mbsf), and 113-690C-22X-3, 113–120 cm (314.2–314.3 mbsf).

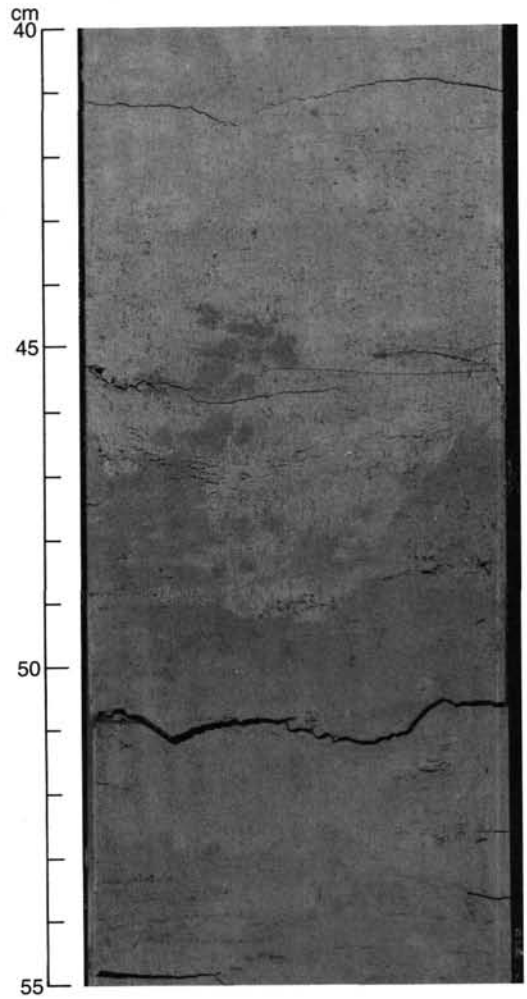

Figure 8. A 3-cm-deep scour mark in foraminifer-bearing nannofossil ooze at 106.8 mbsf (Sample 113-690B-12H-6, 40–55 cm). Small rounded clasts of the underlying, very pale brown (10YR 8/3) sediment occur within the overlying white (10YR 8/2) sediment, and "fine" rapidly upward.

Bioturbation is minor to moderate throughout the section. In many areas it is obscured by coring disturbance.

Unit VI (Depth 317.0–321.2 mbsf)

Sample 113-690C-22X, CC, 30 cm, through Core 113-690C-24X.

See "Basement Rocks" section, this chapter.

Comparison with Site 689

The total sedimentary sequences at Sites 689 and 690 are of comparable thickness, but differ considerably in the thicknesses of specific intervals (Fig. 12). The primary lithologic difference between the two sites is the larger terrigenous component in the upper Maestrichtian to lower Eocene sediments at Site 690.

Biosiliceous ooze of late Miocene to Pleistocene age, Unit I, (Subunit IB at Site 690) is present at both sites with a thickness of 24–32 m. Both sites contain a unit of interlayered siliceous and calcareous oozes (Unit II, which can be divided into Subunits IIA and IIB), but the ages and thicknesses of these units vary considerably. At Site 689, Unit II is almost 120 m thick and ranges in age from the late Miocene to the late Oligocene. In

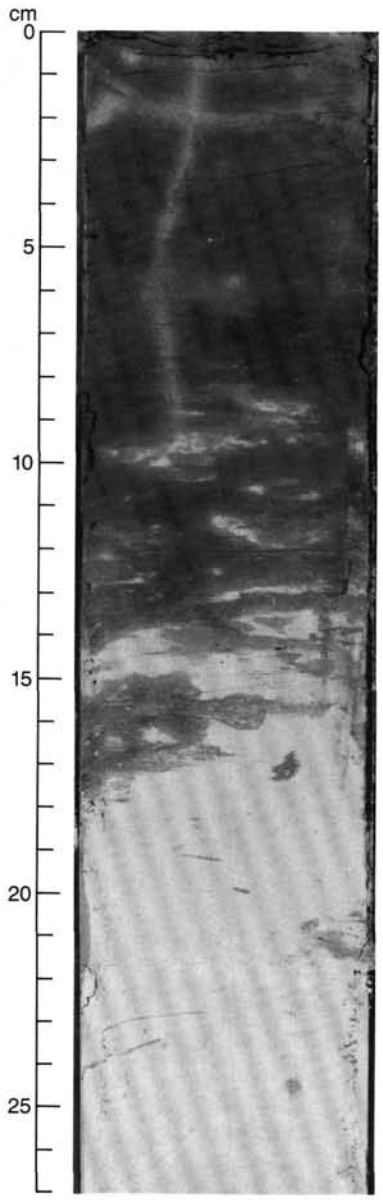

Figure 9. Distinct bioturbated contact between dark brown (7.5YR 5/4) clayey nannofossil ooze and white (5YR 8/0) nannofossil ooze of Subunit IVB, at 206 mbsf (Sample 113-690B-25H-2, 0–27 cm).

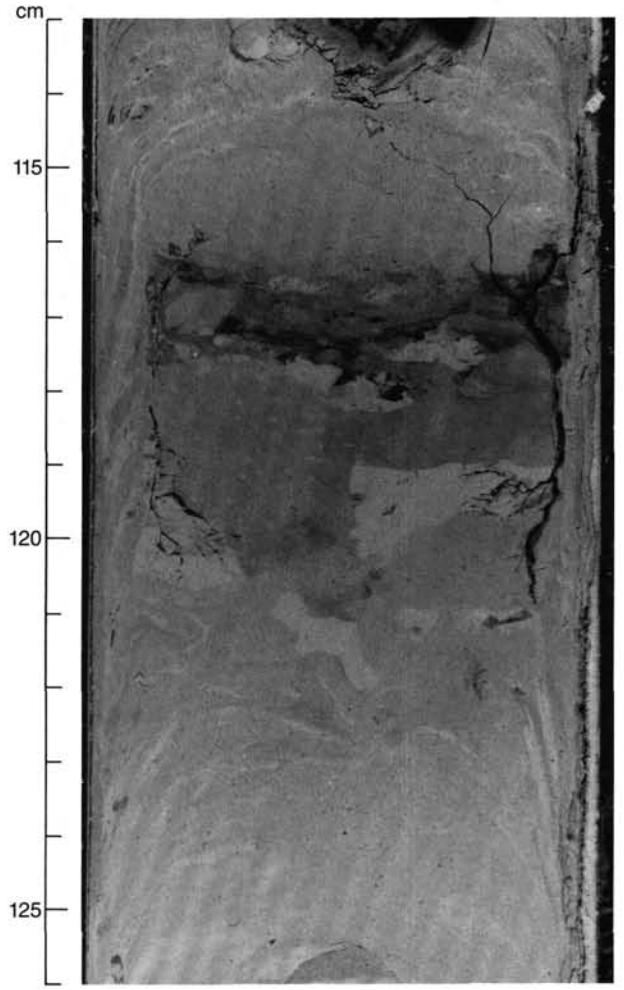

Figure 10. Bioturbated ash layer in mud-bearing nannofossil ooze/chalk at 227.7 mbsf (Sample 113-690C-13X-3, 113–126 cm).

contrast, Unit II is about 65 m thick at Site 690, and ranges in age from Miocene to early Oligocene. Unit III is also present at both sites, but at Site 689 it is almost 150 m thick, consists of Subunits IIIA and IIIB, and ranges in age from the late Eocene to the Cretaceous. At Site 689, it is largely a diagenetic unit, where chalk becomes dominant over ooze and where chert layers are recovered. Unit III at Site 690 is 45 m thick, ranges in age from early Oligocene to early Eocene, and consists of foraminiferal nannofossil oozes.

Terrigenous sediments (quartz, clay, and mica) become a significant component in the lower Eocene at Site 690 and are not observed at Site 689; the terrigenous contribution has created an expanded section at Site 690.

Clay Mineralogy

X-ray diffraction analyses were completed on 44 samples from Holes 690B and 690C (Fig. 13). The purposes of clay mineral studies at Site 690 are: (1) to recognize the major variations of the paleoenvironment as expressed by clay mineral associations at a sampling interval of one per core; (2) to search for cyclic variations of clay associations, in relation to weak lithologic changes (expressed by the changing color of the sediment), using a sampling interval of three per section; (3) to compare the clay associations with those recognized at Site 689 in shallower water depths.

Results

The clay minerals identified include chlorite, kaolinite, illite, and three smectite minerals (Fig. 13). Based on the relative abundances of the clay species, three units were recognized for Site 690; Unit C3 is divided into four subunits.

Unit C1 extends from the seafloor to 41 mbsf and consists of illite (abundant to very abundant), smectite (absent to abundant), and chlorite and kaolinite (absent to common). The stratigraphic range of this unit is lower Miocene to Pliocene. Unit C2, which extends from 41 to 89 mbsf, has a clay association of abundant illite and abundant smectite, often associated with common chlorite and kaolinite. The stratigraphic range of this unit is from the lower Oligocene to the lower Miocene. Unit C3 extends from 89 mbsf to the basement at 317 mbsf. The clay fraction consists mainly of smectite. This unit ranges from upper Campanian/lower Maestrichtian to middle Eocene, and is divided into four subunits. Subunit C3a extends from 89 to 185

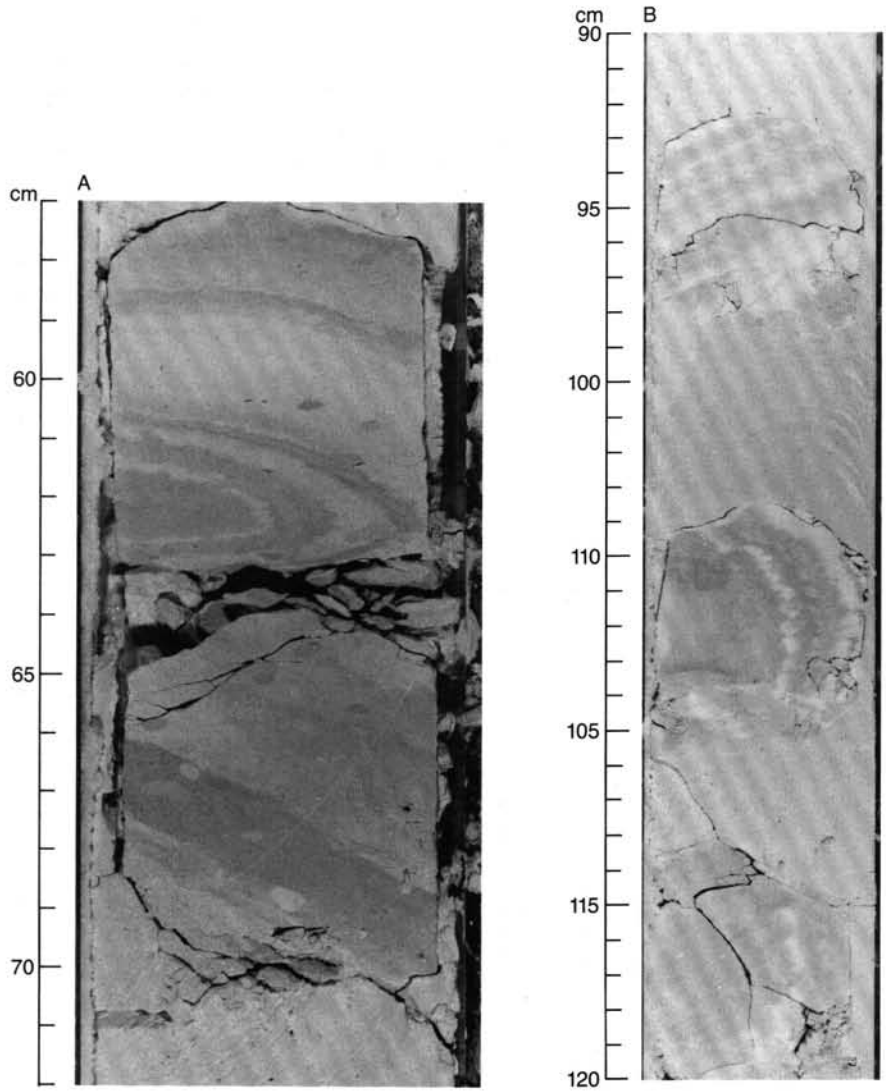

Figure 11. A. Fold, layering, and bioturbation in foraminifer-bearing muddy nannofossil chalk from Subunit IVC, 253.0 mbsf (Sample 113-690C-16X-1, 57–72 cm). B. Microfaults in foraminifer-bearing muddy nannofossil chalk biscuits from Subunit IVC, 266 mbsf (Sample 113-690C-17X-3, 90–120 cm.

mbsf (upper Paleocene to Eocene). The clay association consists of very abundant smectite, rare to common chlorite and kaolinite, and sporadic rare illite. Subunit C3b extends from 185 to 213 mbsf (upper Paleocene). The clay association consists of very abundant to exclusive smectite, generally associated with rare to common chlorite and kaolinite, and sporadically with rare illite. Subunit C3c extends from 213 to 297 mbsf (upper Campanian/lower Maestrichtian to upper Paleocene) and consists of smectite exclusively. Subunit C3d extends from 297 mbsf to the basement at 317 mbsf, and consists of very abundant to exclusive smectite, associated with rare to common illite. This subunit is upper Campanian/lower Maestrichtian in age.

The base of Unit C2 is located near the boundary between lithostratigraphic Units III and IV at 92.9 mbsf, which marks the first appearance of Cenozoic siliceous microfossils. Subunit C3d corresponds to sediments containing abundant volcanic glass.

Paleoenvironmental History

Very abundant and exclusive smectite in Unit C3 (upper Campanian/lower Maestrichtian to middle Eocene) points to predominantly warm climatic conditions with alternating periods of humidity and aridity in low-relief source areas, as described during the same time interval in several Atlantic regions including the southern part of the South Atlantic (Chamley, 1979; Robert, 1987). The clay association is roughly similar to those described in Unit C3 at Site 689, although the sites display minor differences.

Subunit C3d at Site 690 corresponds to Subunit C3b at Site 689 and contains rare to common illite, probably derived from erosion of rugged terrain. A similar weak occurrence of illite, recognized in the Cape Basin at DSDP Site 361 near the K/T boundary (Robert, 1987), suggests that these detrital supplies probably originate from a distant source area.

Subunits C3c to C3a at Site 690 stratigraphically correspond to Subunit C3a at Site 689 which contains exclusive smectite. However, exclusive smectite at Site 690 occurs only in Subunit C3c (upper Campanian/lower Maestrichtian to upper Paleocene).

Subunit C3b (upper Paleocene) shows a weak increase of chlorite, and/or kaolinite content, as compared with C3c and C3d. This event is unknown in the Cape Basin, but the first Cenozoic appearance of kaolinite (in trace amounts as high as 5%)

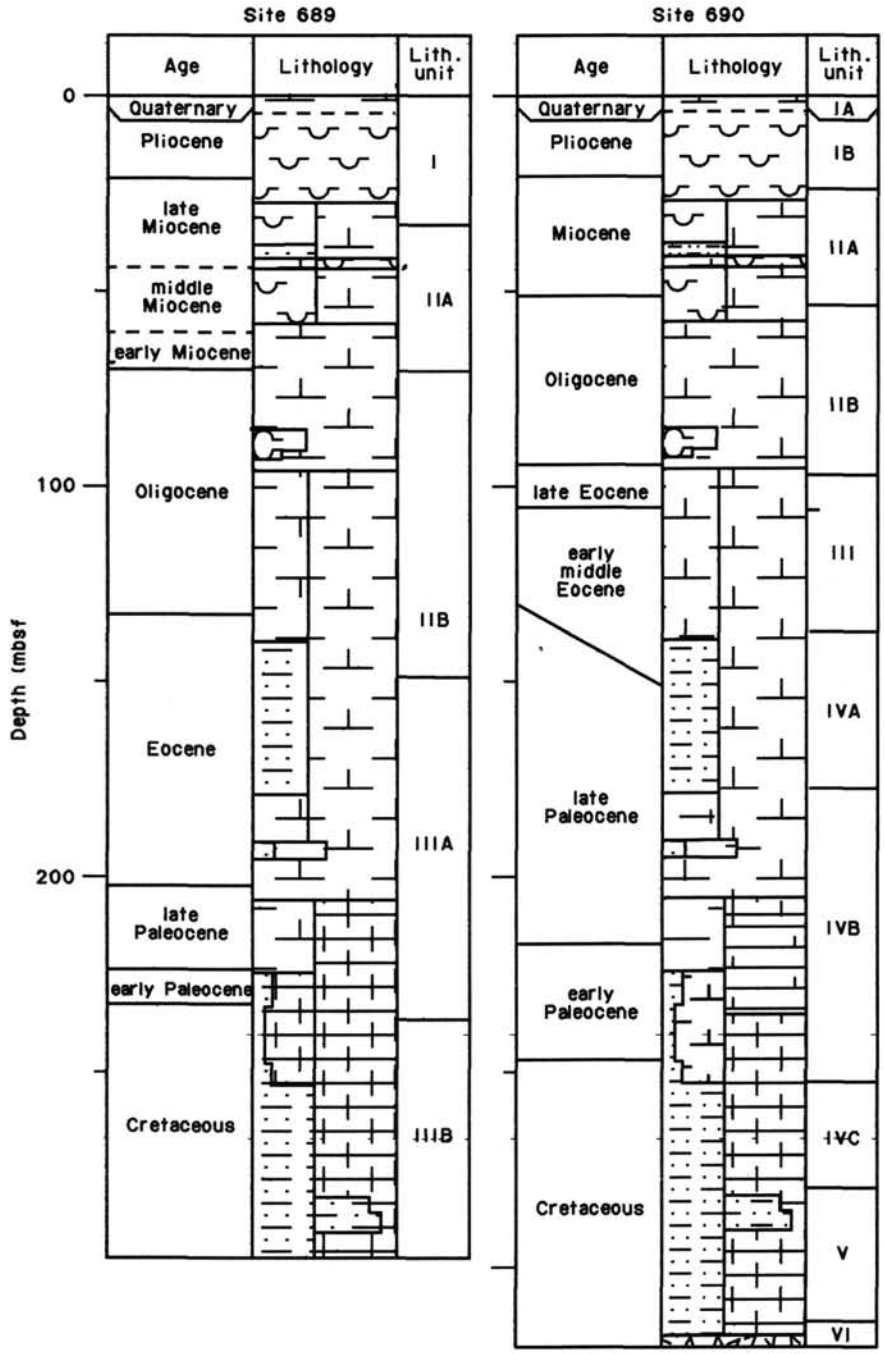

Figure 12. Summary lithologic comparison of Sites 689 and 690. Hiatuses (wiggly line in lithology column) only show when they occur at lithologic boundary.

on the Falkland Plateau at DSDP Sites 327 and 511 was recorded during the Paleocene (Robert and Maillot, 1983). As this event is unknown in other South Atlantic regions (Robert, 1987), it probably originates from Antarctica. This supply was not recorded at shallower water depths (Site 689), suggesting that detrital particles may have been carried northward by intermediate water currents.

In Subunit C3a (upper Paleocene to Eocene), the smectite content slightly decreases upward relative to Subunits C3b through C3d, while chlorite and/or kaolinite increase. Successive increases of chlorite and/or kaolinite during the Paleocene are not related to tectonic events. Indeed, these minerals are not associated with significant increases of the illite content, illite being generally the most abundant clay mineral eroded from tectonically active areas (Chamley, 1979). Besides, tectonic events generally induce sharp and obvious variations of the clay associations (Robert, 1987). Moreover, no tectonic events were reported in the Dronning Maud Land region of Antarctica during the Paleocene (Grikurov, 1982). As a consequence, the slight increase of chlorite and/or kaolinite on Maud Rise throughout the Paleocene probably resulted from slight climatic variations in weathering on Antarctica.

Clay minerals in Subunit C3b (Sections 113-690B-23H-1 and -25H-1) were studied in sediments ranging in color from dark reddish yellow to white (7.5 YR 8/6, 7.5 YR 7/6, 5 YR 7/6, and 5 YR 8/1). Color variations are not directly related to important

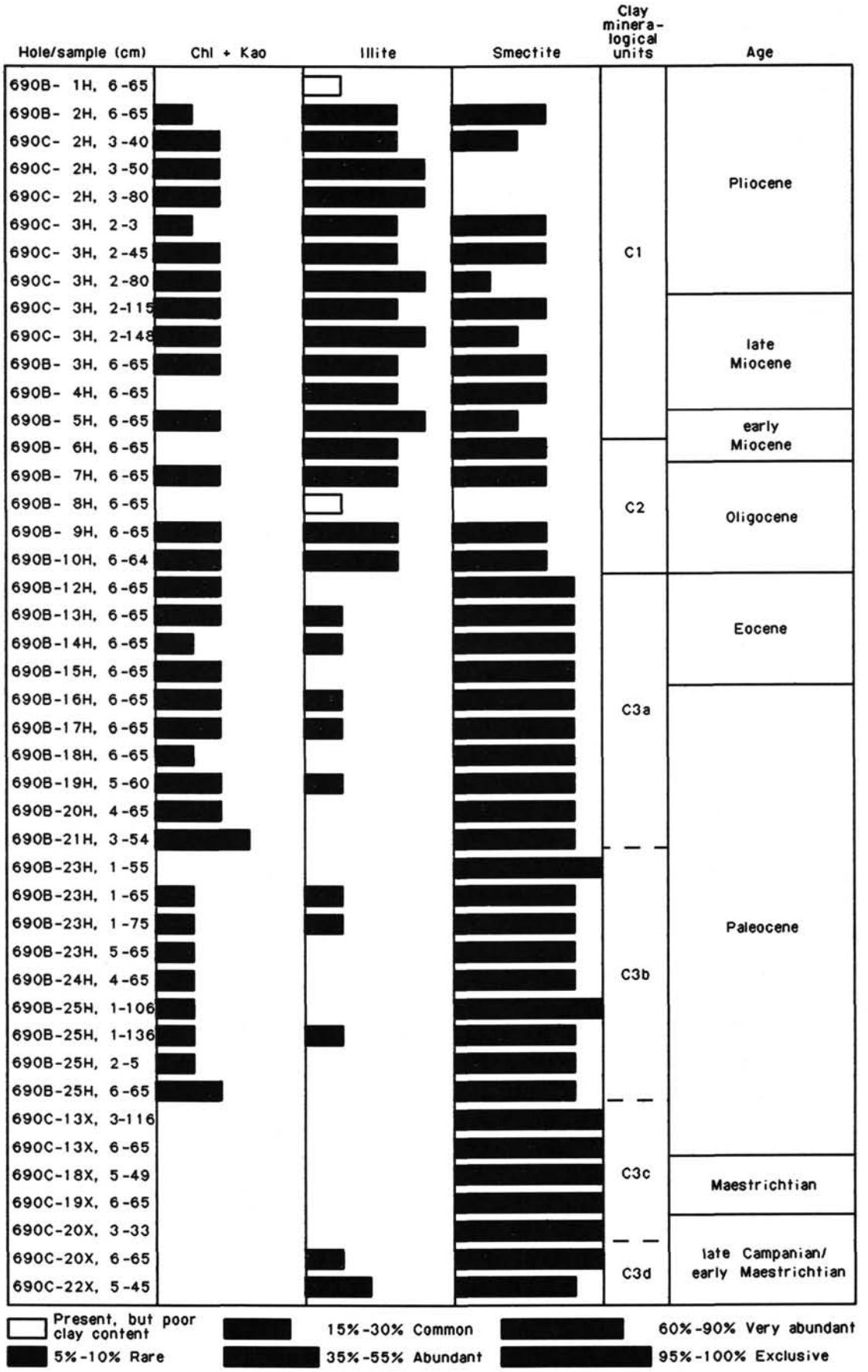

Figure 13. Clay mineralogy, Site 690; Chl = chlorite, Kao = kaolinite.

changes in the clay association, but lighter sediments appear slightly enriched in smectite.

Unit C2 (lower Oligocene to lower Miocene) displays a strong increase of the illite content, associated with a smaller abundance of smectite, suggesting that hydrolysis strongly decreased on Antarctica. This unit correlates with the Oligocene increase of illite at Site 689, and those of DSDP Sites 329 and 511 on the Falkland Plateau (Robert and Maillot, 1983). Increased abundance of illite was also recorded in the Ross Sea region at DSDP Site 274 where it occurred during the early Miocene (Robert et al., in press). This difference in the age of the event between both regions suggests that cold and/or arid conditions prevailed earlier in continental regions near Maud Rise.

Unit C1 (lower Miocene to Pliocene) is mainly characterized by fluctuations in the illite and smectite contents of the clay fraction, and also by a slight increase of the smectite content. As at Site 689, smectite probably results from the removal of ancient smectite-rich sediments outcropping on or around Antarctica. In this unit, alternating white and light yellowish brown sediments were studied in Section 113-690C-2H-3, and gray grading to grayish brown sediments in Section 113-690C-3H-2. Variations of the clay association are not related to the color of the sediment. However, cyclic variations of the clay association are apparent. Sediments characterized by abundant smectite and illite alternate with sediments containing very abundant illite associated with common to rare smectite, and sometimes devoid of smectite. Similar cyclic variations were described in upper Pleistocene sediments off Kapp Norvegia where smectite-rich sediments were deposited during colder periods, and smectite-poor sediments during warmer periods (Grobe, 1986). Cyclic variations on Maud Rise during the Pliocene probably proceed from the same mechanisms.

BASEMENT ROCKS

Introduction

Between 317 and 321.6 mbsf, 1.7 m of basalt was recovered on Maud Rise. The rocks are dark gray, amygdaloidal, and sparsely olivine phyric. Based on the major and trace element geochemistry, they can be classified as oceanic alkali basalts. The low silica content and high concentration of incompatible elements (Ti, K, P, Zr, Nb) indicate a mantle peridotite source with a low degree of partial melting. They have the composition of basalts found on ocean islands and seamounts.

The low Si and Mg content, coupled with high concentration of Ti, Zr, Sr, and the alkalis, is comparable to basalts from the Tristan da Cunha Island, a modern hot-spot; to basalts dredged from the Rio Grande Rise, and to alkali basalts dredged from the Tuzo Wilson and Bowie seamounts.

Basalt Stratigraphy

The basalt recovered at Maud Rise is dark gray, amygdaloidal, and contains as much as 20% vesicles filled with calcite, zeolites, and some chlorite (Fig. 14). Extensive fracturing is apparent throughout the rock, and calcite veins crosscut and/or connect the calcite-filled amygdules.

Two separate flow units are identified within the 1.7-m-long basalt interval, both about equal in thickness. The topmost 10-cm section of the flows is glass and is characterized by perlitic texture. Perlites are concentric fractures common in quenched lavas (Figs. 15 and 16). The number of phenocrysts increases downhole and within each flow unit, and the glass is replaced by slender crystals of magnetite-ilmenite and biotite in the matrix. There is an increase in magnetite content with depth.

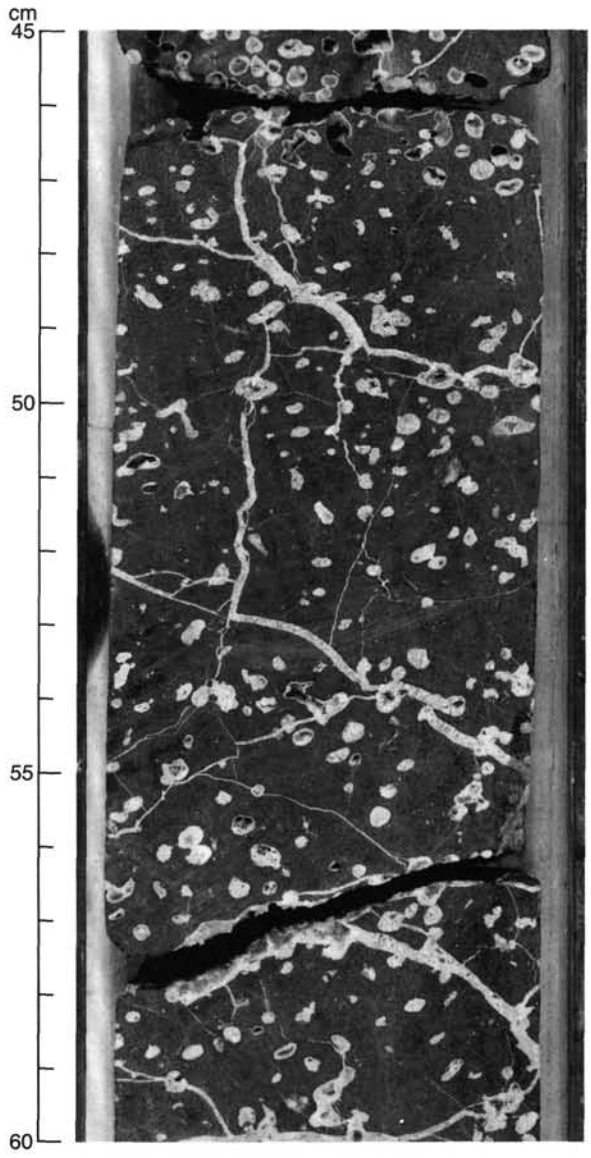

Figure 14. Amygdules in basalt core, Sample 113-690C-24X-1, 45–60 cm.

Petrography and Alteration

In thin section the rock has a glomeroporphyritic texture; it is sparsely olivine-phyric, with rare pyroxene phenocrysts. The olivine phenocrysts show quench texture, and are euhedral to skeletal (Fig. 17) and range in size between 0.2 and 0.5 mm. Most phenocrysts occur as glomeroporphyries (Fig. 18) in a glassy or devitrified matrix of magnetite, biotite, and apatite.

Minerals were optically identified on board, and their composition was checked by microprobe analysis at the Department of Geology, University of Toronto. Olivine phenocrysts are altered to iddingsite, but relict olivine cores are common. The forsterite component of olivine is about Fo_{86}. Other phenocrysts have not been identified, but the shape of some carbonate-altered grains resembles pyroxene. Cumulus olivine occurs as 1–3-mm-size aggregates that are altered to iddingsite, and are speckled with minute inclusions of magnetite. Apatites are abundant in the matrix, and occur as quench textured, hollow, elongate, "hopper olivine"-shaped grains, or as hexagonal basal sections.

Figure 15. Perlite in palagonitized glass, Unit I, Sample 113-690C-23X-1, 4–6 cm (50X).

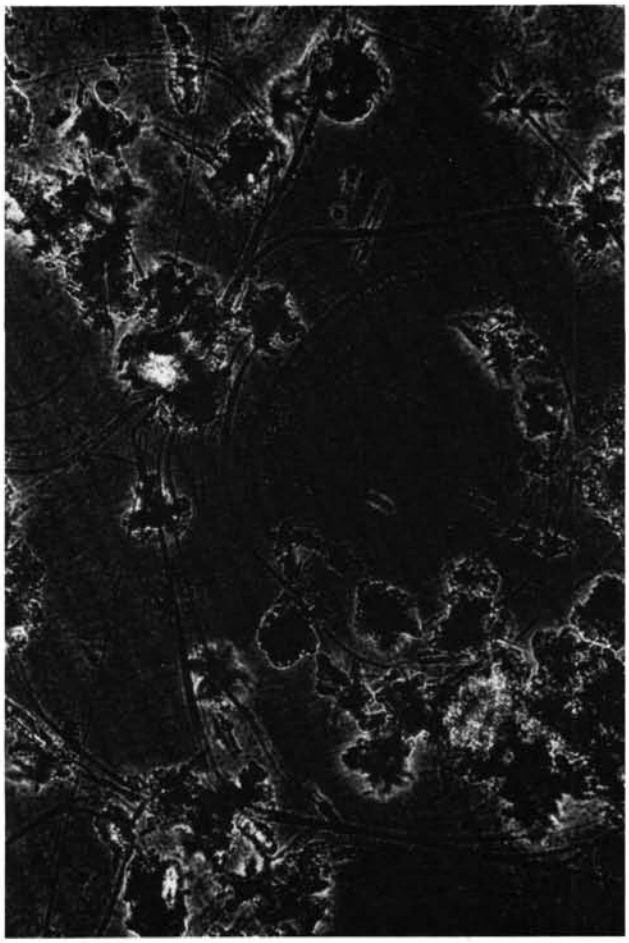

Figure 16. Perlite in palagonitized glass, Unit II, Sample 113-690C-24X-1, 18–20 cm (50X).

They have a high relief, and basal sections are dark under crossed polars. Magnetites occur as blocky grains associated with olivine, but also as needle-shaped or fernlike aggregates. Strongly pleochroic brown biotites occur as radiating needles, nucleating from the glass. Interstitial glass is present in the matrix in variable proportions.

A variety of xenoliths was found in the basalt, including apatite, orthopyroxene, and brown chromite rimmed by magnetite. Chromite attached to anhedral olivine grains indicates a common source for both minerals. Apatites are anhedral, often twinned, cloudy due to the large number of inclusions, and as large as 1.5 mm in size. The grain boundaries are uneven and show signs of absorption. Chromites are anhedral to subhedral, transparent brown, and range in size from 0.5 to 4.0 mm. Grain boundaries are smooth, and a number of xenoliths are subrounded. Titaniferous magnetite rims all chromite grains, and inclusions are not present in the chromite grains. The orthopyroxene xenoliths are relatively fresh and slightly subrounded. Most grains are rimmed by yellow-orange iddingsite, and these rims act as a barrier to chemical reactions between the pyroxene and the melt.

Some minerals in the basalt are altered. All olivine grains are rimmed by a platy, orange-yellow mineral optically identified as iddingsite, but the chemical composition of this mineral ranges between chlorite and amphibole. Iddingsite is an iron-rich hydrous mineral, and it is a common alteration product of olivine. In the upper part of both units carbonate replaces olivine and possibly pyroxene phenocrysts, but in the lower section carbonate alteration is uncommon.

Geochemistry

The major and trace element geochemistry of eight whole-rock samples from Hole 690C is shown in Table 3, together with the microprobe analyses of the glass from the two flow tops; the chemical analyses of basalts from the Walvis Ridge, Tristan da Cunha Island, and Rio Grande Rise; and the composition of an average oceanic basalt.

Basalts from Maud Rise have high Zr, TiO_2, P_2O_5, K_2O; low SiO_2 and MgO contents. This composition is typical of alkali basalts. The alkali trend is evident when $Na_2O + K_2O$ values are plotted against SiO_2 (Fig. 19). Data points plotted on the AFM diagram (Fig. 20) cluster in the alkali field. The diagram of Pearce and Cann (1973) was used for further classification of the basalt (Fig. 21). This diagram was constructed on the assumption that Ti, Y, and Zr are immobile trace elements during weathering and low-grade metamorphism. Data points in Figure 21 cluster on the periphery of the "within plate basalts" (WPB) section of the diagram. By definition, the WPB is a basalt series formed by hot-spot-related volcanic activity (Pearce, 1976, unpublished manuscript). These basalts can range from tholeiitic to calc-alkalic composition, and are formed in ocean island and continental rift environments.

Chemical variations between the two flows are examined. Figure 22 is a visual representation of the major and trace element concentrations with depth. It appears that, apart from slight variations, both units have similar major and trace element contents. The oscillations in some sections of the diagram

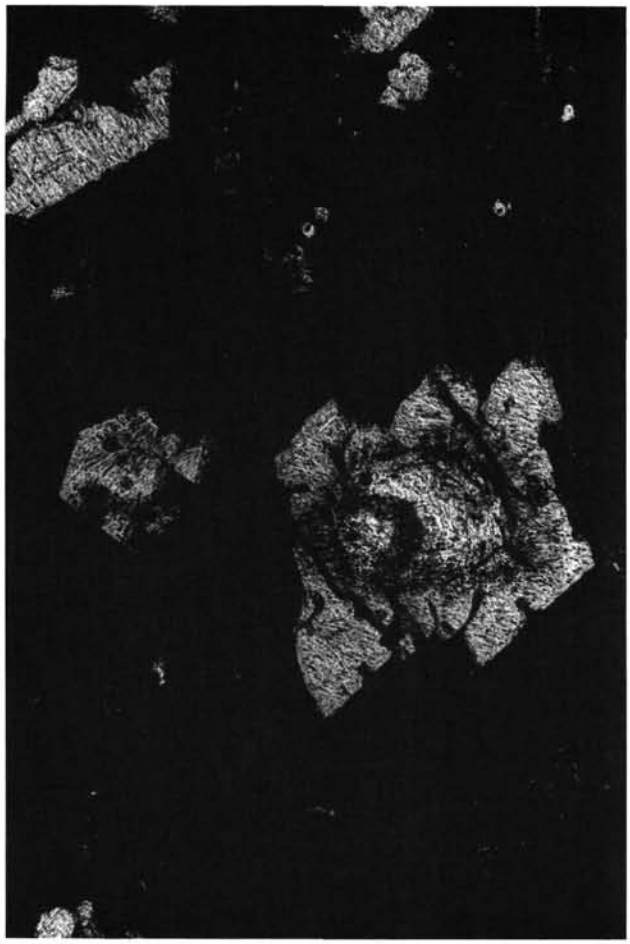

Figure 17. Skeletal olivine (altered to iddingsite), Sample 113-690C-24X-1, 93–96 cm (50X).

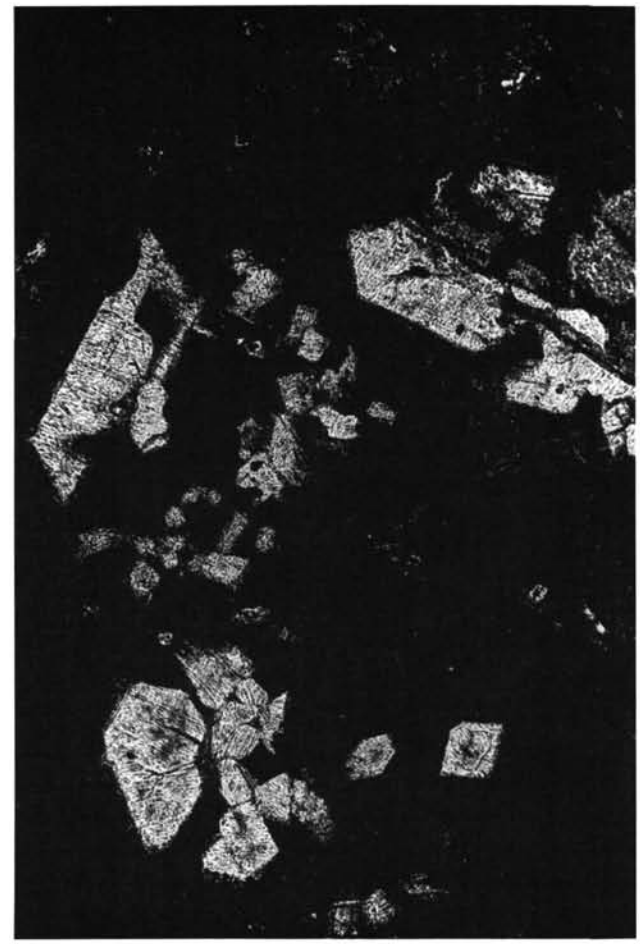

Figure 18. Olivine glomeroporphyries (altered to iddingsite) Sample 113-690C-24X-1, 93–96 cm (50X).

may be an effect of close sampling intervals. However, as the basalt is highly vesicular, and vesicles are filled with calcite, zeolite, and minor quartz, concentrations should not be taken as absolute values. Nb, Zr, Ti, Na_2O, K_2O, and Al_2O_3 values are similar in both flows, whereas there is an increase in SiO_2 and MgO toward the top of Unit I. To check for the true concentrations of major and some trace elements, the glass in both flow tops was analyzed by electron microprobe, and results are shown in Table 3. The glass in the overlying flow is slightly more hydrated, as shown by the lower totals. It is important to note that there is a 20% decrease in MgO from the top of Unit II to the top of Unit I, which is not supported by the whole-rock analysis.

Microprobe analysis of the forsterite content in the relict olivine core is about Fo_{86}, we can calculate the MgO content of the liquid in equilibrium with the olivine by using the equation of Roeder and Emslie (1970):

$$K_D = \frac{(FeO)^{OL}}{(MgO)} \frac{(MgO)^{LIQ}}{(FeO)} = 0.30$$

Assuming that 40% of the Fe was present in the liquid as Fe_2O_3, the MgO content of the liquid crystallizing the olivine had to be about 10–12 wt% (FeO total of the whole rock is approximately 10 wt%). The MgO content of the whole rock ranges between 5–6 wt%, and in the glass, between 3–4 wt%. Evidently MgO was lost during seawater and basalt interaction, as shown by the 20% loss of MgO in the more hydrated glass at the top. Nonprimary MgO values are supported by the relatively high Ni values.

To check the immobility of some trace elements in the basalt, Nb, Sr, P, Y, Ce, Ba, Ti, and K values are plotted against Zr in Figure 23. It appears that Nb, P, Y, Ce, Ti, and K are relatively immobile, whereas Sr and Ba show a wider scatter. Primary biotite and apatite support the immobility of K and P. The Ba and Sr values are probably influenced by the calcite in the amygdules, as calcite can concentrate both elements. However, the unusually high Sr and Ba values are interpreted as a reflection of the alkali composition of the rock. The Zr/Nb ratio (7.0) in the Maud Rise basalt is comparable to values observed in other ocean-floor alkali basalts.

Discussion

Based on mineralogy and major and trace element geochemistry, the basalts from Maud Rise, Site 690, can be classified as ocean-floor olivine alkali basalts. They are high in Ti, Zr, P, Nb, Sr, Ba, and K, and low in Si and Mg. The high concentration of incompatible elements and low SiO_2 content is indicative of a low degree of partial melting of the mantle (about 2.5%). There is no evidence for significant amount of fractional crystallization in these rocks.

Both major and trace element geochemistry of the Maud Rise basalts are similar to dredged basalts from the Rio Grande Rise and from the Tristan da Cunha Island, a modern hot-spot; to alkali basalts from the Tuzo Wilson and Bowie seamounts;

Table 3. Major and trace element microprobe analyses of basalt from Unit I and Unit II flow tops from Hole 690C; from Rio Grande Rise (Thompson et al., 1983), Walvis Ridge (Thompson and Humphris, 1984), and from an average oceanic alkali basalt (Engle et al., 1965).

113-690C- Core/section (interval in cm)	23X-1 10–12	23X-1 52–53	24X-1 9–10	24X-1 15–17	24X-1 26–28	24X-1 64–67	24X-1 93–96	24X-1 119–121	Rio Grande Rise dredge	Walvis Ridge	Tristan da Cunha	Ocean alkali basalt
Major element analyses on volatile-free basis after ignition at 1000°C (wt%)												
SiO_2	48.73	47.36	48.55	47.53	45.44	45.49	45.10	44.86	47.33	51.14	46.7	47.41
TiO_2	3.39	3.44	3.57	3.50	3.29	3.37	3.30	3.30	3.25	3.03	3.6	2.87
Al_2O_3	14.63	14.94	15.25	14.99	14.34	14.53	14.40	14.63	14.90	16.53	17.30	18.02
Fe_2O_3 (tot)	10.09	9.75	10.19	10.42	9.64	9.84	9.85	9.48	9.60	11.96	10.40	9.97
MnO	0.12	0.12	0.11	0.12	0.11	0.38	0.12	0.12	0.17			
MgO	5.75	4.02	4.99	5.06	5.21	4.57	4.51	4.40	7.19	2.37	4.70	4.79
CaO	8.34	11.68	7.78	8.28	12.41	11.89	12.85	15.93	10.15	7.08	9.70	8.65
Na_2O	2.84	2.64	3.06	2.95	2.53	2.93	2.86	2.57	3.57	2.91	4.10	3.99
K_2O	3.67	3.18	4.23	4.24	4.13	3.88	3.77	3.21	1.73	2.19	3.0	1.66
P_2O_5	1.80	1.72	1.63	1.73	1.78	1.72	1.67	1.80	0.75			0.92
Total	99.36	98.85	99.36	98.82	98.88	98.60	98.43	99.65				
LOI	6.8	9.9	7.8	7.6	10.5	11.95	9.25	13.48				2.45
Trace element analyses on a dried 110°C basis (ppm)												
Nb	77	76	82	81	74	77	77	71	70	20	112	
Zr	542	535	571	562	516	541	533	500	293	200	325	333
Y	29	29	32	32	28	30	28	28	25	46	45	54
Sr	1544	1422	1543	1782	1591	1683	1449	921	928	318	1167	815
Rb	47	49	53	51	49	48	46	36	3		173	
Zn	180	137	140	142	192	135	130	120	103			
Cu	31	28	32	34	32	33	28	25	55	110		36
Ni	184	119	136	129	141	128	139	130	106	55	10	51
Cr	129	101	163	122	129	103	124	103	146	73	28	67
V	150	158	173	162	158	173	166	157	271	437	230	252
Ce	190	186	208	205	189	197	198	185		65		
Ba	921	1062	1491	1748	1756	1122	859	675	1156	384	913	498

and to alkali basalts from ocean islands. These basalts typically represent alkalic volcanism associated with mantle plumes. The highly vesicular nature of the basalt from Maud Rise indicates high concentration of volatiles in the melt. It has been suggested by Moore et al. (1982) that volatiles behave as strongly incompatible elements in the mantle, and concentrate in the liquid phase. Consequently, we find vesicular alkali basalts associated with the initial growth phase of an ocean island or seamount, and also with the final stage. The abundance of unusual xenoliths in the Site 690 basalts, such as brown chromite and apatite, suggests a mantle source.

It is not possible to make assumptions about the composition of the underlying rocks because of the short length of recovered basalt (2 m). It should be noted, however, that the relative thinness of the individual flows (1 m) suggests that they may form only a cap on basalts of tholeiitic composition.

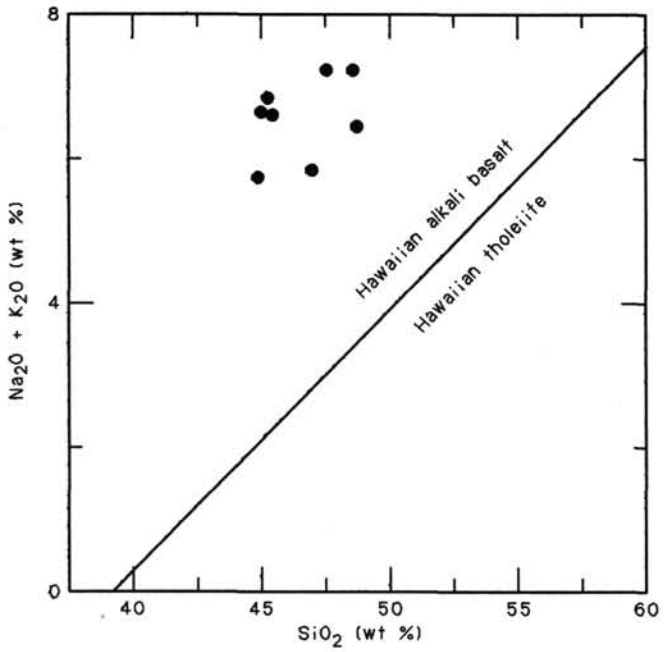

Figure 19. Calc-alkalic and tholeiitic fields on $Na_2O + K_2O$ vs. SiO_2 plot. Dots = Hole 690C basalt samples.

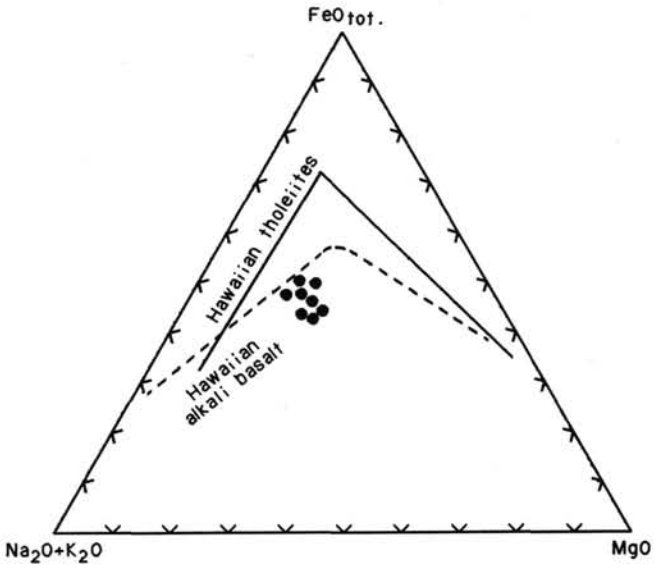

Figure 20. AFM diagram showing tholeiitic and calc-alkalic fields. Dots = Hole 690C basalt samples.

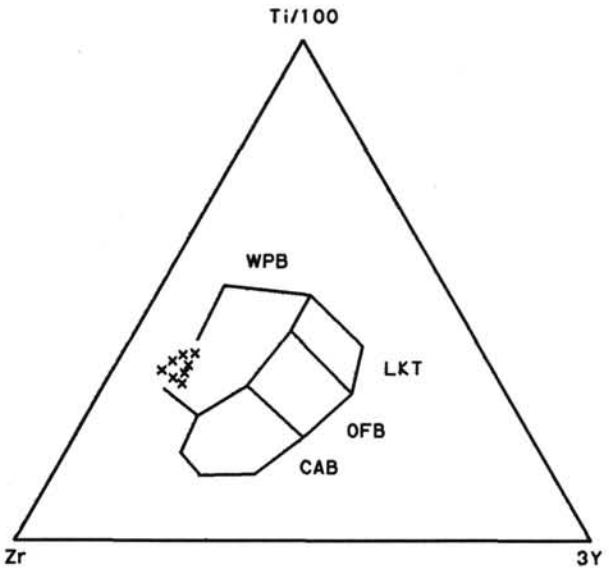

Figure 21. Ti-Zr-Y diagram of Pearce and Cann (1973), X = Hole 690C basalt samples. WPB = within-plate basalt; OFB = ocean floor basalt; LKT = low k tholeiites; CAB = calc-alkalic basalt.

The mineralogical and geochemical evidence suggests that the basalt recovered from Maud Rise represents alkalic volcanism, generally associated with the building of ocean islands and seamounts. Apart from the alteration of olivine to iddingsite and the filling of vesicles with zeolites and carbonate, the basalt is relatively unaltered, and does not show evidence of subaerial weathering.

PHYSICAL PROPERTIES

Index properties measured on samples from approximately every other section in each core are listed in Table 4. Profiles of bulk density, water content (dry basis), and grain density (Fig. 24) and porosity (Fig. 25) illustrate the large variations in index properties. At Hole 690B, bulk densities range from a low of 1.24 g/cm^3 at 12.6 mbsf to a high of 2.19 g/cm^3 at 174.9 mbsf. Water content mirrors bulk density and ranges from a high of 289% at 6 mbsf to a low of 34% at 148.1 mbsf. Grain density ranges from a high of 3.09 g/cm^3 at 172.9 mbsf to a low of 1.89 g/cm^3 at 3 mbsf. The grain density at this site is unusual in that it is inversely related to water content and directly related to bulk density. In most marine sediments the grain density is unrelated to either of these measures, essentially being a constant with a value between 2.65 and 2.75 g/cm^3. Grain density in the upper 70 m of Hole 690B is inversely related to porosity. These unusual relationships reflect the influence of the presence of diatoms and the low density (specific gravity) of biogenic silica (2.02 g/cm^3). The presence of diatom ooze accounts for the large variations in the index properties because of diatoms' very low bulk density and ability to form a strong fabric.

Silica content was not determined for Hole 690B sediments but the percent calcium carbonate was measured (Fig. 26 and Table 5). The calcium carbonate content reflects the amount of silica present if the sediment contains only siliceous and calcareous components. The decreases in $CaCO_3$ content at various levels within the section is reflected in the index properties; bulk density, water content, grain density, and porosity (Figs. 24 and 25). As the $CaCO_3$ content stabilizes downhole a steady decrease of porosity and water content and a steady increase in bulk density is observed with only minor perturbations. These variations are attributed to diagenetic alterations in the form of compaction (consolidation) and possible cementation.

Five lithostratigraphic units containing seven subunits (Fig. 3) were identified (see "Lithostratigraphy" section, this chapter). They are as follows: Unit I ranges from 0 to 24.4 mbsf, Pliocene to Miocene siliceous, dominantly diatom ooze; Subunit IIA ranges from 24.4 to 53.4 mbsf, siliceous and calcareous sediments; Subunit IIB ranges from 53.4 to 92.9 mbsf, a calcareous-rich sediment of Oligocene age. Unit III contains a calcareous sediment of lower Eocene to upper Paleocene age, ranging from 92.9 to 137.8 mbsf. Unit IV, from 137.8 to 281.1 mbsf, contains three subunits. Subunit IVA contains mostly calcareous sediment with a large terrigenous component. Subunit IVB is almost pure calcareous material, and Subunit IVC is calcareous-rich material with a terrigenous component. Unit V, at 281.1–317.0 mbsf, contains calcareous sediment with a large terrigenous content.

Nine geotechnical stratigraphic units were determined by the examination of the physical properties at Hole 690B: Unit G-I, 0–2.1 mbsf, contains high grain density, low water content sediments; Unit G-II, 2.1–19 mbsf, high velocity, low bulk and grain density, and very high water content and porosities; Unit G-III, 19–24 mbsf, high velocities, decreasing grain and bulk density and increasing porosity; Unit G-IV, 24–32 mbsf, high velocities, decreasing bulk and grain densities, and increasing porosity, with a steep porosity gradient; Unit G-V, 32–55 mbsf, fluctuating porosity, bulk density, and water content; Unit G-VI, 55–138 mbsf, increasing bulk density, shear strength, and velocity, and decreasing porosity and water content. Unit G-VI may be further divided at 85 mbsf on the basis of large changes of velocity starting at 85 mbsf. Unit G-VII, 138–158 mbsf, is characterized by increasing bulk and grain densities, shear strength, and velocity. Unit G-VIII, 158–180 mbsf, contains increasing porosity, velocity, and water content and decreasing bulk density and shear strength. Unit G-IX, 180–317 mbsf, contains the highest velocity in the section, low shear strength, and decreasing bulk and grain densities. Figure 27 illustrates the relationship between the lithostratigraphic units of Site 690 and the geotechnical units of Sites 689 and 690.

Compressional Wave Velocity

Sonic velocities (V_p) in sediment were measured using two methods. A continuous measurement of V_p was made through the whole core using a *P*-wave logger (PWL) installed next to the gamma ray attenuation porosity evaluator (GRAPE) source and detector. Individual measurements were made on samples removed from the core with one measurement from each section, usually three per core. V_p was measured in only one direction; the sediments in Hole 690B are bioturbated, and acoustic anisotropy was at a minimum. Measurements on competent core "biscuits" were made on sediments obtained by the XCB. The Hamilton Frame Velocimeter was utilized for the laboratory determination of V_p using procedures outlined by Boyce (1976).

Figures 28 and 29 are V_p profiles (Hamilton Frame) for Hole 690B sediments. Figure 29 is a V_p profile on an expanded scale for sediments in the upper 200 m of the section. Table 6 lists the V_p determinations. Figure 30 is a continuous V_p profile as determined by the PWL for sediments recovered by the use of the APC core technique for Hole 690B sediments. The V_p in the radiolarian-diatom ooze of lithostratigraphic Subunit IB is relatively high for such low-density, high-porosity sediments. In this unit the density of the sediment appears to be the major factor that governs acoustic velocity. Within the siliceous ooze the V_p velocity increases with increasing bulk density, attesting to the strong sediment fabric created by the diatoms. The lowest velocities in the section are found at a depth of 74–88 mbsf, the upper part of Unit G-VI, a carbonate-rich sediment.

In the upper 100 m the highest velocities are found in the upper 20 mbsf. In the upper 90 m the velocity gradient is essen-

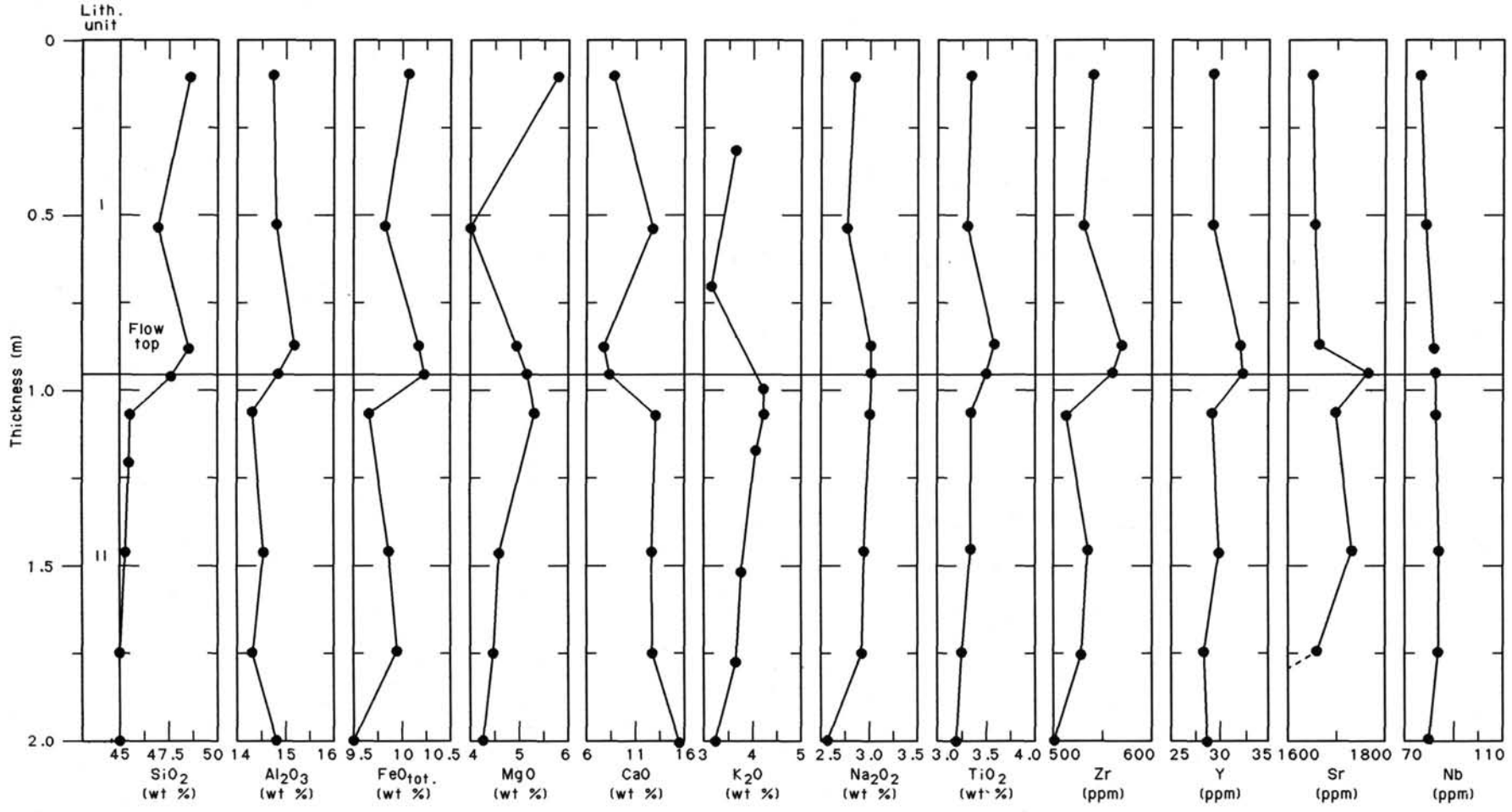

Figure 22. Major and trace element variations with depth for Hole 690C basalt samples.

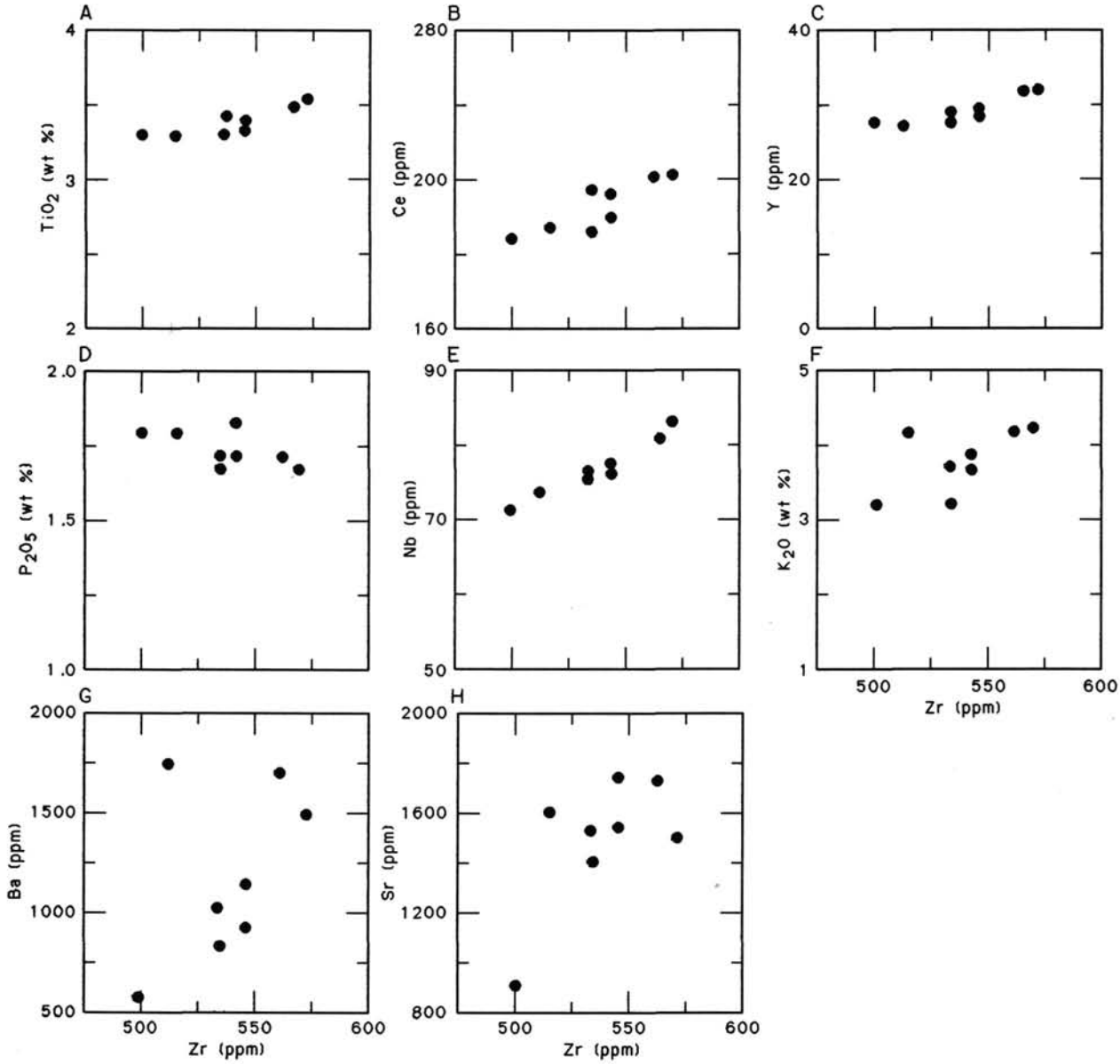

Figure 23. Zr plotted against various trace elements in basalt. A. TiO_2. B. Ce. C. Y. D. P_2O_5. E. Nb. F. K_2O. G. Ba. H. Sr.

tially zero or slightly negative. From 100 to 180 mbsf the velocity gradient is equal to 2 m/s/m. From 150 to 210 mbsf the velocity decreases and has a zero gradient. Although no velocities were measured over the interval between 220 to 270 mbsf the velocity gradient from 212.3 to 291.6 mbsf is very high, approaching 5 m/s/m. The highest velocities occur at a depth of 275–290 mbsf.

Shear Strength

The undrained shear strength of the sediment was determined using a Wykeham-Farrance motorized vane shear device. Standard 1.2-cm equidimensional miniature vanes were used with the Wykeham-Farrance device. Its operation and calculations follow procedures outlined by Boyce (1976).

The shear strengths determined for Hole 690B are listed in Table 7 and illustrated in Figure 31. In the upper 50 mbsf the shear strengths range from 14 to 56 kPa, the highest strengths being in the upper section. The strength gradient in this zone is essentially zero. The strength gradient from 50 to 150 mbsf is fairly high at 1 kPa/m. Below 150 mbsf, the shear strength decreases and becomes quite erratic. The introduction of terrigenous material appears to have decreased the overall strength of the sediment or made it more sensitive to coring disturbance. No attempts were made to measure the residual strength as outlined in the procedure handbook. The residual strength of noncohesive sediment such as diatom or nannofossil ooze was considered unmeasureable with the existing equipment.

Thermal Conductivity

The thermal conductivity of the sediments sampled at Hole 690B was measured following the methods of Von Herzen and Maxwell (1959) using the needle-probe technique. The needle-probe was inserted through a drilled hole in the core liner so that the probes were oriented perpendicular to the core axis.

Thermal conductivity ranged from a low of 1.007 W/m-K at 27.9 mbsf to a high of 1.611 W/m-K at 131.7 mbsf (Table 8 and Fig. 32). Thermal conductivity is directly related to bulk density and inversely related to water content.

Table 4. Water content, porosity, bulk density, and grain density measured on samples from Site 690.

Core, section top (cm)	Depth (mbsf)	Water content (% dry weight)	Porosity (%)	Bulk density (g/cm^3)	Grain density (g/cm^3)
113-690A-					
1H-2, 90	0.9	92.28	73.46	1.57	2.85
1H-4, 90	5.3	168.48	80.41	1.31	2.26
1H-6, 87	8.8	268.18	88.48	1.24	2.45
1H-7, 57	9.8	225.00	86.11	1.27	2.52
113-690B-					
1H-1, 90	0.9	83.38	70.40	1.59	2.77
1H-2, 20	1.7	85.60	70.05	1.56	2.70
2H-2, 90	3.0	188.07	80.20	1.26	1.89
2H-4, 90	6.0	229.90	86.05	1.27	2.34
2H-6, 90	9.0	169.89	80.15	1.30	2.37
3H-2, 90	12.6	185.72	78.45	1.24	2.27
3H-4, 90	15.6	198.54	84.62	1.30	2.40
3H-6, 90	18.6	99.04	70.63	1.45	2.40
4H-1, 89	22.3	155.41	94.23	1.59	2.68
4H-3, 89	25.3	90.21	72.27	1.56	2.56
4H-5, 88	28.3	57.10	62.28	1.76	2.94
5H-1, 88	31.0	57.95	63.01	1.76	2.86
5H-3, 89	34.0	112.71	75.67	1.46	2.38
5H-5, 89	37.0	113.52	80.13	1.54	2.53
6H-1, 89	41.9	113.74	78.29	1.51	2.58
6H-3, 90	44.9	79.29	69.68	1.61	2.79
6H-5, 89	47.9	94.72	74.28	1.56	2.66
7H-1, 89	51.3	80.14	73.10	1.68	2.69
7H-3, 89	54.3	63.20	68.36	1.81	2.96
7H-5, 89	57.3	53.53	62.09	1.82	2.79
8H-1, 89	61.0	56.89	61.88	1.75	2.79
8H-3, 89	64.0	78.69	69.71	1.62	2.67
8H-5, 89	67.0	63.86	66.17	1.74	2.70
9H-1, 89	70.7	63.30	66.29	1.75	2.61
9H-3, 90	73.7	73.00	70.69	1.72	2.79
9H-5, 88	76.7	64.96	64.67	1.68	2.63
10H-2, 90	81.8	64.72	64.46	1.68	2.72
10H-4, 90	84.8	63.93	64.45	1.69	2.64
10H-6, 90	87.8	69.49	64.67	1.62	2.62
11H-1, 90	90.0	55.25	62.36	1.80	2.83
11H-3, 90	93.0	69.12	65.98	1.65	2.72
11H-5, 90	96.0	61.44	62.83	1.69	2.65
12H-2, 90	101.2	60.27	67.62	1.84	2.63
12H-4, 85	104.2	61.33	63.85	1.72	2.65
12H-6, 90	107.2	58.58	61.41	1.70	2.70
13H-2, 90	110.9	50.85	59.51	1.81	2.76
13H-4, 90	113.9	56.47	61.68	1.75	2.74
13H-6, 90	116.9	52.84	57.55	1.71	2.62
14H-1, 90	119.1	55.79	60.31	1.73	2.64
14H-2, 90	120.6	51.58	60.67	1.83	2.88
14H-3, 90	122.1	44.87	58.61	1.94	2.77
14H-4, 90	123.6	47.27	58.39	1.86	2.75
14H-6, 90	126.6	46.03	55.45	1.80	2.79
15H-2, 90	130.2	51.35	58.25	1.76	2.65
15H-6, 90	136.2	39.30	52.17	1.89	2.75
16H-1, 91	138.4	40.84	57.59	2.04	3.00
16H-3, 90	141.4	37.98	53.39	1.99	2.86
16H-5, 90	144.4	34.88	53.43	2.12	2.87
17H-1, 90	148.1	34.05	53.58	2.16	2.95
17H-3, 90	151.1	35.05	53.75	2.12	2.96
17H-5, 90	154.1	36.80	52.99	2.02	2.96
18H-1, 90	157.8	33.77	52.04	2.11	2.98
18H-3, 90	160.8	38.52	50.93	1.88	2.58
18H-5, 90	163.8	34.53	50.62	2.02	2.55
19H-1, 90	167.5	34.70	55.88	2.22	3.05
19H-3, 90	170.5	38.63	54.27	2.00	2.85
20H-1, 90	174.9	36.66	57.27	2.19	3.26
20H-3, 90	177.9	35.46	55.04	2.15	3.09
21H-2, 90	183.9	39.51	54.08	1.96	2.82
21H-4, 10	183.1	38.19	54.63	2.03	2.75
22H-2, 90	187.3	41.20	52.87	1.86	2.71
22H-4, 90	190.3	39.54	52.01	1.88	2.81
23H-2, 90	191.8	43.66	54.75	1.85	2.74
23H-4, 90	194.8	39.15	52.02	1.89	2.77
24H-2, 93	200.3	38.58	52.27	1.92	2.76
24H-4, 93	203.3	41.77	53.44	1.86	2.72
25H-2, 90	206.3	36.25	49.86	1.92	2.74

Table 4 (continued).

Core, section top (cm)	Depth (mbsf)	Water content (% dry weight)	Porosity (%)	Bulk density (g/cm^3)	Grain density (g/cm^3)
113-690B-					
25H-4, 90	209.3	34.55	48.25	1.93	2.67
25H-6, 90	212.3	29.31	45.70	2.07	2.83
113-690C-					
17X-7, 2	271.6	24.72	43.74	2.26	2.89
18X-1, 1	271.8	20.35	37.60	2.28	2.84
18X-4, 68	277.0	29.34	44.97	2.03	2.57
19X-1, 40	281.9	34.01	49.16	1.98	2.79
19X-4, 105	287.1	31.38	46.80	2.01	2.73
20X-1, 34	291.6	40.18	56.47	2.02	2.83

Summary

The results of physical-property measurements at Site 690 demonstrate the effect that density, in this case low-density biogenic silica and high-density calcium carbonate ooze, can have on the index properties and compressional wave velocities. The siliceous sediments have a low bulk density and high velocity compared to the high bulk density and low velocity of the calcareous sediments. It was also demonstrated that physical properties can delineate geotechnical boundaries which in most cases can be associated with lithostratigraphic boundaries and seismic horizons. Figure 27 shows the association of lithostratigraphic and geotechnical units within Site 690. The boundary between geotechnical Units G-III and G-IV was marked by a high velocity and a large porosity gradient. This boundary corresponds to the boundary between lithostratigraphic Units I and II. The geotechnical boundary that corresponds to the lithostratigraphic boundary between lithostratigraphic Subunits IIA and IIB is marked by increasing bulk density, velocity, and shear strength. At the boundary between lithostratigraphic Units II and III a large increase in velocity was noted. The geotechnical boundary between Units G-VI and G-VII, which corresponds to the boundary between lithostratigraphic Units III and IV, was delineated on increasing velocity, shear strength, bulk density, and grain density and decreasing porosity.

Thus the geotechnical units designated in Figure 27 are based on the changes and rate of change of the index properties, acoustic velocities, and shear strength. The dashed lines between the two geotechnical columns (Sites 689 and 690, Fig. 27) designate tentative correlations.

SEISMIC STRATIGRAPHY

Site 690 was chosen originally, as W2B, at shotpoint 870 on multichannel seismic line UB Maud-2 (University of Bergen Seismological Observatory, Norway). UB Maud-2 (Fig. 2) was shot 12-fold, at a 50-m shot spacing, using one 600-in.^{3} Bolt air gun. Also in the vicinity were a single-channel *Islas Orcadas* 1277 line and several multichannel lines acquired aboard *Polarstern* early in 1986 (see track chart, Fig. 1). The drilling target was a 350 millisecond (ms) sedimentary section on the flank of a small bank of sediments on the southern slope of Maud Rise. Final site selection was a compromise between preserving the assumed Neogene and upper Oligocene section while keeping basement accessibly shallow, and risking an Eocene-Oligocene boundary hiatus. Because of the hiatuses in the Neogene record at Site 689, the risk was taken in order to improve the chance of sampling a more complete Neogene section.

These considerations made the drilling target quite precise; since the area was not well reconnoitered, we decided to approach the site nominally along the track of UB Maud-2 (Fig. 1),

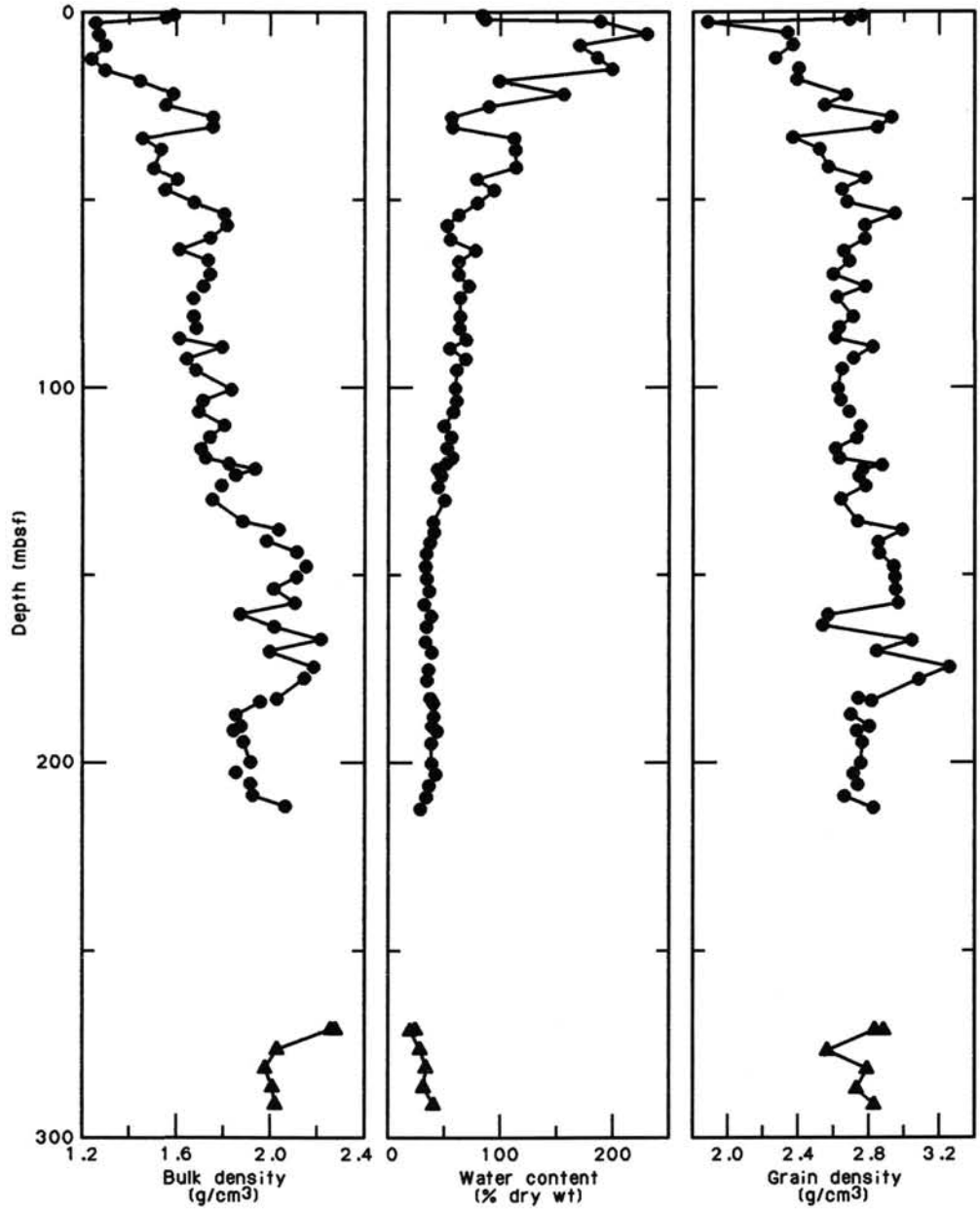

Figure 24. Profiles of bulk density, water content, and grain density in Holes 690B (dots) and 690C (triangles).

to avoid confusion. *JOIDES Resolution* passed over the site and then dropped the beacon on the return track. Similarly, on leaving the site, *JOIDES Resolution* looped away to the north-northeast to stream the seismic gear (see "Introduction and Explanatory Notes" chapter, this volume), before crossing over the position of the site heading along 222° for Site 691. The 3.5-kHz profile obtained on leaving the site is shown in Figure 33.

As at Site 689, there was no logging, and shipboard velocity measurements were used to establish a time-depth relationship. PWL data and a derived velocity-depth model are shown in Figure 34. Hamilton Frame measurements of velocity are similar (see Fig. 29). As for Site 689, the model is biased high over the depth range sampled by the APC (0–210 m), compared with both kinds of shipboard measurements, to allow for the changes from *in-situ* conditions. Below 210 mbsf the Hamilton Frame measurements are again higher than all but the very highest PWL values. The model compromises between these extremes, on the assumption that with the incomplete recovery typical of XCB drilling, the harder and thus faster-velocity lithologies will be preferentially recovered and measured.

The velocity-depth model is different in detail from that of Site 689, reflecting for example the slightly higher velocities between 120 and 170 mbsf at Site 690. The resulting time-depth relations, however, coincide within 2 m down the entire section. These two time-depth curves do depart from that calculated by Carlson et al. (1986), by more than 10 m in the depth range 180–250 mbsf (but by less at greater depth). This departure is small considering the end-member nature of the biogenic, largely calcareous sections at the two sites. It strongly supports the conclusions of Carlson et al. (1986), that velocity-depth relations derived from sonobuoy wide-angle reflection data, which show very different features for carbonates than for terrigenous or siliceous sediments in the deep sea, are not useful in the context of ocean drilling. Similar reservations must apply to the use of

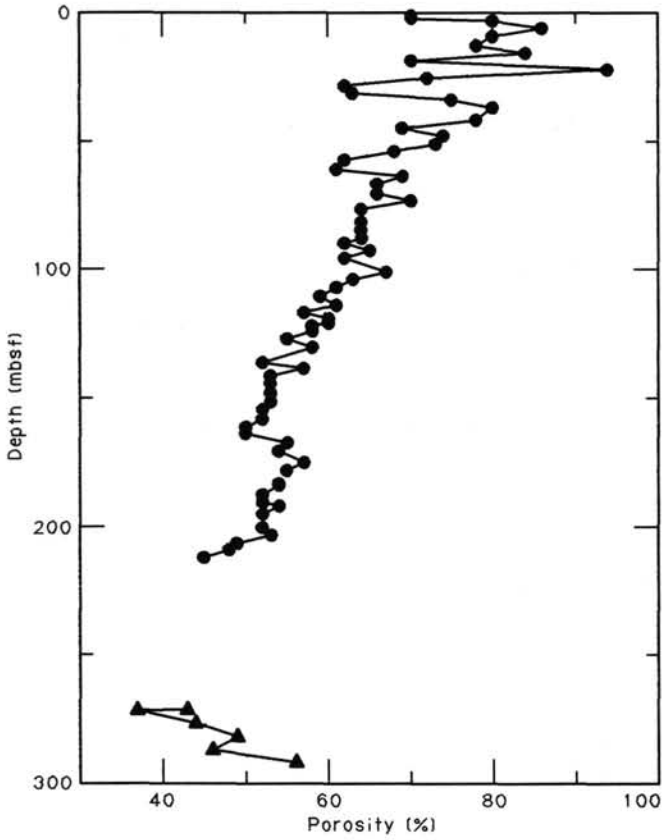

Figure 25. Profile of porosity in Holes 690B (dots) and 690C (triangles).

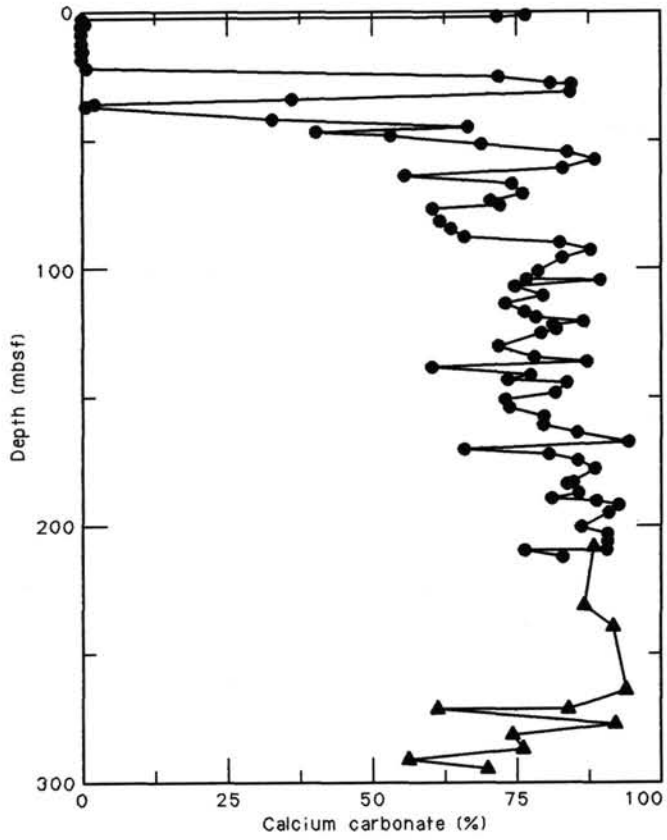

Figure 26. Profile of percent calcium carbonate in Holes 690B (dots) and 690C (triangles).

multichannel seismic interval stacking velocities, a widespread and prejudicial practice during site proposal review. Except in sections suspected of having had overburden stripped off, or of having been tectonically deformed, the velocity-depth relation determined by Carlson et al. (1986; V(m/s) = 1590 exp. (0.00033Z · m)) provides the most useful first approximation.

In Figure 35, the lithologic section is compared with *JOIDES Resolution*'s water-gun profile acquired on leaving the site. The interpreted depth and nature of the more prominent reflectors are listed in Table 9. In general, as at Site 689, the abundant reflectors at shallow depth correspond to the calcareous/siliceous alternations of the top 100 m, the transparent middle section represents the uniform, mainly calcareous oozes beneath, and some reflectors not far above basement correspond to diagenetic changes. There are differences between the sites, but they are minor.

Not all of the reflectors seen on the water-gun and 3.5-kHz profiles coincide. This is a natural effect of the different frequency content of the two sound sources. In the upper part of the record, where both systems produce reflections, the water-gun record (Fig. 35) is dominated by the calcareous/siliceous lithologic alternations, probably because the dominant periods of those changes are 30–40 ms (20–30 m) where also there is adequate water-gun energy. The 3.5-kHz profile (Fig. 33) however, sees much shorter events, of the order of 1 or 2 ms, which the water-gun system cannot resolve. For example, consider the seabed reflection itself: the uppermost 2 m at the site is a foraminiferal ooze, of a reasonably high density (Fig. 24) and thus high acoustic impedance contrast with the water. Beneath it lies a diatom ooze with a very high porosity and low bulk density, making its acoustic impedance very low, approaching that of the water column. The 3.5-kHz profile properly defines the top and bottom of the foraminiferal ooze, the former with a strong reflection. Because of the small thickness of the foraminiferal ooze, however, the water-gun system hardly detects it, producing a very low amplitude reflection from the seabed, as if the relevant acoustic impedance contrast was that of water to diatomaceous ooze. The 3.5-kHz profile also shows a sequence of reflectors between 27–37 ms (20–28 m) caused by the transition from nannofossil to diatom ooze.

The 3.5-kHz profile of Figure 33, acquired while leaving the site, shows that we could have been much less fortunate in its location. The fine-scale reflectors between about 38 and 75 ms at the site (30 and 58 m, covering much of Miocene and upper Oligocene sedimentation) are pinched out or drastically thinned both up- and downslope. Biostratigraphic indications are that the hiatus at the Oligocene/Miocene boundary at the site was of short duration, and an improvement on Site 689. This shows the value of regional high-resolution site surveys for shallow (APC) paleoceanographic targets: it may have been possible to find sections without a hiatus, if more time had been available to search.

Below the depth of 3.5-kHz penetration, the water-gun record shows that the reflectors between 126 and 140 ms (95–105 m, including the Eocene/Oligocene boundary) at the site are associated with an unconformity of regional extent. However, this is not the same erosional event or period of nondeposition as was seen at Site 689, where late or middle Oligocene erosion was inferred.

Deeper in the record, there are no reflectors above basement as strong as those associated with the cherts which brought an end to drilling at Site 689. Some weak discontinuous reflectors below about 340 ms (275 m) appear related to the presence of large amounts of clay, and then volcanic glass, in the Upper Cretaceous sediments at Site 690. Basement lies at 317 m, corre-

Table 5. Percent of calcium carbonate present in sediments from Holes 690B and 690C.

Core, section, interval (cm)	Depth (mbsf)	$CaCO_3$ (%)
113-690A-		
1H-2, 90	0.9	80.1
1H-4, 90	5.3	0.8
1H-6, 87	8.8	0.7
1H-7, 57	9.8	0.3
113-690B-		
1H-1, 90	0.9	76.6
1H-2, 90	1.7	72.0
1H-6, 90	2.6	86.1
2H-2, 90	3.0	0.0
2H-3, 145	5.1	0.6
2H-4, 90	6.0	0.0
2H-6, 90	9.0	0.0
3H-2, 90	12.6	0.0
3H-4, 90	15.6	0.0
3H-4, 120	15.9	0.3
3H-6, 90	18.6	0.0
4H-1, 89	22.3	0.8
4H-3, 89	25.3	71.9
4H-4, 145	27.4	80.9
4H-5, 88	28.3	84.6
5H-1, 88	31.0	84.3
5H-3, 89	34.0	36.3
5H-4, 145	36.1	0.0
5H-5, 89	37.0	0.8
6H-1, 89	41.9	32.8
6H-3, 90	44.9	66.6
6H-4, 120	46.7	40.4
6H-5, 89	47.9	53.3
7H-1, 89	51.3	69.0
7H-3, 89	54.3	83.9
7H-5, 89	57.3	88.6
8H-1, 89	61.0	83.1
8H-3, 89	64.0	55.7
8H-5, 89	67.0	74.4
9H-1, 89	70.7	76.1
9H-3, 90	73.7	70.5
9H-4, 117	75.5	72.2
9H-5, 88	76.7	60.3
10H-2, 90	81.8	61.7
10H-4, 90	84.8	63.6
10H-6, 90	87.8	66.0
11H-1, 90	90.0	82.6
11H-3, 90	93.0	87.9
11H-5, 90	96.0	83.0
12H-2, 90	101.2	78.7
12H-4, 85	104.2	76.9
12H-4, 120	104.6	89.7
12H-6, 90	107.2	74.7
13H-2, 90	110.9	79.6
13H-4, 90	113.9	73.1
13H-6, 90	116.9	76.4
14H-1, 90	119.1	78.4
14H-2, 90	120.6	86.6
14H-3, 90	122.1	81.3
14H-4, 90	123.6	81.9
14H-5, 90	125.1	79.3
15H-2, 90	130.2	72.1
15H-5, 91	134.7	78.1
15H-6, 90	136.2	87.3
16H-1, 90	138.4	60.3
16H-3, 90	141.4	77.5
16H-4, 120	143.2	73.6
16H-5, 90	144.4	83.7
17H-1, 90	148.1	81.7
17H-3, 90	151.1	73.1
17H-5, 90	154.1	74.0
18H-1, 90	157.8	79.7
18H-3, 90	160.8	79.8
18H-5, 90	163.8	85.5
19H-1, 90	167.5	94.5
19H-3, 90	170.5	66.1
19H-4, 112	172.2	80.8
20H-1, 90	174.9	85.7
20H-3, 90	177.9	88.7
21H-2, 90	183.9	83.7
21H-4, 10	184.1	84.6
22H-2, 90	187.3	85.8
22H-3, 120	189.1	81.1
22H-4, 90	190.3	89.0
23H-2, 90	191.8	92.7
23H-4, 90	194.8	91.2
24H-2, 92	200.3	86.4
24H-4, 93	203.3	91.1
25H-2, 90	206.3	91.1
25H-4, 90	209.3	90.9
25H-4, 112	209.5	76.6
25H-6, 90	212.3	83.1
113-690C-		
11X-3, 112	208.3	71.5
13X-5, 147	231.1	83.2
14X-4, 115	238.9	88.7
17X-2, 115	264.1	89.1
17X-CC, 2	271.6	83.8
18X-1, 1	271.8	61.1
18X-4, 68	277.0	92.1
19X-1, 40	281.9	74.3
19X-4, 105	287.1	76.1
20X-1, 34	291.6	56.2
20X-3, 145	294.4	64.7

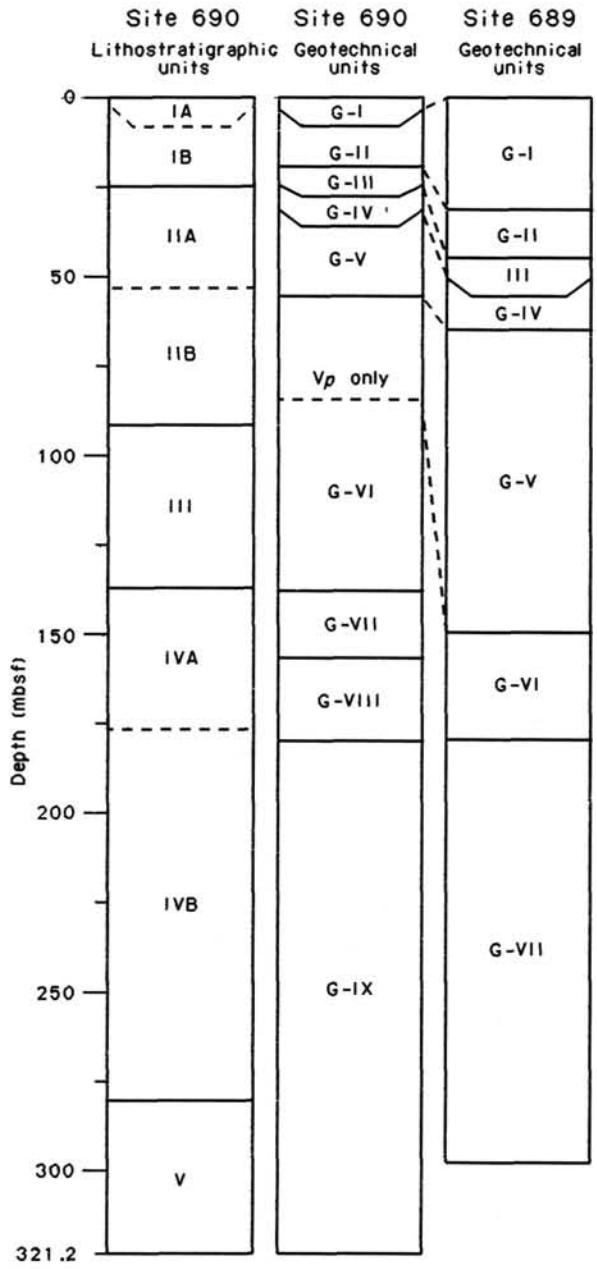

Figure 27. Relationship between lithostratigraphic units of Site 690 and the geotechnical units of Sites 689 and 690. Dashed lines between the two geotechnical columns designate tentative correlations.

sponding to a strong, discontinuous reflector at 385 ms. To the southwest of the site (Fig. 2), this strong reflector is replaced laterally by a set of more planar, weaker onlapping reflectors. This suggests that basement at the site may have been an isolated topographic high, subaerial for some time after its formation. If so, then the absence of any shallow-water indicators in the overlying sediments, and their comparative youth, might be explained.

BIOSTRATIGRAPHY

Site 690 was drilled in 2914 m of water on the flank of Maud Rise to obtain a biosiliceous and carbonate-rich Upper Cretaceous and Cenozoic sequence at high southern latitudes away from terrigenous sediment sources and unstable sediments. This was the deepest of a two-hole transect to study the history of vertical-water-mass structure on Maud Rise. Site 690 penetrated to 317 mbsf in Quaternary to Campanian(?) sediment with an average core recovery in the three holes of 94%. Beneath a thin layer of Quaternary foraminiferal ooze there was some 25 m of middle Pliocene to upper Miocene biosiliceous sediment with only minor carbonate. The remainder of the Neogene consisted of alternating calcareous nannofossil oozes and diatom-bearing nannofossil oozes, the former dominant in the lower Neogene. The Oligocene to Cretaceous part of the section consisted almost entirely of nannofossil ooze and chalk. In Hole 690C we recovered a possibly complete K/T boundary section.

All depths referred to are depths below seafloor, and samples are from the core catcher unless otherwise specified. On the summary biostratigraphic correlation chart (Fig. 36), the age or biostratigraphic zone assigned to a given core catcher is extrapolated to the midpoint of the overlying and underlying core. The section is described from the top down.

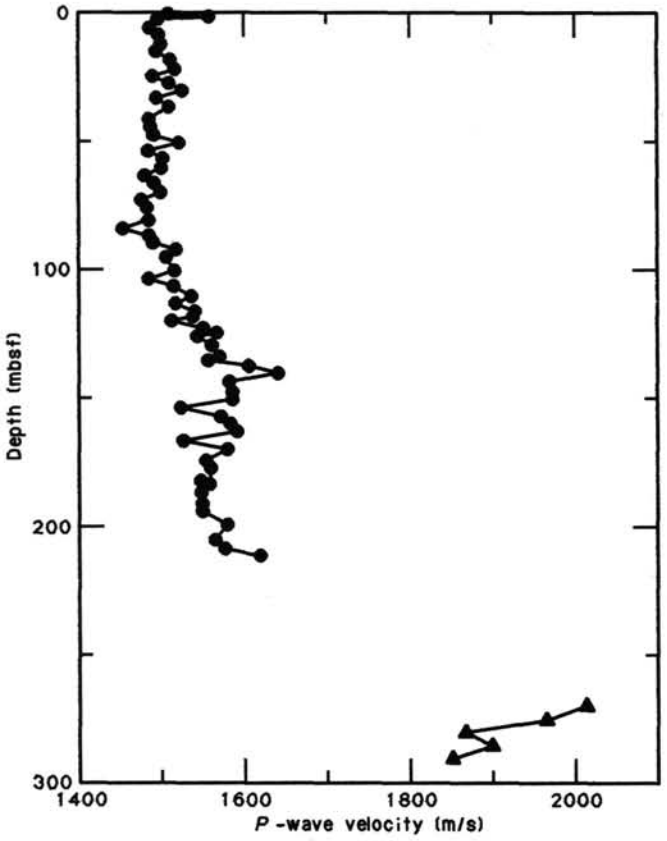

Figure 28. Compressional wave velocity profile (Hamilton Frame), Holes 690B (dots) and 690C (triangles).

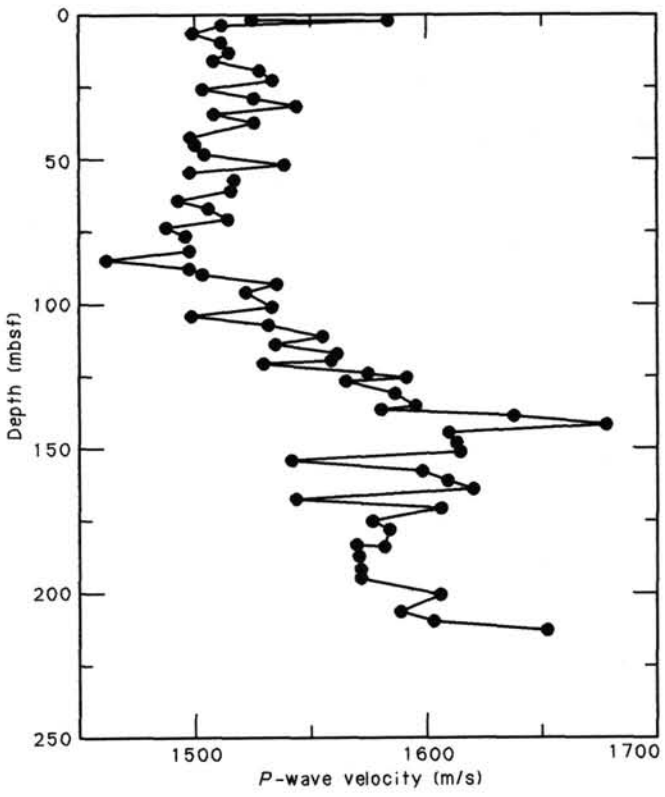

Figure 29. Compressional wave velocity profile (Hamilton Frame) for upper 200 m, Hole 690.

lated to the midpoint of the overlying and underlying core. The section is described from the top down.

Planktonic Foraminifers

Planktonic foraminifers were examined from each core catcher and several additional samples from each core from Holes 690B and 690C in order to identify the major stratigraphic boundaries.

In general, the planktonic foraminiferal assemblages at this site are similar to those of Site 689. Differences occur where dissolution has altered the assemblage or where a hiatus exists at one of the sites. Preservation of planktonic foraminifers varies considerably downsection in both holes. Preservation is good in the Quaternary but relatively poor through the Neogene. Fluctuating preservation is particularly evident in the lower Miocene. Planktonic foraminifers are well preserved in the uppermost lower Miocene in Hole 690B, but poorly preserved in the lowermost Miocene where the effects of dissolution are pronounced. Preservation continues to be moderate through the Oligocene and is good from Eocene through Upper Cretaceous.

The abundance of planktonic foraminifers varies considerably downsection. The Quaternary is marked by abundant planktonic foraminifers, whereas the Pliocene to lower Miocene contains few planktonic foraminifers. Abundances are notably lower in the Neogene at Site 690 than at Site 689. Apparently dissolution has effectively removed much of the upper Neogene planktonic foraminiferal record at Site 690. The uppermost lower Miocene contains abundant planktonic foraminifers, but the lower Miocene, marked by pronounced dissolution, contains only a few dissolution-resistent forms such as *Catapsydrax unicavus*. Abundances increase considerably in the Eocene and continue to be high through the Upper Cretaceous.

Quaternary

A layer of Quaternary planktonic foraminiferal ooze occurs at the top of Holes 690B and 690C. This layer consists almost entirely of *Neogloboquadrina pachyderma*. *Globigerinita glutinata* is rare in Section 113-690C-1H, CC.

Neogene

Except for rare occurrences, planktonic foraminifers are absent from the Pliocene and upper Miocene. By contrast, the lower Miocene in Section 113-690B-5H, CC, contains abundant cool temperate species including *Globorotalia zealandica*, *Globorotalia miozea*, *Globigerina woodi*, and *Globigerina connecta*. Less common are *Globigerina brazieri* and *Catapsydrax* spp. The incursion of these temperate species into the Southern Ocean seems to coincide with a period of warmth indicated by lower $\delta^{18}O$ values at several DSDP sites (Shackleton and Kennett, 1975; Savin et al., 1975; Savin et al., 1981; Hodell and Kennett, 1985) as well as by biogeographic data (Haq, 1980; Woodruff, 1985). This supports previous suggestions that the early Miocene was a period of global warmth. It should be noted, however, that diatom biostratigraphy places this sample in the lower middle Miocene.

It is not possible to place the Miocene/Oligocene boundary on planktonic foraminiferal evidence, because Cores 113-690B-6H and -7H are marked by increased dissolution that has resulted in disproportionate numbers of resistant and long-ranging species such as *Catapsydrax unicavus* and *Globorotaloides suteri*. The extensive dissolution also precludes any estimate of diversity trends. The lower Miocene assemblages observed in Section 113-690B-5H, CC, however, do reflect a brief interval of increased diversity similar to that seen in the lower Miocene at the Subantarctic and cool temperate latitudes (Jenkins, 1975; Jenkins and Srinivasan, 1985).

Table 6. Compressional wave velocities measured on Hamilton Frame of samples from Site 690.

Core, section, top (cm)	Depth (mbsf)	Velocity (m/s)
113-690A-		
1H-2, 90	0.9	1583
1H-4, 90	5.3	1538
1H-6, 87	8.8	1513
1H-7, 57	9.8	1515
113-690B-		
1H-1, 90	0.9	1524
1H-2, 20	1.7	1581
2H-2, 90	3.0	1511
2H-4, 90	6.0	1499
2H-6, 90	9.0	1511
3H-2, 90	12.6	1514
3H-4, 90	15.6	1508
3H-6, 90	18.6	1527
4H-1, 89	22.3	1533
4H-3, 89	25.3	1503
4H-5, 88	28.3	1525
5H-1, 88	31.0	1543
5H-3, 89	34.0	1508
5H-5, 89	37.0	1525
6H-1, 89	41.9	1498
6H-3, 90	44.9	1500
6H-5, 89	47.9	1504
7H-1, 89	51.3	1538
7H-3, 89	54.3	1498
7H-5, 89	57.3	1517
8H-1, 89	61.0	1515
8H-3, 89	64.0	1493
8H-5, 89	67.0	1506
9H-1, 89	70.7	1514
9H-3, 90	73.7	1488
9H-5, 88	76.7	1496
10H-2, 90	81.8	1498
10H-4, 90	84.8	1463
10H-6, 90	87.8	1498
11H-1, 90	90.0	1504
11H-3, 90	93.0	1535
11H-5, 90	96.0	1522
12H-2, 90	101.2	1533
12H-4, 85	104.2	1499
12H-6, 90	107.2	1532
113-690B-		
13H-2, 90	110.9	1555
13H-4, 90	113.9	1535
13H-6, 90	116.9	1561
14H-1, 90	119.1	1559
14H-2, 90	120.6	1530
14H-4, 90	123.6	1574
14H-5, 90	125.1	1591
14H-6, 90	126.6	1565
15H-2, 90	130.2	1586
15H-5, 90	134.7	1595
15H-6, 90	136.2	1580
16H-1, 91	138.4	1637
16H-3, 90	141.4	1676
16H-5, 90	144.4	1609
17H-1, 90	148.1	1613
17H-3, 90	151.1	1614
17H-5, 90	154.1	1542
18H-1, 90	157.8	1598
18H-3, 90	160.8	1609
18H-5, 90	163.8	1620
19H-1, 90	167.5	1544
19H-3, 90	170.5	1606
20H-1, 90	174.9	1577
20H-3, 90	177.9	1584
21H-2, 90	183.9	1582
21H-4, 10	183.1	1570
22H-2, 90	187.3	1571
23H-2, 90	191.8	1572
23H-4, 90	194.8	1572
24H-2, 93	200.3	1606
25H-2, 90	206.3	1589
25H-4, 90	209.3	1603
25H-6, 90	212.3	1652
113-690C-		
17X-7, 2	271.6	2103
18X-4, 68	277.0	2048
19X-1, 40	281.9	1937
19X-4,105	287.1	1973
20X-1, 34	291.6	1918

Paleogene

Section 113-690B-8H,CC, contains common *Chiloguembelina cubensis*. In the Atlantic, *C. cubensis* became extinct between 29.5 and 30.5 Ma (Hess and Stott, 1987, unpublished data) and its last appearance datum (LAD) is used to mark the top of the lower Oligocene (Berggren et al., 1985). The lower Oligocene assemblages are low in diversity (between three and five species) and similar in composition to those at Site 689. *Subbotina angiporoides*, *C. cubensis*, and *Globorotaloides suteri* are the dominant species. The last appearance of *Globigerinatheka index* is observed in Sample 113-690B-11H-4, 35–39 cm, and is used to mark the Oligocene/Eocene boundary. Diatom evidence and calcareous nannofossils suggest that there is a short hiatus between the lower Oligocene and uppermost Eocene. Such a hiatus is not readily evident in the planktonic foraminiferal record, although *Subbotina brevis*, a species that ranges briefly across this boundary at Site 689, was not observed in samples examined from Hole 690B. In addition to *G. index*, the upper Eocene assemblages contain abundant *S. angiporoides* and *C. cubensis*, with fewer numbers of *Subbotina linaperta* and *Subbotina eocaena*.

The boundary between the upper and middle Eocene is placed at a distinct faunal change in Sample 113-690B-12H-2, 110–114 cm, marked by the last appearance of several *Acarinina* species including *Acarinina coalingensis* and *Acarinina aculeata*. Species richness increases notably at this level, from an average of 6 species in the upper Eocene to an average of more than 13 species in the middle Eocene. Placement of the upper/middle Eocene boundary at this level means that the upper Eocene in Hole 690B is condensed within a short interval between the base of Core 113-690B-11H and the upper portion of Core 113-690B-12H.

The boundary between the middle and lower Eocene is difficult to identify owing to the absence of zonal index species and presence of only relatively long ranging species. At Site 690 the boundary is approximated within a broad interval marked by the first appearances of *S. eocaena* and *Acarinina pentacamerata* and the last appearance of *Acarinina soldadoensis* within Core 113-690B-13H. The diversity of lower Eocene assemblages appears similar to that of the middle Eocene, ranging from 10 to 15 species.

The morozovellid species used to delineate the lower Eocene and upper Paleocene biozones in the low latitudes are not present in Leg 113 sites. The boundary between the lower Eocene and upper Paleocene (P6a/P6b) is alternatively placed at the first evolutionary appearance of *Pseudohastigerina wilcoxensis*. In Hole 690B the evolutionary transition leading from *Planorotalites chapmani* to *P. wilcoxensis* (characterized by the gradual migration of the aperture to a completely marginal position) occurs within Section 113-690B-15H-3, with *P. wilcoxensis* present in Sample 113-690B-15H-2, 36–40 cm. Placement of the boundary at this level does not agree, however, with calcareous nannofossil data (see "Calcareous Nannofossils" discussion below) that would place the boundary near the top of Core 113-690B-17H at the first appearance of *Tribrachiatus bramlettei*. Nonetheless, few continuous deep-sea sequences exist where the first appearance of *P. wilcoxensis* and *T. bramlettei* have been well documented. The expanded nature of the upper Paleocene at Hole 690B, due in part to an abundant admixture of clay (see "Lithostratigraphy" section, this chapter) may highlight a stratigraphic offset between these two datum levels that has not previously been recognized.

The expanded nature of the Paleocene at Site 690 also allows identification of a number of distinct biostratigraphic horizons that could not easily be recognized in the condensed and somewhat fragmented Paleocene sequence in Hole 689B. Cores 113-690B-15X through -19X contain diverse assemblages (12–14 species) which are dominated by *Subbotina patagonica*, *Subbotina triangularis*, *Turborotalia reissi*, *Planorotalites planoconica*, and *Planorotalites australiformis* as well as several *Acarinina* and small *Morozovella* species. Common to abundant *Planorotalites pseudomenardii* occur in Cores 113-690B-17H and -18H. In lower latitude sequences the total range of this form is usually used to delineate the top and bottom of Zone P4, a relatively long zone according to the chronology of Berggren et al. (1985). It appears that the total range of this form at high latitudes is shortened and can be used only to approximate Zone P4. Of particular interest, however, is the presence within this interval at Hole 690B of *Morozovella convexa* and *Morozovella djanensis*, small forms whose occurrence on the Falkland Plateau during the late Paleocene occurred during a period of increased marine temperatures. In this warm period, marked by low $\delta^{18}O$ values, the morozovellids expanded their biogeographic range into higher latitudes (Boersma and Premoli-Silva, 1983). The same marine conditions seem to be recorded in Hole 690B, thus extending the apparent influence of warm boundary currents well into the Antarctic Ocean.

A dramatic drop in diversity occurs in Core 113-690B-20X. From this level to the base of Hole 690B the assemblages are dominated by *Subbotina* spp. These include *Subbotina triloculinoides*, *Subbotina patagonica*, *Subbotina triangularis*, and *Sub-*

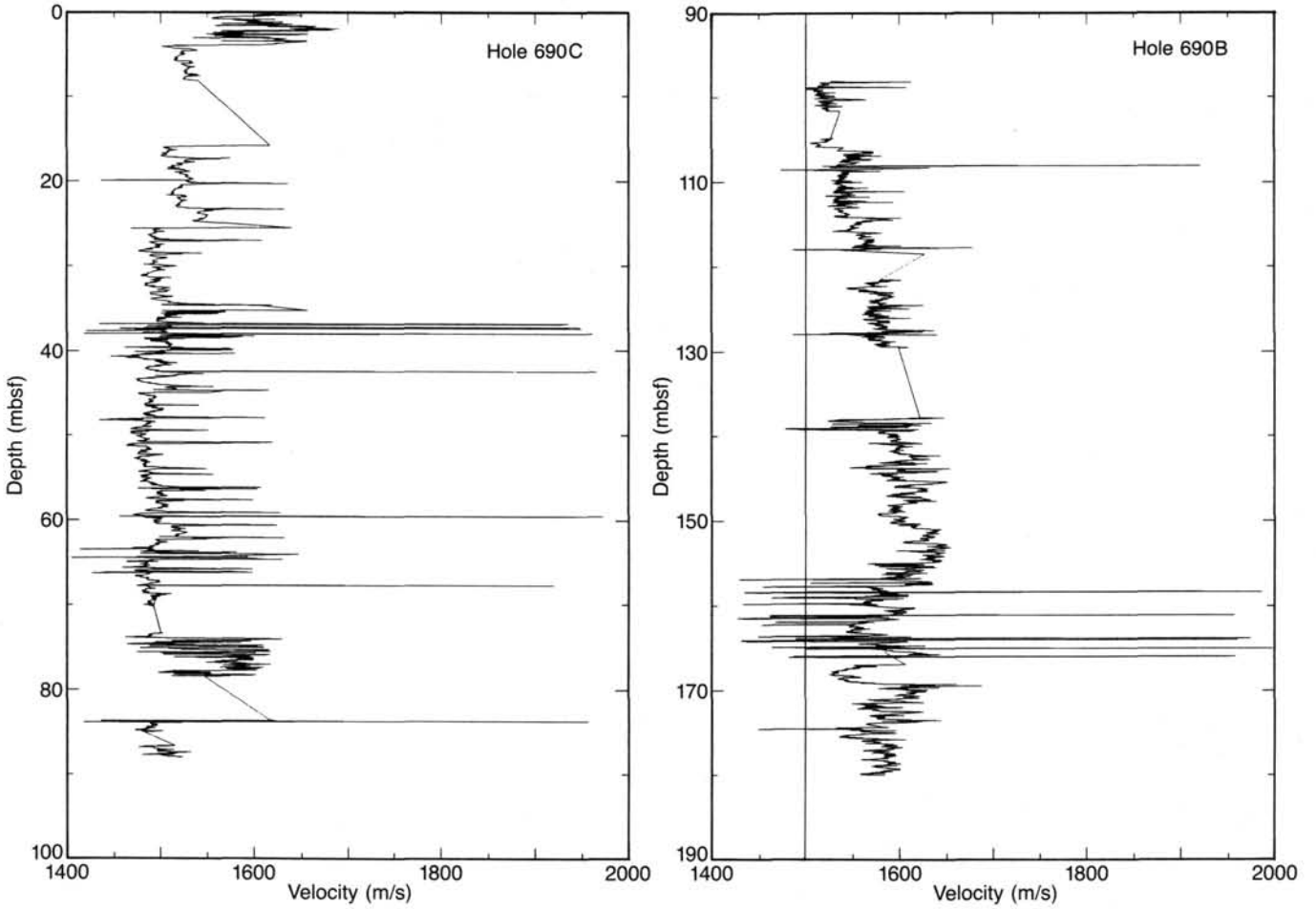

Figure 30. Compressional wave velocity profile (PWL) for upper 180 m, Hole 690.

botina varianta. *Planorotalites* spp. form a small component in Cores 113-690B-24X and -25X. These include *Planorotalites imitata* and *Planorotalites compressa*. Boersma and Premoli-Silva (1983) noted a similar diversity pattern at middle latitude sites in the Atlantic Ocean in Zone P3 and continuing into Zone P4. They also noted an increase in $\delta^{13}C$ isotopic values in the lower part of Zone P4 following a gradual increase through the lower Paleocene. They suggested that the increased carbon isotope values resulted from increased productivity and fertility in the ocean, a pattern that seems to coincide with the beginning of increased diversification of planktonic foraminifers during the late Paleocene. However, very few data have previously been available for this interval from the South Atlantic, particularly from Zone P3 which is often marked by increased dissolution. Preliminary evidence from Hole 690B suggests that the interval extending from Cores 113-690B-20H to -25X and 113-690C-11X is approximately equivalent to Zones P3 and P4. Few *Acarinina* species occur in this interval, although those that do occur, such as *Acarinina mckannai* and *Acarinina chasconona* are consistently present. *Acarinina spiralis*, a species with a range restricted to Zones P2 and lower P3, was observed only in Core 113-690C-11X.

It may be possible to recognize the P3/P2 zonal boundary in Site 690 on the basis of the last appearance of *Morozovella inconstans* in Sample 113-690C-13X-2, 38–42 cm, slightly above the last appearance of *Globoconusa daubjergensis* at Sample 113-690C-13X-4, 36–40 cm. The last appearance of *G. daubjergensis* is used to mark the P1c/P2 boundary. The short interval between this datum level and the last appearance of *M. inconstans* approximates the extent of Zone P2. Calcareous nannofossil data (see "Calcareous Nannofossils" discussion below) suggests the existence of a hiatus near the LAD of *M. inconstans*, which could explain the apparent brevity of Zone P2 in Site 690.

The P1c/P1b boundary is placed at the first appearance of *Morozovella trinidadensis* which is observed at Sample 113-690C-15X-6, 36–40 cm. Zone P1b extends down to at least Sample 113-690C-15X-4, 8–10 cm, where *Subbotina pseudobulloides*, *Chiloguembelina*, and *Subbotina eobulloides* are the conspicuous components of the planktonic foraminiferal assemblage. The first appearance of *Subbotina fringa* is slightly above this within Section 113-690C-15X-3. At present, the P1a/P1b boundary is extrapolated to a position midway between Sample 113-690C-15-5, 8–10 cm, and the position of the K/T boundary at Sample 113-690C-15X-4, 48–50 cm, identified on calcareous nannofossil evidence. Section 113-690C-15X-4 is characterized by extensive bioturbation, and more detailed sampling and analysis are needed to accurately characterize the assemblages in this interval and identify the P1b/P1a boundary.

The boundary between the Tertiary and Cretaceous occurs at Sample 113-690C-15X-4, 48–50 cm, across a distinct color change in the sediment (see "Lithostratigraphy" section and "Calcareous Nannofossils" discussion, this chapter) based on calcareous nannofossil evidence. Sample 113-690C-15X-5, 4–7 cm, taken from the lighter sediments just below the color change, contains a diverse assemblage of Upper Cretaceous

Table 7. Undrained shear strength measured on samples from Site 690.

Core, section top (cm)	Depth (mbsf)	Shear strength (kPa)	Core, section top (cm)	Depth (mbsf)	Shear strength (kPa)
113-690A-			113-690B-		
1H-4, 83	5.3	24.5	12H-6, 84	107.2	66.4
1H-6, 130	8.8	95.6	13H-2, 84	110.9	59.4
			13H-4, 84	113.9	80.4
113-690B-			13H-6, 84	116.9	84.0
			14H-1, 84	119.1	81.6
1H-2, 20	1.7	16.3	14H-2, 84	120.6	91.0
2H-2, 84	3.0	21.0	14H-3, 84	122.1	129.4
2H-4, 84	6.0	56.0	14H-4, 84	123.6	87.4
2H-6, 84	9.0	26.8	14H-5, 84	124.1	119.0
3H-2, 84	12.6	14.0	14H-6, 84	126.6	100.3
3H-4, 84	15.6	56.0	15H-2, 83	130.2	96.8
3H-6, 84	18.6	54.8	15H-5, 83	130.7	130.6
4H-1, 83	22.3	23.3	15H-6, 83	136.2	61.8
4H-3, 85	25.3	17.5	16H-1, 83	138.4	136.4
4H-5, 84	28.3	10.5	16H-3, 84	141.4	138.8
5H-1, 84	31.0	10.5	16H-5, 85	144.4	73.4
5H-3, 84	34.0	30.3	17H-1, 85	148.1	105.0
5H-5, 84	37.0	47.8	17H-3, 85	151.1	112.0
6H-1, 86	41.9	31.5	17H-5, 85	154.1	148.1
6H-3, 85	44.9	23.3	18H-1, 85	157.8	144.6
6H-5, 86	47.9	43.1	18H-3, 85	160.8	160.9
7H-1, 85	51.3	61.5	18H-5, 85	163.8	82.8
7H-3, 84	54.3	21.0	19H-1, 85	167.5	23.3
7H-5, 85	57.3	24.5	19H-3, 85	170.5	186.6
8H-1, 85	61.0	31.5	20H-1, 85	174.9	92.1
8H-3, 85	64.0	57.1	20H-3, 85	177.9	115.4
8H-5, 85	67.0	47.8	21H-2, 85	183.9	68.8
9H-1, 85	70.7	57.1	21H-4, 7	183.1	93.3
9H-3, 95	73.7	51.3	22H-2, 84	187.3	66.5
9H-5, 60	76.7	37.3	22H-4, 84	190.3	94.5
10H-2, 84	81.8	59.4	23H-2, 84	191.8	49.0
10H-4, 84	84.8	57.1	23H-4, 84	194.8	63.0
10H-6, 84	87.8	89.0	24H-2, 84	200.3	82.8
11H-1, 84	90.0	49.0	24H-4, 84	203.3	64.1
11H-3, 84	93.0	71.1	25H-2, 90	206.3	84.0
11H-5, 84	96.0	86.3	25H-4, 90	209.3	52.5
12H-2, 84	101.2	111.9	25H-6, 90	212.3	135.5
12H-4, 84	104.2	74.6			

planktonic foraminifers including *Abathomphalus mayaroensis*. Because of the severe bioturbation through this interval, the precise location of the P1a Zone/*Abathomphalus mayaroensis* Zone boundary will require detailed analysis of the planktonic foraminiferal assemblages.

Cretaceous

The Cretaceous planktonic foraminiferal assemblages from Hole 690C are similar to assemblages observed in Hole 689B. These assemblages exhibit low diversity (a maximum of 17 species) and are dominated by simple globigerine morphotypes. The upper Maestrichtian *Abathomphalus mayaroensis* Zone is recognized from Sample 113-690C-18X-5, 46–49 cm, through Sample 113-690C-15X-5, 4–7 cm. This interval also yields the keeled forms *Abathomphalus intermedius*, *Rugotruncana circumnodifer*, and *Globotruncana arca*. *Abathomphalus intermedius* occurs without *A. mayaroensis* in Sample 113-690C-19X-1, 19–123 cm, indicating a late middle Maestrichtian age for this sample. Keeled planktonic forms are rare below Section 113-690C-19X-5 to the bottom of the hole. The dominant simple globigerine taxa include *Heterohelix* spp., *Globigerinelloides multispinatus*, *Hedbergella monmouthensis*, and ?*Rugoglobigerina* n. sp. The unusual acarininid-like forms found in the Maestrichtian of Hole 689B also occur in low to moderate abundances in Hole 690C, ranging from Sample 113-690C-22X-2, 118–122 through Sample 113-690C-17X-3, 119–123 cm. This confirms at least a local distribution for this unusual taxon in the Maestrichtian of Maud Rise.

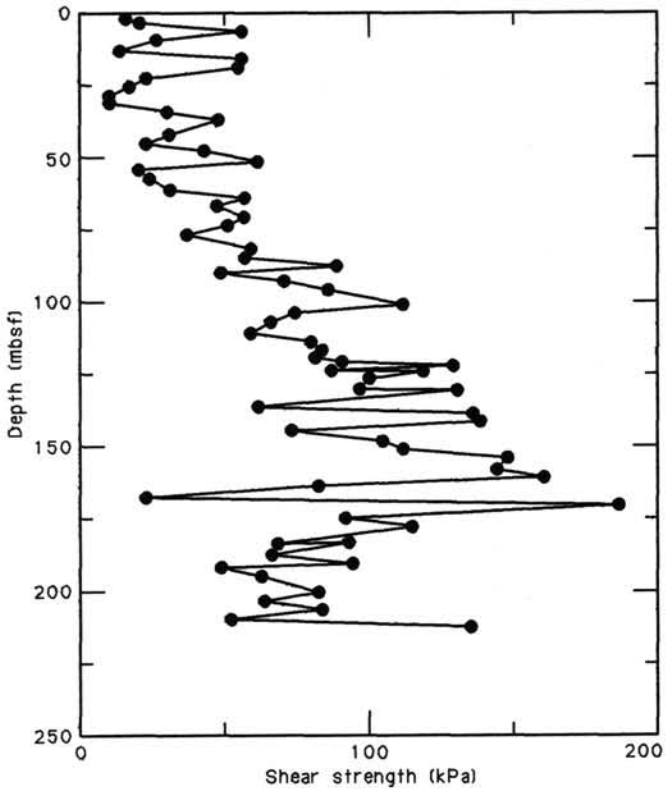

Figure 31. Undrained shear strength profile of Hole 690B.

The lowermost sediments of Hole 690C are probably coeval with the oldest sediments recovered in Hole 689B based on correlation of the last appearance of *Globigerinelloides impensus*. This form ranges from Sample 113-690C-22X-4, 118–122 cm, through Sample 113-690C-22X-1, 118–122 cm. This interval is considered to be no younger than early Maestrichtian and no older than late Campanian, based on correlation with its last occurrence at Falkland Plateau Hole 327A, where it was dated as late Campanian by Sliter (1977) and late Campanian-early Maestrichtian by Krasheninnikov and Basov (1983).

The Upper Cretaceous planktonic foraminifers recovered from Maud Rise are typical of the extratropical Austral Province. Diversity is low, keeled morphotypes are rare (with the exception of the *Abathomphalus mayaroensis* Zone assemblages) and simple globigerine forms dominate. Several species are endemic to the Austral Province. Prior to Leg 113, *Rugotruncana circum-*

Table 8. Thermal conductivity measured on samples from Site 690.

Core, section, top (cm)	Depth (mbsf)	K (W/m-K)
4H-5, 50	27.9	1.007
5H-3, 90	34.0	1.106
6H-3, 90	44.9	1.111
7H-3, 89	54.3	1.387
8H-3, 89	64.0	1.166
9H-3, 90	73.7	1.225
10H-3, 90	83.3	1.374
11H-3, 90	93.0	1.310
12H-3, 90	102.7	1.349
13H-3, 90	112.4	1.531
14H-3, 90	122.1	1.558
15H-3, 90	131.7	1.611

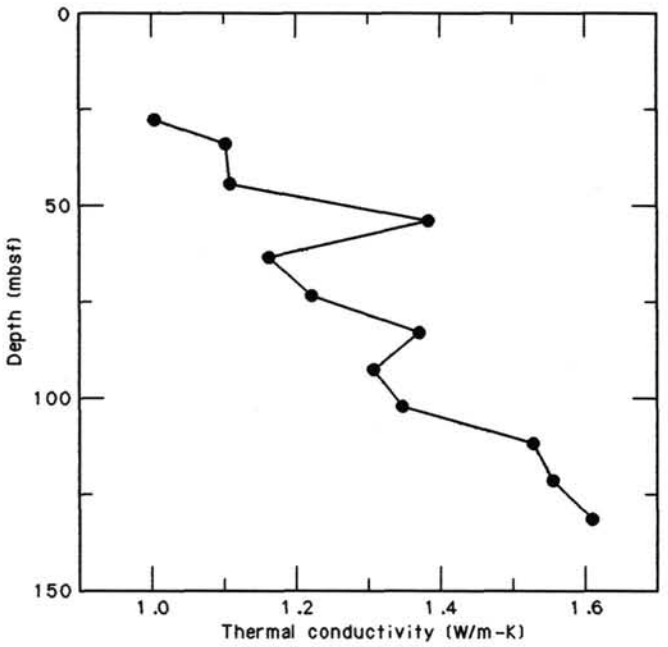

Figure 32. Thermal conductivity profile of Hole 690B.

nodifer was only reported from New Zealand, the Lord Howe Rise (DSDP Hole 208) and a single specimen from Seymour Island, Antarctic Peninsula (Huber, in press). The occurrence at Maud Rise of *Globigerinelloides impensus* is the first known outside the Falkland Plateau. Specimens designated as *Rugoglobigerina* n. sp. are common in the Campanian-lower Maestrichtian of Falkland Plateau Holes 327A and 511, Seymour Island, and Maud Rise, but have not been reported elsewhere. The spinose acarininid-like forms have not been reported away from Maud Rise, and thus may have had only a local distribution. The coherence of the Austral Province assemblage indicates that there was communication, perhaps via trans-Antarctic passages, between the southern southwest Pacific and the southernmost South Atlantic. The significant occurrence of keeled zonal taxa in the upper Maestrichtian may be interpreted as resulting from penetration of warm water into the high latitudes, or adaptation of the keeled planktonic species to the high-latitude environment. Oxygen isotopic analyses of the planktonic foraminiferal tests should characterize variations in the thermal history of the surface waters through the Upper Cretaceous sequences.

Benthic Foraminifers

Benthic foraminifers were studied in a mud-line sample, all core-catcher samples from Hole 690B and from Hole 690C below the washed interval (Sections 113-690C-11X, CC, through -22X, CC). Additional samples were studied from intervals where the benthic foraminiferal assemblages show major changes. Samples from Core 113-690B-3H are barren of benthic foraminifera, and Section 113-690B-2H, CC, contains only 13 specimens (probably derived from the higher sediments by burrowing). Another interval barren of benthic foraminifers extends from Sample 113-690B-5H-2, 40–43 cm, through Sample 113-690B-5H-6, 40–43 cm. All other samples contain at least 200 specimens of benthic foraminifers. Benthic foraminifers are rare compared to planktonic microfossils in all samples. Preservation is good to moderate, except in the lowermost cores; no data are included on Cores 113-690C-21X and -22X because preservation did not allow recognition of most species. Samples from Cores 113-690B-11H and -12H show evidence of considerable reworking (variable preservation, presence of many broken and corroded specimens, presence of older specimens).

Relative abundances of species were determined in all samples (see "Explanatory Notes" chapter, this volume for methods). The benthic foraminiferal fauna in all samples studied is predominantly calcareous with only few species and specimens of agglutinated forms.

Depth estimates using Paleogene and older faunas are tenuous, but comparison of Site 690 faunas with faunas described from the South Atlantic (Tjalsma and Lohmann, 1983; Dailey, 1983; Van Morkhoven et al., 1986) leads to an estimate of upper abyssal for assemblages 1 through 6 (2500 m or deeper). Assemblages 7 and 8 may indicate middle to lower bathyal depths (1000–2500 m).

Study of the benthic foraminiferal faunas at the low time resolution presented here shows clearly that higher resolution studies are necessary for an understanding of the evolution of benthic foraminiferal faunas through the Cenozoic.

Benthic foraminiferal faunas at Site 690 were divided into eight assemblages: (1) the mud-line sample, Section 13-690B-1H, CC (Quaternary-Pliocene), and Samples 113-690B-4H-4, 40–43 cm, through -5H-1, 40–43 cm (upper Miocene, 26.31 through 31.53 mbsf); (2) Section 113-690B-5H, CC, through Sample 113-690B-11H-3, 40–43 cm, lower Miocene through Oligocene?, 40.78 through 92.51 mbsf); (3) Samples 113-690B-11H-4, 40–43 cm, through -12H-2, 40–43 cm (upper through middle? Eocene, 94.01 through 100.71 mbsf); (4) Samples 113-690B-12H-3, 40–43 cm, through -15H-4, 40–43 cm (middle Eocene, 102.21 through 133.01 mbsf); (5) Samples 113-690B-15H-5, 40–43 cm, through -19H-3, 40–43 cm (middle Eocene to uppermost Paleocene?, 134.51 through 170.31 mbsf); (6) Sample 113-690B-19H-4, 40–43 cm, through Section 113-690C-12X, CC (upper Paleocene, 171.81 through 218.06 mbsf); (7) Samples 113-690C-13X-1, 40–43 cm, through -18X-2, 40–43 cm (lower Paleocene-upper Maestrichtian, 224.01 through 273.31 mbsf); (8) Sections 113-690C-18X, CC, through -20X, CC (lower Maestrichtian, below 278.37 mbsf).

Assemblage 1 (Quaternary; upper to middle Miocene)

Assemblage 1 is a mostly calcareous fauna, dominated by *Epistominella exigua* (28%–41%), and with abundant *Fursenkoina* spp. and *Bolivina* spp. in some samples (see below). Other species present in samples from Core 113-690B-1H are *Eilohedra weddellensis, Melonis sphaeroides*, *Pullenia* spp., and *Oridorsalis* spp. Section 113-690B-4H, CC, contains 23% *Fursenkoina* spp., and *Oridorsalis* spp., *Gyroidinoides* spp., and *Pullenia* spp. are common. *Bolivina decussata* is abundant (29%) in Sample 113-690B-4H-4, 40–43 cm, and *Fursenkoina* spp. are abundant (31%) in Sample 113-690B-5H-1, 40–43 cm. The diversity is relatively low (about 30–41 species, average 34) compared with the diversity of Holocene deep-sea faunas in other areas (e.g., Douglas and Woodruff, 1981). The fauna differs from that in the upper samples at Site 689 by the greater relative abundance of *E. exigua* at Site 690 (6% at Site 689). This difference is probably caused by the greater depth at Site 690. There is a barren interval between samples with assemblage 1 and assemblage 2 (31.53 through 40.78 mbsf).

Assemblage 2 (lower Miocene-Oligocene?)

Assemblage 2 is characterized by the presence of common to abundant *Stilostomella* spp. (8%–31%) and *Nuttallides umbonifera* (5%–46%). The diversity is low (31–48 species, average 39), but somewhat higher than in assemblage 1. *Epistominella exigua* is common (2%–17%). Other common species are *Pullenia* spp. (2%–11%), *Cibicidoides mundulus* (6%–10%), *Oridorsalis* spp. (2%–14%), and *G. subglobosa* (2%–8%). *Bulimina alazanensis* is common (8%) in Section 113-690B-5H, CC.

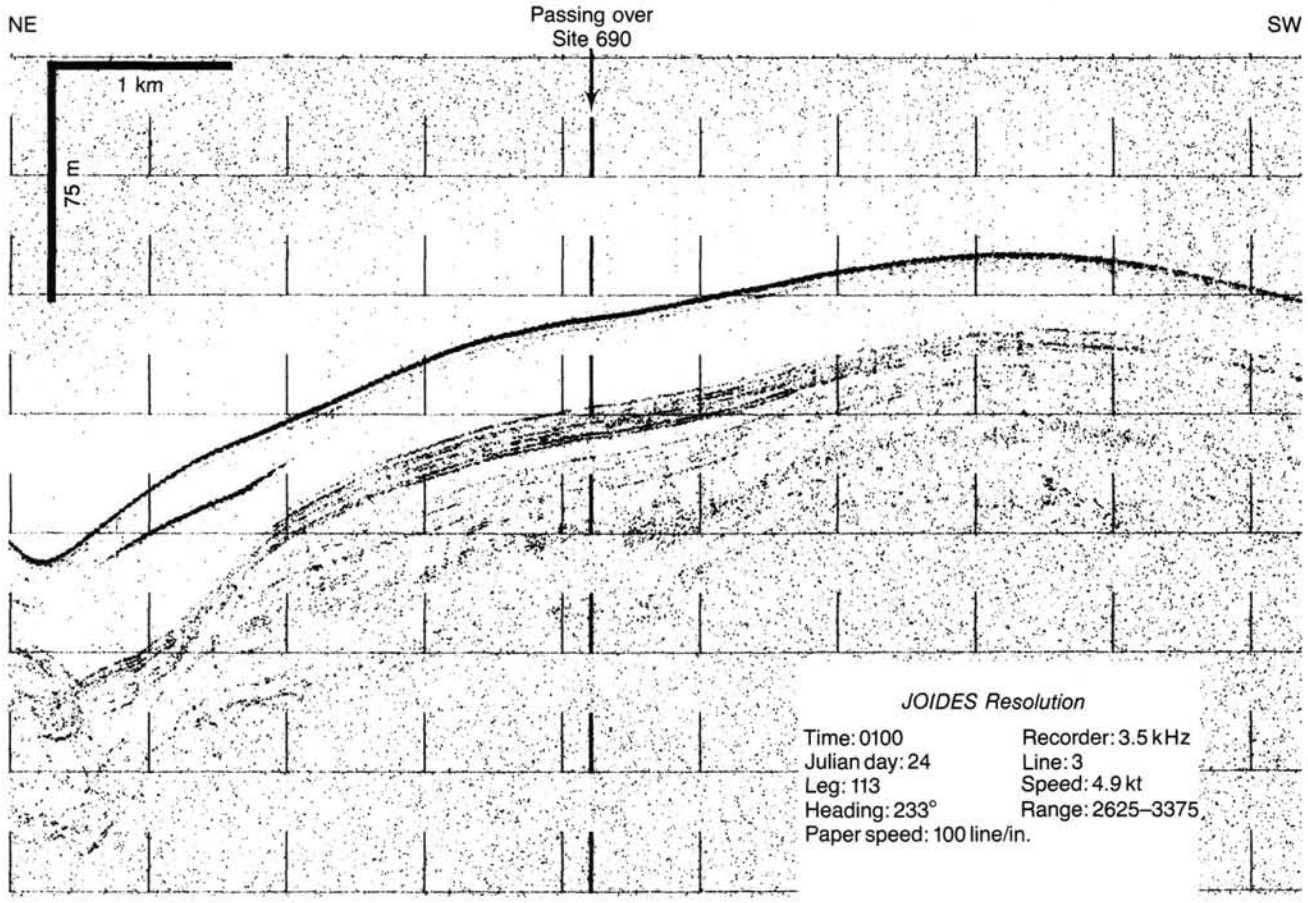

Figure 33. The 3.5-kHz profile obtained aboard *JOIDES Resolution* crossing Site 690 after departure (see also Fig. 35 and, for location, Fig. 1).

The co-occurrence of rare *Cibicidoides wuellerstorfi*, *Spiroplectammina spectabilis*, and *Vulvulina spinulosa* in Section 113-690B-5H, CC, suggests that the age of this sample is latest early Miocene (e.g., Thomas, 1985, 1987). *Turrilina alsatica* is abundant (10%–31% in Samples 113-690B-10H, CC, through -11H-3, 40–43 cm (89.10 through 92.51 mbsf). The lower boundary is taken above the LAD of *Bulimina elongata* which is abrupt (no gradual decrease in abundance; there is probably a hiatus at this boundary; see "Calcareous Nannofossils" discussion below.

Assemblage 3 (upper to middle? Eocene)

Assemblage 3 resembles assemblage 2 because it contains common to abundant (as much as 20%) *Stilostomella* spp. and as much as 14% *N. umbonifera*. Assemblage 3, however, contains common (as much as 4%) *Nuttallides truempyi* and up to 33% *Bulimina elongata*. This species is most abundant just below the boundary with assemblage 2; this suggests that there is a hiatus between the two assemblages at Site 690. The LAD of *N. truempyi* occurs in the same sample as the l.a. of *B. elongata* (113-690B-11H-4, 40–43 cm). The diversity is similar to that in assemblage 2 (31–42 species, average 37). The lower boundary was taken at the LAD of *Bulimina semicostata;* this species is very rare just below its LAD, and there is considerable reworking in Cores 113-690B-11H and -12H. Thus the location of this boundary is uncertain and might be lower than in Sample 113-690B-12H-3, 40–43 cm.

Assemblage 4 (middle Eocene)

This assemblage is characterized by the presence of *Bulimina semicostata* and *Siphogenerinoides eleganta*, and is a *Nuttallides truempyi* fauna, with the nominate species at 4%–22% (e.g, Tjalsma and Lohmann, 1983). Common species are *Bulimina semicostata* (as much as 22%), *Siphogenerinoides eleganta* (as much as 13%), *Stilostomella* spp. (10%–15%), and *Bolivina huneri* (2%–14%). Also present are *Bulimina simplex* (1%–3%) and *Bulimina trinitatensis* (1%–4%). The diversity is high (40–65 species, average 52). *Bulimina elongata* is present (as much as 16%) in the higher samples of the assemblage. *Pullenia* spp., *Oridorsalis* spp., and *Gyroidinoides* spp. are common accessory species (all 2%–8%). The lower boundary was taken at the f.a. (first appearance) of *B. semicostata*, an abrupt boundary at a change in lithology in Section 113-690B-15H-4.

Assemblage 5 (middle Eocene? through uppermost Paleocene?)

This assemblage is characterized by common *Tappanina selmensis* (1%–38%), *Siphogenerinoides brevispinosa* (1%–16%), *Bolivinoides* sp. aff. *decorata* (as much as 27%), *Bulimina simplex* (as much as 35%), and (in some samples) *Aragonia semireticulata* (as much as 15%). *Stilostomella* spp. are common to abundant (2%–46%), and *Nuttallides truempyi* is common in most samples (2%–15%). The diversity is lower than in assemblage 4 (32–48 species, average 38). The lower boundary was chosen at just above the l.a. of *Stensioina beccariiformis.* The faunal changes between assemblage 5 and assemblage 6 are the most important and most rapid changes at Site 690. At this boundary there are several l.a.'s (see below), and a strong decrease in diversity (66 species in Sample 113-690B-19H-4, 40–43 cm, to 36 species in Sample 113-690B-19H-3, 40–43 cm). The changes occurred at the same time as a major decrease in bulk

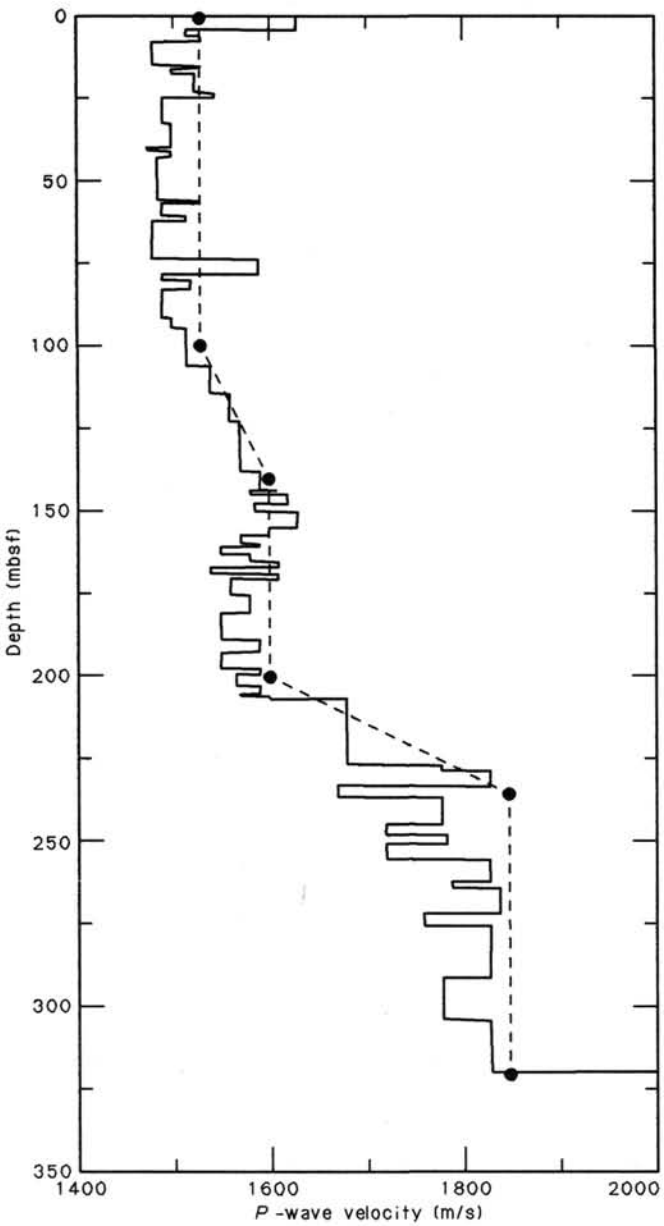

Figure 34. Velocities extracted from PWL records (solid line) of cores from Holes 690B and 690C, with the velocity model (dashed line with dots) used to relate downhole depth to two-way traveltime on the seismic records.

carbon isotope ratios (N. Shackleton, pers. comm., 1987), correlated with the Paleocene/Eocene boundary (e.g, Shackleton, 1986). At Site 690 the biostratigraphic Paleocene/Eocene boundary is difficult to locate, and data on calcareous nannofossils and planktonic foraminifers are not in mutual agreement and do not support the location of this boundary in Core 113-690B-19H. The l.a. of *S. beccariiformis* has been correlated with the top of Zone P5 (Tjalsma and Lohmann, 1983; Van Morkhoven et al., 1986); this would place the top of P5 in Core 113-690B-19H, in agreement with the calcareous nannofossil zonation, but not with the planktonic foraminiferal zonation.

Assemblage 6 (upper Paleocene)

This assemblage is characterized by the presence of *Stensioina beccariiformis* (2%–16%) together with *Bulimina thanetensis* (as much as 30%). *Bulimina midwayensis* is present in most samples (as much as 4%). *Stilostomella* spp. are common (4%–22%), as is *Nuttallides truempyi* (4%–16%). *Cibicidoides pseudoperlucidus* occurs in many samples (as much as 8%). *Pullenia* spp. and *Gyroidinoides* spp. are usually present (1%–5%). *Lenticulina* spp. and uniserial lagenids are common in most samples (on average 35 and 8%, respectively). Diversity is high (52–67 species, average 60). The upper boundary of this assemblage is placed at a sudden drop in diversity which occurs just above the sample with the l.a. of *S. beccariiformis* and *Neoeponides hillebrandti* (see above). The lower boundary is placed at the f.a. of *B. thanetensis.*

Assemblage 7 (lower Paleocene-upper Maestrichtian)

The assemblage is characterized by the presence of *S. beccariiformis* (4%–19%) together with *Osangularia navarroana* (1%–9%), in the absence of *B. thanetensis. Stilostomella* spp. are common (2%–13%), as is *N. truempyi* (8%–18%). Other common species are *Neoeponides hillebrandti* and *N. lunata* (1%–12%). *Gyroidinoides* spp. are common (as much as 10%), and diverse lagenids are present. The diversity is high (58–79 species, 66 average). The K/T boundary is between Samples 113-690C-15X-4, 40–43 cm, and 113-690B-15X, CC. *Stensioina beccariiformis* is less common (4%–5%) from Samples 113-690C-16X, CC, through 113-690C-15X-4, 40–43 cm (in contrast with the other samples in the assemblage, 11%–19%). *Eouvigerina gracilis* is present in all samples, but most common (as much as 5%) just after the K/T boundary. Several species have a last appearance just after the K/T boundary, but most of these do occur in Sample 113-690-15X-4, 40–43 cm (e.g., *Gyroidinoides quadrata, Globorotalites conicus, Alabamina creta*). There are less obvious changes in relative abundances at the K/T boundary at Site 690 than at this boundary at Site 689. The lower boundary of the assemblage is placed at the f.a. of *O. navarroana.*

Assemblage 8 (lower Maestrichtian)

The assemblage is characterized by the presence of abundant *Gyroidinoides* spp. (7%–26%, mainly *G. nitida, G. globosus, G. quadratus, G. subangulatus*, and *G. vortex*). *Stensioina* spp. are common (9%–22%), as are *Coryphostoma* spp. (as much as 15%), *Reussella szajnochae* (as much as 8%), *Praebulimina reussi* (as much as 8%), *Neoeponides hillebrandti* (as much as 8%), and *Nuttallides truempyi* (as much as 12%). Similar faunas have been described by Hemleben and Troester (1984) from the Rio Grande Rise, and Sliter (1977) and Basov and Krashninnikov (1983) from the Falkland Plateau. These authors differ on the details of the environmental interpretation, but in general decided on a depth of lower to middle bathyal (1000–2000 m). The ranges of Campanian-Maestrichtian benthic foraminifers are not well-defined, but comparison of the Site 690 fauna with the fauna at Site 516 (Dailey, 1983) suggests that the oldest sediment at Site 690 is lower Maestrichtian.

Comparison of Faunas at Sites 689 and 690

All assemblages can be recognized at the two sites, but relative abundances are different. For instance, *N. truempyi* is usually more common at Site 690 (the deeper site), whereas *S. beccariiformis* is usually more common at Site 689, in agreement with reported depth preferences of these species. In general, the buliminid species that dominate assemblages 4 and 5 at the two sites are relatively more abundant at Site 690. Generally, the diversity of each assemblage is higher at Site 690.

The assemblage boundaries appear to be coeval between the two Maud Rise sites (at the present resolution of data on calcareous nannofossils, see Fig. 37). Some apparent discrepancies between benthic foraminiferal correlation and nannofossil correlation occur in cores where the sedimentation rate is very low and reworking is common. This occurrence of coeval faunal changes

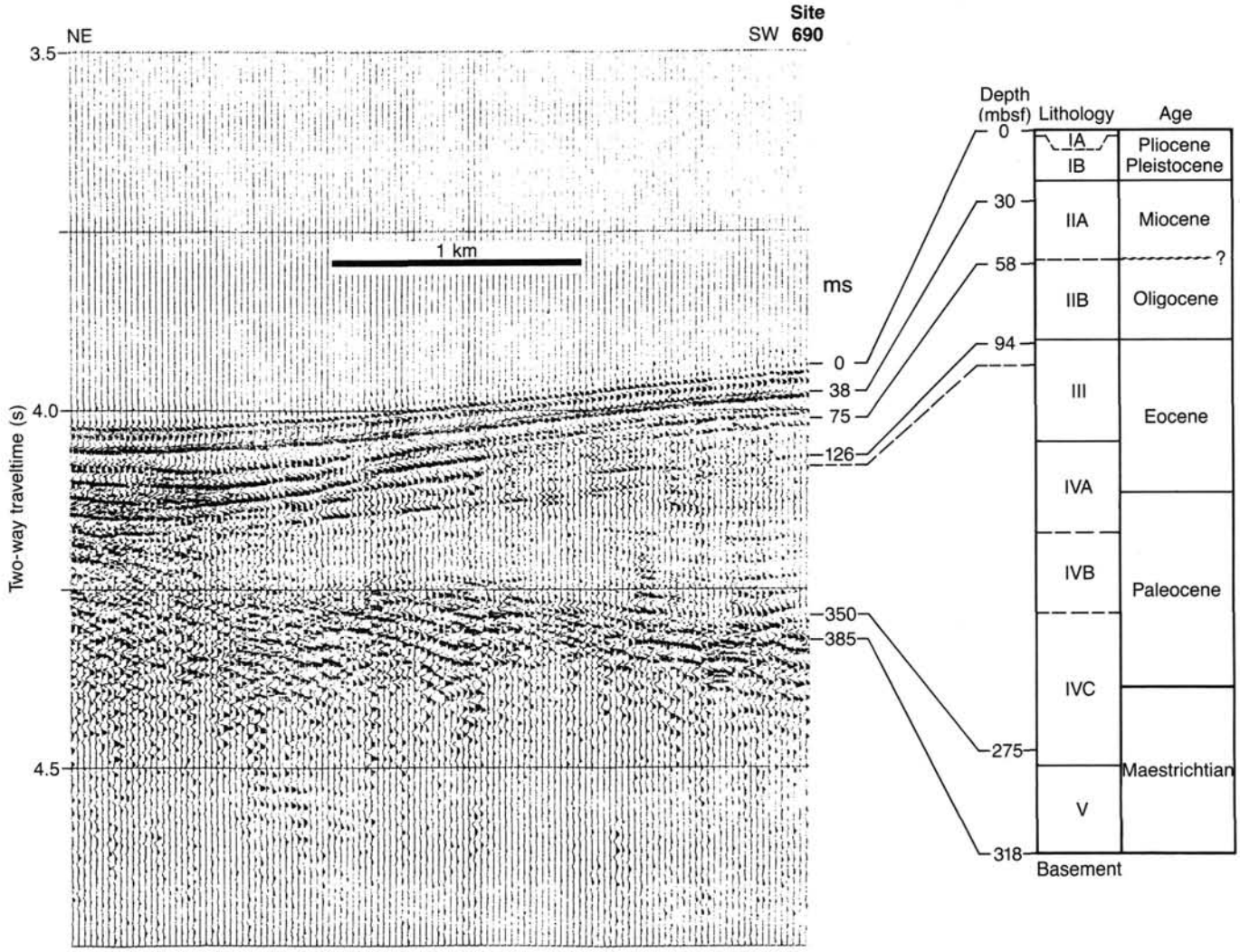

Figure 35. Section of water-gun profile (on left) acquired while crossing over Site 690 after departure, compared with cored section, using velocity-depth model of Figure 34. (See also the 3.5-kHz profile of Figs. 2 and 33 for comparison.)

at sites of different depth suggests that the environmental changes at these times were major. These times are: early to middle Maestrichtian (boundary *Biscutum magnum/Nephrolithus frequens* Zones; assemblage 7/8); early to late Paleocene (hiatus in CP4, assemblage 6/7); boundary Paleocene/Eocene or latest Paleocene (assemblage 5/6); end of the early Eocene (CP10, assemblage 4/5); the end of the middle Eocene (assemblage 3/4); the earliest Oligocene (assemblage 2/3); and the early to middle Miocene (barren interval between assemblage 2 and 1). The most severe changes occurred at the end of the Paleocene. At the K/T boundary the temporary changes in relative abundance were more severe at the shallower site than at the deeper site, and several species appeared to change their depth range toward shallower levels at this time for a short period only (e.g., *N. truempyi*). The duration of benthic foraminiferal assemblages was relatively long in the Maestrichtian and from the Oligocene to Holocene. The relatively short (several millions of years) duration of assemblages in the upper Paleocene through Eocene suggests that the structure of the deep-water masses of the oceans might have been less stable during this period than it was earlier and later.

Table 9. Main seismic reflectors at Site 690.

Two-way traveltime (ms)	Depth (mbsf)	Sediment age	Comments
27–37	20–28	Miocene/Pliocene	Density rise, top of nannofossil ooze (see 3.5-kHz profile).
(38)	(30)	Miocene	(Reflectors between these levels are truncated away from site; see 3.5-kHz profile).
(75)	(58)	Oligocene	
126	94	Eocene/Oligocene (boundary hiatus)	Underlying reflectors truncated at this level.
140	102–104	late Eocene	
350	275	Maestrichtian	Abrupt rise in clay and volcanic glass(?) in chalk/mudstones.
385	318	?(basement)	Strong irregular reflector.

These overall faunal changes need to be better defined, the timing needs to be related to carbon and oxygen isotopic events, and the variability within each assemblage must be better established. The record at Sites 689 and 690, however, appears to be excellent for evaluation of the development of deep waters during the Cenozoic.

Calcareous Nannofossils

Calcareous nannofossils are rare in the foraminiferal ooze of lithostratigraphic Subunit IA (Hole 690B), absent in the subjacent Pliocene diatomaceous ooze (Subunit IB), common to abun-

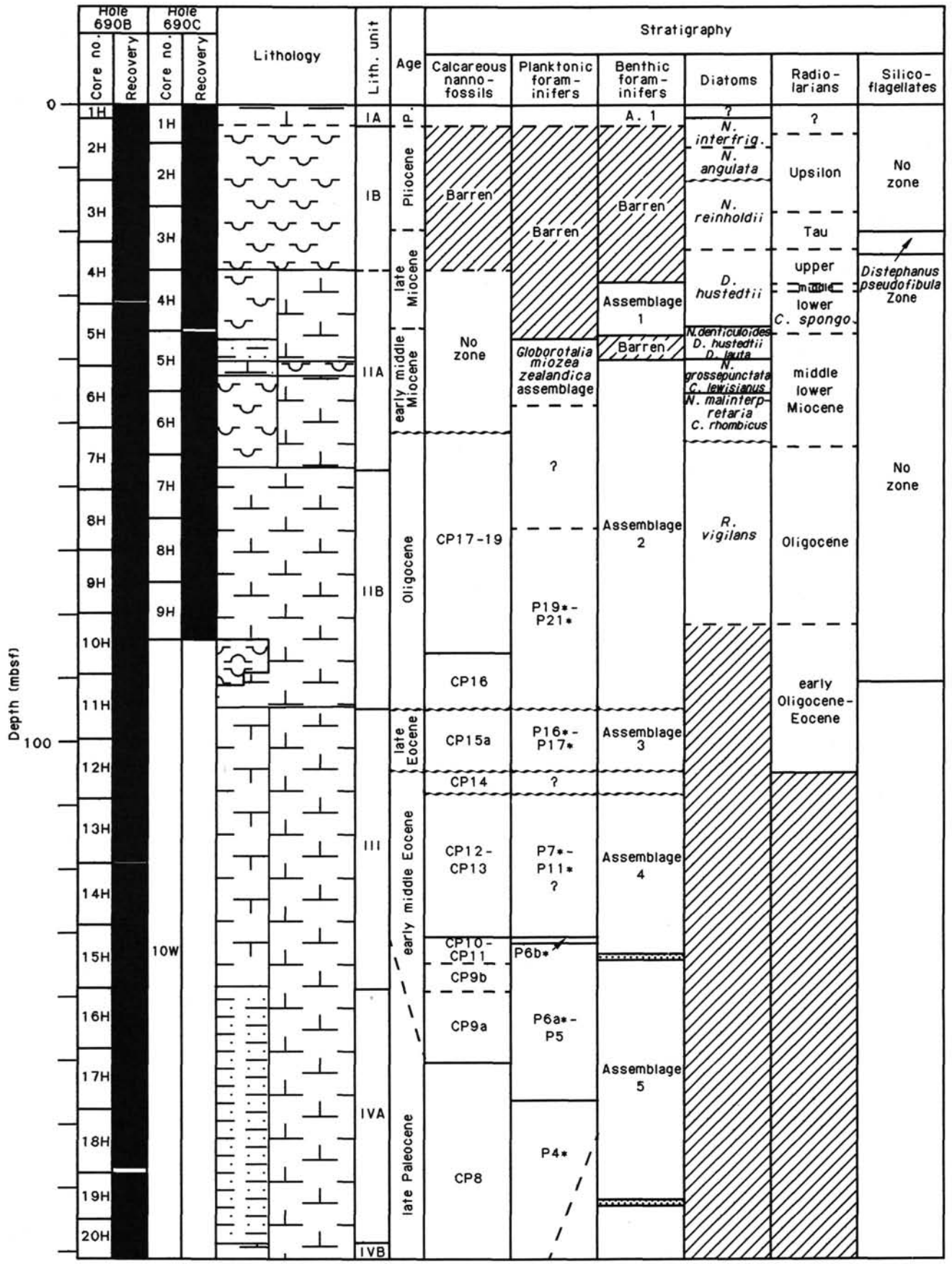

Figure 36. Summary biostratigraphic correlation chart, Site 690; * designates zonal equivalence.

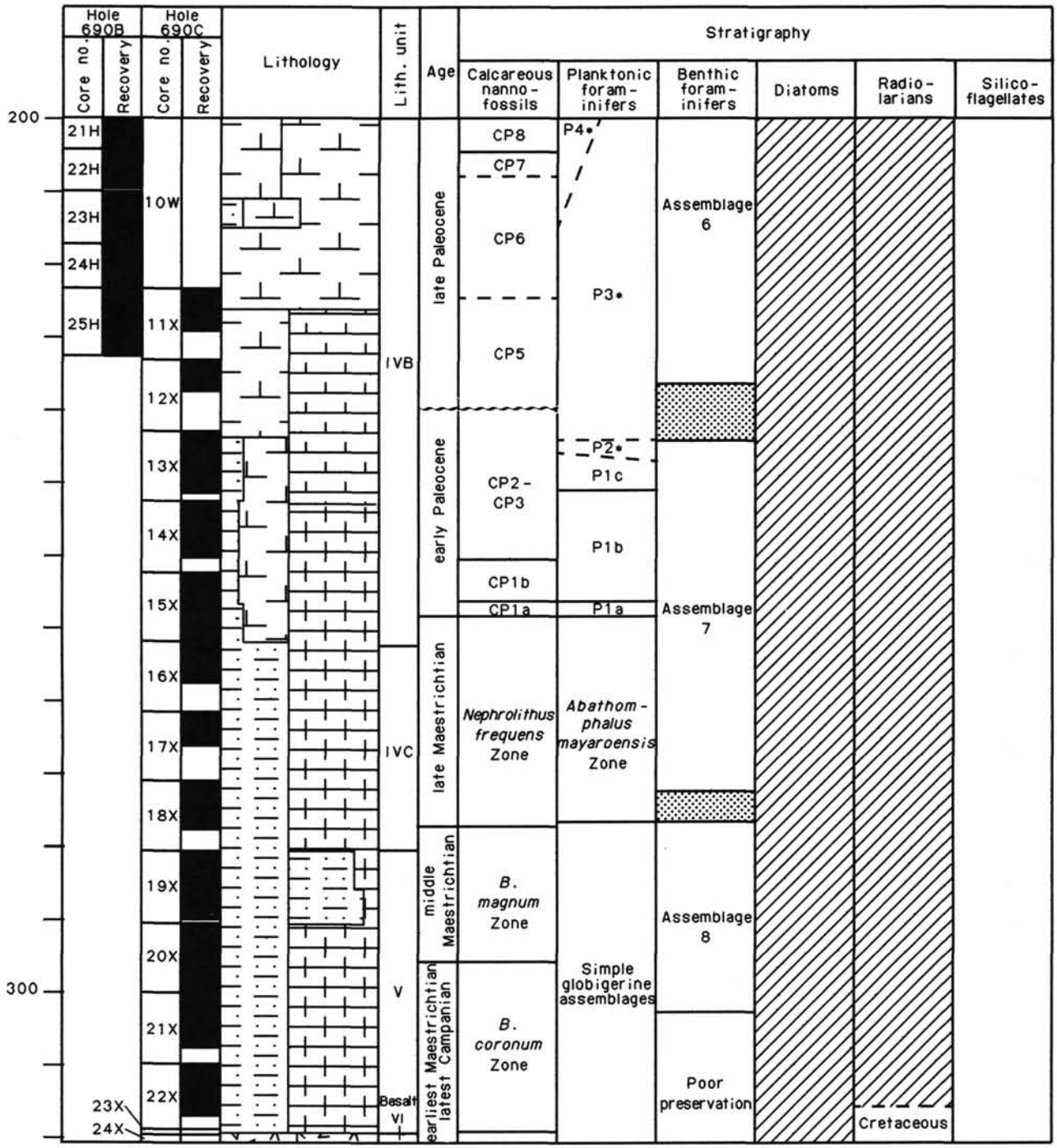

Figure 36 (continued).

dant at most levels in the Miocene below 24.3 mbsf, and abundant throughout the remainder of the section. Preservation is generally good in the Miocene and Oligocene, moderate in the middle Eocene, and moderate to good in the lower Eocene, Paleocene, and Upper Cretaceous through Core 113-690C-20X. Coccoliths in the lowermost two cores immediately above basement are poorly preserved, but preservation throughout the section is markedly better than at Site 689 due to the higher clay content at the present site, particularly in the Eocene-Cretaceous (lithostratigraphic Units IV and V).

The following is a description of nannofossils from a composite section drilled at this site; it covers Cores 113-690B-1H to -25H, plus Cores 113-690C-11X to -22X. Cores 113-690C-1H to -9H from the redundant APC hole at the top of the section are not discussed.

Neogene

The foraminiferal ooze at the top of the section (Core 113-690B-1H) contained rare *Pseudoemiliania lacunosa* and *Coccolithus pelagicus*. The latter specimens exhibited a central area

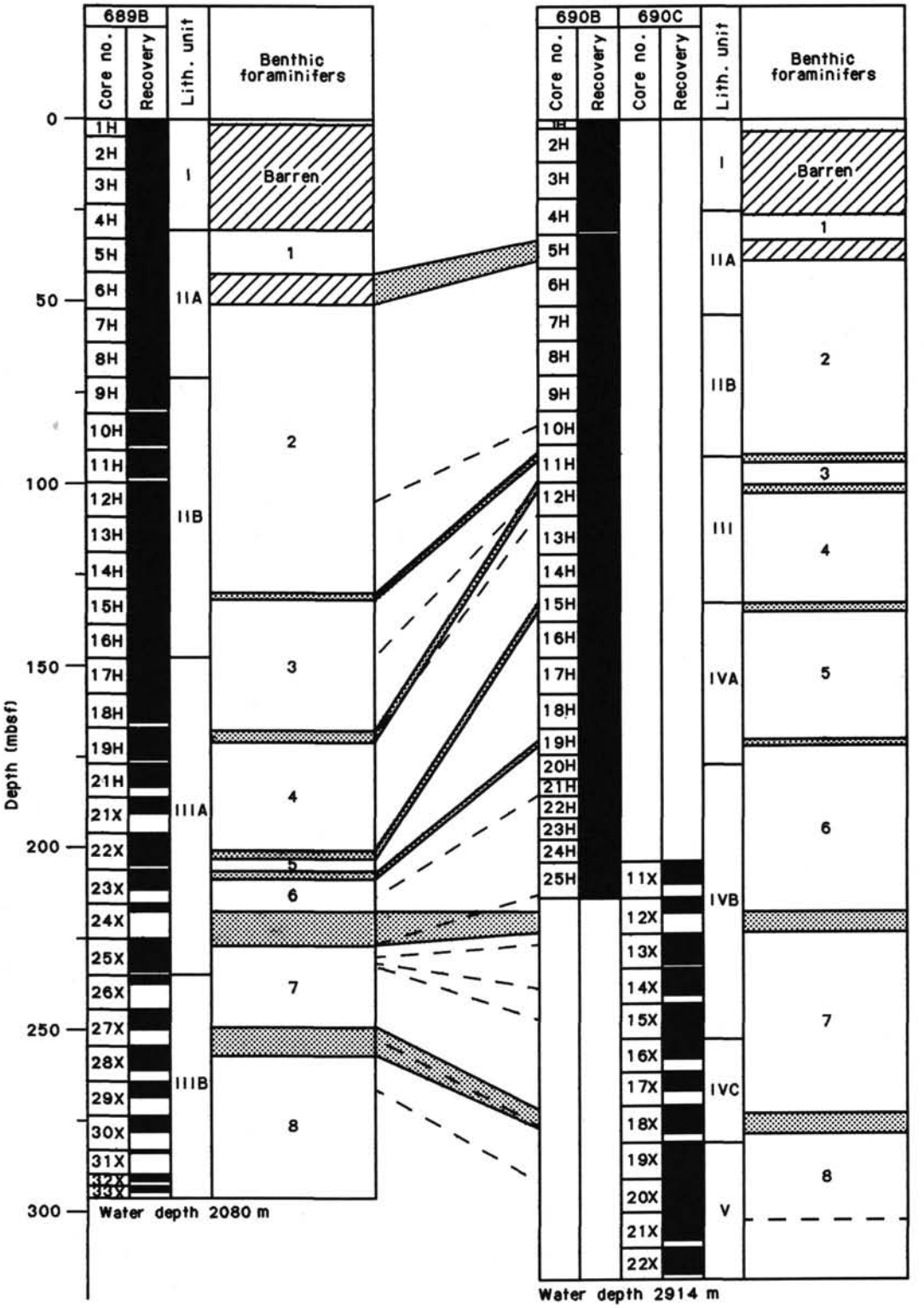

Figure 37. Benthic foraminiferal assemblages at Sites 689 and 690. Dense stippled pattern indicates uncertainty interval of boundary. Diagonal pattern indicates barren intervals.

bar, a feature characteristic of many Pleistocene representatives of the species. *Coccolithus pelagicus* is reported to have been absent from the Southern Hemisphere since about the middle Holocene, but persists today in the Northern Hemisphere where it has a temperature preference between 6° and 14°C (McIntyre and Bé, 1967). This suggests that at some time during the Pleistocene, interglacial conditions were sufficiently warm to allow this taxon to exist at this site. There are no records, however, of coccolithophorids living at this latitude today; and coccolithophorids are not present in the Pliocene sediments recovered at this site (Cores 113-690B-2H and -3H).

The highest occurrence of upper Miocene nannofossil ooze spans the interval from Cores 113-690B-4H-3 to 5H-3, and the assemblage is composed of over 99% *Reticulofenestra perplexa*

with *Coccolithus pelagicus* accounting for the remainder. The remainder of Core 113-690B-4H is barren except for the core-catcher sample, which consists of 100% *C. pelagicus* except for a few chiasmolith rims reworked from the Oligocene. This limited diversity accompanied by strong alternations in dominance among taxa is characteristic of Miocene sections at these latitudes. The number of reworked chiasmolith rims increases in Section 113-690B-6H, CC, where the bulk of the assemblages consists of strongly etched *C. pelagicus* among the diatomaceous sediments. A reworked specimen of *Reticulofenestra umbilica* (lower Oligocene) suggests the proximity of a disconformity, which is placed between Sections 113-690B-7H-1 and -2.

Paleogene

Below the hiatus in Core 113-690B-7H is a relatively pure, presumably upper Oligocene, nannofossil ooze, as indicated by very abundant *Chiasmolithus altus* (central area bars generally not preserved). Small reticulofenestrids (*Reticulofenestra daviesi*) are also very abundant, and *Coccolithus pelagicus* is few to rare, but consistently present. The assemblage in Core 113-690B-8H is similar except for the addition of few *Cyclicargolithus abisectus*. Diversity increases in Core 113-690B-9H, where *C. floridanus* is common, *C. abisectus* few, and the first downhole occurrence of *Reticulofenestra bisectus* (few) is noted. At DSDP Site 513 on the Falkland Plateau, *R. bisectus* ranged higher than *Chiasmolithus altus* in a section subject to strong dissolution and possible reworking (Wise, 1983). Compared to Site 513, the LAD's of these taxa appear in reverse order at the present site. The distribution of *R. bisecta* is sporadic in this section (W. Wei, oral comm., 1987). One must conclude, therefore, that *R. bisecta* cannot be used to mark the Oligocene/Miocene boundary at these high latitudes.

Reticulofenestra bisecta is common in portions of Core 113-690B-10H, which also contains the first *in-situ* downhole occurrences of *Reticulofenestra umbilica* and *R. hillae* (Sample 113-690B-10H-5, 26 cm). The LAD's of these taxa denote the top of nannofossil Subzone CP16c at lower latitudes (34.6 Ma). As at DSDP Site 513, the LAD of *R. umbilica* is nearly coincident with the FAD (first appearance datum) of *Cyclicargolithus abisectus*. The assemblage is little changed in Core 113-690B-11H, except that *C. floridanus* is abundant in selected samples.

Isthmolithus recurvus is common in Sections 113-690B-11H-2 and -3. Section 113-690B-11H-4 contains an upper Eocene assemblage with *Reticulofenestra reticulata*, which is assigned to Subzone CP15a. Thus most of the lower Oligocene *Blackites spinosus* Zone (including the interval with *Reticulofenestra oamaruensis* at Site 689) and all of the upper Eocene Zone 15b appear to be missing. A second disconformity representing a shorter time interval lies at a color change and scour mark in Sample 113-690B-12H-6, 48 cm (see Fig. 8). There appears to be considerable mixing of nannofossils across these two disconformities, but the presence of *R. umbilica* suggests that the interval between them can be assigned to Zones CP14 and CP15a.

Preservation improves and diversity increases downhole in Core 113-690B-14H where discoasters are noted for the first time in this section. Unfortunately, most of these are rare, nondescript seven-rayed forms which are not age-diagnostic. These do indicate, however, that warmer water conditions had persisted over Maud Rise until some time in the middle Eocene. Rare and poorly preserved *Discoaster sublodoensis* are present at least down to Section 113-690B-15H-1, and the FAD of *Discoaster lodoensis* is tentatively placed at Sample 113-690B-15H-5, 30 cm. The LAD of *Tribrachiatus orthostylus* (top of Martini's Zone NP12; Martini, 1971) is in the section immediately above. The base of Subzone CP9b is tentatively placed at Sample 113-690B-16H-1, 28 cm, where *T. contortus* is rare but clearly distinguishable (J. Pospichal, oral comm., 1987). *Tribrachiatus bramlettei* is also present (rare to common) through most of Subzone CP9a, and has been traced by Pospichal down to Sample 113-690B-17H-1, 130 cm. The presence of members of the genus *Tribrachiatus* at Site 690, far from a continental margin, indicates that the distribution of this form is limited by water depth rather than by an affinity for neritic environments, as is sometimes suggested.

The FAD of *Tribrachiatus bramlettei* marks the traditional nannofossil Eocene/Paleocene boundary and the top of CP8, the *Discoaster multiradiatus* Zone. *Discoaster multiradiatus* ranges in this section as high as the base of Core 113-690B-15H where it is rare to common. It is consistently common in Core 113-690B-17H where it is accompanied by *Hornibrookina australis* and fasciculiths. In Core 113-690B-19H, a complete assemblage of upper Paleocene taxa are present, including *Toweius eminens*, *H. australis, F. involutus, Prinsius bisulcus,* and *D. multiradiatus*. Most of these taxa, like *D. multiradiatus*, range a short distance into the basal Eocene. Apparently, the Eocene/Paleocene transition is quite expanded in this section, and the exact placement of that boundary might be adjusted with further study.

The *Discoaster multiradiatus* Zone (CP8) extends downsection through Core 113-690B-21H, below which a plexus of helioliths can be traced generally in small numbers to the bottom of the hole (Core 113-690B-25H; 213.4 mbsf; J. Pospichal, oral comm., 1987). *Heliolithus riedelii*, the originally proposed zonal marker for CP7, is present in Sample 113-690B-22H-2, 28 cm, and *H. universus* is abundant in the section below. In addition, Pospichal found a few *Discoaster mohleri* in Sample 113-690B-24H-2, 29 cm, which could extend Zone CP6 down at least to that level. *Heliolithus kleinpellii* is tentatively identified in Core 113-690B-25H, which places the basal core of the hole in Zone CP5.

Core 113-690C-11X from the slightly offset Hole 690C was taken between 204.2 and 213.9 m, in an effort to overlap coverage with Core 113-690B-25H. Unfortunately, only 5.53 m were recovered, and Core 113-690C-12X was highly disturbed when the liner shattered. Nevertheless, despite the potential problems with contamination, it appears that the desired overlap was achieved between the two holes in that *Heliolithus kleinpellii* and other helioliths are common in portions of Core 113-690C-12X, which is assigned to Zone CP5 (J. Pospichal, oral comm., 1987).

Core 113-690C-13X contains abundant *Chiasmolithus bidens, C. danicus*, few *Cruciplacolithus tenuis*, and can be assigned to the combined Zones CP3-CP2. As at Site 689, the *Fasciculithus tympaniformis* Zone (CP4) appears to be missing, and the disconformity is believed to lie between Cores 113-690C-12X and -13X. Zones CP2-CP3 cannot be further divided because *Ellipsolithus macellus* is not present at this site.

Chiasmolithus danicus can be traced at least down to Sample 113-690B-14X-3, 28 cm, and marks the base of Zone CP2. This interval contains *Hornibrookina teuriensis* (J. Pospichal, oral comm., 1987), *Cruciplacoliths edwardsii, C. tenuis,* and *C. primus*. The FAD of *C. tenuis* is placed below Sample 113-690C-15X-3, 151 cm, to mark the base of Subzone CP1b, and a CP1a Subzone is present at this site.

Cretaceous/Tertiary (K/T) Boundary

On the basis of a cursory shipboard study, the K/T boundary is placed between 48 and 50 cm in Section 113-690C-15X-4. As at Site 689, the boundary is approximately at a prominent color change between a white upper Maestrichtian (*Nephrolithus frequens* Zone) ooze below and a darker, clay-rich Danian unit above. At this site, however, the volcanogenic Danian sediments are brownish rather than greenish as at Site 689. In common

with Site 689, the boundary has been intensely bioturbated, but at the present site the sequence is considerably expanded. Thus it is possible to delineate a definite CP1a Subzone which lacks *Cruciplacolithus* (the *Markalius astroporus* Zone of authors). A strong *Zygodiscus sigmoides* acme accompanied by *Markalius inversus* is noted in Sample 113-690C-15X-4, 6–8 cm, well above the K/T contact. The presence of such an interval could not be established unambiguously at Site 689 due to the strong bioturbation of a more condensed sequence.

Zeolites, glass shards, and volcanic alteration products are also present in the smear slides of the brownish Danian material, thus it appears that at this site, as well as at Site 689, color can serve as guide to the presence of Danian coccolith assemblages. If so, then a visual inspection of the boundary shows Danian material distributed well below the inferred K/T contact, with Cretaceous material well above that level.

It is difficult to determine by visual inspection, however, if some of the Cretaceous chalky ooze inset within the Danian material may possibly represent clasts dislodged by erosion of the Maestrichtian strata. If that has been the case, then one might suspect that a portion of Zone CP1a may be missing. If, on the other hand, the Maestrichtian has not been eroded, and if the boundary has simply been distorted by intense bioturbation, then the original contact before bioturbation may have been as high in Section 113-690C-15X-4 as about 41–42 cm (for further analysis of the nature of this contact, see "Calcareous Nannofossils" discussion in "Site 689" chapter, this volume).

Upper Cretaceous

The upper Maestrichtian *Nephrolithus frequens* Zone corresponds roughly to lithostratigraphic Unit IVc, and extends from the K/T contact down through Sample 113-690C-18X-5, 36 cm (see "Introduction and Explanatory Notes" and "Site 689" chapters, this volume, for the zonal definitions and usage employed here). The presence of *N. frequens* rather than *N. corystus* has been determined by scanning electron microscopy (J. Pospichal, oral comm., 1987). Preservation near the top of the zone is good to moderate, but begins to deteriorate in Core 113-690C-17X. Preservation improves considerably, however, in Core 113-690C-18X due to an increase in clay content. The nannofossil flora in Core 113-690C-19X (lithostratigraphic Unit V) is essentially pristine, rivaling that of the Maestrichtian at DSDP Site 327 on the Falkland Plateau, where the sediment facies is very similar.

The interval from Section 113-690C-18X, CC, to Sample 113-690C-20X-2, 28 cm, is assigned to the *Biscutum magnum* Zone; the nominate species is abundant.

The remaining cores in this hole belong to the *Biscutum coronum* Zone; *B. coronum* are few, but are accompanied by *Monomarginatus* and related forms. The preservation changes downhole to moderate in Core 113-690C-21X, and core disturbance is considerable in the core-catcher samples (Paleocene contaminants are common). Sediment clasts and finely interbedded dark and light layers in the core suggest mixing by downslope processes.

The nannofossil assemblages from the basal sediment in the hole (Section 113-690C-22X, CC) are poorly preserved, strongly contaminated, and were essentially undatable aboard ship. It would seem from the previous core, however, that the hole bottomed near the Campanian/Maestrichtian boundary before entering basaltic basement.

On the whole, the sequence of nannofossil zones in the Upper Cretaceous section at this site is quite similar to that of Site 689. This suggests that the basal sediments may be of similar age at both sites. This cannot be demonstrated conclusively because basement could not be reached at Site 689 due to the presence of chert layers above basement.

Diatoms

Abundant, well-preserved diatoms are present in Pleistocene to upper Miocene sediment. Below the upper Miocene, diatom preservation gradually deteriorates with a concomitant drop in abundance and species diversity. No diatoms were observed in sediments older than Oligocene.

Hole 690A

Hole 690A was abandoned after recovery of the first core because the top was situated below the mud line. The top core contains few to common Quaternary diatoms. The co-occurrence of *Hemidiscus karstenii* and *Actinocyclus ingens* at this level indicate an interval in the uppermost *Coscinodiscus elliptopora/Actinocyclus ingens* Zone. Section 113-690A-1H, CC, belongs to the lower Pliocene *Nitzschia angulata* Zone. Diagnostic taxa in the well-preserved diatom assemblage include *Nitzschia praeinterfrigidaria*, *Cosmiodiscus intersectus*, and *Nitzschia angulata*.

Hole 690B

Section 113-690B-1H, CC, is a foraminiferal ooze with rare to few, poor to moderately well-preserved diatoms. The 41 m just below this level (Cores 113-690B-2H through -6H-1) contain, in general, common to abundant, moderate to well-preserved diatoms. Below this, the diatom component is diluted by biogenic carbonate (coccoliths), and the abundance drops off from few to rare until only traces of diatoms are encountered in Sections 113-690B-9H, CC, and -10H, CC. We also note dilution by coccoliths in the interval in Sections 113-690B-4H-3 through 113-690B-5H-2. In Sections 113-690B-11H, CC, to -13H, CC, we found zeolites, suggesting that biogenic silica had originally been deposited in these sediments but had subsequently been dissolved and reprecipitated.

Based on an additional investigation of smear slides taken in every section of Cores 113-690B-1H to -7H we can assign more accurate diatom zonal boundaries to the uppermost sediment interval. Core 113-690B-1H can be placed in the Pleistocene *Coscinodiscus elliptopora/Actinocyclus ingens* Zone. Prominent species are *Nitzschia kerguelensis*, *Eucampia balaustium* (= *E. antarctica*), *Actinocyclus ingens*, *A. actinochilus*, and *Thalassiosira lentiginosa*. Within Cores 113-690B-2H and -3H we found the middle and lower Pliocene *Nitzschia interfrigidaria* and *Nitzschia angulata* Zones (Sample 113-690B-2H-1, 15 cm, to 113-690B-2H-3, 28–29 cm, and 113-690B-2H-3, 28–29 cm, to 113-690B-3H-6, 28–29 cm, respectively). In addition to the nominate taxa, *Thalassiosira gracilis*, *Rhizosolenia barboi*, *Rouxia naviculoides*, *Cosmiodiscus intersectus*, and *Thalassiothrix longissima*, the latter of which dominates in the *N. interfrigidaria* Zone, are also present. We note a marked increase in *Ethmodiscus rex* fragments in the interval from Sample 113-690B-2H-5, 120 cm, to Sample 113-690B-2H-7, 27–28 cm. This occurs below the first appearance of *N. angulata*.

The first consistent occurrence of *Denticulopsis hustedtii* in Sample 113-690B-3H-6, 125 cm, identifies the top of the upper Miocene to lower Pliocene *D. hustedtii* Zone. Species belonging to the *Coscinodiscus marginatus* group are common to abundant in the upper part of this zone, whereas *Denticulopsis dimorpha* is common to abundant in its lower part (Sections 113-690B-4H-3 to 113-690B-5H-2). In addition, we found, particularly in the upper part of this zone, *Nitzschia januaria*, *N. donahuensis*, *N. claviceps*, and *N. efferans*. These forms may be useful in further dividing the long *D. hustedtii* Zone. Similarly, abundance changes in *Denticulopsis dimorpha* may be used to refine the resolution within the lower part of this zone.

The underlying *Denticulopsis hustedtii/D. lauta* and *Nitzschia denticuloides* Zones occur between Section 113-690B-5H-1

and Sample 113-690B-5H-6, 28–29 cm. In addition to the nominate taxa, these zones are characterized by an increase in abundance of *Denticulopsis praedimorpha*. The *Nitzschia grossepunctata* and *Coscinodiscus lewisianus* Zones extend down to Sample 113-690B-6H-3, 28–29 cm. Within the interval of these latter middle Miocene zones falls the f.a. of *Denticulopsis hustedtii* (Sample 113-690B-5H-7, 28–29 cm) and the l.a. of *Rhaphidodiscus marylandicus* (Sample 113-690B-6H-2, 28–29 cm). Common to abundant members of the *Actinocyclus ingens* group were also encountered. As in the Miocene sediments of Site 689 we did not find *Coscinodiscus lewisianus* in this site.

The *Nitzschia malinterpretaria* and *Coscinodiscus rhombicus* Zones (upper middle to middle lower Miocene) can be placed within Sample 113-690B-6H-3, 28–29 cm, through an interval between Samples 113-690B-6H-7, 28–29 cm, and 113-690B-7H-1, 28–29 cm. In addition to *Nitzschia malinterpretaria*, *N. pusilla*, and *N. efferans*, the assemblage within these zones is dominated by *Thalassiosira spinosa* and *T. spinosa* var. *aspinosa*, which are indicative of lower Miocene. Below Section 113-690B-7H-1 the sediments contain few diatoms. Prominent species are *Rocella gelida*, which is found only in Section 113-690B-6H, CC, as well as *Rocella vigilans*, *Synedra jouseana*, and *Lisitzina ornata*. The occurrence of *R. vigilans* and *L. ornata* indicates the upper Oligocene. The absence of the indicator species for the lowermost Miocene (*Bogorovia veniamini*) and the occurrence of *Rocella vigilans* in Sample 113-690B-7H-1, 114–115 cm, suggests an unconformity spanning the lowermost Miocene to the uppermost Oligocene. Sections 113-690B-8H, CC, and -9H, CC, contain few to rare diatoms, indicating the upper Oligocene.

Hole 690C

The sequence of diatoms in Hole 690C is similar to Hole 690B. As in Hole 690B, we examined samples at closer spaced intervals (one to two samples per section). Biostratigraphic results can be summarized as follows:

Core 113-690C-1H top to -1H-3: *Thalassiosira lentiginosa* Zone, Quaternary;

Section 113-690C-1H-4: *Nitzschia interfrigidaria* Zone, middle Pliocene;

Sections 113-690C-1H-5 to -3H-3: *Nitzschia angulata—Nitzschia reinholdii* Zones, lower Pliocene;

Sections 113-690C-3H-4 to -4H-4: *Denticulopsis hustedtii* Zone, lowermost Pliocene to upper Miocene;

Sections 113-690C-4H-4 to -5H-3: *Denticulopsis hustedtii/D. lauta-Nitzschia denticuloides* Zones, upper to middle Miocene;

Section 113-690C-5H-3: top of *Nitzschia grossepunctata* Zone, lower middle Miocene;

Section 113-690C-5H, CC: boundary of *Nitzschia grossepunctata-Coscinodiscus lewisianus* Zones to *Nitzschia malinterpretaria-Coscinodiscus rhombicus* Zones, lowermost middle Miocene;

Section 113-690C-8H, CC, and 690C-9H, CC: Oligocene.

Summary

At Site 690 we recovered a well-preserved, more or less continuous, diatom stratigraphic record ranging from Quaternary to lower Miocene. Upper Oligocene diatoms are sparse and poorly preserved, and there are some indications of unconformities in the lower middle Miocene and at the Miocene/Oligocene boundary.

We noted that some discrepancy exists between the planktonic foraminiferal biostratigraphical age assignment at Core 113-690B-5H and that of the *N. grossepunctata* and *Coscinodiscus lewisianus* Zones. Planktonic foraminiferal evidence indicates an age of late early Miocene, whereas the diatom zones place this interval in the early middle Miocene.

Prominent abundance fluctuations occur in species such as *Denticulopsis praedimorpha*, *D. dimorpha*, the *Actinocyclus ingens* group, and the *Coscinodiscus marginatus* group in the Miocene, and *Thalassiothrix longissima* and *Ethmodiscus rex* in the Pliocene. These abundance fluctuations are certainly associated with surface-water paleoceanographic changes. Such processes are also apparent in the alternation of biogenic siliceous (mostly diatoms) and biogenic calcareous (mostly coccoliths) sediments in the middle and upper Miocene of Site 689. Quantitative analysis of Neogene diatom distribution tied to similar investigations on radiolarians and biogenic calcareous components and to isotopic, sedimentologic, and magnetostratigraphic studies should help provide detailed information about the paleoceanographic events which led up to the development of the modern Southern Ocean. Thus Site 690, along with Site 689, provides a very exciting opportunity for paleoceanographic investigations. (See comments on general stratigraphic problems with diatom biostratigraphic zonation in "Biostratigraphy" section, "Site 697" chapter, this volume.)

Radiolarians

Radiolarians are abundant and well preserved in Neogene sediments (upper 40 m), abundant but poorly preserved in the Oligocene (approximately 50-100 mbsf), and virtually absent below this level in both Holes 690B and 690C.

Radiolarian stratigraphy for each hole is based on examination of strewn slides prepared from core-catcher samples. The stratigraphic indicators found in each hole are as follows:

Section 113-690A-1H, CC, is dated as middle Pliocene (lower Upsilon Zone) based on the occurrence of common *Desmospyris spongiosa*, *Antarctissa ewingi, Eucyrtidium calvertense, Clathrocyclas bicornis, Helotholus vema*, and *Prunopyle titan*. Based on the diatoms, this sample is lower Pleistocene. Radiolarian stratigraphy for the Pliocene and Pleistocene of the Antarctic is based exclusively on LAD's, and thus cannot be used to distinguish a mixed Pliocene/Pleistocene assemblage from an unreworked Pliocene assemblage. This sample may therefore represent a reworked Pliocene sediment with some admixture of Pleistocene material.

Sections 113-690B-1H, CC, and -2H, CC, are also dated as middle Pliocene in age (lower Upsilon Zone). Rare reworked lower Pliocene and upper Miocene specimens were seen in Section 113-690B-1H, CC, including *Lychnocanium grande* and *Antarctissa conradae*.

Section 113-690B-3H, CC, is assigned to the upper *Cycladophora spongothorax* Zone, based on the common occurrence of *C. spongothorax*, *D. haysi*, *Eucyrtidium pseudoinflatum*, *A. conradae*, *P. hayesi*, *L. stigi*, and *S. universus*, together with rare specimens of *P. titan* and *C. bicornis*. Section 113-690B-4H, CC, is assigned to the lower part of the *C. spongothorax* Zone, based on the co-occurrence of the nominate species and *Actinomma tanyacantha*, and on the absence of upper *C. spongothorax* Zone indicators such as *E. pseudoinflatum*. All Hole 690B radiolarian assemblages in samples below Section 113-690B-4H, CC, are poorly preserved, and age assignments are questionable. Section 113-690B-5H, CC, contains *E. cienkowski*, *P. hayesi*, *E. calvertense*, *Sethoconus sp.* Chen (1975), *D. megalocephalis*, *Lithatractus timmsi*, *Amphistylus angelinus*, *C. tetrapera*, and one specimen of *S. dilli*. This assemblage, in the absence of *A. tanyacantha*, indicates the middle or lower Miocene. One specimen each of *C. spongothorax* and *D. spongiosa* was encountered as well, indicating minor contamination of the sample by younger material. Section 113-690B-6H, CC, is tentatively assigned to the lower Miocene based on the occurrence of *C. isopera*, *A. angelinus*, *P. hayesi*, *Lithomelissa stigi*, *C. semipolita*, *S. dilli* (one specimen), and *C. tetrapera* (also only one specimen).

Sections 113-690B-7H, CC, through -9H, CC, could not be assigned an age due to poor preservation. Sections 113-690B-10H, CC, and -11H, CC, however, had a sufficient number of stratigraphically useful specimens to assign them to the lower Oligocene or Eocene. Species include *Cyclampterium* sp. cf. *milowi*, *Arachnocalpsis* sp., *L. challengerae*, *C. semipolita*, and *P. decora*. All samples examined below this level are barren of Radiolaria.

At Hole 690C we recovered a sequence very similar to the upper nine cores of Hole 690B, although no evidence of reworking was detected in the 690C core-catcher samples. Radiolarians in Section 113-690C-1H, CC, include *D. spongiosa*, *E. calvertense*, *A. ewingi*, *H. vema*, *C. bicornis*, *S. universus*, and *P. c. trilobum*. No *P. titan* or *C. davisiana*(?) were seen even though the entire slide was scanned. This sample is assigned to the middle part of the Upsilon Zone (Gauss equivalent age interval, middle-upper Pliocene). Section 113-690C-2H CC, contains an unusually low-diversity assemblage of radiolarians, despite excellent preservation and an abundance of silicoflagellates (*Distephanus* sp.) and diatoms. The presence of *C. bicornis*, *E. calvertense*, *A. ewingi*, *A. strelkovi*, and *E. pseudoinflatum* indicates the lower Pliocene, while the absence of *D. spongiosa*, *H. vema*, and *L. grande* further constrains the age to between the top of the C3N-3 normal subchron and base of the C3N-1 normal subchron of the Gilbert Chron (upper Tau Zone). Section 113-690C-3H, CC, is assigned to the upper or middle part of the *C. spongothorax* Zone, based on the presence of *C. spongothorax*, *D. haysi*, *A. conradae*, *P. titan*, and *E. pseudoinflatum* (this last very rare).

Section 113-690C-4H, CC, is assigned to the *A. tanyacantha* Zone, based on the presence of *A. tanyacantha* and the absence of *C. spongothorax*, *C. g. golli*, or other lower or upper Miocene indicators. Section 113-690C-5H, CC, contains a typical lower middle or lower Miocene assemblage, including *E. punctatum*, *C. g. golli*, *C. g. regipileus*, *C. tetrapera*, *Sethoconus* sp. Chen (1975), *C. isopera*, *A. angelinus*, and *L. timmsi*. Radiolarians from Sections 113-690C-6H, CC, -7H, CC, and -8H, CC, indicate the Oligocene. Species include *C. semipolita*, *C. isopera*, *Cyclampterium* sp. cf. *milowi*, and *L. challengerae*. Section 113-690C-9H, CC, contains *Cyclampterium* sp. cf. *milowi*, *Sethoconus* sp. Chen (1975), and *P. decora* and is lower Oligocene to upper Eocene. All remaining core-catcher samples (i.e., below the washed interval) are barren of Radiolaria, with the exception of 113-690C-21H, CC, and -22H, CC, which contain poorly preserved radiolarians. These latter two samples could not be cleaned sufficiently to allow abundance estimates or taxonomic analyses to be made.

Discussion

At Site 690 we recovered a radiolarian stratigraphic record very similar to that recovered at Site 689. The same assemblages and preservation variations were observed in both sites. Site 690 samples, however, do not contain the well preserved lower Oligocene/upper Eocene and Upper Cretaceous assemblages recovered at Site 689. It was more difficult to extract Radiolaria from the lower Neogene sediments at Site 690, perhaps due to the higher clay content of the sediments. Site 690, like Site 689, contains an excellent Miocene and Pliocene radiolarian record for biostratigraphy and paleoceanographic analysis.

Silicoflagellates

The silicoflagellate stratigraphy at this site is similar to that of Site 689, except that abundances are low in the Oligocene, and the lowermost Oligocene is missing due to a hiatus. Missing are the *Mesocena apiculata* Subzone of the *Dictyocha deflandrei* Zone and the acme of *Naviculopsis trispinosa*, which was present near the bottom of the Oligocene section at Site 689.

Silicoflagellates are well represented in the Pliocene at Site 690, where silicoflagellate-diatom oozes are dominated by *Distephanus speculum* from Cores 113-690B-1H to -5H. The last appearance datum of *Distephanus boliviensis* is in Core 113-690B-7H, below which this taxon alternates in dominance with *D. speculum* downsection to Section 113-690B-3H-3. The *Distephanus pseudofibula* Zone spans Cores 113-690B-3H and -4H (Gilbert Chron in age according to Shaw and Ciesielski, 1983), and, as at Site 689, the nominative taxon is represented by an abundance of all three morphotypes of this plexus. Silicoflagellates are sparse below this interval, and the Miocene-Oligocene section is not zoned here.

Palynology

Smear slides of core-catcher samples of Leg 113, Site 690 are barren of sporomorphs, organic-walled dinocysts or other land-derived and marine organic particles. The organic chemical studies ("Organic Geochemistry" section, this chapter) confirm the paucity of organic matter.

Calcareous dinoflagellates (calcispherulids) of Maestrichtian age were found in core-catcher samples of the lower part of Hole 690C (113-690C-15X to -22X). Lithologically, all samples represent a foraminiferal and nannofossil ooze or chalk. Several different morphotypes represent distinct species, phenotypic variants of the same species or diagenetic alterations and changing environmental parameters. This problem is discussed in detail by Fütterer (1984). In the present report we use the taxonomic nomenclature of Bolli (1974).

The elongated, ovoidal *Pithonella krasheninnekova* is the most abundant species, with a range from lower Coniacian to the lowermost Paleocene (after Fütterer, 1984). The strictly spherical, two-layered *Pithonella globosa* is also common. Its range was considered to be from middle Maestrichtian to lower Paleocene by Fütterer (1984), and its lower range has now been extended to include the lower Maestrichtian. Both species were formerly described from DSDP sites on the Walvis Ridge, Southeastern Atlantic Ocean, Leg 74.

Summary

At Site 690 we sampled a 321-m section ranging from Quaternary to uppermost Campanian(?) and consisting of pure siliceous (Pliocene to uppermost Miocene) and calcareous (Eocene through Upper Cretaceous) oozes, with the transition between the two facies (upper Miocene through Oligocene) marked by a mixed siliceous/calcareous ooze. There was minor ice-rafted and other terrigenous detritus in the Neogene part of the section, whereas part of the Paleocene and Cretaceous sequence is marked by an increase in largely silt-sized particles, possibly of eolian origin or products of nepheloid deposition. The presence of Pliocene to upper Miocene siliceous oozes make this an excellent site (in combination with Site 689) for the study of upper Neogene diatom and radiolarian biostratigraphy and paleoceanography. Similarly, the recovery of upper Miocene through Upper Cretaceous calcareous oozes will allow us to establish a high-latitude reference section for stable isotopes and calcareous microfossils and nannofossils. In addition, the alternation of calcareous and diatom-bearing calcareous oozes in the middle and upper Miocene will provide a chronology for the transition from a predominately "Subantarctic" type facies to an "Antarctic" type facies during the middle to late Miocene.

Lithostratigraphic Unit I is divided into two subunits with the upper consisting largely of foraminiferal ooze of Quaternary age. Minor components include diatoms, radiolarians, and rare coccoliths. The lower subunit consists of a siliceous ooze ranging from uppermost Miocene to lower upper Pliocene. Diatoms dominate this part of the section, but radiolarians are also abundant and well preserved, and silicoflagellates (*Distephanus*

speculum, *D. boliviensis*, *D. plexus*) are important in at least one part of the section (lower Pliocene). An interval in the lower Pliocene (near the base of the diatom *N. angulata* Zone) has increased abundance of *Ethmodiscus rex* fragments.

An abundant, low-diversity, polar planktonic foraminiferal assemblage is present in the Quaternary, but the upper Miocene and Pliocene contain only a few dissolution-resistant forms. The Quaternary contains a relatively low-diversity, calcareous benthic foraminiferal assemblage, but the upper Miocene and Pliocene contain very few benthics. Therefore, zonation of the uppermost Miocene and Pliocene was dependent upon the biosiliceous component. The existing diatom zonation seem to be applicable, although originally determined on sediments from the Subantarctic region.

There is an obvious unconformity at 2.1 mbsf (Quaternary/lower upper Pliocene). In the upper Miocene (upper part of lithologic Subunit IIA) biosiliceous sediment and diatom-bearing nannofossil ooze alternate. The nannofossil asemblage has a low diversity; two species (*Reticulofenestra perplexa* and *Coccolithus pelagicus)* alternate in dominance. These species are characteristic of the upper Miocene at high southern latitudes. The foraminifers (benthic and planktonic) exhibit low diversity and are poorly preserved in the upper Miocene. The alternating biosiliceous and nannofossil facies may represent repeated passage of an oceanographic front over this site, with the diatom-bearing nannofossil ooze facies roughly equivalent to sediments beneath the present-day Subantarctic zone and the siliceous facies equivalent to sediments beneath the present-day Antarctic zone south of the Polar Front. This latter facies became the sole sediment type in the uppermost Miocene and Pliocene.

The lower part of lithologic Subunit IIA (lower Miocene to Oligocene) is marked by a gradual downhole reduction in the siliceous (diatom and radiolarian) component and a corresponding increase in the calcareous component. Radiolarian preservation is good through the middle Miocene. Below that it is poor although radiolarians were well preserved and abundant at some intervals. Similarly, diatom preservation becomes poor below the middle Miocene, although diatoms persist into the Oligocene and there are generally enough stratigraphic markers available to identify zones in the lower Miocene and Oligocene. The calcareous nannofossils are monospecific or near-monospecific assemblages, characterized by the high-latitude forms mentioned previously. They change to more temperate and diverse assemblages in the lowermost Miocene and Oligocene.

The planktonic foraminiferal faunas consisted of cool to temperate species in the lower Miocene, an interval characterized by lower $\delta^{18}O$ values at other sites. The lower Miocene benthic foraminiferal assemblages are somewhat more diverse than younger faunas.

Data from all planktonic fossil groups suggest the presence of a hiatus or interval with drastically reduced sedimentation rates across the Miocene/Oligocene boundary, at about 51 mbsf (top of Core 113-690B-7H).

The lower Oligocene to lower Eocene (lower part of lithologic Unit IIb to Unit III) is dominated by a nannofossil ooze with appreciable admixture of foraminifers and, in the lower Oligocene, minor biosiliceous components. Zeolites are present in the Eocene, indicating that biogenic silica has been dissolved and reprecipitated. Calcareous microfossils indicate one major and several smaller disconformities in Cores 113-690B-11H and -12H. There is a hiatus at the Oligocene/Eocene boundary (Section 113-690B-11H-4). There are only a few meters of upper Eocene sediments in the lower part of Core 113-690B-11H and the upper part of Core 113-690B-12H. There is considerable mixing, via bioturbation, of coccoliths across the unconformity, and considerable reworking of foraminifers within Core 113-690B-12H. Benthic foraminifers decrease in diversity upsection across the Eocene/Oligocene hiatus, and several buliminid species have their l.a. at this level.

The nannofossils increase in diversity in the lower Eocene where the first discoasters were encountered in the hole (Core 113-690B-14H). This occurrence of lower-latitude forms at this site allows us to use a restricted "standard" zonation in the lower Paleogene. Increased planktonic foraminiferal diversity and the occurrence of warmer-water forms makes it possible to subdivide the Oligocene and Eocene, with reservations, within the context of lower-latitude zonations. The Oligocene section contains a diverse assemblage of benthic foraminifers with abundant *Nuttallides umbonifera*, similar to that of Site 689. The character of the fauna may indicate the presence of a water mass corrosive to calcium carbonate.

The Eocene-Paleocene interval is subdivided into two lithologic units with Subunit IVA (middle Eocene to uppermost Paleocene) separated from Subunit IVB (Paleocene) on the basis of increased terrigenous content (as much as 15%) in the latter. Calcareous microfossil preservation and diversity are generally good through the Eocene and Paleocene. Determination of the location of the Paleocene/Eocene boundary is difficult because of discrepancies between calcareous nannofossils and planktonic foraminiferal age determinations (see "Sedimentation Rates" section, this chapter). The uppermost Paleocene belongs to the *Discoaster multiradiatus* Zone. Unit IVA contains a low-diversity benthic foraminiferal assemblage with common *Tappanina selmensis* and *Aragonia semireticulata*. A major change occurs in the benthic faunas between Sample 113-690B-19H-3, 41 cm, and Sample 113-690B-19H-4, 41 cm. Faunas in the latter sample and below contain common *Stensioina beccariiformis* and other "relict" Cretaceous specimens that became extinct at the end of the Paleocene (Tjalsma and Lohmann, 1983); the diversity drops considerably upsection. This is the most important benthic faunal change of the Cenozoic, and occurs below the Paleocene/Eocene boundary as defined by planktonic groups. Because of the absence of some key stratigraphic markers, a precise calcareous nannofossil zonation cannot be applied throughout the Paleocene. However, it does appear that a complete basal Danian sequence was cored.

The absence of some stratigraphic markers and indefinite ranges of others makes it difficult to assign precise zonal boundaries to the planktonic foraminifers. However, as with the calcareous nannofossils, the planktonic foraminiferal evidence indicates that the basal Danian is expanded and complete. Near the K/T boundary, planktonic foraminiferal preservation and diversity drop off sharply. This depauperate fauna contrasts with the benthic foraminiferal fauna, which remains diverse across the boundary. Benthic faunas have a lower diversity below the *N. frequens* Zone/*B. magnum* Zone boundary.

On the basis of calcareous microfossils, the Cretaceous/Tertiary boundary is placed at about 48–50 cm in Section 113-690C-15X-4. The boundary is marked by a prominent color change between white, upper Maestrichtian ooze below and a reddish yellow, clay-rich Danian unit above. As in Site 689, the boundary layer has been considerably bioturbated and, because of this, the boundary may prove to be somewhat higher than our original estimate. Nannofossil preservation just below the boundary is good to moderate but improves downcore. Benthic foraminiferal faunal changes are much less obvious than at the K/T boundary at Site 689. A decrease in the relative abundance of *S. beccariiformis* started below the K/T boundary, as at Site 689. The basal sediment shows poor nannofossil and benthic foraminiferal preservation (though not for the planktonic foraminifers), but it was possible to date the sediment just above basement as Campanian?/early Maestrichtian.

PALEOMAGNETISM

Introduction

Site 690 lies in a water depth approximately 800 m deeper than at Site 689 on the southwestern flank of Maud Rise. Because of its slope setting, a greater variation in sedimentation rates might be expected due to slumps and changes in biogenic input. As a consequence of the lower carbonate content, the sedimentation rate was expected to be lower than at Site 689, apart from the intervals with terrigenous input, and therefore a sampling interval of 25 cm was retained.

Cenozoic Sediments

We measured the natural remanent magnetization (NRM) of 287 samples (Fig. 38), about one third of all the paleomagnetic samples taken at this site. Although the intensities were slightly higher than for Site 689, the overprint by the Brunhes geomagnetic field seems to be stronger. The distribution of the inclination values for Hole 690B (Fig. 39) appears to be similar to Hole 689B, but, assuming the same cutoff value of −30°, nearly 67% of all samples are interpreted as normal. Only 15% show negative inclination, as opposed to 26% for Hole 689B. Thus an interpretation of the polarity pattern is much more difficult, especially because of two apparent long, normal magnetozones of more than 30 m in length. They separate a shorter part of the polarity pattern, which cannot be assigned unequivocally to a time interval of the geomagnetic polarity time scale.

The NRM intensities range from 0.03 to 19.7 mA/m. There is a general correlation between intensity and lithology, shown most markedly by the intensity peak of Core 113-690B-17H (Fig. 38), which reflects the muddy nannofossil ooze (see "Lithostratigraphy" section, this chapter) encountered in this core. As at Site 689, the siliceous intervals have higher intensities than the calcareous intervals.

The basic assumptions for the development of an age-depth relationship are nearly constant sedimentation rates over long time periods and a minimum number of hiatuses. Both can be fulfilled by the assignment to the geomagnetic polarity time scale as shown in Figure 40, although this tentative interpretation is not unequivocal, nor is it integrated with the biostratigraphy. This suggests an average sedimentation rate for the Neogene of approximately 3 m/m.y. with a slight decrease in the late Pliocene to 2 m/m.y. The very low sedimentation rate provides a sampling interval of 100,000 yr and a measuring interval of 300,000 yr. Our interpretation suggests that an increased sedimentation rate of approximately 4.4 m/m.y. prevailed during late Paleogene time. A more reliable interpretation based on the detection of shorter polarity intervals requires detailed shore-based demagnetization and measurement of all samples. A detailed resampling of certain intervals may be necessary for better definition of such short polarity intervals.

Igneous Rocks

Approximately 1 m of amygdaloidal, olivine-phyric basalt was recovered in Core 113-690C-24X. Three 10-cm^3-diameter minicores were drilled from separate pieces of the basalt chosen to assure full representation of the recovered interval. We measured the NRM of all samples and progressively demagnetized (alternating field) them up to 80 mT (Table 10). Their NRM intensities show an increase by a factor of 2 downsection and are of a magnitude that is comparable to other drilled oceanic basalts. The typical demagnetization behavior, as shown in Figure 41 (Sample 113-690C-24X-1, 13–15 cm), indicates that the basalts have high stability, typified by a median destructive field of more than 70 mT. NRM directions and the end point after demagnetization all indicate a steeply-dipping (−70°) normally magnetized vector. This inclination is some 7° shallower than the axial dipole field inclination at this site.

SEDIMENTATION RATES

Biostratigraphic and Magnetostratigraphic Data

The sedimentation rate curve for Site 690 (Figs. 42 and 43) is constructed from two different data sources. Biostratigraphic ages derived from planktonic and benthic foraminifers, diatoms, radiolarians, and calcareous nannofossils provided the primary source of age information. Biostratigraphic data used to construct the age-depth relationship (Table 11) consist of selected datum levels and zonal assignments which have been correlated to the chronostratigraphic scale. The accuracy of the calibration between biostratigraphy and chronostratigraphy varies considerably for different fossil groups and time intervals. In particular, the pre-Pliocene diatom and radiolarian stratigraphies are not well calibrated with the chronostratigraphy.

Figure 42 was constructed as follows: The curve is based on biostratigraphic data (data points plotted with identifying number labels). Magnetostratigraphic data in comparison are shown as line segments with unlabeled datum points (solid boxes). Error boxes for paleomagnetic data represent the distance in depth between two samples of different polarities assigned to different magnetozones. From the preceding and the following magnetozone boundaries a sedimentation rate, and from this a corresponding error in the age determination, is calculated. This age error is represented by the horizontal box size. Biostratigraphic data are of three types. First and last occurrences of species are known only to occur within a finite depth interval, although the age of the datum is generally reported without any associated error estimate. These data thus plot as vertical lines. Age ranges for individual samples by contrast have a finite age range but do not have any depth uncertainty, and plot as horizontal lines. Finally, a few FAD's and LAD's for which uncertainty estimates are available are plotted as boxes. Many samples have more than one age-range estimate from different fossil groups. To make the overlap between multiple dates clear, small solid circles are used to mark the end of each datum which plots as a line. FAD's and LAD's represent, respectively, the oldest and youngest possible ages for a depth interval. Arrows are plotted to indicate datums of this type, with the direction indicating the time direction during which the species occurs.

Magnetostratigraphy provided a second source of age information. Magnetic polarity data were matched to a best-fitting correlation with the geomagnetic polarity reversal time scale of Berggren et al. (1985) (see "Paleomagnetism" section, this chapter). This correlation was constructed without recourse to biostratigraphic data. Magnetostratigraphic ages are determined by the comparison of the inferred downhole polarity pattern to a geomagnetic polarity time scale. Due to an average time span between the measured samples of approximately 100,000 yr a number of short polarity intervals are naturally overlooked, and thus the potential high-frequency information cannot be used for an unequivocal identification of polarity patterns. The preliminary interpretation is based on a relatively small number of polarity reversals which are fitted to the polarity time scale under the assumption of fairly constant sedimentation and a minimum number of hiatuses. Overprinting on about 25% of the samples makes the interpretation more difficult and open for later reinterpretation. Shore-based study including magnetic cleaning by stepwise demagnetization is required to obtain a more complete polarity record.

Age-Depth Curve, Site 690

The upper Pliocene to Quaternary section at Site 690 is marked by very low rates of deposition, or possibly by a hiatus (see "Biostratigraphy" section, this chapter), and it is not possible at present to infer sedimentation rates for this time interval. Sedimentation rates during the Pliocene at Site 690 (~1–20.5 mbsf) are estimated to be 12 m/m.y. (Fig. 43). This estimate is

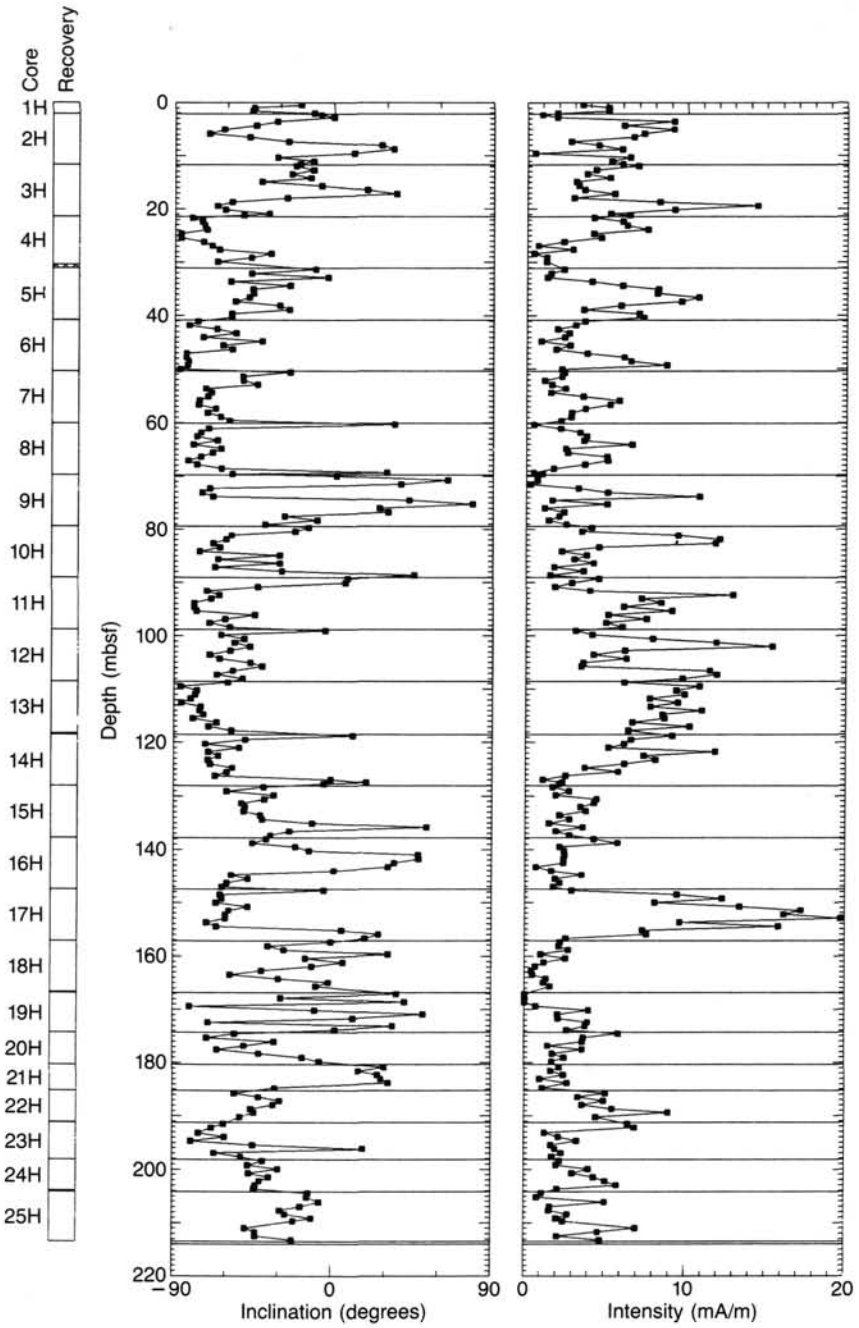

Figure 38. Downhole variation in NRM inclination and intensity for Hole 690B. Pattern indicates no recovery.

based on biostratigraphic data. The original magnetostratigraphic interpretation for the same interval assumes slower, but continuous, sedimentation during the Pliocene and late Miocene. Using the age constraints given by the chronostratigraphically calibrated radiolarian and diatom stratigraphies (an age equal to subchrons C3N3 and C3N4 in the depth interval 18–20.5 mbsf), an improved magnetostratigraphic interpretation can be given for the upper 21 m of Site 690 (Fig. 43, stippled line). All polarity intervals of the geomagnetic time scale can be assigned to the inferred polarity pattern, if a discontinuous sedimentation with a hiatus at a depth of 20.5 mbsf is assumed. An explanation is needed, however, for the two reversed magnetozones (2.0–2.3 mbsf, 2.8–3.2 mbsf), now placed in the uppermost Gauss normal Subchron.

Miocene sediments range from 21 to 51 mbsf. Construction of a sedimentation rate curve for this interval is difficult, and the present interpretation is tentative. Biostratigraphic estimates of age for this interval of the Miocene are not well established (Fig. 42).

An important exception occurs in Section 113-690B-5H, CC, for which planktonic and benthic foraminiferal evidence suggests a late early Miocene age. The discrepancy between ages indicated by planktonic foraminifers and those derived from diatom biostratigraphy highlights the lack of an accurate cali-

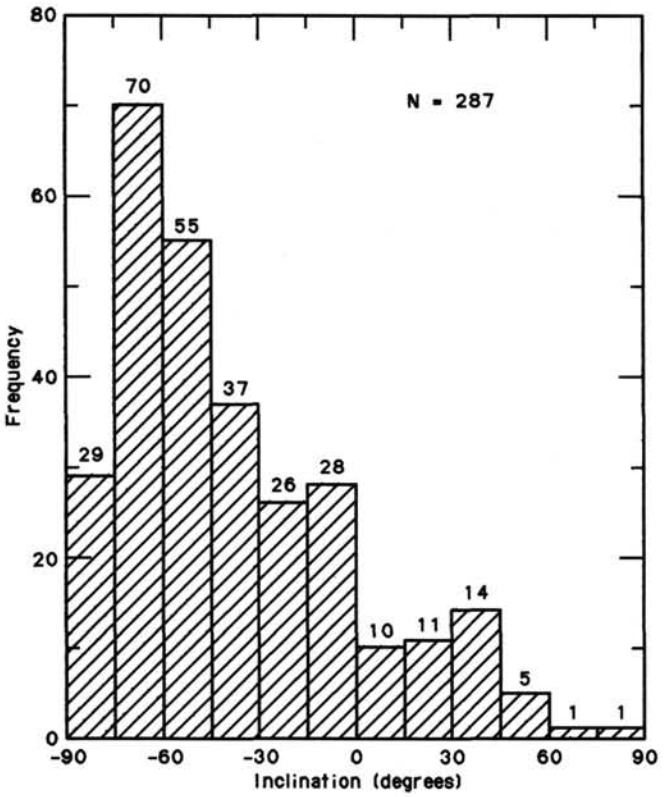

Figure 39. Frequency distribution of NRM inclination values for Hole 690B.

bration between these fossil groups. At present, the planktonic foraminiferal age estimate may provide the closest approximation to an actual geochronologic age, because it draws on data from the Subantarctic and temperate latitudes where correlations with low-latitude sequences have been carried out in more detail.

Also important is the biostratigraphic evidence (see "Biostratigraphy" section, this chapter) for a hiatus spanning the lower Miocene and uppermost Oligocene within the top of Core 113-690B-7H (approximately 51 mbsf). Magnetostratigraphic age estimates for this interval show an increasing discrepancy with the biostratigraphic estimates with increasing depth in the hole, and a difference of 4 m.y. exists between the magnetostratigraphic and biostratigraphic age estimates for Section 113-690B-5H, CC (40.8 mbsf), probably due to a lack of short polarity intervals expected in Chron C5A. The sedimentation rate curve drawn in Figure 42 satisfies the biostratigraphic constraints of an early Miocene age in Section 113-690B-5H, CC, and substantial hiatuses in the upper Miocene to basal Pliocene, and lower Miocene to uppermost Oligocene. The sedimentation rate implied by these correlations is only 2 m/m.y., and the existence of additional hiatuses within the Miocene section seems probable, although they cannot be identified with the shipboard stratigraphic data.

The interval between 51 and 93 mbsf is dated by several different microfossil groups as middle upper Oligocene to lower Oligocene. Magnetostratigraphic age estimates are much lower based on the detection of a larger number of reversals, whereas the geomagnetic time scale defines only three reversals in the lower Oligocene. A straight line fitted to the biostratigraphic data gives a sedimentation rate of 5.5 m/m.y. A hiatus exists in Section 113-690B-11H-3, across the Eocene/Oligocene boundary. The exact duration is not clear, but the hiatus is longer than the coeval one at Site 689 (where it was at least 1 m.y.).

Another hiatus is indicated by microfossil data at about 101 mbsf. Between 5 and 10 m.y. of section is missing in this hiatus, which separates upper Eocene from middle to lower Eocene sediments. Planktonic foraminifer and nannofossil dates in the lower Eocene through Paleocene indicate a relatively constant sedimentation rate of 10 m/m.y. There may be a short hiatus (corresponding to calcareous nannofossil Zone CP4, duration 0.4 m.y.) between Section 113-690B-25X, CC, and Sample 113-690B-13X-1, 124 cm. On the other hand, the short zone may not have been found because of poor recovery in the interval between beds. Magnetostratigraphic age estimates for this interval are much lower, due (at least) to the fact that the high number of reversals in the inferred polarity pattern cannot be found in the lower Eocene and Paleocene (Chrons C23 to C29). Further shore-based demagnetization studies may reveal a certain number of overprinted samples and result in a cleaned polarity sequence, which also gives the opportunity for detection of further short polarity reversals not yet included in the geomagnetic time scale.

Summary

Site 690 sediments were deposited at relatively low rates of between 2 and 12 m/m.y. Upper Cretaceous and lower Paleogene rates of sedimentation of between 7.5 to 10 m/m.y. decrease in the Oligocene to 5.5 m/m.y. Very low overall rates of deposition (2 m/m.y.) are seen in the Miocene, and undetected hiatuses may be present in this interval. Sedimentation rates reached a maximum of 12 m/m.y. in the early Pliocene. Prominent hiatuses occur in the section at 51 mbsf (lower Miocene to upper Oligocene); 93 mbsf (Eocene-Oligocene); and ~101 mbsf (upper and middle Eocene).

INORGANIC GEOCHEMISTRY

Introduction and Operation

Data on the chemical composition of interstitial water are presented for Holes 690B and 690C. Thirteen whole-round squeezed sediment samples (seven of 5-cm and six of 10-cm thickness) were analyzed. The four deeper whole-rounds are from XCB cores, the others from APC cores. The chemical data are summarized in Table 12.

Evaluation of Data

For overall evaluation of the data, a charge balance was carried out. The data do not include sodium; there have been no reports of Na/Cl ratios of interstitial waters from pelagic sediments diverging significantly from that of seawater. Sodium is calculated by multiplying the Na/Cl ratio of seawater by the measured chloride concentration. The calculations reveal that apparently, all samples have excess positive charge. The excess increases erratically from 3.6 meq/L in the shallower sample to 8 meq/L at the bottom of the hole. This trend is the same as that observed at Site 689 (see "Site 689" chapter, this volume) and may be related to a systematic error in one of the methods, or it may indicate that the assumption of a constant Na/Cl ratio is not valid. The very high excess positive charge (23 meq/L) in the deepest sample is caused by the low chloride value. Unfortunately, there was not enough sample to repeat the analysis.

Few of the parameters determined differ substantially from seawater, thus contamination by the latter may be suspected. The seawater used for circulation, however, is taken through the ship's water intake (approximately 10 m below sea surface). At this time of year (a few weeks after the retreat of the ice) diatoms are blooming and keep the level of dissolved silica below 0.01 mmol/L in the upper euphotic zone (Sverdrup et al., 1942). The lowest pore-water silica concentration measured is 0.14 mmol/L. This low silica concentration occurs in the same depth interval as the sulfate low, thus it is evident that contamination of the samples by seawater is minor.

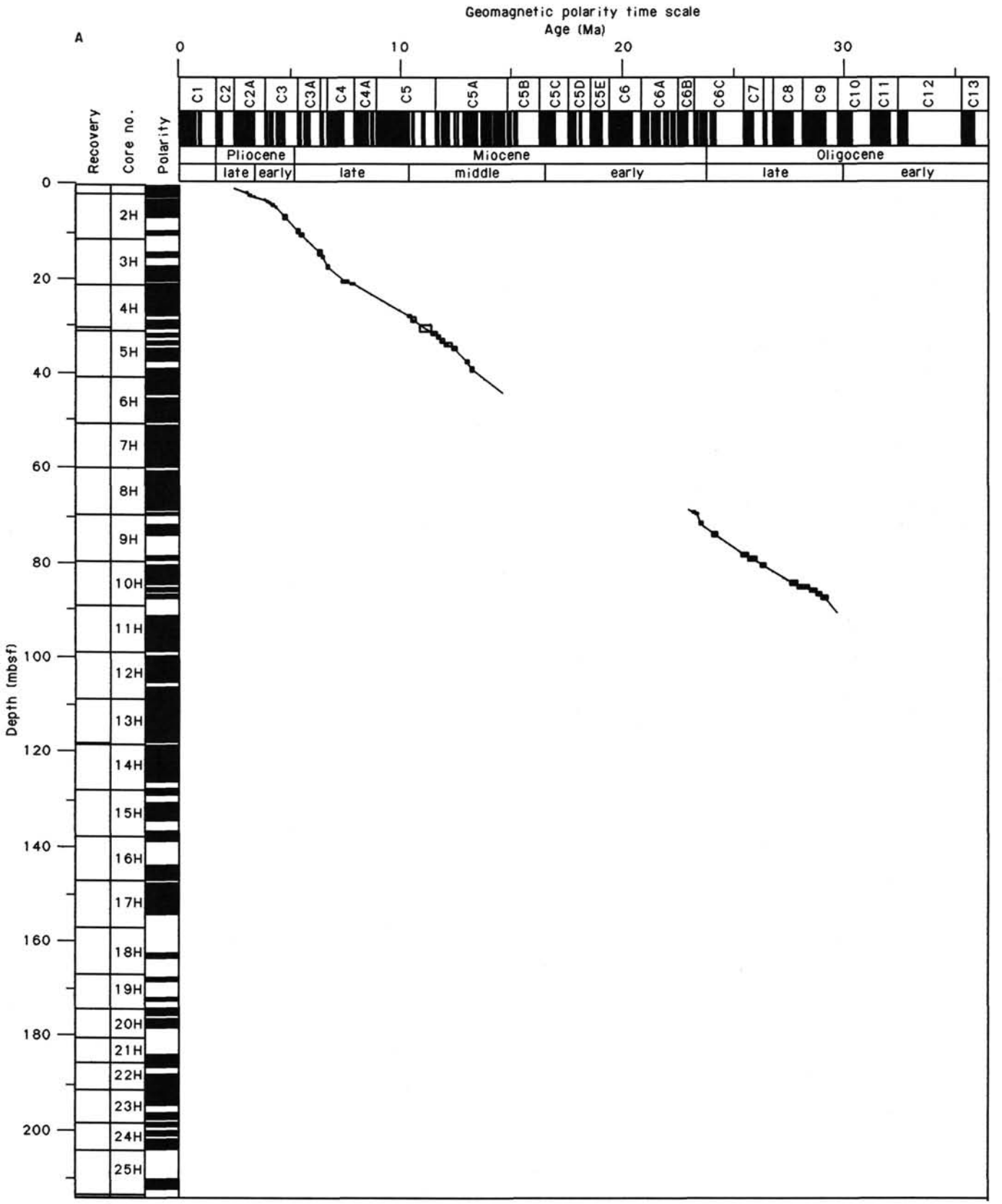

Figure 40. Assignment of the inferred magnetostratigraphy for Hole 690B to the established geomagnetic polarity timescale. A. Neogene. B. Paleogene.

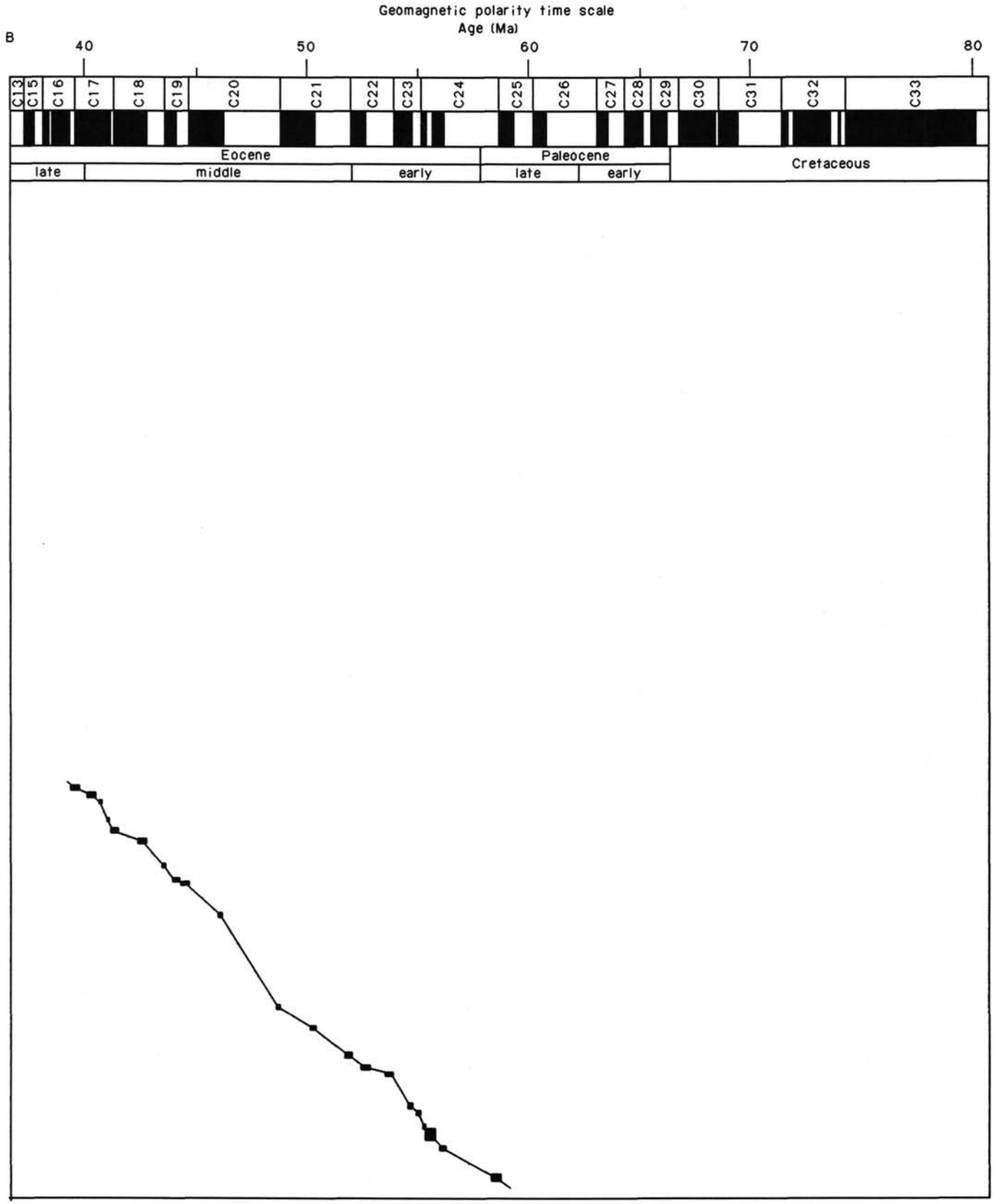

Figure 40 (continued).

Table 10. Natural and characteristic remanent magnetization after alternating field demagnetization of basalt samples from Hole 690C.

Sample	NRM Inclination (°)	NRM Declination (°)	Intensity (mA/m)	Characteristic RM Inclination (°)	Characteristic RM Declination (°)	Median destructive field (mT)
113-690C-24X-1, 13	−74.2	180	1991	−71.8	170.5	70
113-690C-24X-1, 50	−76.9	289	2939	−70.2	264.3	>80
113-690C-24X-1, 101	−70.2	329	4427	−69.2	319.2	>80

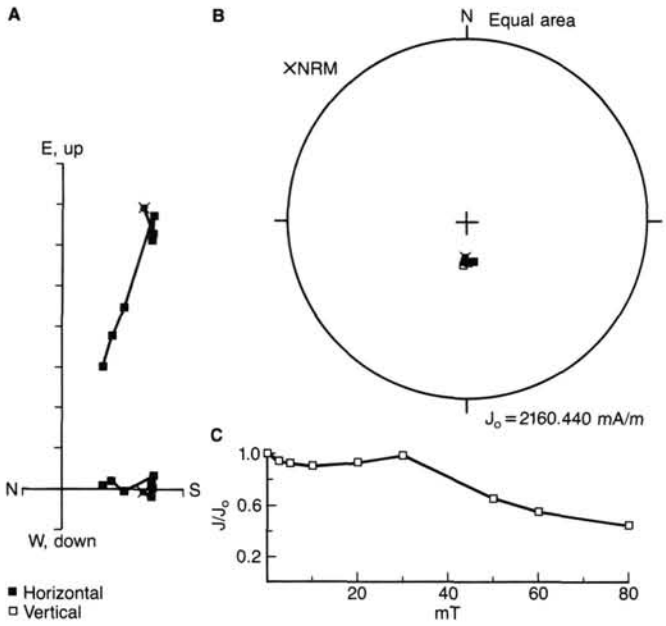

Figure 41. Alternating field demagnetization of basalt Sample 113-690C-24X-1, 13–15 cm. A. Zijderveld orthogonal vector plot. B. Equal-area stereographic projection of resultant vector. C. Normalized intensity decay curve.

Chlorinity and Salinity

Chloride data are presented in Figure 44A and Table 12. The average concentration of chloride corresponds to a seawater salinity of 35.2 ‰. There are no significant variations, although a slightly decreasing trend downhole may be present. In the region where the data from the two holes overlap, the concentration of chloride is the same in the two data sets, within analytical precision. Possibly the low value at 296 mbsf (529.2 mmol/L) is an experimental error, but this sample may have been diluted by some dilute calcium-containing water, most probably during sample handling. This is also suggested by the salinity measurements (Table 12). For all other samples there is no correlation between chlorinity and salinity.

pH

The pH (Fig. 44B and Table 12) varies between 7.52 and 7.96 without any trend. The pH data from the two holes are continuous. The measured pH is on the average 0.3 pH-units higher than that calculated for *in-situ* calcite saturation (see "Inorganic Geochemistry" section in "Site 689" chapter, this volume), indicating that the pH has changed during retrieval of the samples.

Alkalinity and Sulfate

The alkalinity data are presented in Figure 44C. The low level of phosphate (see below) and undetectable (by smell) hydrogen sulfide concentrations make corrections of the titration alkalinity unnecessary. The titration alkalinity is an accurate estimate of the carbonate alkalinity. The alkalinity level varies from 2.8 meq/L in the upper sample to 4.0 meq/L at 143 mbsf. Below 143 mbsf it decreases to 3.1 meq/L. Microscopic examination of the sediments revealed the presence of authigenic calcite overgrowths on nannofossils. The decreasing alkalinity below 143 mbsf (Table 12) is probably caused by precipitation of calcite as calcium is released from another source (see below). Thus, the very low alkalinity levels are caused partly by precipitation and partly by the low rate of microbial generation.

The sulfate profile (Fig. 44D) also suggests a low bacterial activity. Sulfate decreases from seawater concentrations in the upper section and reaches a level of 20–22 mmol/L below 250 mbsf. The profile represents a balance between diffusive supply and bacterial consumption.

Phosphate and Ammonia

The concentration profile for phosphate is presented in Figure 44E. The concentration of dissolved phosphate shows a subsurface maximum at 17.4 mbsf (6.5 mmol/L) and decreases toward a level of about 1 mmol/L at 180 mbsf. The maximum is caused partly by the bacterial preference for phosphorus-containing organics, and partly by a longer time for adsorption in the lower part of the sequence. The levels are low and confirm the low bacterial activity.

The concentrations of ammonia (Fig. 44F) are low. The two high readings (at 17.4 and 239 mbsf) are suspected to be caused by contamination introduced during sample handling. The concentration of nitrate is probably minor since the redox level established by the sulfur system renders nitrate unstable relative to ammonia. Thus, the ammonia level also reflects the low bacterial activity. The increasing level at the base of the sequence may represent a temperature effect on an adsorption/desorption equilibrium, although this is highly speculative.

Calcium and Magnesium

Calcium and magnesium data are presented in Figures 44G and 44H, respectively. The concentration of calcium increases linearly from seawater levels to a nearly constant value of about 13 mmol/L below 100 mbsf. The high reading at 296 mbsf is probably an artifact (see discussion above on chloride). The concentration of magnesium decreases from seawater levels at the top of the site and stabilizes at about 49 mmol/L below 170 mbsf. A slight increasing trend in the lower part is indicated. Both calcium and magnesium vary less than at Site 689 (see "Site 689" chapter, this volume) and less than usually observed in deep-sea sediments. This may be related to the abundance of mica, volcanic glass, and zeolites below 150 mbsf. It seems that this mineral combination buffers the levels of alkaline earths and masks the effect of seawater/crust interactions inferred to take place at Site 689. The Mg/Ca ratio (Fig. 44I) decreases linearly with increasing depth to a constant level below 200 mbsf.

Potassium

The concentration of potassium decreases linearly from 12.8 mmol/L in the uppermost section to 9.2 mmol/L at the bottom of the hole (Fig. 44J). The concentration of potassium in the upper section is about 20% higher than one would expect in 35‰ seawater. the profile may be controlled by diffusion from the seawater to a reaction zone situated either in the mica/zeolite interval or, as suggested for Site 689, at the sediment/crust interface.

Dissolved Silica

The concentration of dissolved silica (Fig. 44K) varies between 1126 μmol/L (at 17.4 mbsf) and 140 μmol/L (at 173 mbsf). In all samples the levels fall between quartz saturation and amorphous silica saturation. The declining silica profile from the surface toward 100 mbsf parallels the distribution of diatoms. The subsurface minimum between 150 and 200 mbsf coincides with the highest abundance of mica (visually quantified). In this interval the silica concentrations plot in the stability field of mixed-layer illite-montmorillonite as provided by Wollast (1974) for seawater at 25°C. The increase toward the bottom takes place in the interval where volcanic glass becomes abundant (5%–20%). Quartz is present from 40 mbsf down but, for kinetic reasons, does not control the concentration of dissolved silica.

ORGANIC GEOCHEMISTRY

Headspace Analyses for Low-Molecular-Weight Hydrocarbons

Holes 690B and 690C penetrated the Upper Cretaceous and Cenozoic section on the west flank of Maud Rise in the eastern Weddell Sea. Sixteen samples were collected and analyzed in the same manner as at Site 689. Once again, extremely low levels of methane were encountered, maximally 9.6 mL of gas per liter of moist sediment. Data are presented in Table 13.

At Site 690, analyses were carried out on the Carle Series 100 gas chromatograph using a Porapak column. Although in the standard operating mode (range 1, output 4) it is less sensitive than the natural gas analyzer, it was believed to have the advantage of a wide calibrated range and the apparent absence of memory phenomena.

The Carle 100 was found to yield a concentration for methane in laboratory air of 5.2 ppm, abnormally high. The headspace measurements were therefore corrected to this extent. Certain sediment analyses were followed by an air analysis which revealed equal concentrations of methane in air and "sample." Numerous sediments are therefore devoid of indigenous methane. A rationale for this phenomenon involving continuous highly oxic conditions at the site of deposition, without significant sulfate reduction at shallow depths, and minimal activity of methanogenic bacteria, is invoked once again. Because of the low sample levels of methane, and the significance of the background level of the gas in laboratory air, both the Carle and the Hewlett Packard natural gas analyzer were evaluated at low sample concentrations. They behaved differently. In the Carle, zero-grade helium gave a double peak for methane, at an indicated concentration of 0.45 ppm. On the other hand, the Hewlett Packard analyzer, which proved to be substantially more sensitive, gave no response to helium. An artifact appears to be involved.

Analyses of laboratory air on the natural gas analyzer were variable over a period of 24 hr, averaging 2.6 ppm (eight analyses), ranging from 2.0 to 4.2 ppm, excluding the two highest, 5.4 and 8.5 ppm late in the evening. All of these data were inexplicable at the time, as the pristine atmosphere contains approximately 1.5 ppm methane. However, it was later found that the counter-gas of the X-ray fluorescence elemental analyzer (argon-plus-10% methane) is discharged into the air in an adjacent laboratory. This represents a probable source of atmospheric contamination.

Rock-Eval Analyses

The data of Holes 690B and 690C are closely comparable to those of Hole 689B. Total organic carbon (TOC) is very low in the Eocene-Pliocene, averaging 0.08% (eight analyses). Paleocene values (five) average 0.12%, while two Cretaceous values are relatively high, 0.36% and 0.53%. Data are given in Table 14.

An appraisal of kerogen type is possible for only one sample, that from Section 113-690C-20X-3, Cretaceous, which is extremely immature and of type III, terrestrial, or of type II, planktonic, but highly oxidized.

The greater number of samples appear to contain highly mature, oxidized, refractory kerogen, probably in a second or later sedimentary cycle. Most yield no hydrocarbons upon pyrolysis. Three hydrogen index values exceed 1000 mg (hydrocarbons)/g (organic carbon). They are probably spurious, as they are accompanied by extremely high T_{max} values. As at Site 689, these values represent diatomites.

DOWNHOLE MEASUREMENTS

Heat Flow Measurement

A temperature measurement was made with the Von Herzen APC temperature recording device #5, in Hole 690C. The device was used three times (Cores 113-690C-4H, -6H, and -9H). Reliable data, however, were taken on only two measurements (Cores 113-690C-4H and -9H). The data from Core 113-690C-6H could not be recovered, probably due to a mechanical pin connection problem. Two temperature records were collected at 35.2 (Fig. 45) and 83.6 (Fig. 46) mbsf. Just before pulling out of the hole, the observed temperatures were 5.214°C and 6.043°C, respectively. The estimated true formation temperatures are 4.6°C at 35.2 mbsf and 5.4°C at 83.6 mbsf. They were calculated using "DECAY3" and "FITTING3" computer programs as described in the downhole measurement section for Site 689 (see "Site 689" chapter, this volume).

SUMMARY AND CONCLUSIONS

Site 690 lies on the southwestern flank of Maud Rise at 65°9.629′S; 1°12.296′E and at a water depth of 2914 m. Site 690 is the deeper of two sites on Maud Rise on a depth transect for studies of vertical-water-mass stratification and biogenic sedimentation during the late Mesozoic and Cenozoic around Antarctica. Objectives were similar to those at Site 689, located only 116 km to the northeast: to obtain a high-quality (APC-XCB), continuously-cored, Cenozoic-upper Mesozoic calcareous-siliceous biogenic sequence beneath the present-day Antarctic water mass, and to monitor long-term changes in major biogenic components resulting from paleoceanographic developments. This site is isolated from influences of terrigenous sediment transport from Antarctica except for wind-blown and ice-rafted components, as was Site 689. Single-channel seismic reflection profiles at Site 690 are similar to those at Site 689 and indicate the presence of a relatively thin (0.35 s two-way traveltime) sequence of draped and mounded, weakly reflective sediments inferred to be pelagic oozes.

Three holes were drilled at Site 690: Hole 690A consists of a single APC core to 9.86 mbsf; Hole 690B consists of 25 APC cores to 213.4 mbsf. Hole 690C consists of 9 APC cores to 83.6 mbsf, a washed interval from 83.6 to 204.2 mbsf, and 14 XCB cores from 204.2 m to 321.2 mbsf. At the base of the hole 1.71 m of normally magnetized amygdaloidal pyroxene-olivine basalt was recovered. Sediments directly overlying basement are

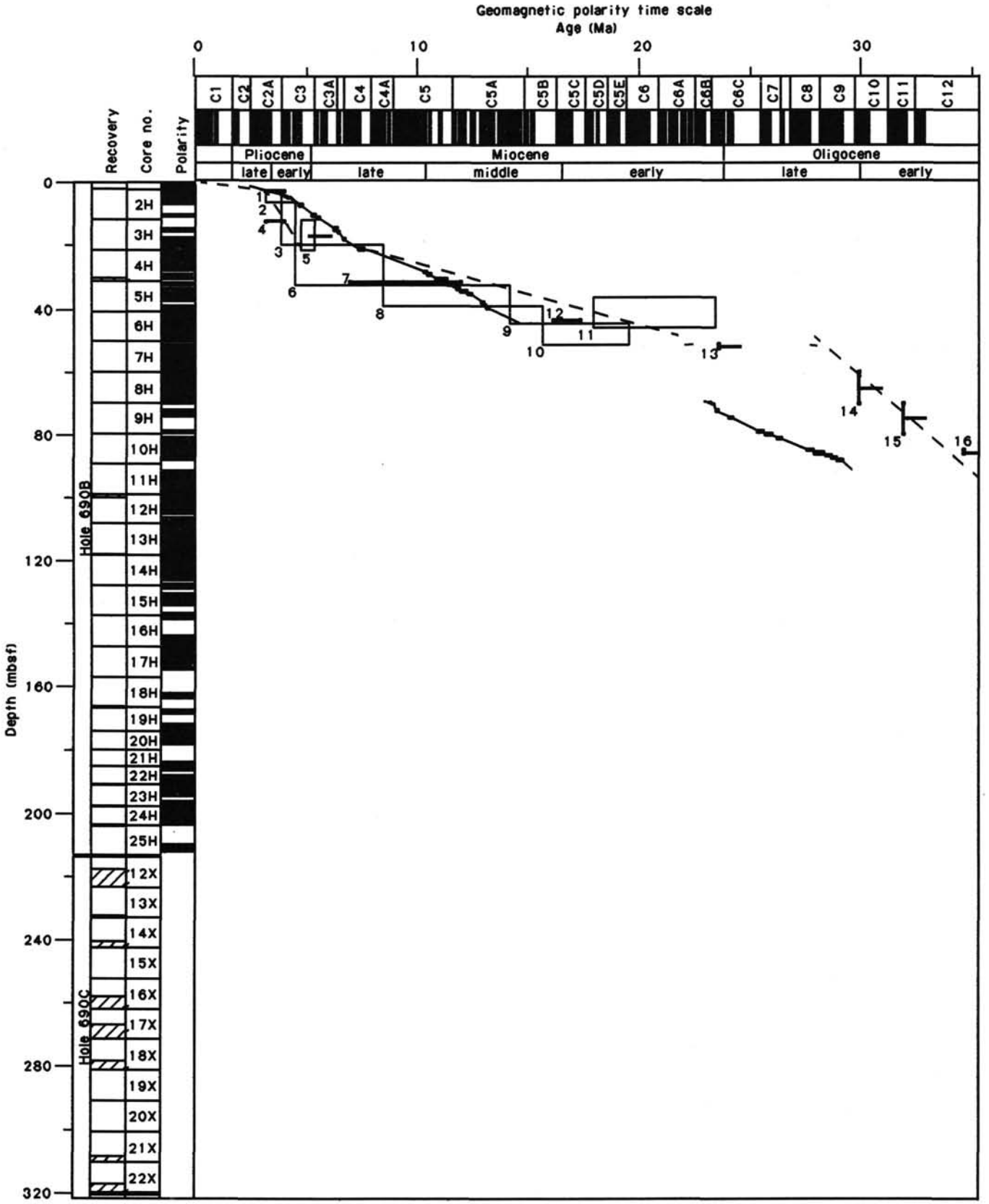

Figure 42. Age-depth interpretation of Site 690 based on Holes 690B and 690C. Age-depth curve shown by dashed line based on biostratigraphic data (Table 11) and hiatuses indicated by wavy lines. See text for explanation.

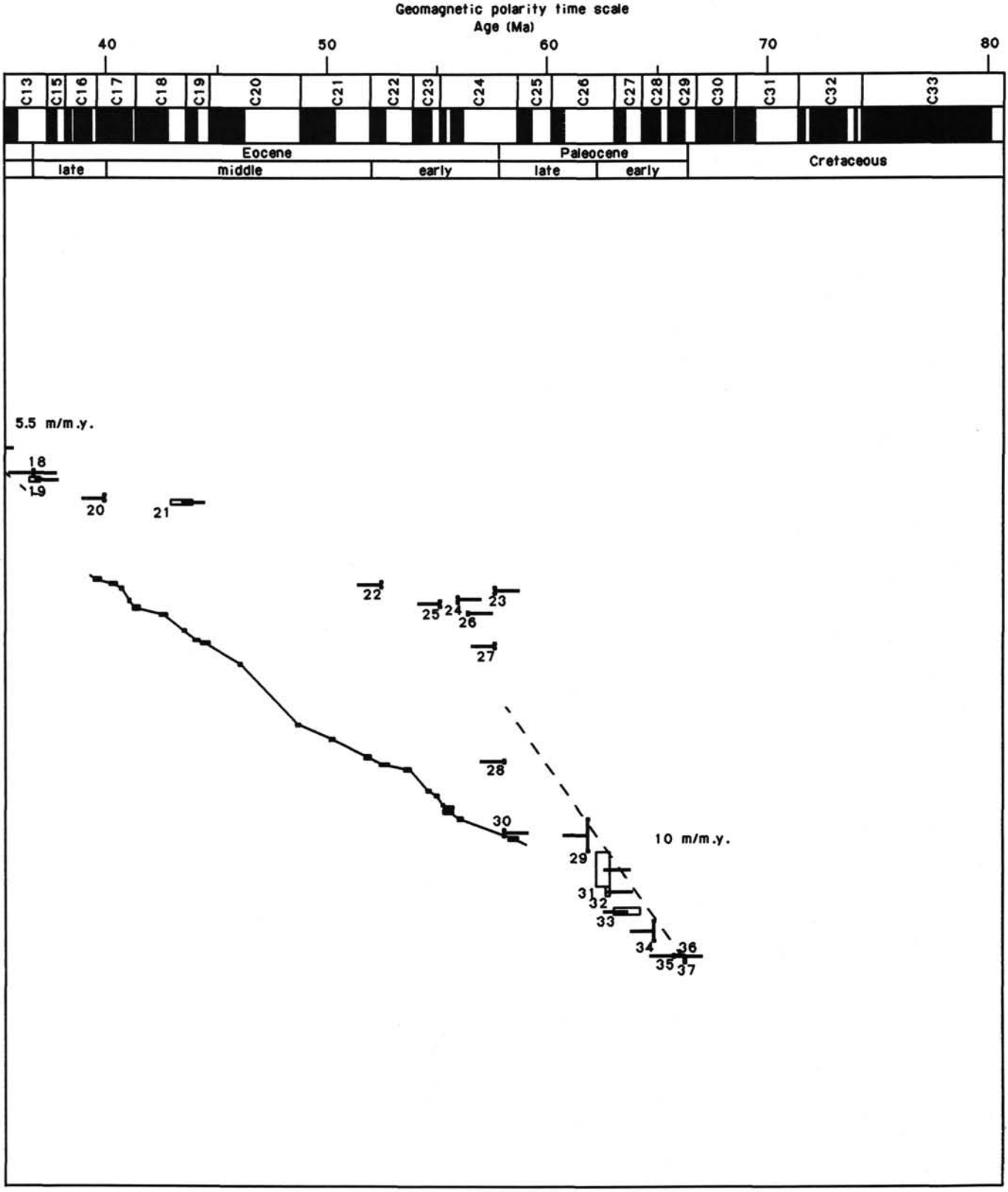

Figure 42 (continued).

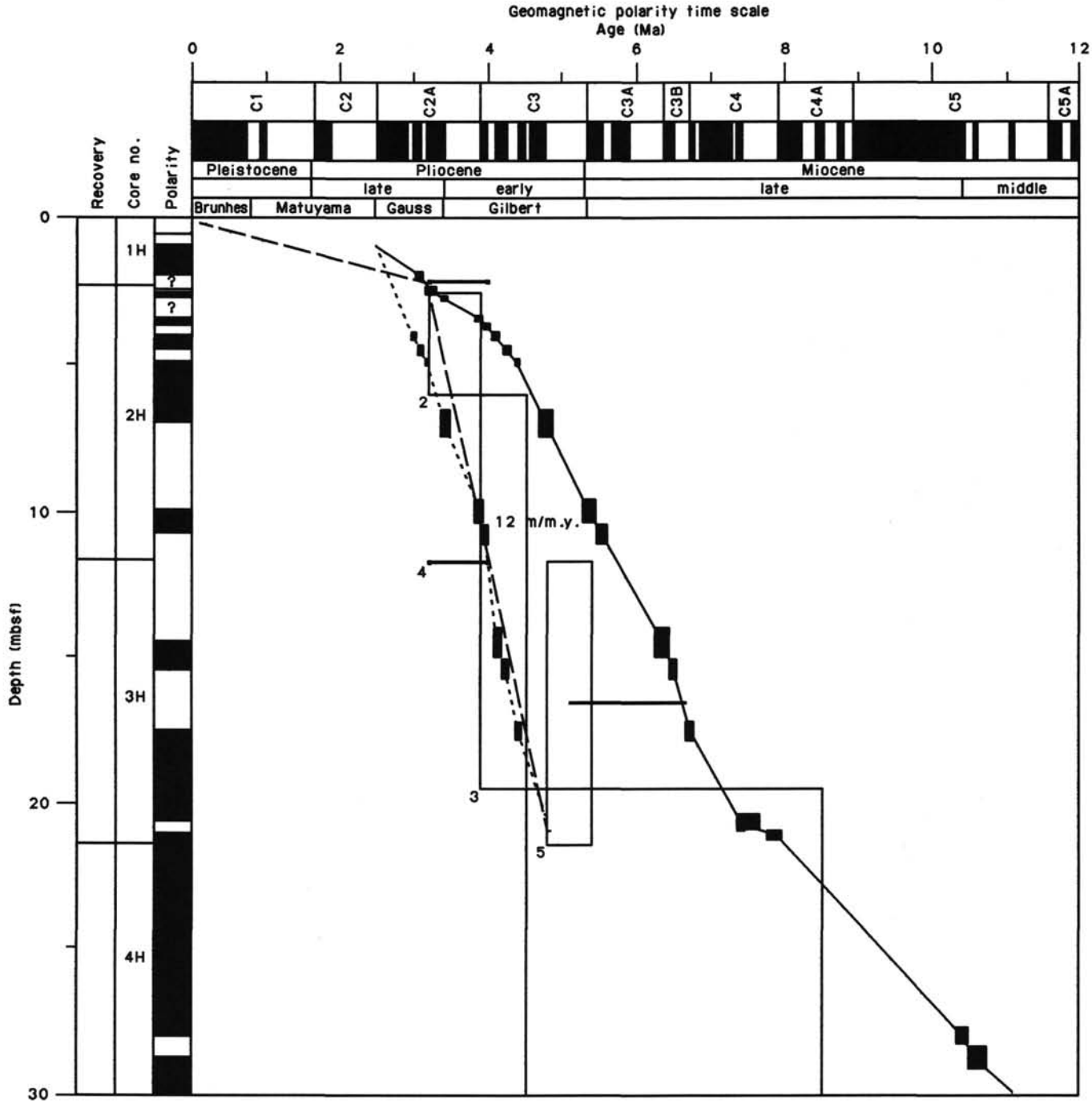

Figure 43. Enlargement of late Miocene to Quaternary portion of Figure 42 to show more clearly the different magnetostratigraphic and biostratigraphic interpretations (Table 11). Age-depth curve shown by dashed line. The original magnetostratigraphic assignment is shown by a solid line connecting data points, the improvement based on biostratigraphic tiepoints is represented by the stippled line. Other plotting conventions explained in Figure 42.

most probably upper Campanian to lower Maestrichtian. The APC part of the section extends from the seabed through the upper Paleocene. The quality of the cores is generally excellent, with marked disturbance only in the uppermost cores in each hole.

Drilling at Site 690 sampled 317 m of almost pure siliceous and calcareous oozes in the upper half of the sequence and mixed calcareous ooze/chalk and terrigenous sediments in the lower half. Minor cherts occur in the basal sediments. Major hiatuses span the middle-upper Eocene and part of the lower Oligocene. Additional hiatuses may be present across the Miocene/Oligocene boundary and the lower/upper Paleocene boundary. The uppermost Miocene and the upper Pliocene/lower-middle Quaternary hiatuses are present, as at Site 689. The magnetostratigraphy is comparable to Site 689 in that it is well established for the upper Neogene, with excellent prospects for all Cenozoic sediment recovered. An increase in NRM intensity in the lower part of the sequence is correlated with increased terrigenous sediment deposition. The magnetostratigraphic studies have been strengthened by the coring of two nearby sites.

Table 11. Biostratigraphic data used to construct sedimentation rate curve in Figure 42.

	Datum	Depth range (m)	Age range (m.y.)
1	top lower Upsilon Zone—R	2.1	3.2–4.0
2	*N. interfrigidaria* Zone—D	2.5–6.0	3.2–3.9
3	*N. angulata-N. reinholdii* Zone—D	6.0–19.5	3.9–4.52
4	bottom lower Upsilon Zone—R	11.7	3.2–4.0
5	LAD *C. spongothorax*—R	11.7–21.4	4.8–5.4
6	*D. hustedtii* Zone—R	19.5–32.2	4.52–8.5
7	lower *C. spongothorax* Zone—R	31.1	7.0–12.0
8	*D. hustedtii-D. lauta-N. denticuloides* Zone—D	32.2–38.8	8.5–14.25
9	*N. grossepunctata-C. lewisianus* Zone—D	38.8–44.2	14.25–15.7
*	hiatus (Oligocene/Miocene boundary)—D	±51	??
10	*N. malinterpretaria-C. rhombicus* Zone—D	44.2–51.0	15.7–19.6
11	*G. miozea* assemblage—PF	36.0–45.6	18.5–23.5
12	*C. wuellerstorfi* assemblage—BF	38.6–40.8	16.2–17.4
13	LAD *C. altus*—N	50.7–52.2	23.6
14	LAD *C. cubensis*—PF	60.1–69.8	30.0
15	LAD *S. angiporoides*—PF	69.8–79.4	32.0
16	LAD *R. umbilica*—N	84.2–85.7	34.7
*	hiatus (Eocene/Oligocene boundary)—N, PF, BF	±93	??
17	FAD *I. recurvus*—N	92.4–93.9	37.0
18	LAD *R. reticulata*—N	92.4–93.9	36.7
19	LAD *G. index*—PF	92.5–94.0	36.5–37.0
*	hiatus (upper-middle Eocene)—N, PF, BF	±101	??
20	FAD *C. oamurensis*—N	100.6–102.1	40.0
21	LAD *Acarinina* spp.—PF	102.1–103.6	42.0–43.0
22	FAD *D. sublodoensis*—N	128.4–129.9	52.6
23	FAD *P. wilcoxensis*—evolutionary—PF	130.0–130.7	57.8
24	LAD *T. selmensis*—BF	133.0–134.5	56.1
25	LAD *D. lodoensis*—N	134.4–135.9	55.3
26	LAD *T. contortus*—N	137.8–138.1	56.7
27	FAD *T. bramlettei*—N	147.8–149.3	57.8
28	FAD *D. multiradiatus*—N	185.2–185.5	59.2
*	hiatus (?) (Zone CP4 missing)—N	213.4–224.8	61.6–62.0
29	FAD *F. tympaniformis*—N	204.0–214.0	62.0
30	LAD *S. beccariiformis*—BF	170.3–171.9	58.2
31	LAD *M. inconstans*—PF	214.3–225.5	62.3–63.0
32	LAD *G. daubjergensis*—PF	227.0–228.5	62.8–63.0
33	FAD *M. trinidadensis*—PF	232.2–233.3	63.0–64.5
34	FAD *C. danicus*—N	236.5–242.9	65.0
35	FAD *C. tenuis*—N	247.4–248.0	66.0
36	Range *P. eugubina*—PF	247.5–248.1	66.4–65.8
37	K/T boundary—N	249.2–249.6	66.4

Note: Depth ranges of first and last appearance datums (FAD's and LAD's) and zones. A single value in the depth range column indicates a sample with a zonal or assemblage age assignment. Age range given for zones, and in some instances for uncertainty in age calibration of a FAD or LAD. Letters following each name refer to the fossil group: D = diatoms; R = radiolarians; N = calcareous nannofossils; PF = planktonic foraminifers; BF = benthic foraminifers. * = duration of hiatuses is given as the minimum value, i.e., the duration of the biostratigraphic zone not represented in the sediment.

Site 690 provides a fine biostratigraphic section that reinforces and adds to the biostratigraphy of Site 689. Its Paleogene calcareous biostratigraphic sequence is reasonably complete except possibly for an interval near the lower/upper Paleocene boundary, the middle to upper Eocene, and the upper Eocene-lowermost Oligocene. The middle Eocene to lower Oligocene interval is preserved in Site 689. The "middle" Paleocene hiatus is present at both sites but much more pronounced at Site 689. Together, therefore, the two sites seem to provide a complete Paleogene sequence except for an undefined interval in the middle Paleocene and across the Eocene/Oligocene boundary. The Maestrichtian and upper Paleocene are highly expanded because of the addition of clays, permitting high-resolution biostratigraphic, paleomagnetic, and isotopic work.

Preservation of the calcareous microfossils is moderately good to excellent throughout. Because of the greater depth of deposition at Site 690, the Neogene has less calcium carbonate due to increased dissolution. Siliceous microfossils are better preserved because of this reduction in carbonate. As at Site 689, there is a marked lack of sediment- and microfossil-reworking by bottom currents except for Cores 113-690B-11H, 113-690B-12H, and 113-690B-25H (i.e., close to hiatuses). Calcareous benthic foraminiferal assemblages are moderately abundant throughout.

The sedimentation across the Paleocene/Eocene boundary appears continuous at Site 690, unlike the second hole at Site 689. Sedimentation across the K/T boundary was also continuous at Site 690, and the boundary is associated with a clay that appears to be of volcanogenic origin, as at Site 689. The boundary (Section 113-690C-15X-4, between 48 and 50 cm) is marked by a prominent color change between a white, upper Maestrichtian ooze overlain by a darker, clay-rich Danian unit. At this site, however, the inferred volcanogenic clays are brownish rather than greenish, as at Site 689. The boundary has been strongly bioturbated, but is expanded at Site 690 compared with Site 689.

Apart from a thin (2.1 m) uppermost layer of foraminiferal ooze of Quaternary age, the upper part of the sequence (upper Miocene and Pliocene) is represented entirely by biosiliceous ooze, above a sequence of upper Miocene to Oligocene interbedded diatom and calcareous nannofossil oozes. This in turn is underlain by an interval of Eocene foraminifer-bearing nannofossil ooze. Lower in the section is upper Maestrichtian to lower Eocene nannofossil ooze mixed with terrigenous sediments, and the lowest part (Maestrichtian/Campanian) has an even stronger terrigenous component mixed with calcareous nannofossils.

The sediment becomes more indurated with depth; calcareous sediments approximately 210 mbsf (upper Paleocene) are entirely ooze. Sediments between 210 and 281 mbsf (upper Paleocene to middle Maestrichtian) consist of semilithified ooze to chalk, with chalk becoming dominant near 242.9 mbsf. Chalk without ooze occurs below 281 mbsf, beginning in the middle Maestrichtian.

The sequence contains volcanic glass, including a few distinct layers in its lower part (220 mbsf to basement) in the lower Paleocene and Upper Cretaceous. The most abundant occurrence is in the basal 20 m (upper Campanian to lower Maestrichtian). Glacial dropstones are even more rare at Site 690 than at Site 689, and were found only rarely in middle upper Miocene to Quaternary sediments. This is a more restricted distribution than at Site 689 nearby, where they range through the entire Neogene with one occurrence in the upper Oligocene. An absence of dropstones in the sedimentary sequence is clearly not an accurate record of continental glaciation, at least in the Maud Rise region, which is 700 km north of the continent. The organic content, as at Site 689, is very low. Sediments are generally light colored in the upper part of the sequence (Quaternary to lower Eocene). In the middle part of the sequence (lower Eocene and Paleocene) colors are more variable and include reddish-yellows and light browns with color changes often gradual and cyclic. The most vivid colors are found in the upper Paleocene. Cretaceous sediments have gray to greenish colors. The sediments throughout lack pyrite or other evidence of sediment reduction. As in Site 689, all evidence suggests deposition in a highly oxidizing environment, at least for the Cenozoic.

The sequence at Site 690 has been divided into five lithostratigraphic units based upon compositional differences (see Fig. 4).

Unit I extends from the seafloor to 24.4 mbsf (upper Miocene to Quaternary). The sediment is composed of an upper 2.2 m of foraminiferal ooze (Subunit IA; Quaternary). The lower part is a diatom ooze with varying amounts of other biosiliceous components.

Unit II extends from 24.4 to 92.9 mbsf and consists of a wide variety of pure and mixed biogenic siliceous and biogenic calcareous oozes (upper Miocene through Oligocene). The upper part (Subunit IIA; upper Miocene to uppermost Oligocene) consists of interbeds of diatom-bearing calcareous ooze and calcareous nannofossil ooze; the lower part (Subunit IIB; Oligocene)

Table 12. Summary of shipboard interstitial water data, Holes 690B and 690C.

Core, section interval (cm)	Depth (m)	Vol. (mL)	pH	Alk. (mmol/L)	Sal. (g/kg)	Mg (mmol/L)	Ca (mmol/L)	Cl (mmol/L)	SO_4 (mmol/L)	PO_4 (μmol/L)	K (mmol/L)	NH_4 (mmol/L)	SiO_2 (μmol/L)	Mg/Ca
113-690B-														
2H-3, 145-150	6.55		7.70	2.84	35.0	54.13	10.80	547.5	29.2	5.00	12.8	0.01	738	5.01
3H-4, 120-125	17.40		7.52	2.93	37.0	54.10	10.83	556.6	29.2	6.50	12.9	0.94	1126	5.00
6H-4, 120-125	46.50		7.96	3.11	35.7	54.36	11.59	553.7	27.6	3.8	12.4	0.01	707	4.69
9H-4, 120-125	75.50	31	7.81	3.75	35.7	52.70	11.69	553.7	26.5	3.0	12.0	0.06	721	4.51
12H-5, 120-125	106.00	41	7.69	3.79	34.9	54.15	12.77	550.3	24.7	1.8	11.5	0.05	394	4.24
16H-4, 120-125	143.50	25	7.90	4.04	34.7	51.38	13.01	545.1	22.9	2.3	10.6	0.01	238	3.94
19H-4, 115-125	172.55	65	7.83	3.82	34.5	48.76	12.83	550.8	22.3	0.6	10.0	0.08	140	3.80
22H-3, 120-125	189.40	29	7.77	3.84	34.5	49.00	13.00	550.8	24.6	1.4	11.1	0.12	193	3.77
25H-4, 115-125	209.85	55	7.74	3.87	34.7	48.37	13.00	547.9	22.7	1.0	10.6	0.01	225	3.72
113-690C-														
11X-3, 115-125	208.35	27	7.95	3.27	34.3	50.17	12.91	545.5	21.9	1.5	10.0	0.04	278	3.89
14X-4, 115-125	238.85	35	7.75	3.87	34.1	48.49	13.10	548.4	20.1	1.4	9.8	1.04	365	3.70
17X-2, 115-125	264.45	27	7.63	3.47	35.0	50.76	13.13	559.4	22.9	2.5	9.6	0.33	642	3.87
20X-4, 115-125	296.45	23	7.86	3.10	33.7	51.27	16.12	529.2	21.02		9.2	0.66	619	3.18

is dominated by calcareous nannofossil ooze, but with diatom-bearing horizons.

Unit III extends from 92.9 to 137.8 mbsf and consists of foraminiferal nannofossil oozes (Eocene, or Eocene to uppermost Paleocene). The boundary between Units II and III occurs at an erosional hiatus (Section 113-690B-11H-3 at 82 cm) which spans the Eocene/Oligocene boundary.

Unit IV extends from 137.8 to 281.1 mbsf, and consists of nannofossil ooze-chalk with varying amounts of terrigenous sediments (quartz, clay, mica; middle Maestrichtian to uppermost Paleocene or lowermost Eocene). This unit has been divided into three subunits: Subunit IVA, from 137.8 to 177.3 mbsf (lower Eocene or upper Paleocene), is dominated by nannofossil ooze but contains at least 15% terrigenous material, including a significant but highly variable component of mica; Subunit IVB, from 177.3 to 252.5 mbsf (upper Paleocene to uppermost Maestrichtian), contains lower amounts of terrigenous material. Chalk is dominant over ooze. Subunit IVC, from 252.5 to 281.1 mbsf (upper to middle Maestrichtian), is marked by increased amounts of terrigenous sediments.

Unit V extends from 281.1 to 317 mbsf (uppermost Campanian(?) to middle Maestrichtian) and is dominated by terrigenous components, volcanic glass, and carbonate ooze and chalk. Foraminifers are much more important than in the overlying units. Dominant sediments are muddy chalk, calcareous mudstone, and nannofossil-bearing mudstone. Unit V is directly underlain by basaltic basement. Unit VI extends from 317 to 321.6 mbsf and consists of 1.71 m of amygdaloidal pyroxene-olivine basalt.

The dominant microfossil components change through the sequence as follows: Upper Cretaceous to lower Oligocene—calcareous nannofossils and planktonic foraminifers; upper Oligocene—calcareous nannofossils and diatoms; Miocene—diatoms and calcareous nannofossils; upper Miocene to Pliocene—diatoms and silicoflagellates; Quaternary—planktonic foraminifers.

Planktonic foraminifers are generally abundant from the Upper Cretaceous to the lower Oligocene, rare to common in the upper Oligocene to Pliocene and abundant in the Quaternary. Preservation is good from the Upper Cretaceous through the Eocene, moderate in the Oligocene, relatively poor in the Neogene, and good in the Quaternary. Calcareous nannofossils are abundant in the Cretaceous to the base of the Neogene, common to abundant through much of the Miocene, absent in the Pliocene, and rare in the Quaternary. Preservation is moderate to good from the Upper Cretaceous to the lower Eocene, moderate in the middle Eocene, and good in the Miocene and Oligocene. Preservation is markedly better at Site 690 than at Site 689, due to higher clay content, especially in the Cretaceous to Eocene. Diatoms are absent below the lower Oligocene. Above this level diatom preservation gradually improves, with a concomitant increase in species abundance, species, and diversity; diatoms are well preserved from the upper Miocene to the Quaternary. Radiolarians are virtually absent in sediments older than the Oligocene except for one level in the Cretaceous, are abundant but poorly preserved in the Oligocene, and are abundant and well preserved in the Neogene. Benthic foraminifers occur throughout the Upper Cretaceous and Paleogene, but are generally poorly represented in the Neogene (except for the Quaternary).

Paleoenvironmental History of Site 690

The paleoenviromental history of Site 690 is similar to that of Site 689, and hence a detailed summary such as is provided for Site 689 is not repeated here. Nevertheless, the absence of some hiatuses at Site 690 that occur in Site 689, the greater water depth of Site 690, and the presence of a fine-grained terrigenous sediment component in the Upper Cretaceous through uppermost Paleocene or lower Eocene at Site 690 (not present at Site 689) have added paleoceanographic and paleoclimatic information for the Antarctic region.

The Upper Cretaceous and Cenozoic sediments at Site 690 were laid down in a pelagic, open-ocean environment at lower and middle bathyal depths, deeper than at Site 689. As at Site 689, the sediment sequence and biotic changes reflect a sequential cooling of the Antarctic water mass, with biosiliceous facies progressively replacing carbonates during the late Cenozoic. Initial siliceous sedimentation probably occurred during the late Eocene (but this interval is not present at Site 690 as a result of a hiatus), a major increase in siliceous sedimentation occurred in the latest Oligocene, and exclusively siliceous sedimentation commenced in the late Miocene. The rate of sediment accumulation was low throughout, except for an interval in the late Paleocene to early Eocene, and decreased with time, whereas rates of sedimentation increased with time at Site 689. During the early-middle Neogene, sedimentation rates decreased to about 2 m/m.y. and then increased to 12 m/m.y. in the early Pliocene.

Sedimentation at Site 690 commenced on oceanic basement, most probably during the late Campanian to early Maestrichtian. Sediments consist of nannofossil-rich, foraminiferal-rich clays containing abundant volcanic glass. The depths at which these earliest sediments were deposited is not yet clear, because benthic foraminiferal assemblages are poorly preserved. Never-

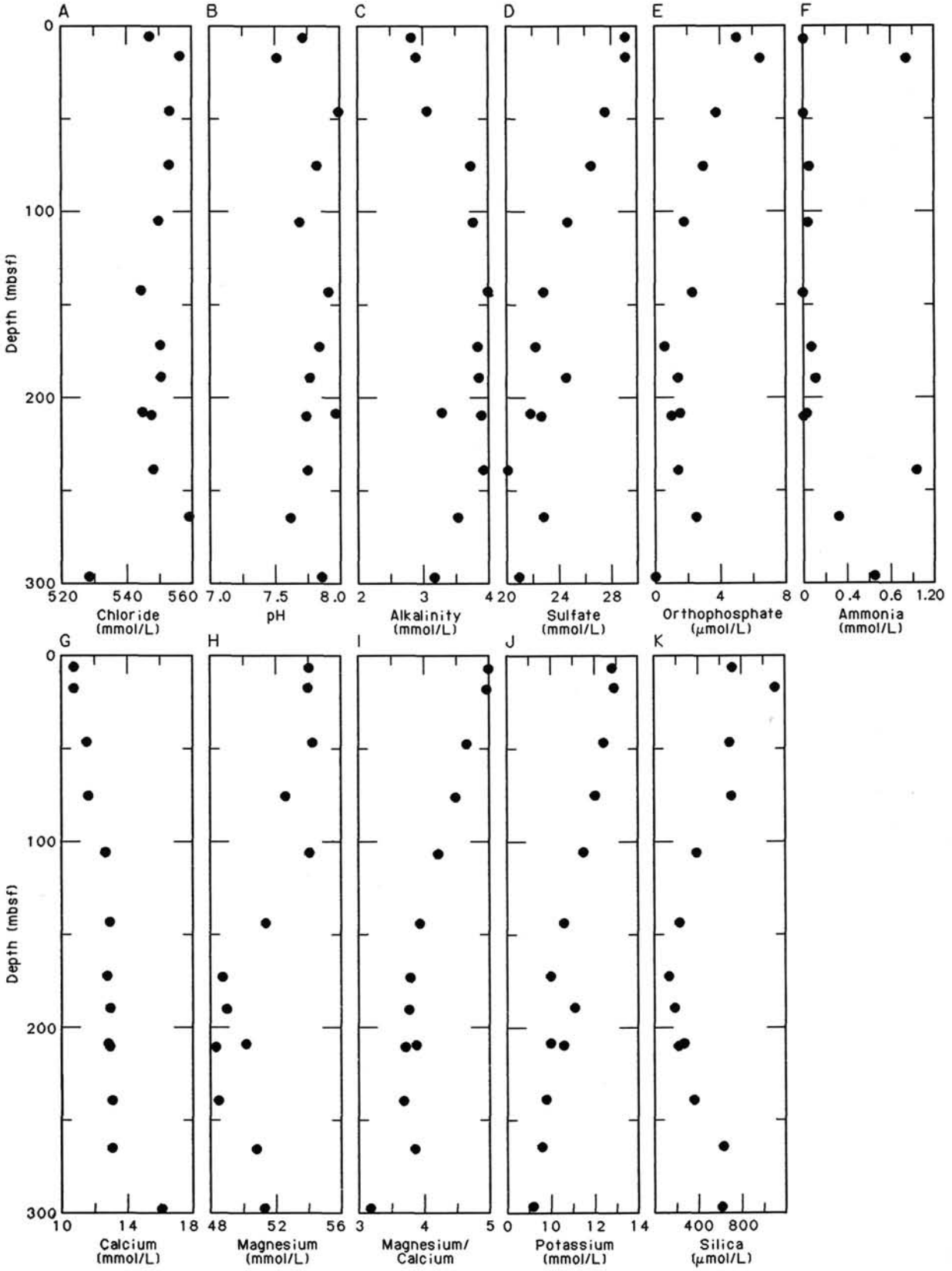

Figure 44. Concentrations vs. depth for Site 690. A. Chloride. B. pH. C. Alkalinity. D. Sulfate. E. Phosphate. F. Ammonia. G. Calcium. H. Magnesium. I. Mg/Ca ratios. J. Potassium. K. Dissolved silica..

Table 13. Low-molecular-weight hydrocarbon determinations by headspace analysis, Holes 690B and 690C.[a]

Core, section interval (cm)	Depth (mbsf)	Methane	Ethane	Propane	Age
		(μL/L)			
113-690B-					
2H-3, 145–150	6.6	0.0	0.0	0.0	Pliocene
3H-4, 120–125	17.5	0.0	0.0	0.0	Pliocene
4H-4, 145–150	27.4	1.6	0.0	0.0	Late Miocene
5H-4, 145–150	37.1	2.2	0.0	0.0	Miocene
6H-4, 117–120	46.5	2.6	0.0	0.0	Miocene
9H-4, 117–120	75.5	0.8	0.0	0.0	Oligocene
12H-5, 117–120	106.0	0.0	0.0	0.0	Eocene/Oligocene
13H-5, 147–150	116.0	0.0	0.0	0.0	Eocene
16H-4, 117–120	143.5	0.0	0.0	0.0	Paleocene/Eocene
19H-4, 112–115	172.5	6.2	0.0	0.0	Paleocene
22H-3, 117–120	189.4	7.9	0.0	0.0	Paleocene
25H-4, 112–115	209.8	5.1	0.0	0.0	Paleocene
113-690C-					
11X-3, 112–115	208.3	9.6	0.0	0.0	Paleocene
14X-4, 115–120	238.9	0.9	0.0	0.0	Paleocene
17X-2, 115–120	264.5	0.0	0.0	0.0	Cretaceous
20X-3, 147–150	295.3	0.0	0.0	0.0	Cretaceous

[a] Ratio methane/ethane is zero or infinite in all cases.

theless, they appear to represent deposition at bathyal depths. The seismic stratigraphy suggests that basement at this site could possibly have been an isolated topographic high that was subaerial for some time after its formation. If so, this might explain the absence of shallow-water indicators and the comparative youth of the sediments overlying basement. The basalt, however, is relatively unaltered and does not show evidence of subaerial weathering. An abundance of volcanic glass in the sediments directly overlying basement indicates active regional volcanism during the early stages of sediment accumulation on the Rise or erosion of volcanic material representing earlier volcanism. At the upper/lower Maestrichtian boundary, benthic faunas became more diverse and better preserved, perhaps reflecting an increase in the depth of deposition to upper to middle bathyal depths (1000–2000 m), or a climatic change. Planktonic foraminiferal faunas also showed increased diversity at that time. Very abundant and almost exclusively smectitic clay minerals in the Upper Cretaceous through lower Eocene indicate warm climatic conditions with alternating episodes of humidity and aridity in low-relief source areas.

During the Late Cretaceous, terrigenous sediments (fine-grained quartz, clay, and mica) were a very important component, and continued to be so at various intervals during the Paleocene to earliest Eocene. The prominence of this terrigenous component and its virtual absence in Site 689 is the major difference between the two sites. This clay is likely to be eolian material initially derived from East Antarctica. Its absence in sediments of similar age at Site 689, on the crest of Maud Rise and only 100 km farther away from East Antarctica, is difficult to explain, except in terms of a fortuitously located and persistent atmospheric or oceanographic boundary between the sites, or winnowing of clay minerals away from the crest of Maud Rise and redeposition in the flank area of Site 690. Alternatively, and much less probably, the terrigenous material may have been deposited from a nepheloid layer that originated on the East Antarctic slope to the south, and flowed at depths greater than 2000 m (depth of Site 689). Clays transported in a nepheloid layer from Antarctica should have been previously mixed on the continental shelf and rise, therefore reducing the possibility of sediment cycles being preserved. Furthermore, it may not have been possible for a nepheloid layer to extend that far to the north when currents at such depths were free to move to the west and southwest. In either case, East Antarctica was a rich source of fine-grained terrigenous sediments for Maud Rise during the Late Cretaceous.

As at Site 689, the terminal Cretaceous event at Site 690 is well represented, and exhibits a very similar sedimentary and microfossil record. The benthic foraminifers change less at this boundary at Site 690 than at Site 689. The biotic crisis for the planktonic microfossils apparently coincided with the beginning of an episode of volcanic activity that laid down approximately 70 cm (uncorrected for bioturbation) of inferred volcanogenic sediments (since altered to clay) at this site in the earliest Cenozoic.

The input of terrigenous sediment decreased from the Cretaceous to the Paleocene at Site 690, and calcareous nannofossils became the dominant sedimentary component for the first time. Nevertheless, the presence of a persistent but varying supply of terrigenous sediment distinguishes the Paleocene of Site 690 from Site 689. Hence, sedimentation rates were considerably higher in the Paleocene at Site 690 than at Site 689. The clays are exclu-

Table 14. Rock-Eval analyses of sediments, Holes 690B and 690C.

Core, section	Depth (mbsf)	S1	S2	S3	TOC	HI	OI	T_{max}	PI	S2/S3
		mg(HC)/g(rock)		mg(CO_2)/g(rock)	(%)	mg(HC)/g(C)		(°C)		
113-690B-										
2H-3	6.6	0.04	[a]0.10	0.21	0.01	[a]1000	2100	565	0.29	0.47
3H-4	17.5	0.15	0.79	0.00	0.07	[a]1128	0	586	0.16	—
4H-4	27.4	0.00	0.00	1.92	0.08	0	2400	299	—	0.00
5H-4	37.1	0.14	[a]1.40	0.84	0.12	[a]1166	700	564	0.09	1.66
6H-4	46.5	0.00	0.00	2.23	0.18	0	1238	383	—	0.00
9H-4	75.5	0.00	0.00	2.27	0.07	0	3242	299	—	0.00
12H-5	106.0	0.00	0.00	1.88	0.04	0	4700	484	—	0.00
16H-4	143.2	0.02	0.00	1.57	0.07	0	2242	299	1.00	0.00
19H-4	172.3	0.00	0.00	1.91	0.26	0	734	449	—	0.00
22H-3	189.1	0.02	0.00	1.27	0.08	0	1587	484	1.00	0.00
25H-4	209.67	0.00	0.00	0.86	0.02	0	4300	299	—	0.00
113-690C-										
11X-3	208.4	0.04	0.03	1.57	0.19	15	826	395	0.67	0.01
14X-4	239.0	0.00	0.00	0.85	0.03	0	2833	270	—	0.00
17X-2	265.0	0.02	0.00	1.19	0.36	0	330	270	1.00	0.00
20X-3	295.7	0.12	0.62	4.69	0.53	116	884	395	0.16	0.13

[a] Chart exhibits rising baseline without peaks.

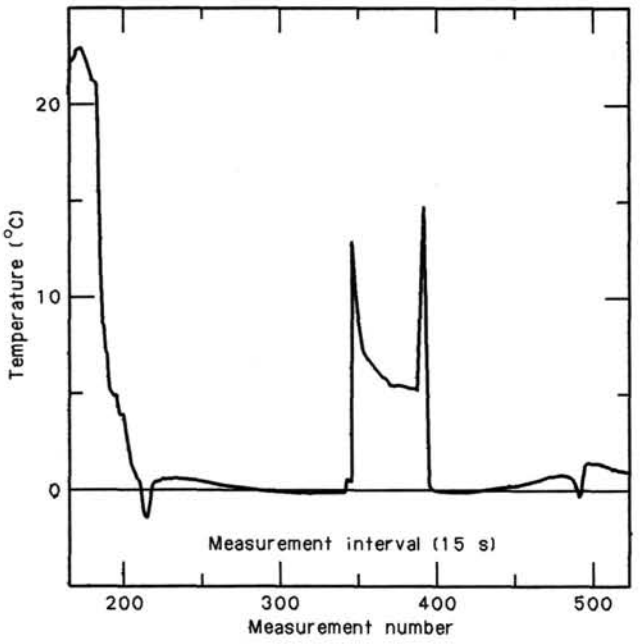

Figure 45. The result of the temperature measurements at Core 113-690C-4H with the Von Herzen APC tool #5 at 35.2 mbsf.

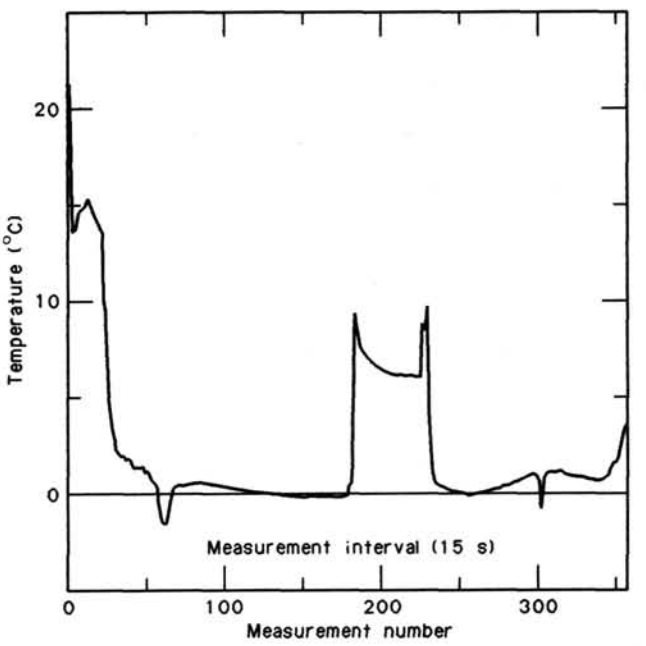

Figure 46. The result of the temperature measurements at Core 113-690C-9H with the Von Herzen APC tool #5 at 83.6 mbsf.

sively smectite in the uppermost Paleocene, with kaolinite-chlorite occurring sparsely through the upper Paleocene. Illite is almost entirely absent. This suggests that conditions were warm and humid during the Paleocene in this sector of East Antarctica, which was probably unglaciated. The reddish-yellow to white cycles are not associated with large changes in clay mineralogy, although the lighter sediments are slightly enriched in smectite, perhaps reflecting slight variations in weathering in Antarctica due to climatic fluctuations. The origin of the reddish colors is still unclear, but probably reflects the climatic conditions of the source area. Distinctive climatic conditions probably existed during the Paleocene, because only this interval exhibits the reddish tints. The cyclicity of the reddish to white intervals supports the eolian origin of the terrigenous fraction. The evidence from the clays and their mineralogy supports the relative warmth of the Paleocene inferred from marine biogeographic evidence. As at Site 689, the Paleocene and the lowermost Eocene at Site 690 is the only interval containing the warmth-loving discoasters. Water depths at Site 690 approached those of the present day (upper abyssal; 2500 m) by Paleocene to early Eocene time.

During the latest Paleocene to early Eocene, an interval not represented at Site 689, there was a further increase in the terrigenous sedimentation rate. Large changes in the benthic foraminiferal assemblages just before the end of the Paleocene probably reflected global faunal changes. At the same time there was an increase in the kaolinite/chlorite content, although Eocene clays continued to be dominated by smectite, suggesting a continuation of relatively warm climatic conditions. Calcareous nannofossils and planktonic foraminifers continued to dominate the biogenic fraction, but the presence of zeolites indicates that an original biosiliceous component was present and has since dissolved and been reprecipitated.

At Site 690 parts of the lower Eocene (parts of calcareous nannofossil zones CP10/CP11) to lowermost Oligocene are not represented in the sediments (Fig. 42). During the early Oligocene, illite first appeared as a major clay mineral, while smectite decreased. This change suggests that hydrolysis strongly decreased on Antarctica, because of major cooling and/or an increase in aridity, supporting inferences drawn from existing biogeographic and stable isotopic data. Benthic foraminiferal assemblages decreased in diversity and lost buliminid species across the Eocene/Oligocene boundary hiatus, possibly reflecting intensification of bottom currents. Biosiliceous sediment first appeared above the Eocene/Oligocene hiatus and consists of diatoms and radiolarians, although sediments continue to be dominated by calcareous nannofossil ooze. At this same level, planktonic foraminifers become unimportant as a sediment component. Near the end of the Oligocene, the diatoms dramatically increased in abundance with a corresponding decrease in the calcareous nannofossils, as at Site 689. Another hiatus or interval of drastically reduced sedimentation rates straddles the Oligocene/Miocene boundary.

The Neogene sedimentary record is very similar to that at Site 689, but overall sedimentation rates were lower at Site 690. Siliceous sediments began to be deposited just before the beginning of the Neogene, reflecting a further major development of the Antarctic water mass. Nannofossil oozes and diatom-bearing to diatom nannofossil oozes were deposited alternately until the middle late Miocene. This alternation may represent the repeated passage of an oceanographic front over the site, or the intermittent existence of a front. During the early part of this transitional period, in the latest Oligocene to early Miocene, the calcareous nannofossils and planktonic foraminiferal assemblages tended to be cool to temperate and relatively diverse, whereas in the middle to late Miocene interval they were essentially monospecific. Diversity of benthic foraminiferal assemblages also decreased, especially at the end of the early Miocene. Calcareous nannofossil and planktonic foraminiferal diversities were highest in the early Miocene, indicating the warmest conditions for the Neogene and supporting inferences from existing stable isotopic data. In general, planktonic foraminifers are less abundant in the Neogene of Site 690 than at Site 689 because of the greater water depths.

Beginning in the middle late Miocene, only biosiliceous sediments were deposited, as at Site 689. The uppermost Miocene is marked by a hiatus probably resulting from increased bottom currents. Siliceous sedimentation continued during the Pliocene

and, as at Site 690, the upper Pliocene and part of the Quaternary are missing in another hiatus. Following this hiatus, a thin (2 m) layer of foraminiferal ooze was deposited, consisting of a single planktonic foraminiferal species *Neogloboquadrina pachyderma*, with a low-diversity fauna of calcareous benthic foraminifers dominated by *Epistominella exigua*, and including rare calcareous nannofossils of two taxa. One of these, *Coccolithus pelagicus*, has been absent from the Southern Hemisphere since the middle Holocene, but still occurs in the Northern Hemisphere where it has a temperature preference of between 6° and 14°C. There are no records of coccolithophorids living at the latitude of Maud Rise in the present day, nor were they recorded from the Pliocene. This suggests that, at some time during the Pleistocene to Holocene, conditions were warmer than any time during the previous 5 m.y.

REFERENCES

Anderson, J. B., 1975. Ecology and distribution of Foraminifera in the Weddell Sea of Antarctica. *Micropaleontology,* 21:69–91.

Baker, D. E., Gass, I. G., Harris, P. G., and le Maitre, R. W., 1964. The volcanological report of the Royal Soc. Exp. to Tristan da Cunha, 1962. *Philos. Trans. R. Soc. London, A,* 256:439–575.

Basov, I. A., and Krasheninnikov, V. A., 1983. Benthic foraminifers in Mesozoic and Cenozoic sediments of the southwestern Atlantic as an indicator of paleoenvironment, Deep Sea Drilling Project Leg 71. *In* Ludwig, W. J., Krasheninnikov, V. A., et al., *Init. Repts. DSDP,* 71: Washington (U.S. Govt. Printing Office), 739–820.

Berggren, W. A., Kent, D. V., Flynn, J. J., and Van Couvering, J. A., 1985. Cenozoic geochronology. *Geol. Soc. Am. Bull.*, 96:1407–1418.

Boersma, A., and Premoli-Silva, I., 1983. Paleocene planktonic foraminiferal biogeography and the paleoceanography of the Atlantic Ocean. *Micropaleontology*, 29:355–381.

Bolli, H. M., 1974. Jurassic and Cretaceous calcisphaerulidae from DSDP Leg. 27, eastern Indian Ocean. *In* Veevers, J. J., Heirtzler, J. R., et al., *Init. Repts. DSDP*, 27: Washington (U.S. Govt. Printing Office), 843–907.

Boyce, R. E., 1976. Definitions and laboratory techniques of compressional sound velocity parameters and water content, wet-bulk density, and porosity parameters by gravimetric and gamma ray attenuation techniques. *In* Schlanger, S. O., Jackson, E. D., et al., *Init. Repts. DSDP*, 33: Washington (U.S. Govt. Printing Office), 931–955.

Bremer, M. L., and Lohmann, G. P., 1982. Evidence for primary control of the distribution of certain Atlantic Ocean benthonic foraminifera by degree of carbonate saturation. *Deep-Sea Res.*, 19:987–988.

Carlson, R. L., Gangi, A. F., and Snow, K. R., 1986. Empirical reflection travel time versus depth and velocity versus depth functions for the deep-sea sediment column. *J. Geophys. Res.*, 91:8249–8266.

Chamley, H., 1979. North Atlantic clay sedimentation and paleoenvironment since the Late Jurassic. *In* Talwani, M., Hay, W., and Ryan, W.B.F., (Eds.), *Deep Drilling Results in the Atlantic Ocean: Continental Margins and Paleoenvironment*: Washington (Am. Geophys. Union), 342–360.

Chen, P. H., 1975. Antarctic radiolaria. *In* Hayes, D. E., Frakes, L. A., et al., *Init. Repts. DSDP*, 28: Washington (U.S. Govt. Printing Office), 407–474.

Cousens, B. L., Chase, R. L., and Schilling, J. G., 1985. Geochemistry and origin of volcanic rocks from Tuzo Wilson and Bowie Seamounts, northeast Pacific ocean. *Can. J. Earth Sci.*, 22: 1609–1617.

Dailey, D. H., 1983. Late Cretaceous and Paleocene benthic foraminifers from Deep Sea Drilling Project Site 516, Rio Grande Rise, Western South Atlantic Ocean. *In* Barker, P. F., Carlson, R. L., Johnson, D. A., et al., *Init. Repts. DSDP*, 72: Washington (U.S. Govt. Printing Office), 757–782.

Douglas, R., and Woodruff, F., 1981. Deep sea benthic foraminifera. *In* Emiliani, C. (Ed.), *The Oceanic Lithosphere* (Vol. 7): New York (Wiley), 1233–1327.

Engle, A.E.J., Engle, C. G., and Havens, R. G., 1965. Chemical characteristics of oceanic basalts and the upper mantle. *Geol. Soc. Am. Bull.*, 76:719–734.

Fütterer, D. K., 1984. Pithonelloid calcareous dinoflagellates from the Upper Cretaceous and Cenozoic of the Southeastern Atlantic Ocean, Deep Sea Drilling Program. *In* Moore, T. C., Jr., Rabinowitz, P. D., et al., *Init. Repts. DSDP*, 74: Washington (U.S. Govt. Printing Office), 533–541.

Grikurov, G. E., 1982. Structure of Antarctica and outline of its evolution. *In* Craddock, C., (Ed.), *Antarctic Geoscience,* I.U.G.S. Series B, 4:791–804.

Grobe, H., 1986. Sedimentation processes on the Antarctic continental margin at Kapp Norvegia during the Late Pleistocene. *Geol. Rundschau*, 75:97–104.

Haq, B. U., 1980. Biogeographic history of Miocene calcareous nannoplankton and paleoceanography of the Atlantic Ocean. *Micropaleontology*, 26:414–443.

Hemleben, C., and Troester, J., 1984. Campanian-Maestrichtian deepwater foraminifers from Hole 543A, Deep Sea Drilling Project. *In* Biju-Duval, B., Moore, J. C., et al., *Init. Repts. DSDP*, 78A: Washington (U.S. Govt. Printing Office), 509–534.

Hodell, D. A., and Kennett, J. P., 1985. Miocene paleoceanography of the South Atlantic Ocean at 22, 16, and 8 Ma. *Geol. Soc. Am. Mem.*, 163:317–337.

Huber, B. T., in press. Upper Campanian-Paleocene foraminifera from James Ross Island region ()Antarctic Peninsula). *In* Feldmann, R. M., and Woodburne, M. O. (Eds.), Geology and Paleontology of Seymour Island: *Geol. Soc. Am. Mem.*, 169.

Jenkins, D. G., 1975. Cenozoic planktonic foraminiferal biostratigraphy of the Southwestern Pacific and Tasman Sea, DSDP Leg 29. *In* Kennett, J. P., and Houtz, R. E., et al., *Init. Repts. DSDP*, 29: Washington (U.S. Govt. Printing Office), 449–467.

Jenkins, D. G., and Srinivasan, M. S., 1985. Cenozoic planktonic foraminifers of the southwest Pacific. *In* Kennett, J. P., and von der Borch, C. C., et al., *Init. Repts. DSDP*, 90: Washington (U.S. Govt. Printing Office), 795–834.

Krasheninnikov, V. A., and Basov, I. A., 1983 Cenozoic planktonic foraminifers of the Falkland Plateau and Argentina Basin, Deep Sea Drilling Project, Leg 71. *In* Ludwig, W. J., Krasheninnikov, V. A., et al, *Init. Repts. DSDP*, 71: Washington (U.S. Govt. Printing Office), 821–858.

Martini, E., 1971. Standard Tertiary and Quaternary calcareous nannofossil zonation. *Proc. II Planktonic Conf.*, Roma 1970: Rome (Ed. Technosciencza), 739–785.

McIntyre, A., and Bé, A.W.H., 1967. Modern Coccolithophoridae of the Atlantic Ocean—1. Placoliths and crytoliths. *Deep-Sea Res.*, 14: 561.

Miller, K. G., and Fairbanks, R. G., 1985. Oligocene and Miocene global carbon isotope cycles and abyssal circulation changes. *In* Sundquist, E. T., and Broecker, W. S. (Eds.), *The Carbon Cycle and Atmospheric CO_2: Natural Variations, Archaen to Present*, Am. Geophys. Union Monogr., 32:469–486.

Moore, J. G., Clague, D. A., and Normark, W. R., 1982. Diverse basalt types from Loihi Seamount, Hawaii. *Geology, 10:88–92.*

Murphy, M. G., and Kennett, J. P., 1986. Development of latitudinal thermal gradients during the Oligocene: oxygen-isotope evidence from the southwest Pacific. *In* Kennett, J. P., von der Borch, C. C., et al., *Init. Repts. DSDP*, 90: Washington (U.S. Govt. Printing Office), 1347–1360.

Pearce, J. A., and Cann, J. R., 1973. Tectonic setting of basic volcanic rocks determined using trace element analyses. *Earth Planet. Sci. Lett.*, 19:290–300.

Robert, C., 1987. Clay mineral associations and structural evolution of the South Atlantic: Jurassic to Eocene. *Palaeogeogr., Palaeoclimatol., Palaeoecol.*, 58:87–108.

Robert, C., and Maillot, H., 1983. Paleoenvironmental significance of clay mineralogical and geochemical data, Southwest Atlantic, DSDP Legs 36 and 71. *In* Ludwig, W. J., Krasheninnikov, V. A., et al, *Init. Repts. DSDP*, 71: Washington (U.S. Govt. Printing Office), 317–343.

Robert, C., Caulet, J. P., and Maillot, H., in press. Evolution climatique et hydrologique en mer de Ross (Site DSDP 274) au Néogéne, d'aprés les associations de Radiolaires, la minéralogie des argiles et la géochimie minérale. *C. R. Acad. Sci. Paris.*

Roeder, P. L. and Emslie, R. F., 1970. Olivine-liquid equilibrium. *Contrib. Mineral. Petrol.*, 29:275–289.

Savin, S., Douglas, R. G., and Stehli, F. G., 1975. Tertiary marine paleotemperatures. *Geol. Soc. Am. Bull.*, 86:1499–1510.

Savin, S. M., Douglas, R. G., Keller, G., Killingley, J. S., Shaughnessy, L., Sommer, M. A., Vincent, E., and Woodruff, F., 1981. Miocene benthic foraminiferal isotope record: A synthesis. *Mar. Micropaleontol.*, 6:423–450.

Shackleton, N. J., 1986. Paleogene stable isotope events. *Palaeogeogr., Palaeoclimatol., Palaeoecol.*, 57:91–102.

Shackleton, N. J., and Kennett, J. P., 1975. Paleotemperature history of the Cenozoic and the initiation of Antarctic glaciation: oxygen and carbon isotope analyses in DSDP Sites 277, 279, and 281. *In* Kennett, J. P., Houtz, R. E., et al., *Init. Repts. DSDP*, 29: Washington (U.S. Govt. Printing Office), 743–755.

Shaw, C. A., and Ciesielski, P. F., 1983. Silicoflagellate biostratigraphy of middle Eocene to Holocene subantarctic sediments recovered by Deep Sea Drilling Project, Leg 71. *In* Ludwig, W. J., Krasheninnikov, V. A., et al., *Init. Repts. DSDP*, 71: Washington (U. S. Govt. Printing Office), 687–737.

Sliter, W. V., 1977. Cretaceous foraminifers from the southwestern Atlantic Ocean, Leg 36, Deep Sea Drilling Project. *In* Barker, P. F., Dalziel, J.W.D., et al., *Init. Repts. DSDP*, 36: Washington (U.S. Govt. Printing Office), 519–574.

Sun, S. S., and Hanson, G. N., 1975. Evolution of the mantle: geochemical evidence from alkali basalt. *Geology*, 3:297–302.

Sverdrup, H. U., Johnson, M. W., and Fleming, R., (Eds.), 1942. *The Oceans: Their Physics, Chemistry and General Biology*: Englewood Cliffs, N.J. (Prentice-Hall).

Thomas, E., 1985. Late Eocene to Recent deep sea benthic foraminifers from the central equatorial Pacific Ocean. *In* Mayer, L., Theyer, F., Thomas, E., et al., *Init. Repts. DSDP*, 85: Washington (U.S. Govt. Printing Office), 655–694.

_____, 1987. Late Oligocene to Recent benthic foraminifers from Deep Sea Drilling Project Sites 608 and 610, northeastern North Atlantic. *In* Ruddiman, W. F., Kidd, R. B., Thomas, E., et al., *Init. Repts. DSDP*, 94: Washington (U.S. Govt. Printing Office), 997–1034.

Thompson, G., Humphris, S. E., and Schilling, G., 1983. Petrology and geochemistry of basaltic rocks from Rio Grande Rise, South Atlantic, Hole 516F. *In* Barker, P. F., Carlson, R. L., Johnson, D. A., et al., *Init. Repts. DSDP*, 72: Washington (U.S. Govt. Printing Office), 457–466.

Thompson, G., and Humphris, S. E., 1984. Petrology and geochemistry of rocks from the Walvis Ridge. DSDP Leg 74, Sites 525, 527 and 528. *In* Moore, T. C., Jr., Rabinowitz, P. D., et al., *Init. Repts. DSDP*, 74: Washington (U.S. Govt. Printing Office), 755–764.

Tjalsma, R. C., and Lohmann, G. P., 1983. Paleocene-Eocene bathyal and abyssal benthic Foraminifera from the Atlantic Ocean. *Micropaleontol., Spec. Publ.*, 4:1–90.

Van Morkhoven, F.P.C.M., Berggren, W. A., and Edwards, A. S., 1986. Cenozoic cosmopolitan deep-water benthic Foraminifera. *Bull. Cent. Rech. Explor. Prod. (Elf-Aquitaine Mem.)*, 11:421.

Von Herzen, R. P., and Maxwell, A. E., 1959. The measurement of thermal conductivity of deep-sea sediments by a needle probe method. *J. Geophys. Res.*, 65:1535–1541.

Weaver, F. M., and Gombos, A. M., 1981. Southern high-latitude diatom biostratigraphy. *SEPM Spec. Publ.*, 32:445–470.

Wise, S. W., 1983. Mesozoic and Cenozoic calcareous nannofossils recovered by Deep Sea Drilling Project Leg 71 in the Falkland Plateau region, southwest Atlantic Ocean. *In* Ludwig, W. J., Krasheninnikov, V. A., et al., *Init. Repts. DSDP*, 71: Washington (U.S. Govt. Printing Office), 481–550.

Wise, S. W., and Wind, F. H., 1977. Mesozoic and Cenozoic calcareous nannofossils recovered by DSDP Leg 36 drilling on the Falkland Plateau, Southwest Atlantic sector of the Southern Ocean. *In* Barker, P. F., Dalziel, I.W.D., et al., *Init. Repts. DSDP*, 36: Washington (U.S. Govt. Printing Office), 269–492.

Wollast, R., 1974. The silica problem. *In* Goldberg, E. D. (Ed.), *The Sea*: New York (Wiley), 5:359–353.

Woodruff, F., 1985. Changes in Miocene deep-sea benthic foraminiferal distribution in the Pacific Ocean: Relationship to paleoceanography. *Geol. Soc. Am. Mem.*, 163:31–172.

Ms 113A-107

SITE 690 HOLE A CORE 1H CORED INTERVAL 2914.3-2922.0 mbsl; 0.0-7.7 mbsf

TIME-ROCK UNIT: LOWER PLIOCENE / UPPER PLIOCENE

BIOSTRAT. ZONE/FOSSIL CHARACTER: LOWER UPSILON Zone (*N. reinholdii - N. angulata*); *C. elliptopora / A. ingens*; C,PM; A,G; B

PALEOMAGNETICS; PHYS. PROPERTIES; CHEMISTRY

SECTION; METERS; GRAPHIC LITHOLOGY; DRILLING DISTURB.; SED. STRUCTURES; SAMPLES

LITHOLOGIC DESCRIPTION

FORAMINIFERAL OOZE and RADIOLARIAN-BEARING DIATOM OOZE

Major lithologies: Foraminiferal ooze, light yellowish brown (2.5Y 6/3). Radiolarian-bearing diatom ooze, white (10YR 8/2), pale yellow (2.5YR 7/3), yellow (10YR 7/4), and light yellowish brown (10YR 6/4). Diatom ooze, white (10YR 8/2), very pale brown (10YR 7/3). Foraminiferal diatom ooze, light yellowish brown (2.5Y 6/3).

Bioturbation is minor to absent. Specific types include *Planolites* and halo burrows. Cyclic and gradational color changes from white to yellow are observed. Color changes are also associated with bioturbation. Ice-rafted dropstones occur in Sections 1, 2, 3, and 5, ranging up to 10 mm in length. They tend to be found where bioturbation is absent.

SMEAR SLIDE SUMMARY (%):

	1, 50 D	2, 50 D	3, 50 D	4, 50 D	5, 50 D	6, 50 D	7, 50 D
COMPOSITION:							
Quartz	Tr	—	—	—	—	—	—
Clay	—	—	—	—	—	Tr	—
Accessory minerals:							
Horneblende	—	Tr	Tr	—	—	—	—
Foraminifers	95	91	30	5	—	—	—
Nannofossils	—	6	—	—	—	1	—
Diatoms	5	3	59	78	90	94	98
Radiolarians	—	—	9	12	10	3	2
Silicoflagellates	—	—	2	5	—	2	—

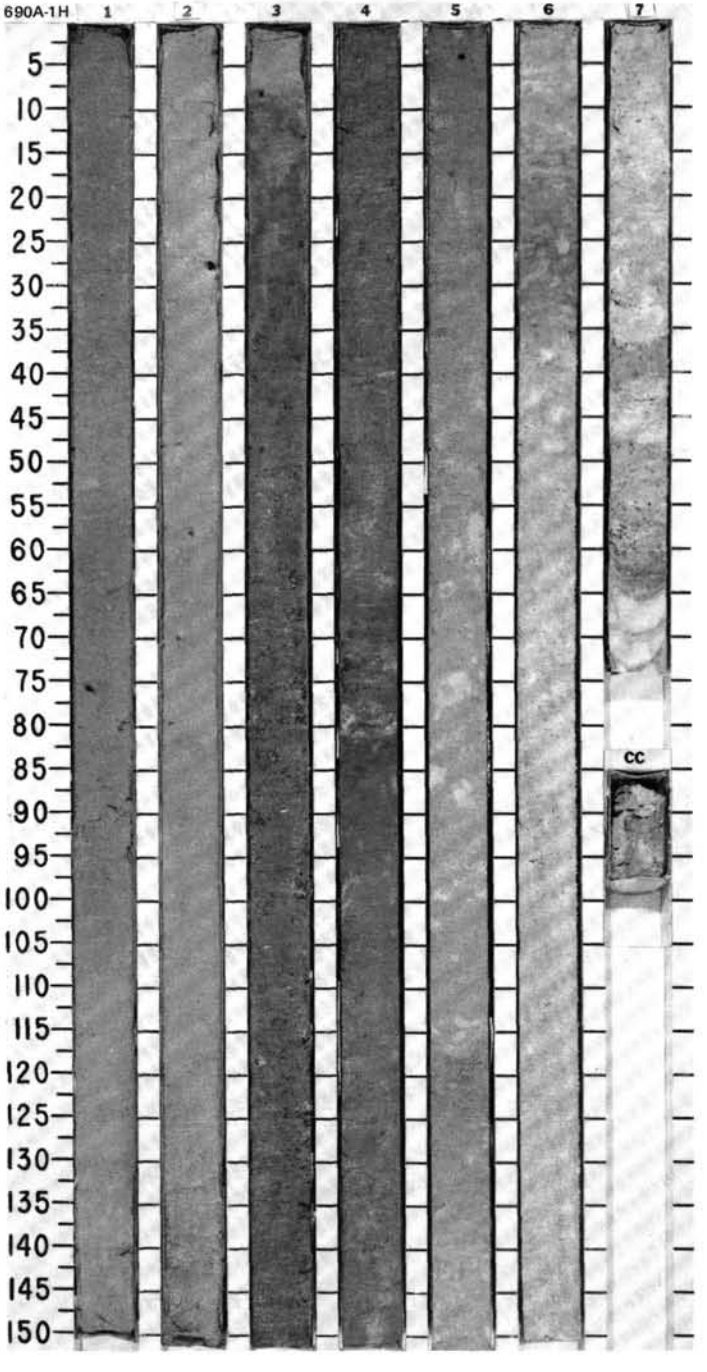

SITE 690 HOLE B CORE 1H CORED INTERVAL 2914.3-2916.4 mbsl; 0-2.1 mbsf

TIME-ROCK UNIT	BIOSTRAT. ZONE/ FOSSIL CHARACTER: FORAMINIFERS	NANNOFOSSILS	RADIOLARIANS	DIATOMS	PALYNOMORPHS	PALEOMAGNETICS	PHYS. PROPERTIES	CHEMISTRY	SECTION	METERS	GRAPHIC LITHOLOGY	DRILLING DISTURB.	SED. STRUCTURES	SAMPLES
UPPER PLIOCENE - QUATERNARY		*Pseudoemiliania lacunosa* Zone	LOWER *Upsilon* (?)	F,P *C. elliptopora* / *A. ingens*			$\phi_{7.70}$ 1.59; V-1581 $\phi_{7.70}$ 1.56	76.6	1	0.5, 1.0	VOID			*
									2					*

LITHOLOGIC DESCRIPTION

FORAMINIFERAL OOZE and DIATOM-BEARING FORAMINIFERAL OOZE

Major lithologies: Foraminiferal ooze, pale yellow (2.5Y 7/3). Diatom-bearing foraminiferal ooze, light gray (2.5 Y 7/2).

Bioturbation is minor and includes *Planolites* and halo burrows.

SMEAR SLIDE SUMMARY (%):

	1, 30 D	2, 30 D
COMPOSITION:		
Quartz	Tr	—
Foraminifers	92	88
Diatoms	8	12

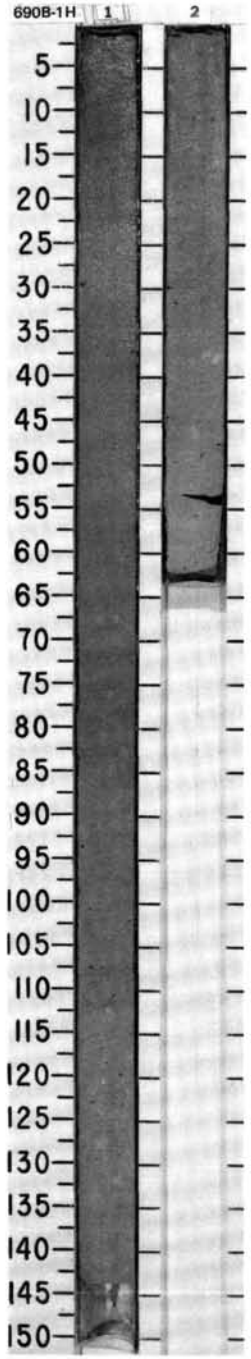

SITE 690 HOLE B CORE 2H CORED INTERVAL 2916.4-2926.0 mbsl; 2.1-11.7 mbsf

TIME-ROCK UNIT: LOWER PLIOCENE

BIOSTRAT. ZONE/FOSSIL CHARACTER: FORAMINIFERS C, G; NANNOFOSSILS B; RADIOLARIANS A, G; DIATOMS A, G; PALYNOMORPHS B

LOWER *Upsilon* Zone

N. angulata - *N. reinholdii*

PALEOMAGNETICS

PHYS. PROPERTIES: V-1511 Φ=80 γ=1.26; V-1499 Φ=86 γ=1.27; V-1511 Φ=86 γ=1.27; V-1511 Φ=80 γ=1.30

CHEMISTRY: 0.0%; 0.6%; 0.0%; 0.0%

SECTION: 1, 2, 3, 4, 5, 6, 7, CC

METERS: 0.5, 1.0

GRAPHIC LITHOLOGY

DRILLING DISTURB.

SED. STRUCTURES

SAMPLES: IW

LITHOLOGIC DESCRIPTION

RADIOLARIAN-BEARING DIATOM OOZE, DIATOM OOZE, and SILICOFLAGELLATE-BEARING DIATOM OOZE

Major lithologies: Radiolarian-bearing diatom ooze, white (10YR 8/2), light gray (10YR 7/2), yellow (10YR 7/4), and very pale brown (10YR 8/3, 10YR 7/4). Diatom ooze, pure white (10YR 8/0), white (10YR 8/2), very pale brown (10YR 7/4), and light yellowish brown (10YR 6/4). Silicoflagellate-bearing diatom ooze, pure white (10YR 8/0), light gray (2.5Y 7/2), and yellowish brown (10YR 5/4).

Minor lithology: Diatom-bearing foraminiferal ooze, light gray (10YR 7/2). Bioturbation and coring disturbance have mixed the boundary. It forms a thin veneer covering many parts of the core.

Bioturbation is minor to moderate throughout the core. Specific types include *Planolites*, halo burrows, *Zoophycos*, and vertical burrows. Distinct light to dark cyclic color changes are present and are particularly well developed in Section 2. Dropstones are present in Section 2, at 45, 90, and 115 cm. They range from 4 to 6 mm in length and tend to occur in the darker units.

SMEAR SLIDE SUMMARY (%):

	1, 120 D	2, 120 D	3, 120 D	4, 120 D	5, 120 D	6, 120 D	7, 30? D
COMPOSITION:							
Quartz	—	—	—	—	—	—	Tr
Foraminifers	—	—	—	—	Tr	—	—
Diatoms	87	80	86	95	95	77	82
Radiolarians	8	15	12	5	3	8	8
Silicoflagellates	5	5	2	Tr	2	15	10

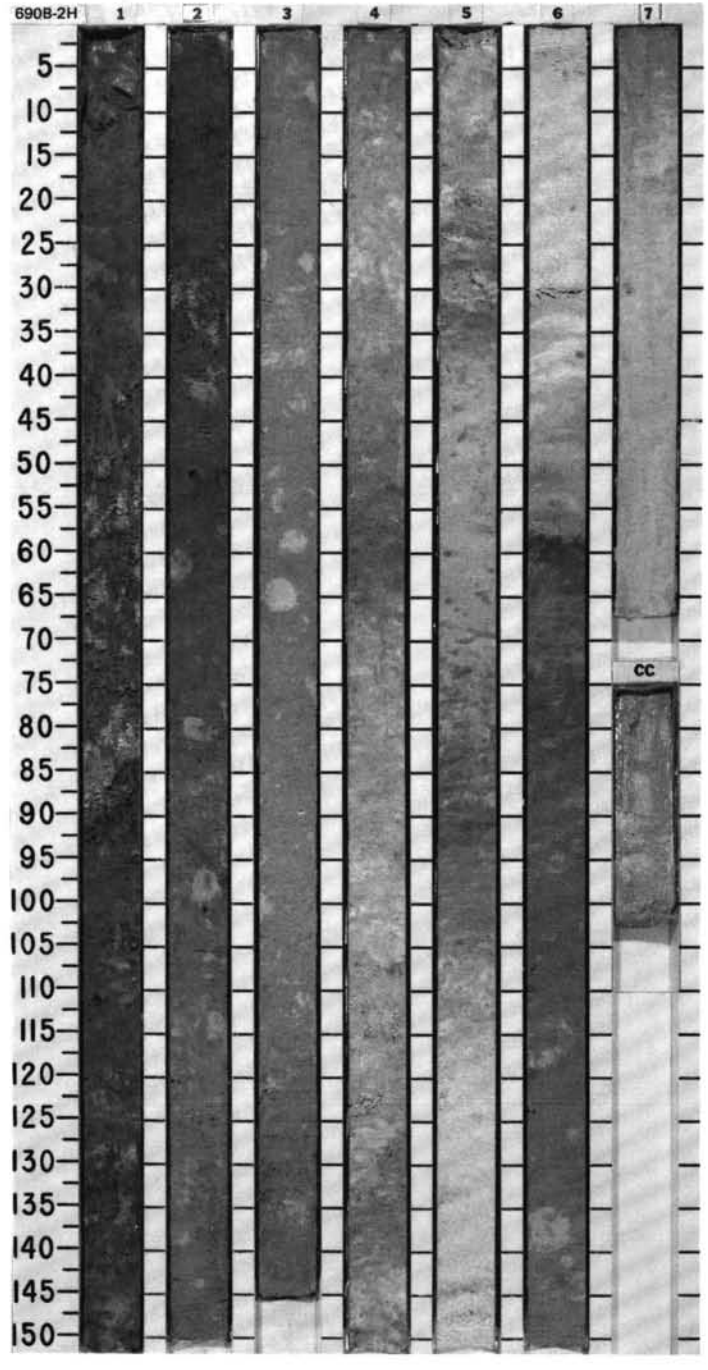

SITE 690 HOLE B CORE 3H CORED INTERVAL 2926.0-2035.7 mbsl; 11.7-21.4 mbsf

TIME-ROCK UNIT	BIOSTRAT. ZONE/ FOSSIL CHARACTER: FORAMINIFERS	NANNOFOSSILS	RADIOLARIANS	DIATOMS	PALYNOMORPHS	PALEOMAGNETICS	PHYS. PROPERTIES	CHEMISTRY	SECTION	METERS	GRAPHIC LITHOLOGY	DRILLING DISTURB.	SED. STRUCTURES	SAMPLES
LOWER PLIOCENE	B	B	A,G UPPER *C. spongothorax*	A,G *D. hustedtii* / *N. reinholdii* - *N. angulata*	B		V=1527 ● ϕ=70 / ±1.45	0.3% ● 0.0%	1	0.5				*
							V=1508 ● ϕ=84 / ±1.30	● 0.0%	2	1.0				*
							V=1514 ● ϕ=78 / ±1.24	● 0.0%	3					*
									4					*
									5					*
									6					*
									7					*
									CC					IW OC

LITHOLOGIC DESCRIPTION

SILICOFLAGELLATE-DIATOM OOZE, SILICOFLAGELLATE-BEARING DIATOM OOZE, SILICOFLAGELLATE- AND RADIOLARIAN-BEARING DIATOM OOZE.

Major lithologies: Silicoflagellate-diatom ooze, white (10YR 8/2) to very pale brown (10YR 8/3) and pale brown (10YR 6/3). Silicoflagellate-bearing diatom ooze, white (2.5Y 8/2) to light gray (2.5Y 7/2). Silicoflagellate- and radiolarian-bearing diatom ooze, white (10YR 8/2) to light gray (2.5Y 7/2) and brown (2.5Y 5/3). Radiolarian-bearing diatom ooze, light gray (2.5Y 7/2) and light olive brown (2.5Y (6/4) to olive brown (2.5Y 4/3).

Bioturbation minor to moderate. Small manganese concretion in Section 5, 68 cm. Dropstones, mm size, in Section 6, 53 and 117 cm.

SMEAR SLIDE SUMMARY (%):

	1, 50 D	2, 50 D	3, 50 D	4, 50 D	5, 50 D	6, 50 D	7, 50 D
COMPOSITION:							
Quartz	—	—	—	—	—	Tr	—
Calcite/dolomite	—	—	—	—	—	Tr	—
Accessory minerals	Tr	—	—	—	—	Tr	—
Diatoms	75	80	55	60	75	70	70
Radiolarians	15	5	5	2	20	30	25
Silicoflagellates	10	15	40	38	5	—	5

SITE 690 HOLE B CORE 4H CORED INTERVAL 2935.7-2945.4 mbsl; 21.4-31.1 mbsf

TIME-ROCK UNIT: UPPER MIOCENE / LOWER PLIOCENE

BIOSTRAT. ZONE/FOSSIL CHARACTER:
- FORAMINIFERS: B
- NANNOFOSSILS: A, G — no Zone — Barren
- RADIOLARIANS: A, G — LOWER *C. spongothorax*
- DIATOMS: A, G — *D. hustedtii*
- PALYNOMORPHS: B

PALEOMAGNETICS: Φ-62 γ-1.76 V-1525 ● | Φ-72 γ-1.56 V-1503 ● | Φ-94 γ-1.59 V-1523 ●

PHYS. PROPERTIES: ●84.5% ●80.9% ●71.9%

CHEMISTRY: ●0.7%

SECTION: 1 2 3 4 5 6 CC

METERS: 0.5 1.0

GRAPHIC LITHOLOGY

DRILLING DISTURB.

SED. STRUCTURES

SAMPLES

LITHOLOGIC DESCRIPTION

DIATOM OOZE, RADIOLARIAN-BEARING DIATOM OOZE, NANNOFOSSIL-DIATOM OOZE, and DIATOM-BEARING NANNOFOSSIL OOZE

Major lithologies: Diatom ooze, light olive gray (2.5Y 6/4). Radiolarian-bearing diatom ooze, light olive gray (2.5Y 6/4). Nannofossil-diatom ooze, white (10YR 8/0, 8/2) and light gray (10YR 7/2, 7/3) to brown (10YR 5/3). Diatom-bearing nannofossil ooze, white (10YR 8/0, 8/1, 8/2).

Bioturbation is minor to moderate throughout core.

SMEAR SLIDE SUMMARY (%):

COMPOSITION:	1, 50 D	2, 50 D	3, 50 D	4, 50 D	5, 50 D	6, 50 D
Quartz	1	Tr	—	—	—	—
Feldspar	Tr	—	—	—	—	—
Volcanic glass	—	1	—	—	Tr	—
Nannofossils	2	—	40	85	75	74
Diatoms	94	87	55	15	25	25
Radiolarians	3	10	2	Tr	Tr	1
Silicoflagellates	Tr	3	3	—	—	—

SITE 690 HOLE B CORE 5H CORED INTERVAL 2945.4-2955.1 mbsl; 31.1-40.8 mbsf

TIME-ROCK UNIT: MIDDLE MIOCENE

BIOSTRAT. ZONE/FOSSIL CHARACTER:
- FORAMINIFERS: C, G — UPPER LOWER MIOCENE
- NANNOFOSSILS: A, G — no Zone
- RADIOLARIANS: C, P — MIDDLE or LOWER MIOCENE
- DIATOMS: F, P — *D. hustedtii* / *D. lauta* - *N. denticuloides*
- PALYNOMORPHS: B — *N. grossepunctata* - *C. lewisianus*

PALEOMAGNETICS

PHYS. PROPERTIES: ϕ=80 γ=1.54 V=1525● ϕ=75 γ=1.46 V=1508● ϕ=83 γ=1.76 V=1543●

CHEMISTRY: ● 0.8% ● 0.0% ● 36.4% ● 84.3%

SECTION: 1, 2, 3, 4, 5, 6, 7, CC

METERS: 0.5, 1.0

GRAPHIC LITHOLOGY

DRILLING DISTURB.

SED. STRUCTURES

SAMPLES

LITHOLOGIC DESCRIPTION

DIATOM-NANNOFOSSIL OOZE, DIATOM-BEARING NANNOFOSSIL OOZE, DIATOM OOZE, MUD-BEARING DIATOM OOZE, and CLAY-BEARING DIATOM OOZE

Major lithologies: Diatom-nannofossil ooze, white (10YR 8/0, 8/1) to light gray (10YR 7/2). Diatom-bearing nannofossil ooze, white (10YR 8/0, 8/1) to pale brown (10YR 6/3) and brown (10YR 5/3). Diatom ooze, light yellowish brown (2.5Y 6/4) to olive brown (2.5Y 4/4). Mud-bearing diatom ooze, olive brown (2.5Y 4/4). Clay-bearing diatom ooze, light yellowish brown (2.5Y 6.4), light olive brown (2.5Y 5/4), and olive brown (2.5Y 4/4).

Bioturbation is minor to moderate in the calcareous oozes and minor to strong in the siliceous oozes.

SMEAR SLIDE SUMMARY (%):

COMPOSITION:	1, 50 D	2, 50 D	3, 50 D	4, 50 D	5, 50 D	6, 50 D
Quartz	—	—	2	5	5	2
Clay	—	—	5	7	5	10
Volcanic glass	—	Tr	—	—	—	—
Accessory minerals:						
Heavy minerals	—	—	—	—	Tr	—
Micronodules	—	—	—	—	Tr	—
Zeolites	—	—	—	—	—	1
Nannofossils	60	68	2	2	3	2
Diatoms	35	25	84	81	80	83
Radiolarians	2	5	7	5	7	2
Silicoflagellates	3	2	—	—	—	—

SITE 690 HOLE B CORE 6H CORED INTERVAL 2955.1-2964.7 mbsl; 40.8-50.4 mbsf

TIME-ROCK UNIT: LOWER MIOCENE

BIOSTRAT. ZONE/FOSSIL CHARACTER:
- FORAMINIFERS: R.P no zone; A.G no Zone; A.P; F.P
- NANNOFOSSILS
- RADIOLARIANS
- DIATOMS: *N. maleinterpretaria - C. rhombicus* : *N. grossepunctata - C. lewisianus*
- PALYNOMORPHS

PALEOMAGNETICS

PHYS. PROPERTIES: γ=1.56 ϕ=74 ● V=1504; γ=1.56 ϕ=70 ● V=1500; γ=1.51 ϕ=79 ● V=1498

CHEMISTRY: ●53.3%; ●40.4%; ●66.6%; ●32.8%

SECTION: 1, 2, 3, 4, 5, 6, 7, CC

METERS: 0.5, 1.0

GRAPHIC LITHOLOGY

DRILLING DISTURB.

SED. STRUCTURES

SAMPLES: IW, OC

LITHOLOGIC DESCRIPTION

NANNOFOSSIL-BEARING DIATOM OOZE, RADIOLARIAN- AND MUD-BEARING DIATOM OOZE, DIATOM-BEARING NANNOFOSSIL OOZE, and NANNOFOSSIL OOZE

Major lithologies: Nannofossil-bearing diatom ooze, white (10YR 8/1) and light gray (10YR 7/2) to light brownish gray (10YR 6/2) and grayish brown (10YR 5/2). Radiolarian- and mud-bearing diatom ooze, light gray (10YR 7/1) and light olive brown (2.5Y 5/4). Diatom-bearing nannofossil ooze, white (10YR 8/1) and light gray (10YR 7/2) to light brownish gray (10YR 6/2) and grayish brown (10YR 5/2). Nannofossil ooze, light brownish gray (10YR 6/2) to grayish brown (10YR 5/2).

Bioturbation is moderate to strong, and includes *Zoophycos* and vertical burrows.

SMEAR SLIDE SUMMARY (%):

	1, 50 D	2, 50 D	3, 50 D	4, 50 D	5, 50 D	6, 50 D
COMPOSITION:						
Quartz	2	7	Tr	Tr	—	3
Clay	7	15	3	—	—	2
Volcanic glass	—	—	—	—	—	Tr
Calcite/dolomite	Tr	—	—	Tr	—	—
Accessory minerals:						
Heavy minerals	—	—	Tr	Tr	Tr	—
Micronodules	—	—	—	—	—	Tr
Nannofossils	15	3	80	91	83	83
Diatoms	71	60	15	7	15	10
Radiolarians	5	15	2	2	2	2
Silicoflagellates	—	—	—	—	Tr	—

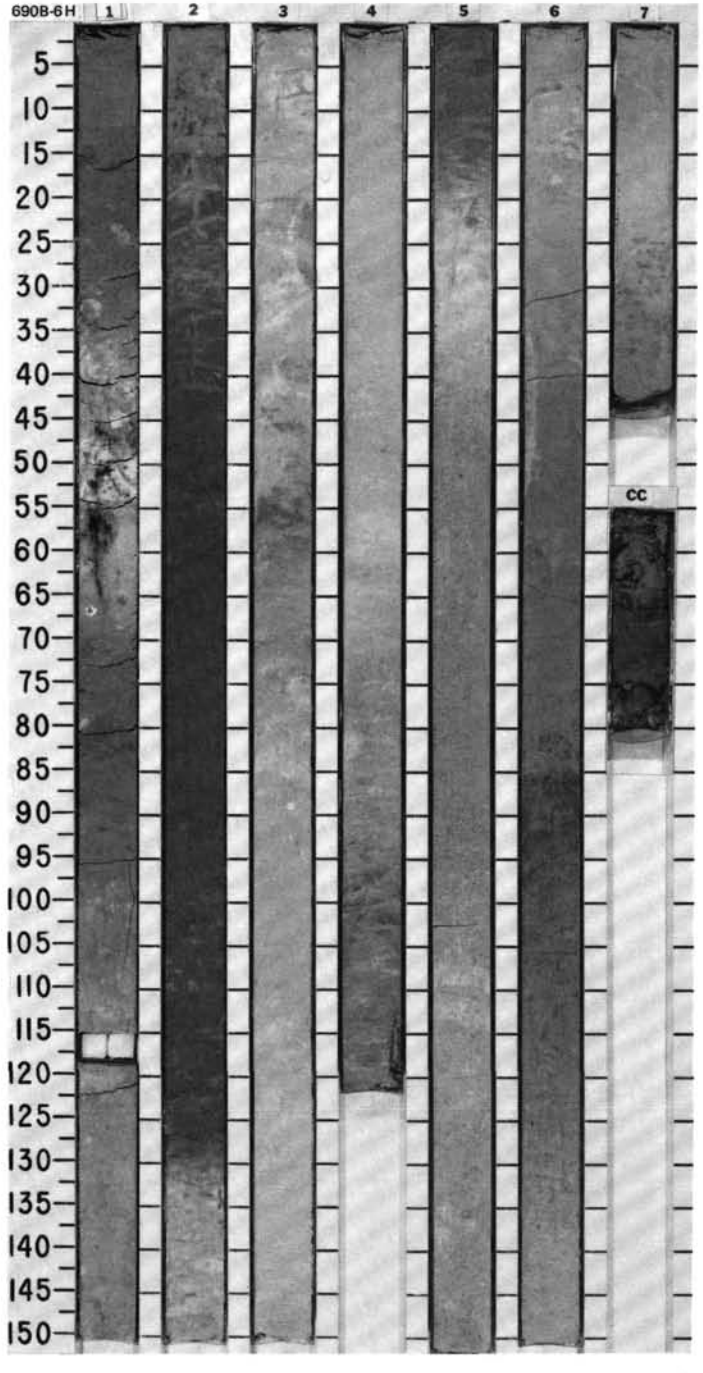

SITE 690 HOLE B CORE 7H CORED INTERVAL 2964.7 -2974.4 mbsl; 50.4-60.1 mbsf

TIME-ROCK UNIT: UPPER OLIGOCENE

BIOSTRAT. ZONE/FOSSIL CHARACTER:
- FORAMINIFERS: C.M — MIOCENE / LOWER MIOCENE ?
- NANNOFOSSILS: C.P — CP17-CP19
- RADIOLARIANS: C.P — no Zone
- DIATOMS: F.P — *Rocella vigilans* (?)
- PALYNOMORPHS: B — *N. maleinterpretaria* - *C. rhumbicus*

PALEOMAGNETICS

PHYS. PROPERTIES: ϕ-73 γ-1.68 V-1538 ● ϕ-68 γ-1.81 V-1498 ● ϕ-62 γ-1.82 V-1517 ●

CHEMISTRY: ● 69.0% ● 83.9% ● 88.6%

SECTION: 1, 2, 3, 4, 5, 6, 7, CC

METERS: 0.5, 1.0

GRAPHIC LITHOLOGY

DRILLING DISTURB.

SED. STRUCTURES

SAMPLES

LITHOLOGIC DESCRIPTION

DIATOM-BEARING NANNOFOSSIL OOZE and NANNOFOSSIL OOZE

Major lithologies: Diatom-bearing nannofossil ooze, light gray (10YR 7/2), slightly to moderately bioturbated (halo burrows, *Planolites*, and vertical burrows), mottled with white (10YR 8/1, 8/2) ooze. Nannofossil ooze, white (10YR 8/2) in Sections 6 and 7, light gray (10YR 7/2) in Sections 4 and 5, light brownish gray (10YR 6/2) in Section 3, and slightly to moderately bioturbated in Sections 3 and 5, mottled with white (10YR 8/1) ooze.

Minor lithology: Radiolarian-, nannofossil-, and mud-bearing diatom ooze, grayish brown (10YR 5/2) to dark grayish brown (10YR 4/2), slightly to moderately bioturbated, containing up to 25% terrigenous components, Section 1, 30-60 cm.

SMEAR SLIDE SUMMARY (%):

	1, 50 M	1, 120 D	2, 50 D	3, 50 D	4, 50 D	5, 50 D	6, 50 D
COMPOSITION:							
Quartz	10	Tr	2	Tr	1	1	1
Feldspar	—	—	—	—	Tr	Tr	—
Clay	15	—	—	—	—	—	—
Accessory minerals:							
Heavy minerals	Tr	—	—	—	—	Tr	Tr
Micronodules	—	—	—	1	—	Tr	—
Nannofossils	15	80	85	92	89	90	94
Diatoms	50	15	10	5	7	7	3
Radiolarians	10	5	3	2	3	2	2
Sponge spicules	—	—	—	—	Tr	—	—

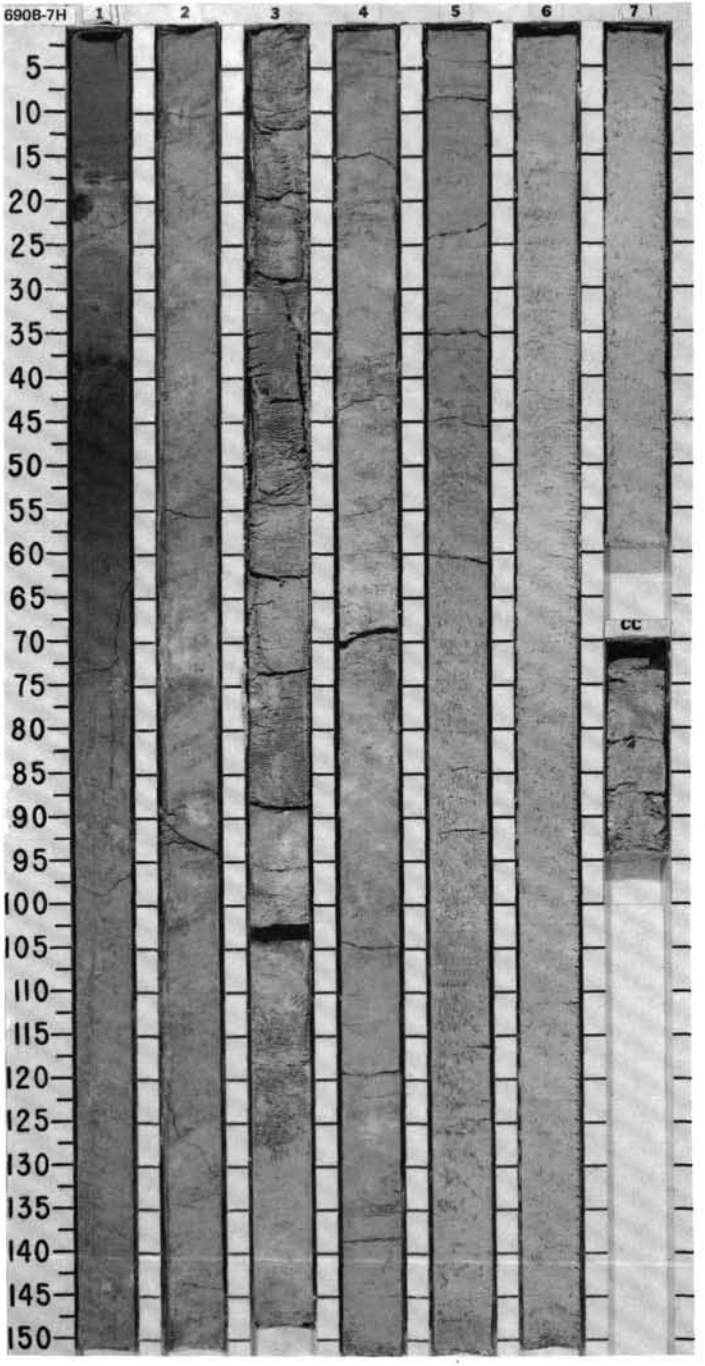

SITE 690 HOLE B CORE 8H CORED INTERVAL 2974.4-2984.1 mbsl; 60.1-69.8 mbsf

TIME-ROCK UNIT	BIOSTRAT. ZONE/ FOSSIL CHARACTER: FORAMINIFERS	NANNOFOSSILS	RADIOLARIANS	DIATOMS	PALYNOMORPHS	PALEOMAGNETICS	PHYS. PROPERTIES	CHEMISTRY	SECTION	METERS	GRAPHIC LITHOLOGY	DRILLING DISTURB.	SED. STRUCTURES	SAMPLES
UPPER OLIGOCENE	A,G	A,G	A,P	F,P	B		ϕ=66 γ=1.74 V=1506 ϕ=70 γ=1.82 V=1493 ϕ=62 γ=1.75 V=1515	● 74.4% ● 55.7% ● 83.0%	1 2 3 4 5 6 7 CC	0.5 1.0	VOID VOID		*	*

OLIGOCENE

CP17-CP19

Rocella vigilans

LITHOLOGIC DESCRIPTION

NANNOFOSSIL OOZE

Major lithology: Nannofossil ooze, light gray (10YR 7/2) to white (10YR 8/2) and light brownish gray (10YR 6/2) from Section 1 through upper part of Section 3 (to about 40 cm). Lower part of Section 3 to upper part of Section 5, light gray (10YR 7/2) and light brownish gray (10YR 6/2, 6/3). Light gray (10YR 7/2) and grayish brown (10YR 5/2) burrows. Bioturbation (*Planolites* and halo burrows) is minor to moderate throughout the core.

SMEAR SLIDE SUMMARY (%):

	1, 50 D	2, 50 D	3, 50 D	4, 50 D	5, 50 D	6, 50 D
COMPOSITION:						
Quartz	Tr	—	Tr	Tr	—	Tr
Volcanic glass	—	Tr	—	Tr	Tr	—
Foraminifers	3	Tr	3	Tr	Tr	Tr
Nannofossils	92	94	91	94	94	95
Diatoms	2	3	3	2	2	2
Radiolarians	2	2	2	3	3	3
Silicoflagellates	1	1	1	1	1	Tr

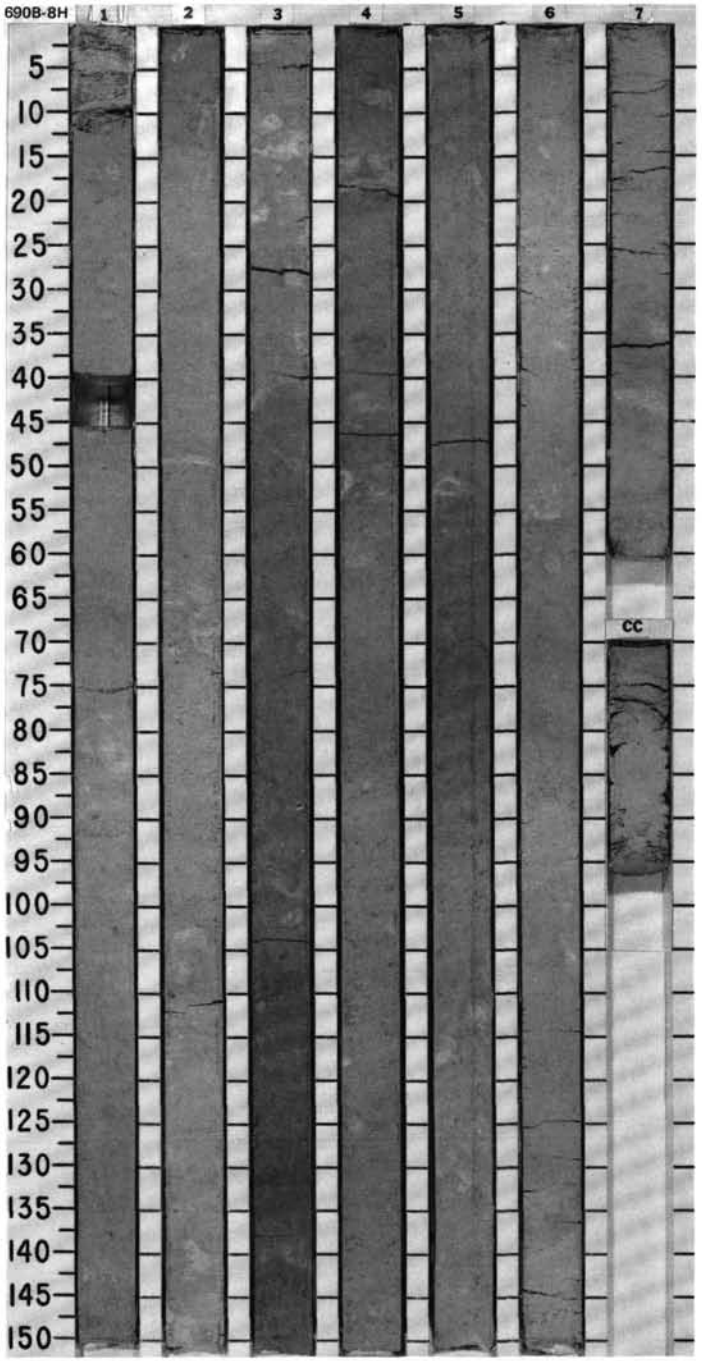

SITE 690 HOLE B CORE 9H CORED INTERVAL 2984.1-2993.7 mbsl; 69.8-79.4 mbsf

TIME-ROCK UNIT: LOWER OLIGOCENE

BIOSTRAT. ZONE/FOSSIL CHARACTER:
- FORAMINIFERS: LOWER OLIGOCENE
- NANNOFOSSILS: CP17-CP19
- RADIOLARIANS: ?
- DIATOMS: OLIGOCENE
- PALYNOMORPHS: B

PALEOMAGNETICS

PHYS. PROPERTIES: φ=65 γ=1.68 V=1496 ● φ=71 γ=1.72 V=1488 ● φ=66 γ=1.75 V=1514 ●

CHEMISTRY: ● 60.3% ● 72.5% ● 70.5% ● 76.0%

SECTION: 1 2 3 4 5 6 7 CC

METERS: 0.5 1.0

GRAPHIC LITHOLOGY

DRILLING DISTURB.

SED. STRUCTURES

SAMPLES: IW OG

LITHOLOGIC DESCRIPTION

NANNOFOSSIL OOZE

Major lithology: Nannofossil ooze, alternating white (10YR 8/2) and light gray (10YR 7/1) in Section 1, light gray (10YR 7/2) and light brownish gray (10YR 6/2) in Section 2, light brownish gray (10YR 6/2) mottled with white (10YR 8/2) and grayish brown (10YR 5/2) in Sections 3 and 4, alternating light gray (10YR 7/2) and light brownish gray (10YR 6/2) in Section 5, and very pale brown (10YR 7/3) in Sections 6 and 7.

Minor to moderate bioturbation throughout the core, producing white (10YR 8/2) mottles in Sections 5, 6, and 7, and light brownish gray (10YR 6/2) and white (10YR 8/2) mottles in Sections 3 and 4. Dark brown silt clasts near the top of Section 4. Black nodules (ice-rafted coal?) and black layers in Section 6.

SMEAR SLIDE SUMMARY (%):

COMPOSITION:	1, 50 D	2, 50 D	3, 50 D	4, 50 D	5, 50 D	5, 146 M	6, 50 D
Quartz	Tr	Tr	Tr	1	Tr	—	—
Volcanic glass	—	—	Tr	1	1	—	—
Nannofossils	95	100	95	91	95	50	97
Diatoms	3	—	3	2	3	—	2
Radiolarians	2	—	2	3	1	—	1
Silicoflagellates	Tr	—	—	2	Tr	—	Tr
Amorphous organic matter	—	—	—	—	—	50	—

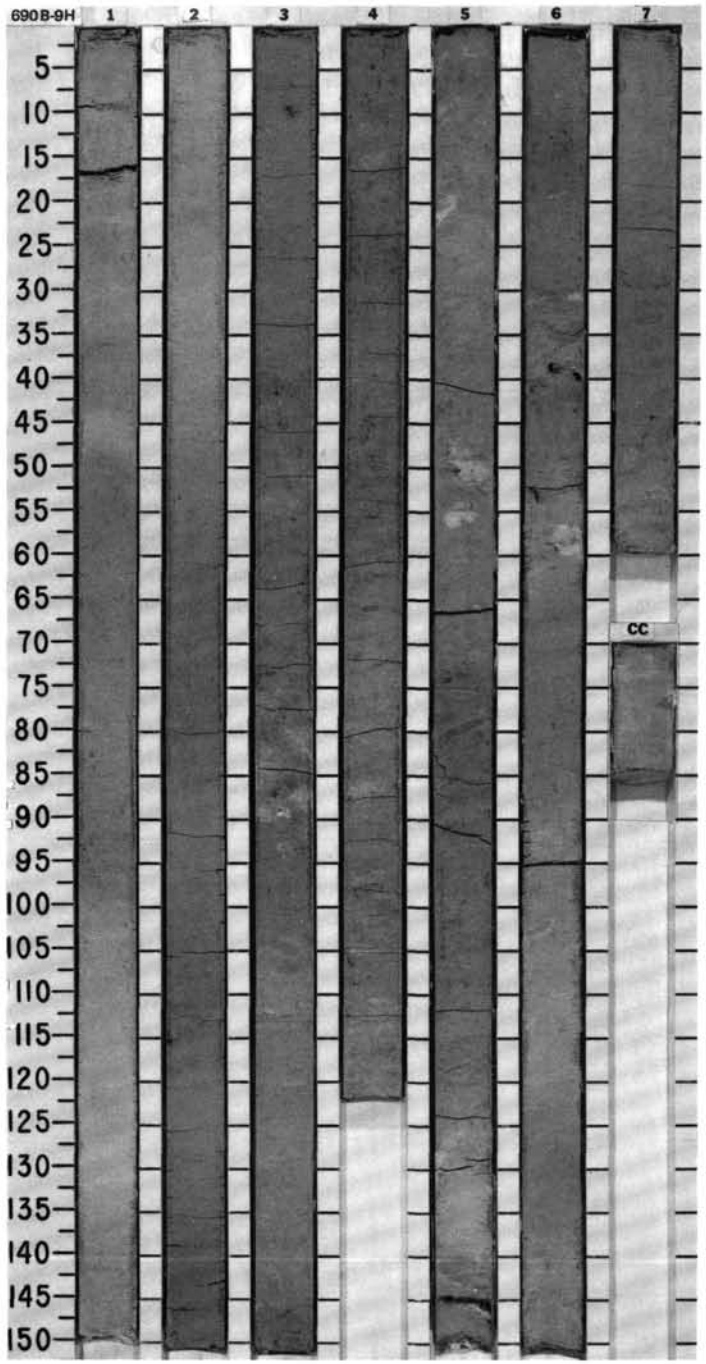

SITE 690 HOLE B CORE 10H CORED INTERVAL 2993.7-3003.4 mbsl; 79.4-89.1 mbsf

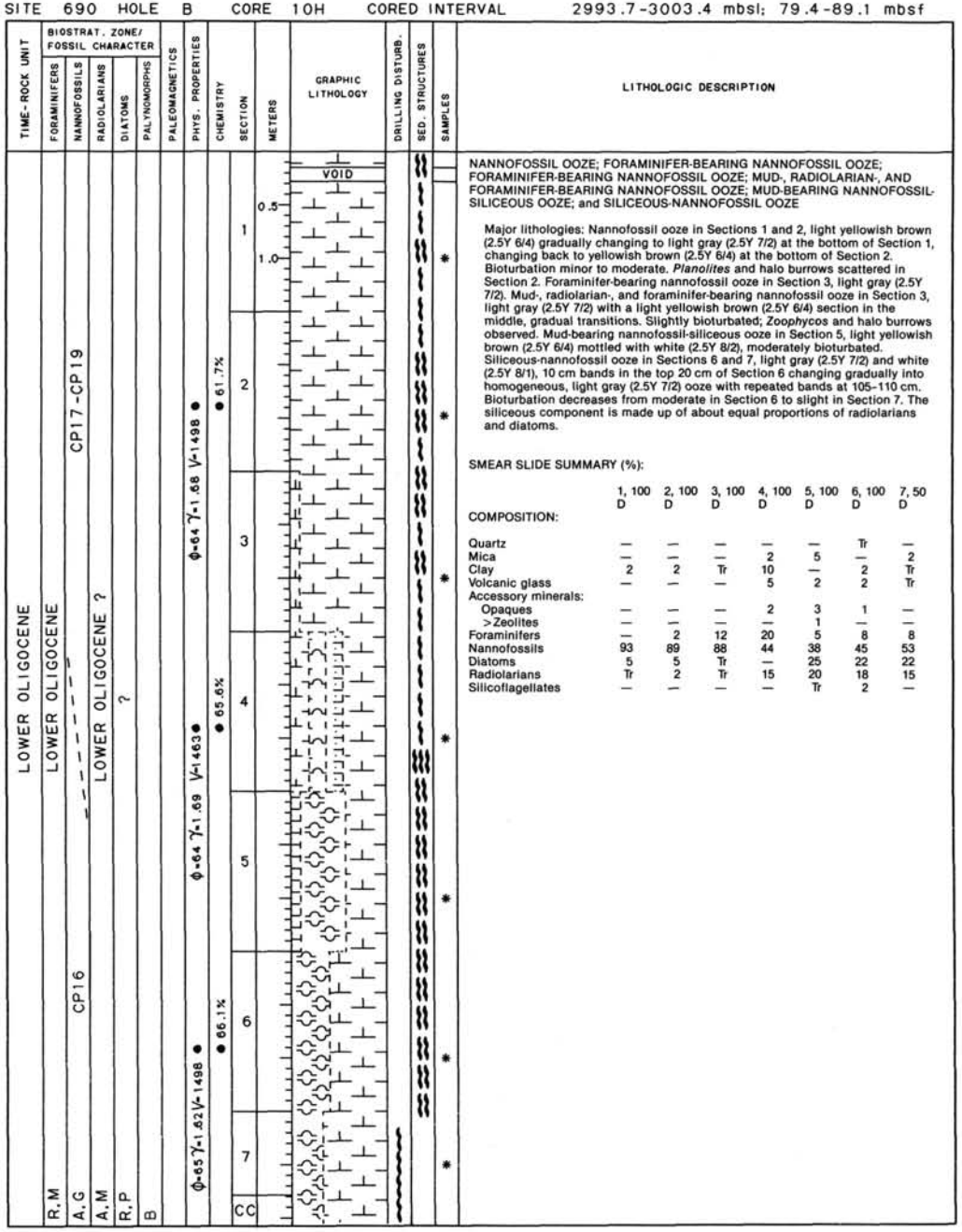

LITHOLOGIC DESCRIPTION

NANNOFOSSIL OOZE; FORAMINIFER-BEARING NANNOFOSSIL OOZE; FORAMINIFER-BEARING NANNOFOSSIL OOZE; MUD-, RADIOLARIAN-, AND FORAMINIFER-BEARING NANNOFOSSIL OOZE; MUD-BEARING NANNOFOSSIL-SILICEOUS OOZE; and SILICEOUS-NANNOFOSSIL OOZE

Major lithologies: Nannofossil ooze in Sections 1 and 2, light yellowish brown (2.5Y 6/4) gradually changing to light gray (2.5Y 7/2) at the bottom of Section 1, changing back to yellowish brown (2.5Y 6/4) at the bottom of Section 2. Bioturbation minor to moderate. *Planolites* and halo burrows scattered in Section 2. Foraminifer-bearing nannofossil ooze in Section 3, light gray (2.5Y 7/2). Mud-, radiolarian-, and foraminifer-bearing nannofossil ooze in Section 3, light gray (2.5Y 7/2) with a light yellowish brown (2.5Y 6/4) section in the middle, gradual transitions. Slightly bioturbated; *Zoophycos* and halo burrows observed. Mud-bearing nannofossil-siliceous ooze in Section 5, light yellowish brown (2.5Y 6/4) mottled with white (2.5Y 8/2), moderately bioturbated. Siliceous-nannofossil ooze in Sections 6 and 7, light gray (2.5Y 7/2) and white (2.5Y 8/1), 10 cm bands in the top 20 cm of Section 6 changing gradually into homogeneous, light gray (2.5Y 7/2) ooze with repeated bands at 105–110 cm. Bioturbation decreases from moderate in Section 6 to slight in Section 7. The siliceous component is made up of about equal proportions of radiolarians and diatoms.

SMEAR SLIDE SUMMARY (%):

COMPOSITION:	1, 100 D	2, 100 D	3, 100 D	4, 100 D	5, 100 D	6, 100 D	7, 50 D
Quartz	—	—	—	—	—	Tr	—
Mica	—	—	—	2	5	—	2
Clay	2	2	Tr	10	—	2	Tr
Volcanic glass	—	—	—	5	2	2	Tr
Accessory minerals:							
Opaques	—	—	—	2	3	1	—
>Zeolites	—	—	—	—	1	—	—
Foraminifers	—	2	12	20	5	8	8
Nannofossils	93	89	88	44	38	45	53
Diatoms	5	5	Tr	—	25	22	22
Radiolarians	Tr	2	Tr	15	20	18	15
Silicoflagellates	—	—	—	—	Tr	2	—

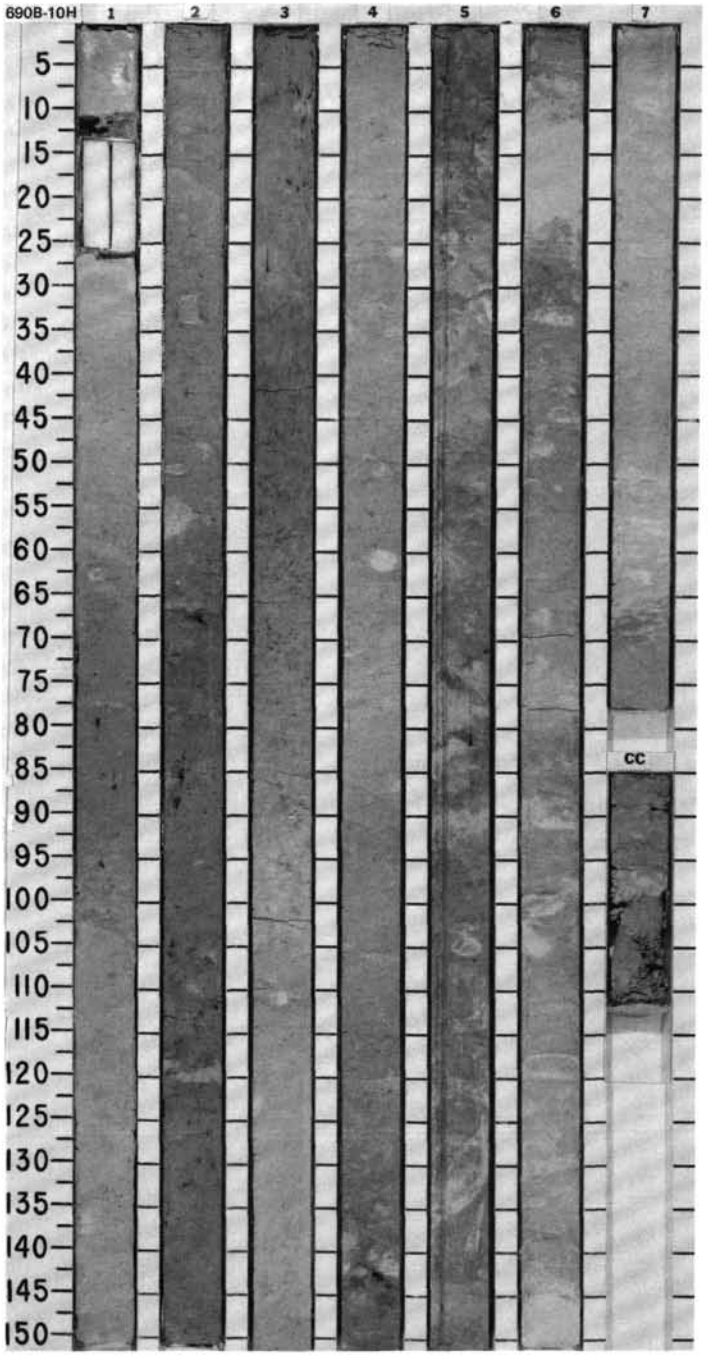

SITE 690 HOLE B CORE 11H CORED INTERVAL 3003.4-3013.1 mbsl; 89.1-98.8 mbsf

TIME-ROCK UNIT	BIOSTRAT. ZONE/ FOSSIL CHARACTER: FORAMINIFERS	NANNOFOSSILS	RADIOLARIANS	DIATOMS	PALYNOMORPHS	PALEOMAGNETICS	PHYS. PROPERTIES	CHEMISTRY	SECTION	METERS	GRAPHIC LITHOLOGY	DRILLING DISTURB.	SED. STRUCTURES	SAMPLES
UPPER EOCENE / LOWER OLIGOCENE	A, G	A, G	F, P		B		ϕ=63 γ=1.69 V=1522 ● ϕ=66 γ=1.65 V=1535 ● ϕ=62 γ=1.80 V=1504 ●	● 83.0% ● 87.9 ● 0%	1 2 3 4 5 6 7 CC	0.5 1.0				*

LITHOLOGIC DESCRIPTION

NANNOFOSSIL OOZE, FORAMINIFER- AND RADIOLARIAN-BEARING NANNOFOSSIL OOZE, and RADIOLARIAN-BEARING NANNOFOSSIL OOZE

Major lithologies: Nannofossil ooze in Sections 3–7, white (2.5Y 8/0, 8/1) mottled with light yellowish brown (2.5Y 6/4) ooze in the upper part of Section 3. Bioturbation absent to moderate. Identifiable types include *Planolites*, *Zoophycos*, and halo burrows. Foraminifer- and radiolarian-bearing nannofossil ooze in Section 1. White (2.5Y 8/2), featureless sediment. Radiolarian-bearing nannofossil ooze, white (2.5Y 8/2), subtle color variations, bioturbation absent to minor.

SMEAR SLIDE SUMMARY (%):

COMPOSITION:	1, 50 D	2, 50 D	3, 50 D	4, 50 D	5, 50 D	6, 50 D	7, 50 D
Quartz	—	—	Tr	—	—	Tr	Tr
Mica	3	4	2	Tr	3	2	4
Clay	5	2	5	2	Tr	3	3
Volcanic glass	—	—	—	4	—	Tr	Tr
Accessory minerals:							
Opaques	—	1	3	1	1	1	—
Zeolites	—	—	—	—	—	2	2
Foraminifers	10	5	5	5	8	8	5
Nannofossils	67	75	83	81	88	82	86
Diatoms	5	5	Tr	2	—	—	—
Radiolarians	10	8	2	5	—	2	Tr

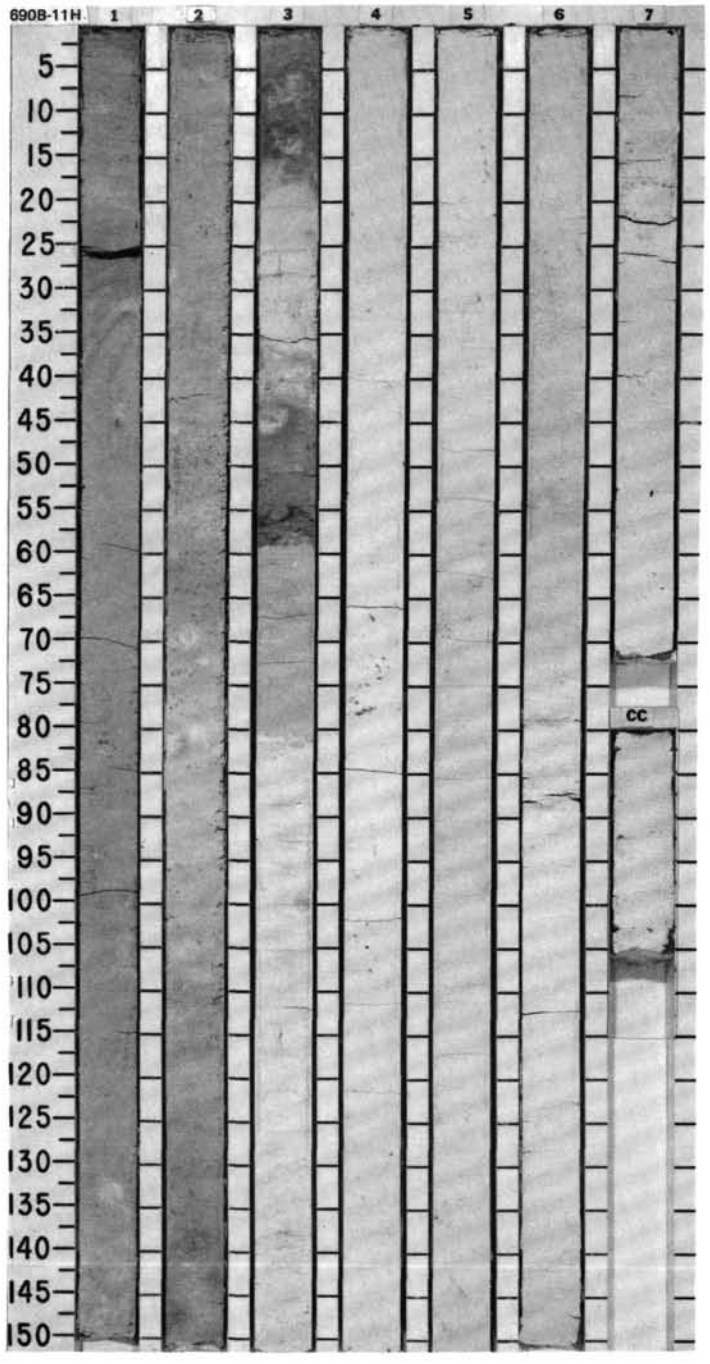

SITE 690 HOLE B CORE 12H CORED INTERVAL 3013.1-3022.8 mbsl; 98.8-108.5 mbsf

TIME-ROCK UNIT: MIDDLE EOCENE / UPPER EOCENE

BIOSTRAT. ZONE/FOSSIL CHARACTER: FORAMINIFERS A,G; NANNOFOSSILS A,M; RADIOLARIANS B; DIATOMS B; PALYNOMORPHS B

PALEOMAGNETICS

PHYS. PROPERTIES: ϕ=67 γ=1.84 V=1533; ϕ=61 γ=1.70 V=1532

CHEMISTRY: 83.0%; 74.7%

SECTION: 1, 2, 3, 4, 5, 6, 7, CC

METERS: 0.5, 1.0

GRAPHIC LITHOLOGY

DRILLING DISTURB.

SED. STRUCTURES

SAMPLES: IW

LITHOLOGIC DESCRIPTION

FORAMINIFER-BEARING NANNOFOSSIL OOZE

Major lithology: Foraminifer-bearing nannofossil ooze, pure white (10YR 8/0), white (10YR 8/2), and very pale brown (10YR 8/3, 8/4) with light gray mottles (2.5Y 7/2). At the base of Section 1 (143–148 cm) and the top of Section 2 (2–8 cm) sediment is chalky.

Bioturbation is absent to moderate. *Planolites*, *Zoophycos*, and halo burrows are present. Mottling, attributed to bioturbation, produces a calico appearance from Section 3, 105 cm, to Section 4, 144 cm. Gradational and cyclic color changes are present and extend for 38–184 cm. Section 6, 47–53 cm, contains a scour(?) mark along a color contact. Subrounded and rounded fragments of sediment, with the color of the scoured-out material, occur as much as 20 cm above the scour, decreasing in size with vertical distance.

SMEAR SLIDE SUMMARY (%):

	1, 80 D	2, 80 D	3, 80 D	4, 80 D	5, 80 D	6, 80 D	7, 25 D
COMPOSITION:							
Quartz	Tr	—	Tr	Tr	Tr	—	—
Mica	1	2	3	4	6	6	1
Clay	—	2	—	—	3	3	—
Volcanic glass	—	—	2	—	—	—	4
Accessory minerals:							
Opaques	—	Tr	Tr	—	Tr	Tr	Tr
Foraminifers	12	22	18	18	12	10	12
Nannofossils	87	74	77	78	79	81	83
Diatoms	Tr	Tr	—	—	—	—	—

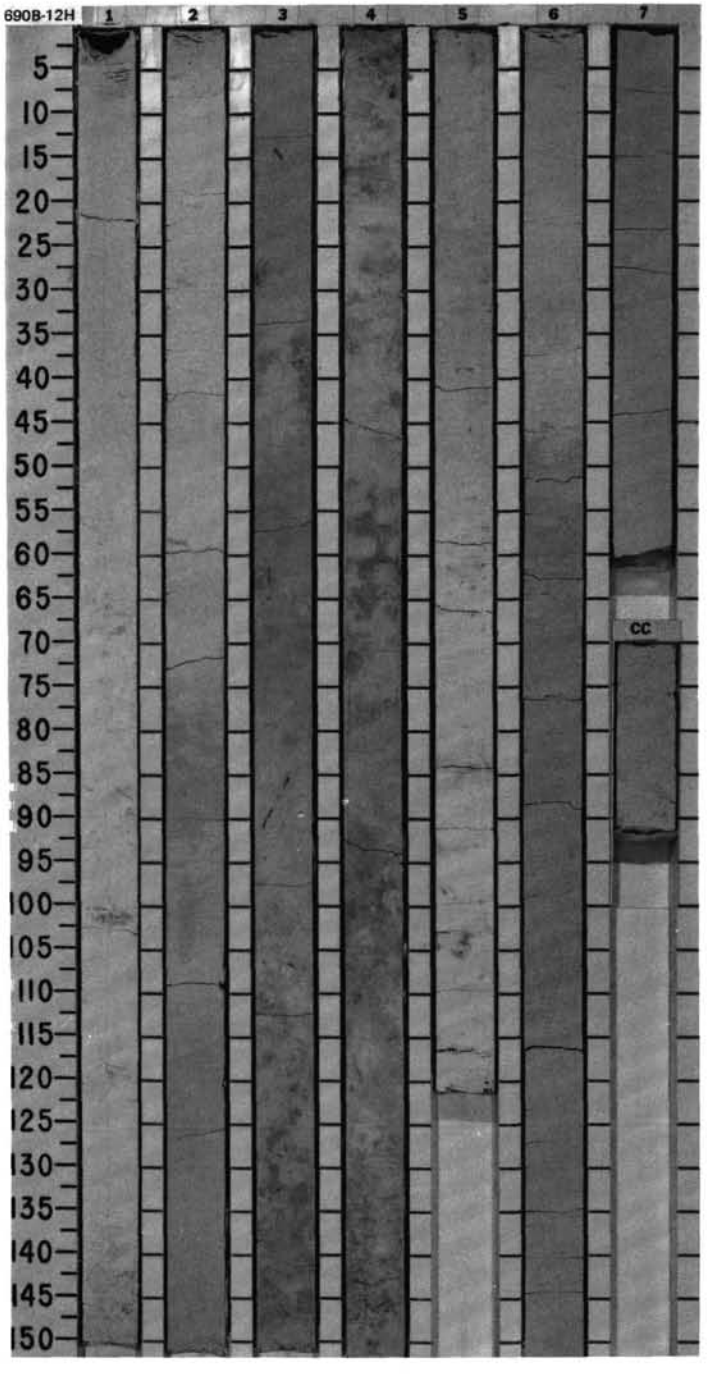

SITE 690 HOLE B CORE 13H CORED INTERVAL 3022.8-3032.8 mbsl; 108.5-118.5 mbsf

TIME-ROCK UNIT: MIDDLE EOCENE

BIOSTRAT. ZONE/FOSSIL CHARACTER:
- FORAMINIFERS: A, G — MIDDLE EOCENE
- NANNOFOSSILS: A, M — CP12-CP13
- RADIOLARIANS: B
- DIATOMS: B
- PALYNOMORPHS: B

PALEOMAGNETICS

PHYS. PROPERTIES: ϕ=57 γ=1.71 V=1561 ● ϕ=62 γ=1.71 V=1535 ● ϕ=59 γ=1.71 V=1555 ●

CHEMISTRY: ● 76.4% ● 73.0% ● 79.5%

SECTION: 1, 2, 3, 4, 5, 6, 7, CC

METERS: 0.5, 1.0

GRAPHIC LITHOLOGY

DRILLING DISTURB.

SED. STRUCTURES

SAMPLES

LITHOLOGIC DESCRIPTION

FORAMINIFER-BEARING NANNOFOSSIL OOZE and FORAMINIFERAL NANNOFOSSIL OOZE

Major lithology: Foraminifer-bearing nannofossil ooze and foraminiferal nannofossil ooze, both white (10YR 8/2), slightly bioturbated sediments. There is a gradual increase in foraminifers downcore from Section 1 to Section 5, where the foraminiferal nannofossil ooze occurs, followed by a decrease in foraminifers in Section 6.

SMEAR SLIDE SUMMARY (%):

	1, 50 D	2, 50 D	3, 50 D	4, 50 D	5, 50 D	6, 50 D	7, 50 D
COMPOSITION:							
Quartz	Tr	—	—	—	Tr	Tr	—
Mica	1	2	1	Tr	Tr	2	—
Clay	—	2	2	—	1	4	—
Volcanic glass	1	—	—	2	2	3	2
Accessory minerals:							
Opaques	Tr	Tr	Tr	Tr	Tr	Tr	—
Zeolites	—	—	Tr	2	6	Tr	2
Foraminifers	16	22	22	24	28	15	22
Nannofossils	82	74	75	72	63	76	74

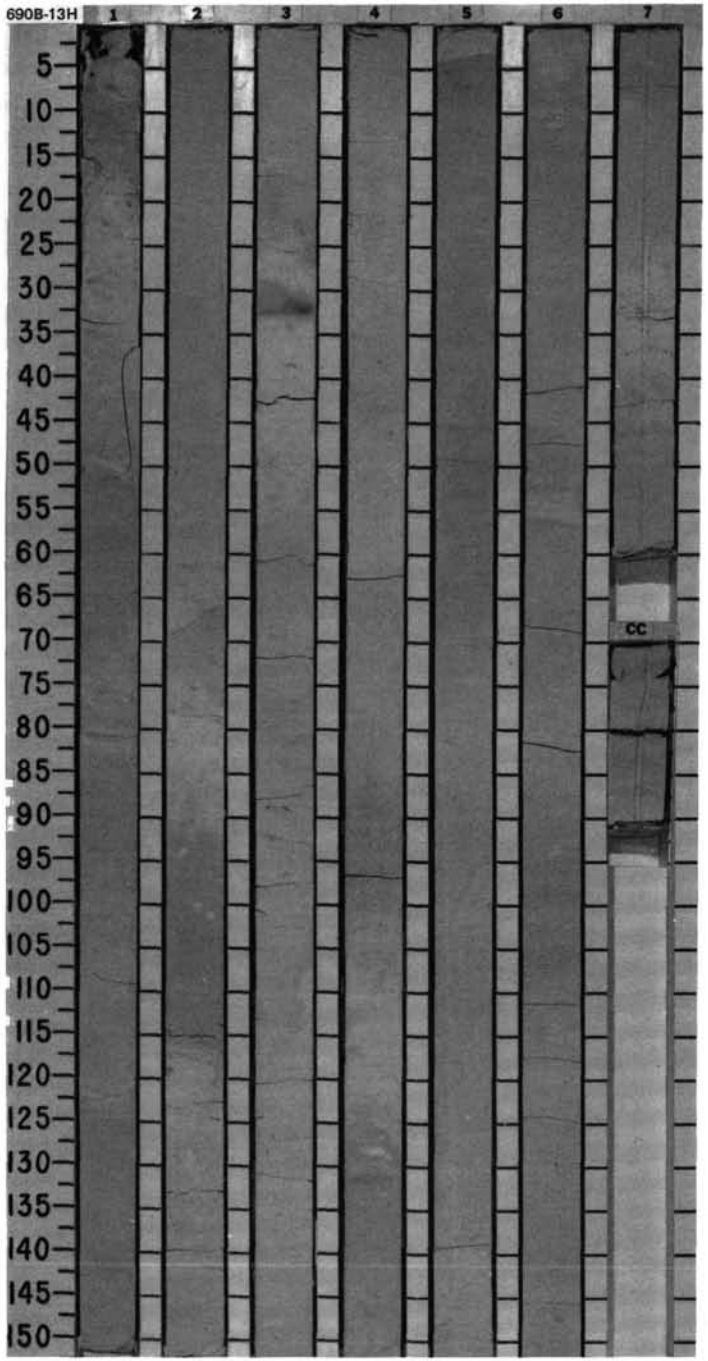

SITE 690 HOLE B CORE 14H CORED INTERVAL 3032.8-3042.4 mbsl; 118.5-128.1 mbsf

TIME-ROCK UNIT: LOWER MIDDLE EOCENE

BIOSTRAT. ZONE/FOSSIL CHARACTER: FORAMINIFERS: A.M; LOWER MIDDLE EOCENE; NANNOFOSSILS: A.M; CP10 - CP11; RADIOLARIANS: F.P; CP12-CP13; DIATOMS: B; PALYNOMORPHS: B

PALEOMAGNETICS

PHYS. PROPERTIES: V-1565 ● 1.80 Ø=55; V-1574 ● 1.86 Ø=58; V-1574 ● 1.94 Ø=58; V-1530 ● 1.83 Ø=61; V-1559 ● 1.73 Ø=60

CHEMISTRY: ● 79.3%; ● 81.9%; ● ; ● 86.6%; ● 78.4%

SECTION: 1, 2, 3, 4, 5, 6, 7, CC

METERS: 0.5, 1.0

GRAPHIC LITHOLOGY: VOID

DRILLING DISTURB.

SED. STRUCTURES: P, P, P, Z

SAMPLES: *

LITHOLOGIC DESCRIPTION

NANNOFOSSIL OOZE, FORAMINIFER-BEARING NANNOFOSSIL OOZE, and FORAMINIFERAL NANNOFOSSIL OOZE

Major lithologies: Nannofossil ooze. Foraminifer-bearing nannofossil ooze. Foraminiferal nannofossil ooze. All white (10YR 8/2), variably bioturbated sediments with very pale brown (10YR 8/3) mottling. The only identifiable bioturbation structure is *Zoophycos*.

SMEAR SLIDE SUMMARY (%):

COMPOSITION:	1, 50 D	2, 50 D	3, 50 D	4, 50 D	5, 50 D	6, 50 D	7, 50 D
Volcanic glass	—	—	Tr	1	2	5	5
Accessory minerals:							
>Zeolites	—	Tr	Tr	3	Tr	3	2
Foraminifers	35	30	9	10	8	15	10
Nannofossils	65	70	91	86	90	77	83
Thoracospheres	—	—	—	—	—	—	Tr

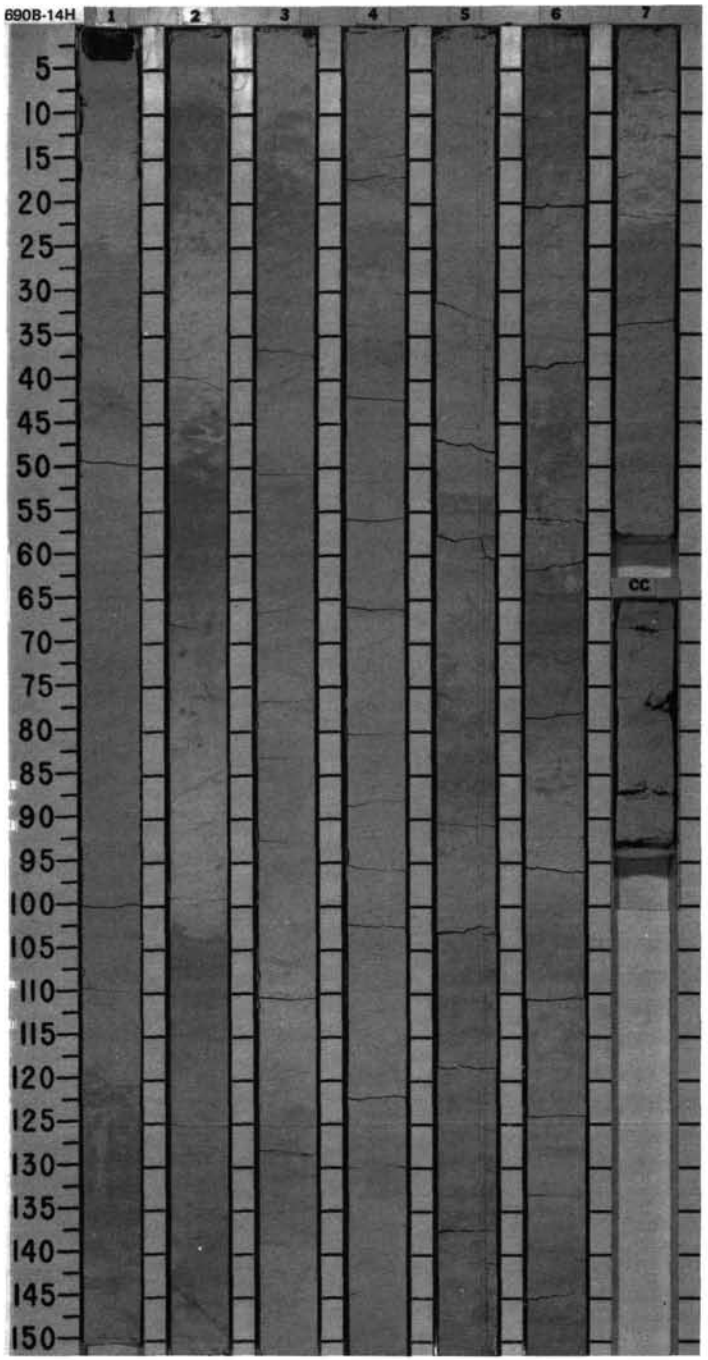

SITE 690 HOLE B CORE 15H CORED INTERVAL 3042.4-3052.1 mbsl; 128.1-137.8 mbsf

TIME-ROCK UNIT: UPPER PALEOCENE - LOWER EOCENE

BIOSTRAT. ZONE/FOSSIL CHARACTER:
- FORAMINIFERS: A,G UPPER PALEOCENE | LOWER EOCENE
- NANNOFOSSILS: A,M CP9b; CP10 - CP11; CP12 - CP13
- RADIOLARIANS: B
- DIATOMS: B
- PALYNOMORPHS: B
- PALEOMAGNETICS
- PHYS. PROPERTIES: φ-52 γ-1.89 V-1580 ● ● V-1595 ● φ-58 γ-1.76 V-1586 ● ● 71.9%
- CHEMISTRY: ● 87.3% ● 78.1%
- SECTION: 1, 2, 3, 4, 5, 6, 7, CC
- METERS: 0.5, 1.0
- GRAPHIC LITHOLOGY
- DRILLING DISTURB.
- SED. STRUCTURES
- SAMPLES

LITHOLOGIC DESCRIPTION

FORAMINIFERAL NANNOFOSSIL OOZE, FORAMINIFER-BEARING NANNOFOSSIL OOZE, and NANNOFOSSIL OOZE

Major lithologies: Foraminifer-bearing nannofossil ooze, white (10YR 8/2), pale brown (10YR 8/3, 8/4), and pink (7.5YR 8/4). Alternation between different colors occurs on a scale of 10-20 cm in lower half of Section 1 and in the upper half of Section 5. In the rest of Section 5 and in Section 4, pale brown and pink predominate. Moderate to strong bioturbation (*Planolites* and *Zoophycos abundant in Section 5*). *Generally decreasing foraminifer content downcore.* Foraminiferal nannofossil ooze, homogeneous pale brown (10YR 8/4), without structures. Nannofossil ooze, pale brown (10YR 8/3) and yellow (10YR 7/6). Minor to moderate bioturbation with vertical burrows and *Chondrites* in top of Section 6. *Zoophycos*, *Planolites*, and *Chondrites* abundant below Section 6, 100 cm, and in parts of Section 7.

SMEAR SLIDE SUMMARY (%):

	1, 50 D	2, 50 D	3, 50 D	4, 50 D	5, 75 D	5, 85? M	6, 50 D
COMPOSITION:							
Quartz	—	—	—	2	Tr	3	1
Feldspar	—	—	—	—	—	Tr	—
Clay	—	—	—	—	—	2	—
Volcanic glass	—	Tr	Tr	1	—	3	2
Accessory minerals:							
Zeolites	2	2	1	—	—	—	—
Foraminifers	20	33	35	20	10	25	7
Nannofossils	78	65	64	77	90	67	90

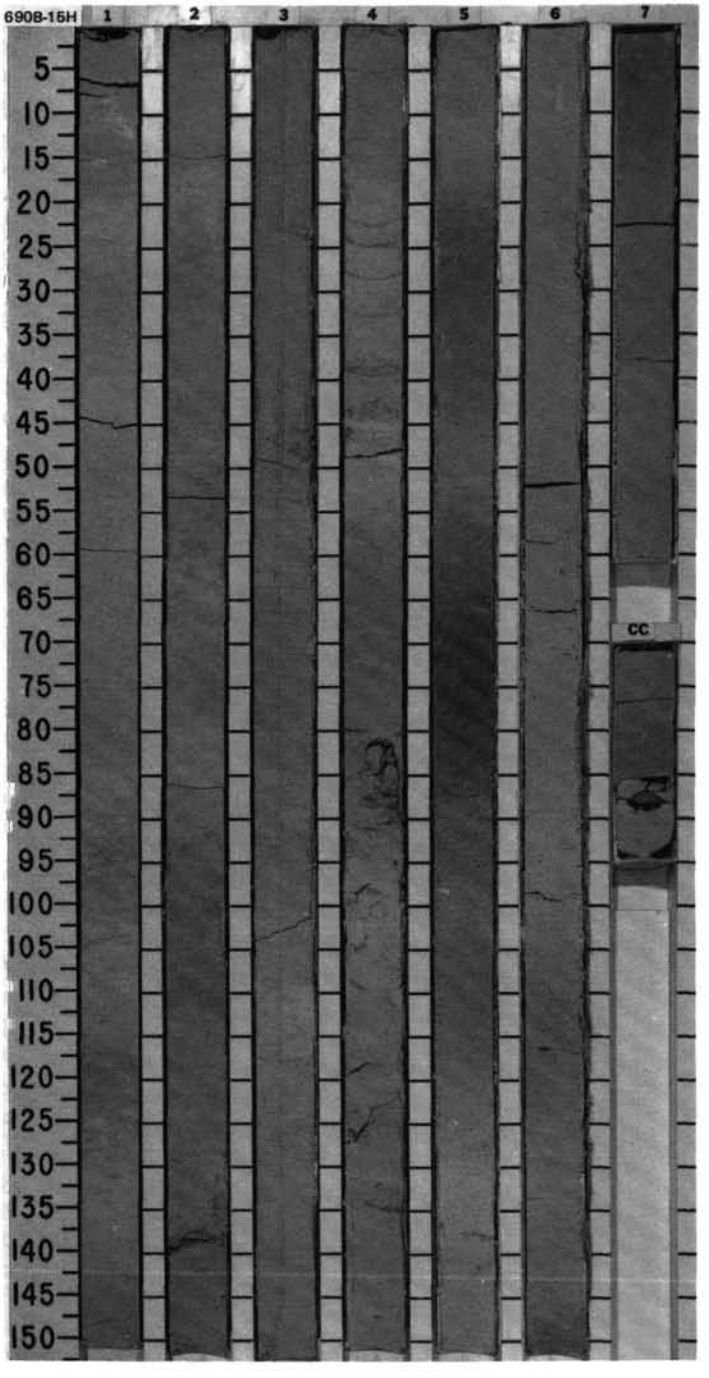

SITE 690 HOLE B CORE 16H CORED INTERVAL 3052.1-3061.8 mbsl; 137.8-147.5 mbsf

TIME-ROCK UNIT: UPPER PALEOCENE – LOWER EOCENE; UPPER PALEOCENE

BIOSTRAT. ZONE/FOSSIL CHARACTER: FORAMINIFERS A, G; NANNOFOSSILS A, M; CP9a; RADIOLARIANS B; DIATOMS B; PALYNOMORPHS B

PALEOMAGNETICS

PHYS. PROPERTIES: ϕ=57 γ=2.04 V=1637 ● ϕ=53 γ=1.99 V=1676 ● ϕ=53 γ=2.12 V=1609 ●

CHEMISTRY: ● 60.3% ● 77.5% ● 83.7%

SECTION: 1, 2, 3, 4, 5, 6, 7, CC

METERS: 0.5, 1.0

GRAPHIC LITHOLOGY

DRILLING DISTURB.

SED. STRUCTURES

SAMPLES: IW, OG

LITHOLOGIC DESCRIPTION

CLAY-BEARING NANNOFOSSIL OOZE and MUD-BEARING NANNOFOSSIL OOZE

Major lithologies: Clay-bearing nannofossil ooze, reddish yellow (7.5YR 7/6, 6/6) and pink (7.5YR 7/4), alternating on a scale of 5–30 cm in Sections 1, 2, and 4. Yellowish brown specks at Section 1, 135–145 cm, and small (< 1 mm) reddish yellow (7.5YR 7/8) spots at Section 3, 80–114 cm. Moderate to minor bioturbation, with *Chondrites* and *Zoophycos* abundant in Sections 1 and 2 and present in Section 3. Mud-bearing nannofossil ooze, reddish yellow (5YR 7/6, 7/8) and pink (5YR 7/4), alternating on a scale of 20–50 cm, all transitions gradational. At the base of Section 7, reddish yellow (5YR 6/6) with very pale brown (10YR 7/3) mottling. Increasing bioturbation, from slight at top of Section 5 to moderate in Section 7. *Chondrites* observed between 50 and 90 cm in Section 4. Vertical burrows, *Chondrites*, and *Planolites* in Section 5.

SMEAR SLIDE SUMMARY (%):

	1, 46 D	2, 50 D	3, 50 D	4, 30 D	5, 90 D	6, 50 D
COMPOSITION:						
Quartz	1	—	1	1	Tr	Tr
Feldspar	Tr	Tr	—	Tr	—	—
Mica	—	—	7	—	10	15
Clay	20	15	5	20	15	15
Volcanic glass	5	5	3	—	—	Tr
Accessory minerals:						
Opaques	1	Tr	2	—	Tr	—
Zeolites	—	—	—	3	—	—
Foraminifers	5	5	5	7	5	1
Nannofossils	68	74	77	69	70	69
Heavy minerals	—	1	2	—	—	—

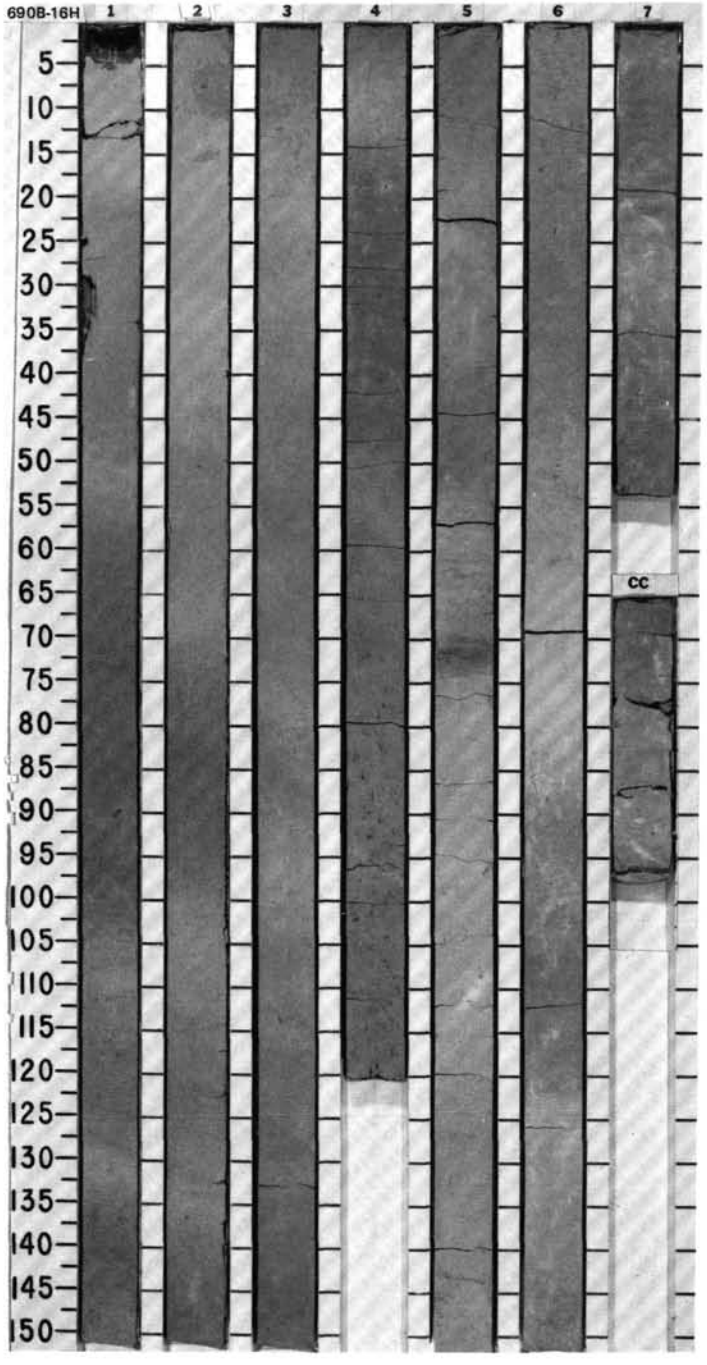

SITE 690 HOLE B CORE 17H CORED INTERVAL 3061.8-3071.5 mbsl; 147.5-157.2 mbsf

TIME-ROCK UNIT	BIOSTRAT. ZONE/ FOSSIL CHARACTER: FORAMINIFERS	NANNOFOSSILS	RADIOLARIANS	DIATOMS	PALYNOMORPHS	PALEOMAGNETICS	PHYS. PROPERTIES	CHEMISTRY	SECTION	METERS	GRAPHIC LITHOLOGY	DRILLING DISTURB.	SED. STRUCTURES	SAMPLES
UPPER PALEOCENE / LOWER EOCENE	A, G	A, G	B	B	B		ϕ=52 γ=2.02 V=1542 ● ϕ=53 γ=2.12 V=1614 ● ϕ=53 γ=2.16 V=1613 ●	● 74.0% ● 73.1% ● 81.7%	1 2 3 4 5 6 7 CC	0.5 1.0				*

LITHOLOGIC DESCRIPTION

MUDDY NANNOFOSSIL OOZE and MUD-BEARING NANNOFOSSIL OOZE

Major lithologies: Muddy nannofossil ooze and mud-bearing nannofossil ooze, mainly very pale brown (10YR 7/3) and pale brown (10YR 6/3); also white (N 8/2, 10YR 8/1), light gray (10YR 7/2), light yellowish brown (10YR 6/4), yellowish brown (10YR 5/4), and brown (7.5YR 5/4). In Sections 3-6, lighter and darker colors alternate in layers 15-50 cm thick. The contacts are gradational and burrowed. In Sections 4 and 5 the following 30-50-cm-thick cycle is common: relatively sharp contact at top, pale brown (10YR 6/3), gradual transition to another pale brown (10YR 7/3), and again relatively sharp contact at base.

Moderate to minor bioturbation, including a long vertical burrow in Section 3 and abundant *Chondrites* in Sections 4-6. Tiny mica flakes are conspicuous on the surface of the core as well as in smear slides.

SMEAR SLIDE SUMMARY (%):

	1, 50 D	2, 50 D	3, 50 D	4, 50 D	5, 50 D	6, 50 D
COMPOSITION:						
Quartz	Tr	1	Tr	Tr	Tr	1
Feldspar	—	—	Tr	—	—	—
Mica	10	15	10	7	15	15
Clay	15	20	15	10	15	20
Volcanic glass	Tr	1	Tr	Tr	1	—
Foraminifers	2	2	3	2	1	3
Nannofossils	73	61	72	81	68	61

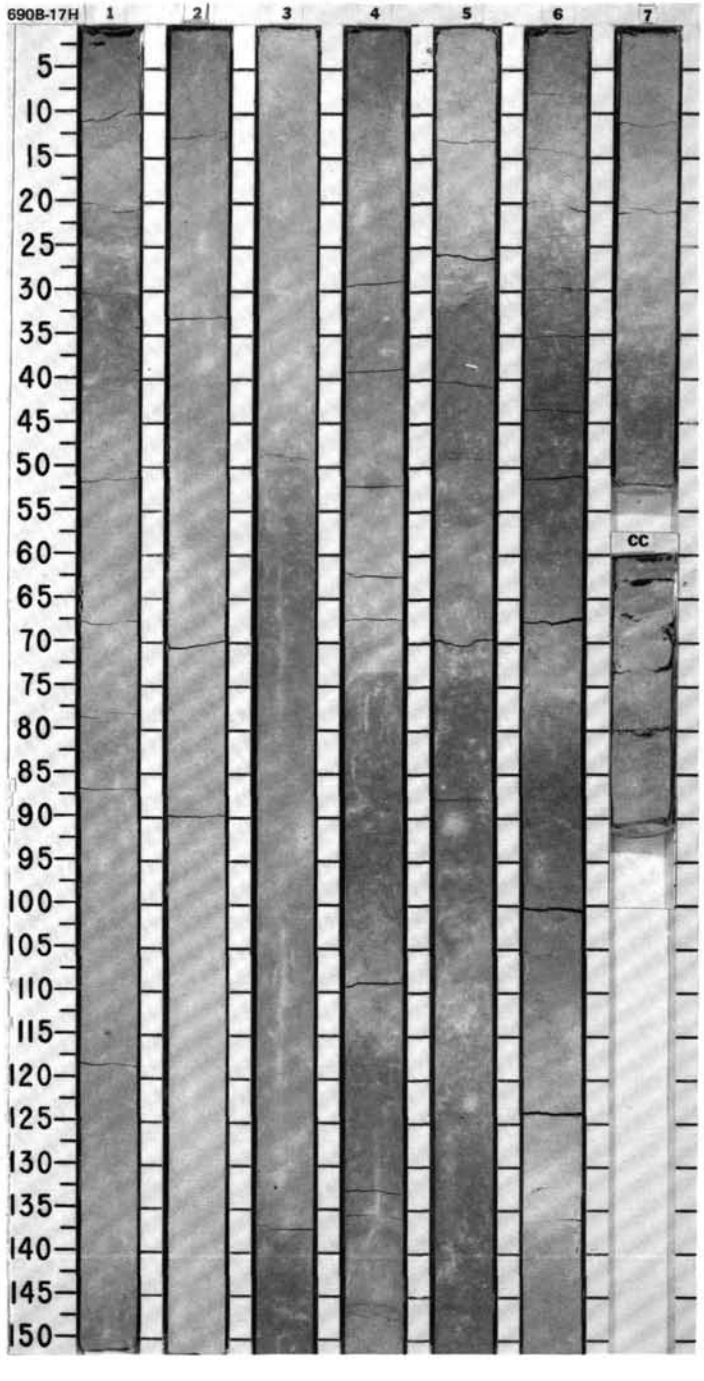

SITE 690 HOLE B CORE 18H CORED INTERVAL 3071.5-3081.2 mbsl; 157.2-166.9 mbsf

TIME-ROCK UNIT	BIOSTRAT. ZONE/ FOSSIL CHARACTER: FORAMINIFERS	NANNOFOSSILS	RADIOLARIANS	DIATOMS	PALEOMAGNETICS	PHYS. PROPERTIES	CHEMISTRY	SECTION	METERS	GRAPHIC LITHOLOGY	DRILLING DISTURB.	SED. STRUCTURES	SAMPLES
UPPER PALEOCENE	A.G	A.G	B	B		ϕ=50 γ=2.02 V=1620 ● ϕ=50 γ=1.88 V=1609 ● ϕ=52 γ=2.11 V=1598 ●	● 85.5% ● 79.8% ● 79.7%	1 2 3 4 5 6 7 CC	0.5 1.0				*

LITHOLOGIC DESCRIPTION

MUDDY NANNOFOSSIL OOZE

Major lithology: Muddy nannofossil ooze, primarily white (2.5Y 8/1) and light gray (10YR 7/1, 7/2). Additional colors in Sections 1-3 include light brownish gray (10YR 6/2), pale brown (10YR 6/3), and light yellowish brown (10YR 6/4). Color boundaries are gradational and burrowed, with layers of each color commonly 30-50 cm thick.

Minor lithology: Nannofossil silty mud, light gray (10YR 7/2), moderately bioturbated, and micaceous in Section 2, 25-65 cm.

Moderately bioturbated, except for Section 4, which is white (2.5Y 8/1) and *apparently structureless.*

Tiny mica flakes are conspicuous on the surface, particularly in darker-colored layers. Small normal faults, thought to result from coring disturbance, displace *Zoophycos* burrows in Section 1, 0-20 cm. Proportion of clay decreases downcore.

SMEAR SLIDE SUMMARY (%):

	1, 50 D	2, 50 M	3, 50 D	4, 50 D	5, 50 D	6, 50 D
COMPOSITION:						
Quartz	—	Tr	—	Tr	Tr	—
Mica	15	40	20	25	30	15
Clay	15	17	20	10	10	10
Accessory minerals:						
Zeolites	Tr	—	—	—	—	—
Chlorite	—	—	Tr	—	—	—
Opaques	—	—	Tr	—	—	—
Foraminifers	3	3	2	2	5	1
Nannofossils	67	40	58	63	55	74

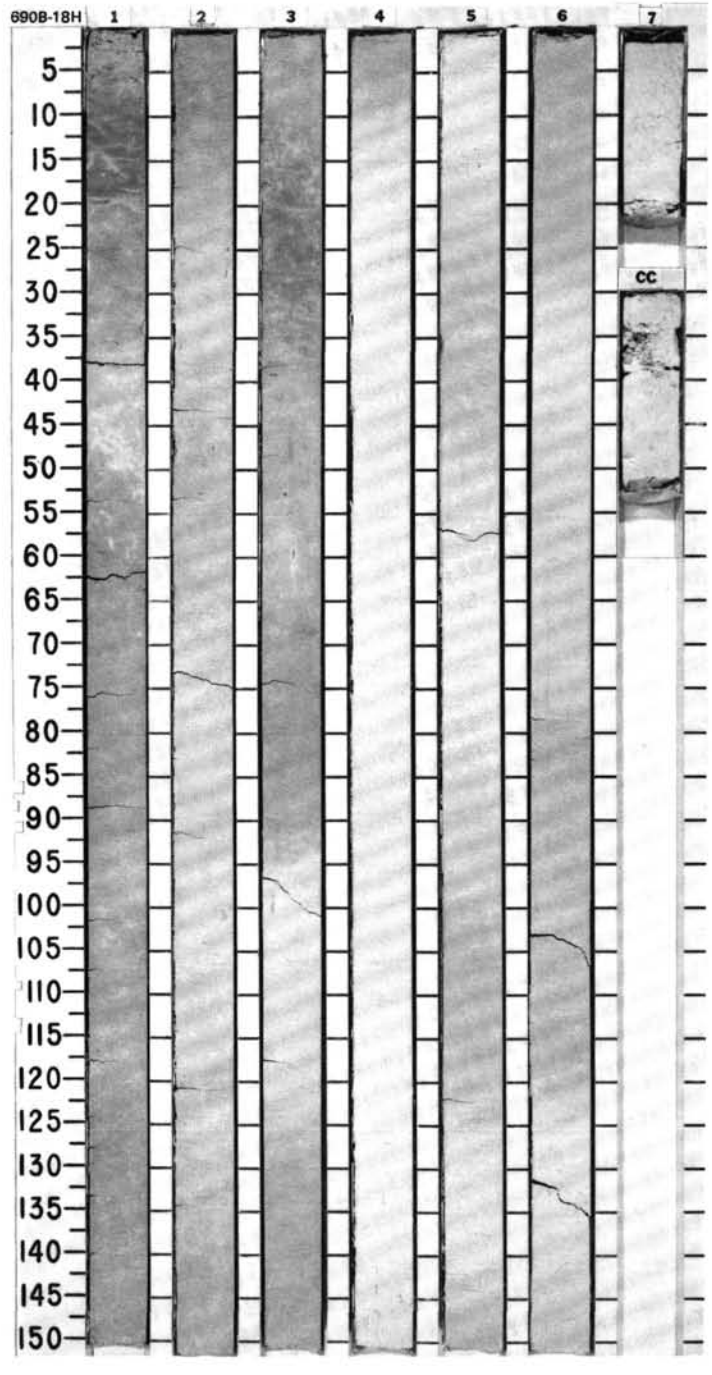

SITE 690 HOLE B CORE 19H CORED INTERVAL 3081.2-3088.6 mbsl; 166.9-174.3 mbsf

TIME-ROCK UNIT	FORAMINIFERS	NANNOFOSSILS	RADIOLARIANS	DIATOMS	PALYNOMORPHS	PALEOMAGNETICS	PHYS. PROPERTIES	CHEMISTRY	SECTION	METERS	GRAPHIC LITHOLOGY	DRILLING DISTURB.	SED. STRUCTURES	SAMPLES
UPPER PALEOCENE	A, G	A, G	B	B	B		ϕ=54 γ=2.00 ν=1606 ● ϕ=56 γ=2.22 ν=1544 ●	● 80.8% ● 66.1% ● 94.5%	1 2 3 4 5 CC	0.5 1.0				IW OG

LITHOLOGIC DESCRIPTION

MUDDY NANNOFOSSIL OOZE, MUD-BEARING NANNOFOSSIL OOZE, and *FORAMINIFER- AND MUD-BEARING NANNOFOSSIL OOZE*

Major lithologies: Muddy nannofossil ooze, mud-bearing nannofossil ooze, and foraminifer- and mud-bearing nannofossil ooze, pure white (2.5Y 8/0), white (2.5Y 8/1) and light gray (2.5Y 7/1, 10YR 7/1) in Sections 1-2; very pale brown (10YR 6/6) and yellowish brown (10YR 5/4, 5/6) in Sections 3-5. Intervals of each color are 30-50 cm thick, with gradational burrowed contacts.

Minor lithology: Altered volcanic ash(?), light greenish gray (5GY 7/1) and gray (2.5Y 6/1), multiple laminae, Section 1, 24-27 cm.

Bioturbation is moderate below Section 2, 50 cm.

SMEAR SLIDE SUMMARY (%):

	1, 50 D	2, 50 D	3, 50 D	4, 50 D	5, 50 D
COMPOSITION:					
Quartz	Tr	1	1	1	Tr
Mica	15	10	10	10	7
Clay	15	5	15	7	10
Volcanic glass	Tr	—	—	—	—
Calcite/dolomite	—	—	—	—	Tr
Foraminifers	1	Tr	3	15	10
Nannofossils	69	84	71	67	73
Diatoms	—	Tr	—	—	—

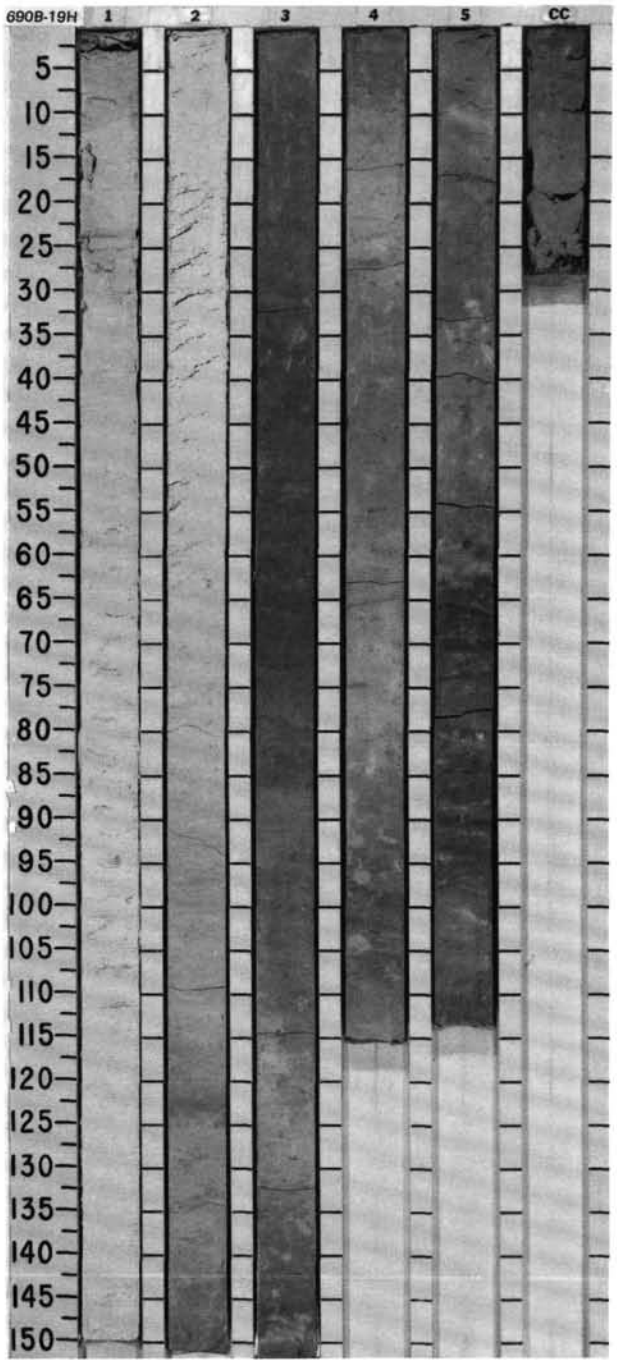

SITE 690 HOLE B CORE 20H CORED INTERVAL 3088.6-3094.6 mbsl; 174.3-180.3 mbsf

TIME-ROCK UNIT	BIOSTRAT. ZONE/ FOSSIL CHARACTER: FORAMINIFERS	NANNOFOSSILS	RADIOLARIANS	DIATOMS	PALYNOMORPHS	PALEOMAGNETICS	PHYS. PROPERTIES	CHEMISTRY	SECTION	METERS	GRAPHIC LITHOLOGY	DRILLING DISTURB.	SED. STRUCTURES	SAMPLES
UPPER PALEOCENE	A, G	A, G	B	B	B		ϕ=54 γ=2.15 V=1584 ϕ=57 γ=2.19 V=1577	● 88.7% ● 85.7%	1 2 3 4 CC	0.5 1.0				* * * *

LITHOLOGIC DESCRIPTION

MUDDY NANNOFOSSIL OOZE, MUD-BEARING NANNOFOSSIL OOZE, and NANNOFOSSIL OOZE

Major lithologies: Muddy nannofossil ooze, mud-bearing nannofossil ooze, and nannofossil ooze, very pale brown (10YR 7/4) and yellowish brown (10YR 5/6) in Section 1; and reddish yellow (7.5YR 6/6), brownish yellow (10YR 6/6), and strong brown (7.5YR 5/6) in Sections 2–4. Intervals of each color are 20–60 cm thick with gradational burrowed contacts; burrow fills tend to be paler than surrounding sediment. Mud content decreases downcore.

SMEAR SLIDE SUMMARY (%):

	1, 50 D	2, 50 D	3, 50 D	4, 50 D
COMPOSITION:				
Quartz	1	Tr	Tr	Tr
Mica	11	5	4	3
Clay	15	18	8	5
Accessory minerals:				
Zeolites	—	2	—	—
Foraminifers	3	5	2	—
Nannofossils	65	70	86	92
Diatoms	2	—	—	—
Radiolarians	3	Tr	Tr	—

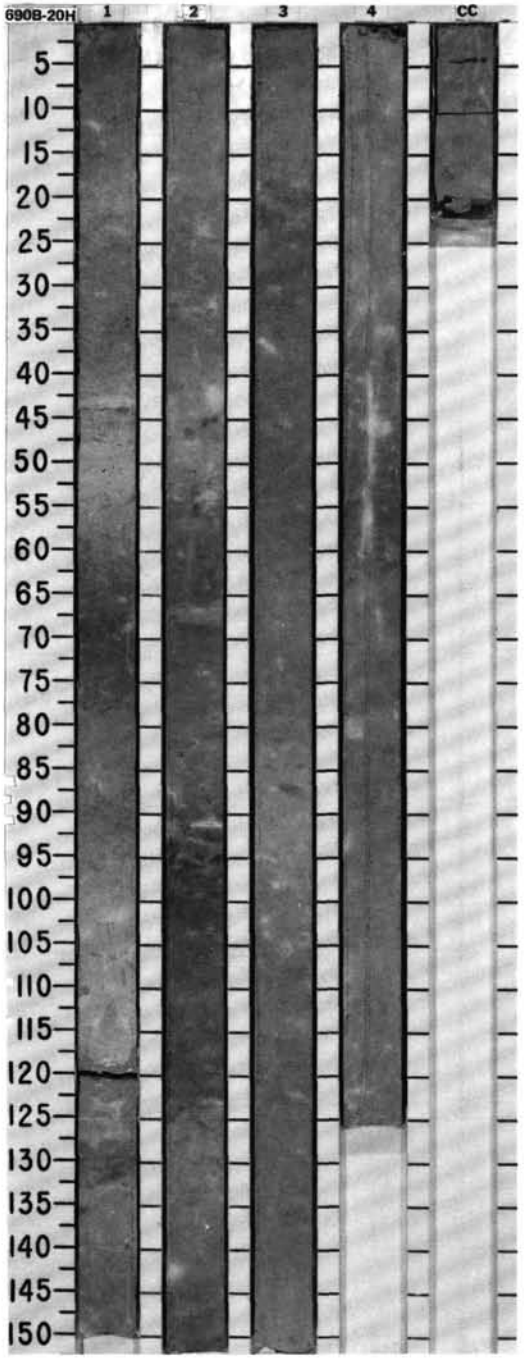

SITE 690 HOLE B CORE 21H CORED INTERVAL 3094.6-3099.5 mbsl; 180.3-185.2 mbsf

TIME-ROCK UNIT	BIOSTRAT. ZONE/ FOSSIL CHARACTER: FORAMINIFERS	NANNOFOSSILS	RADIOLARIANS	DIATOMS	PALYNOMORPHS	PALEOMAGNETICS	PHYS. PROPERTIES	CHEMISTRY	SECTION	METERS	GRAPHIC LITHOLOGY	DRILLING DISTURB.	SED. STRUCTURES	SAMPLES
UPPER PALEOCENE	A, G	A, G	B	B	B		ϕ=54 γ=2.03 V=1570 ● ϕ=54 γ=1.96 V=1582 ●	● 84.6% ● 83.7%	1 2 3 4 CC	0.5 1.0			* * *	

LITHOLOGIC DESCRIPTION

NANNOFOSSIL OOZE

Major lithology: Nannofossil ooze, pink (5YR 8/4, 7.5YR 7/4), light reddish brown (5YR 6/4), and reddish yellow (5YR 6/6); also very pale brown (10YR 7/3) and light reddish brown (5YR 6/4) in Section 1. Intervals of each color are 10–30 cm thick with gradational burrowed contacts. Slight to moderate bioturbation includes abundant *Zoophycos*.

Coring disturbance: liner squeezed flat from about 70 to 135 cm in Section 3.

SMEAR SLIDE SUMMARY (%):

	1, 50 D	2, 50 D	3, 50 D
COMPOSITION:			
Quartz	2	—	—
Feldspar	Tr	—	—
Clay	3	2	10
Volcanic glass	—	Tr	—
Foraminifers	Tr	2	Tr
Nannofossils	95	93	89
Diatoms	Tr	1	Tr
Radiolarians	Tr	2	1

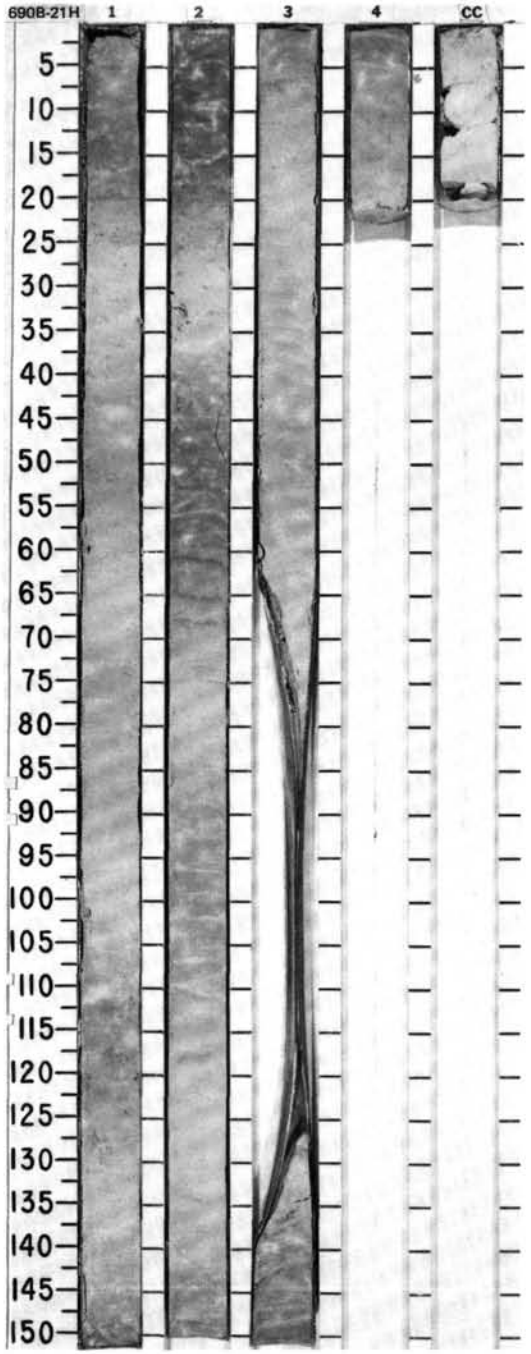

SITE 690 HOLE B CORE 22H CORED INTERVAL 3099.5-3105.5 mbsl; 185.2-191.2 mbsf

TIME-ROCK UNIT	BIOSTRAT. ZONE/ FOSSIL CHARACTER: FORAMINIFERS	NANNOFOSSILS	RADIOLARIANS	DIATOMS	PALYNOMORPHS	PALEOMAGNETICS	PHYS. PROPERTIES	CHEMISTRY	SECTION	METERS	GRAPHIC LITHOLOGY	DRILLING DISTURB.	SED. STRUCTURES	SAMPLES
UPPER PALEOCENE	A, G	A, G	B	B	B		ϕ=53 γ=1.86 χ=1571 ● ϕ=52 γ=1.88 ●	81.13% ●	1 2 3 4 CC	0.5 1.0				* * * IW OG *

LITHOLOGIC DESCRIPTION

NANNOFOSSIL OOZE

Major lithology: Nannofossil ooze, mainly pinkish white (7.5YR 8/2, 8/3; 5YR 8/3). Intervals of reddish yellow (5YR 6/6) in Section 3, and white (5YR 8/1) and pink (5YR 7/3) in Section 4. Intervals of each color are 20–50 cm thick, with gradational burrowed contacts. Slight to moderate bioturbation includes abundant *Zoophycos* in Section 3.

SMEAR SLIDE SUMMARY (%):

COMPOSITION:	1, 80 D	2, 80 D	3, 80 D	4, 80 D
Quartz	—	—	—	Tr
Mica	3	5	5	2
Clay	2	Tr	2	5
Volcanic glass	Tr	—	—	—
Foraminifers	6	10	5	8
Nannofossils	89	85	88	85

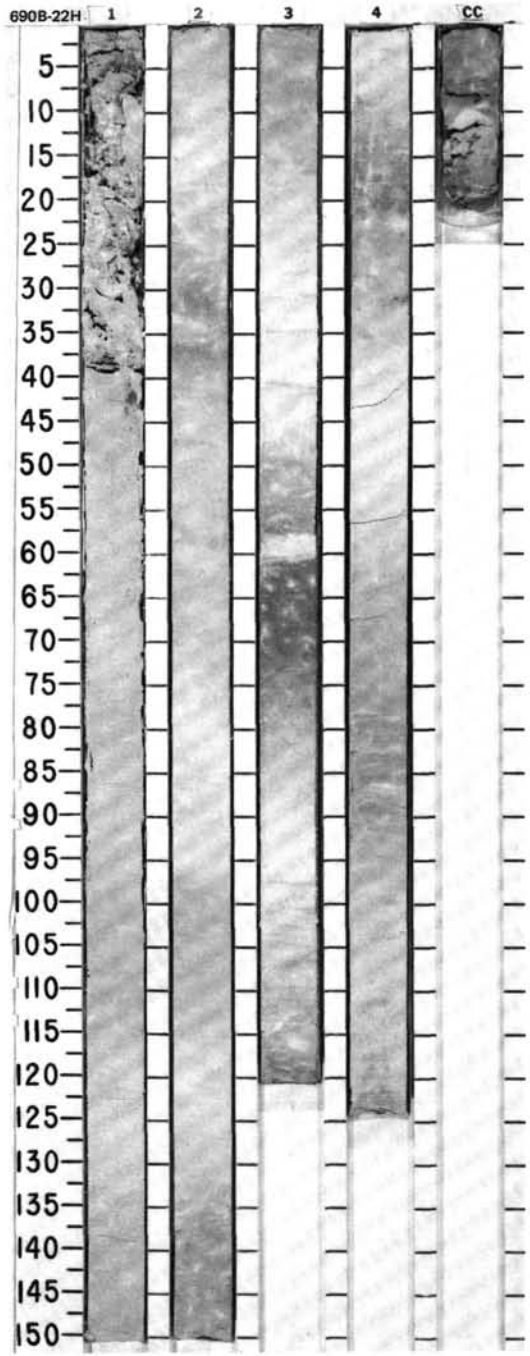

SITE 690 HOLE B CORE 23H CORED INTERVAL 3105.5-3112.5 mbsl; 191.2-198.2 mbsf

TIME-ROCK UNIT	BIOSTRAT. ZONE/ FOSSIL CHARACTER: FORAMINIFERS	NANNOFOSSILS	RADIOLARIANS	DIATOMS	PALYNOMORPHS	PALEOMAGNETICS	PHYS. PROPERTIES	CHEMISTRY	SECTION	METERS	GRAPHIC LITHOLOGY	DRILLING DISTURB.	SED. STRUCTURES	SAMPLES
UPPER PALEOCENE	A, G	A, G	B	B	B		ϕ=52 γ=1.89 V=1572 ● ϕ=54 γ=1.85 V=1572 ●		1 2 3 4 5	0.5 1.0				* * * * *

LITHOLOGIC DESCRIPTION

NANNOFOSSIL OOZE and MUD-BEARING NANNOFOSSIL OOZE

Major lithologies: Nannofossil ooze, pink (7.5YR 8/4) to pinkish white (7.5YR 8/2) and reddish yellow (7.5YR 8/6); Section 1, alternate white and dark layers; color sequences appear to be cyclical. Sections 2–4, white (5YR 8/1) to pinkish white (7.5YR 8/2), with a thin reddish yellow layer (7.5YR 7/6) in Section 3, 91–99 cm. Mud-bearing nannofossil ooze, pink (7.5 YR 8/2), contains long vertical burrows.

There is a chalky layer in Section 5, 58–64 cm. Bioturbation is minor. Identifiable types include *Planolites*, *Zoophycos*, and vertical burrows.

SMEAR SLIDE SUMMARY (%):

	1, 53 D	2, 53 D	2, 180 M	3, 53 D	4, 53 D	5, 53 D
COMPOSITION:						
Mica	3	2	4	6	3	8
Clay	1	5	8	2	6	3
Volcanic glass	Tr	2	4	2	2	2
Accessory minerals	—	—	Tr	—	2	Tr
Foraminifers	9	8	12	4	9	9
Nannofossils	85	83	72	86	78	78
Calcispheres	2	—	—	—	—	—

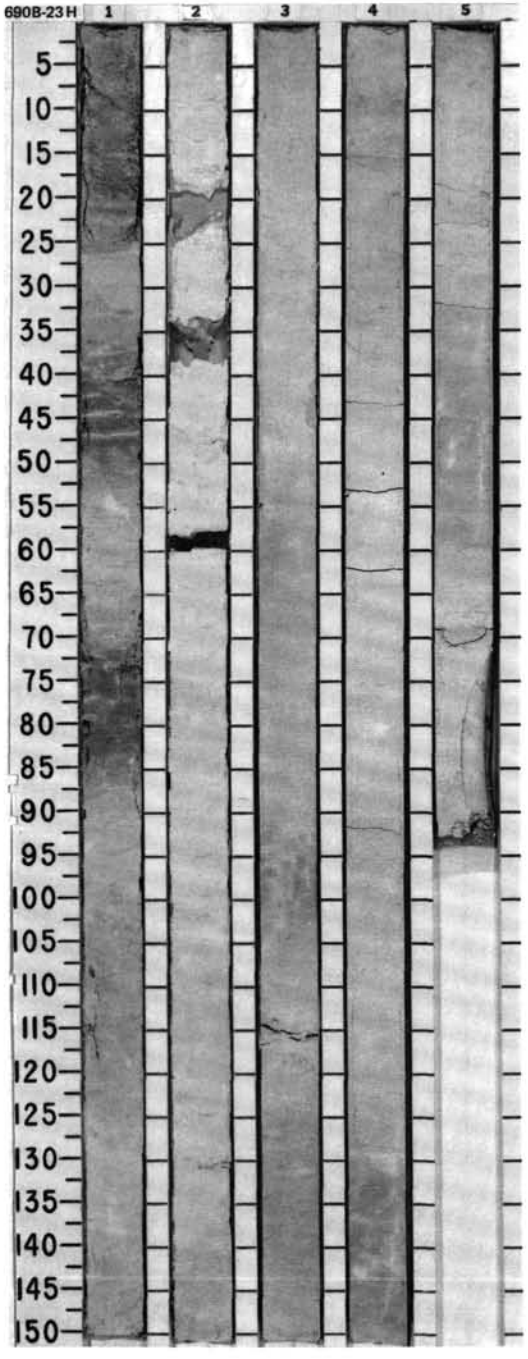

SITE 690 HOLE B CORE 24H CORED INTERVAL 3112.5-3118.5 mbsl; 198.2-204.2 mbsf

TIME-ROCK UNIT	BIOSTRAT. ZONE/ FOSSIL CHARACTER: FORAMINIFERS	NANNOFOSSILS	RADIOLARIANS	DIATOMS	PALYNOMORPHS	PALEOMAGNETICS	PHYS. PROPERTIES	CHEMISTRY	SECTION	METERS	GRAPHIC LITHOLOGY	DRILLING DISTURB.	SED. STRUCTURES	SAMPLES
UPPER PALEOCENE	A,G	A,G	B	B	B		• ϕ=52 γ=1.92 V=1606 • ϕ=53 γ=1.86		1 2 3 4	0.5 1.0			P V C Z T	*

UPPER PALEOCENE — UPPER PALEOCENE — CP5 - CP6

LITHOLOGIC DESCRIPTION

NANNOFOSSIL OOZE and FORAMINIFER-NANNOFOSSIL OOZE

Major lithologies: Nannofossil ooze, grading color cycles of pinkish white (7.5YR 8/2) to white (5YR 8/1). Heavily mottled and bioturbated throughout Section 1; Sections 3 and 4 grading from pink (7.5YR 7/3) to pinkish white (7.5YR 8/2); moderately mottled. Foraminifer-nannofossil ooze, grading color cycles of white (5YR 8/1) to pinkish white (2.5YR 8/2) and reddish yellow (5YR 7/6); moderately to strongly bioturbated.

SMEAR SLIDE SUMMARY (%):

COMPOSITION:	1, 60 D	1, 60 D	3, 60 D	4, 60 D
Quartz	Tr	—	Tr	—
Mica	4	1	2	1
Clay	2	3	1	Tr
Volcanic glass	—	2	—	1
Foraminifers	6	30	6	5
Nannofossils	88	62	91	91
Calcispheres	—	2	—	2

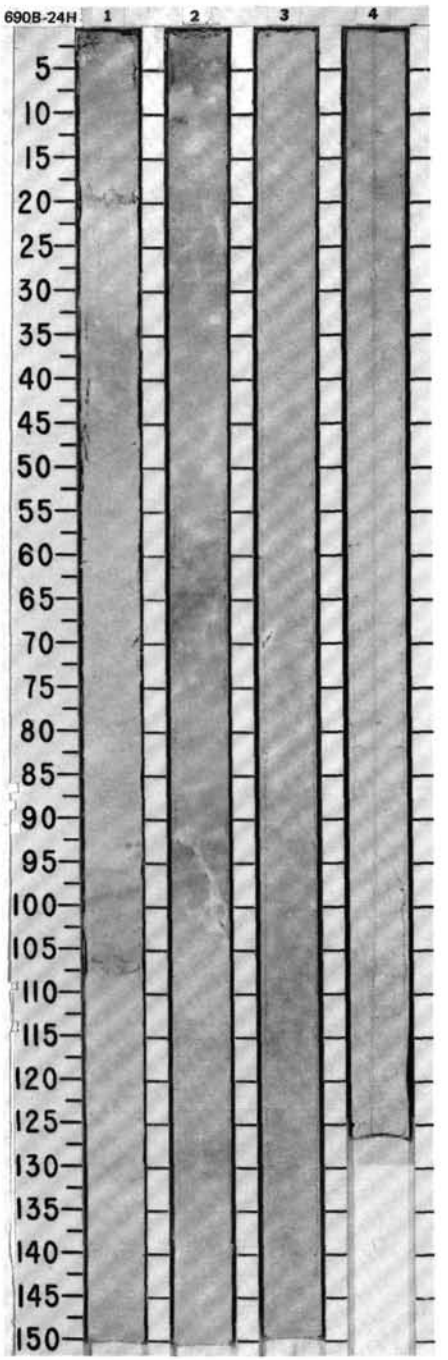

SITE 690 HOLE B CORE 25H CORED INTERVAL 3118.5-3127.7 mbsl; 204.2-213.4 mbsf

TIME-ROCK UNIT	BIOSTRAT. ZONE/ FOSSIL CHARACTER: FORAMINIFERS	NANNOFOSSILS	RADIOLARIANS	DIATOMS	PALEOMAGNETICS	PHYS. PROPERTIES	CHEMISTRY	SECTION	METERS	GRAPHIC LITHOLOGY	DRILLING DISTURB.	SED. STRUCTURES	SAMPLES
UPPER PALEOCENE	AG	G, A	B	B	● ϕ=45 γ=2.07	ϕ=48 γ=1.93 V=1652 V=1602 ● ϕ=50 γ=1.93 V=1602 ●	76.5% ●	1 2 3 4 5 6 7 CC	0.5 1.0				IW OC

LITHOLOGIC DESCRIPTION

NANNOFOSSIL OOZE and MUD-BEARING NANNOFOSSIL OOZE

Major lithologies: Nannofossil ooze, grading cycles of pinkish white (7.5YR 8/2) and white (7.5YR 8/1). Bioturbation absent to moderate; *Zoophycos* present. Mud-bearing nannofossil ooze, pinkish white (7.5YR 8/2) and pink (7.5YR 7/3).

Minor lithology: Clayey nannofossil ooze, strong brown (7.5YR 5/4), Section 1, 113 cm, to Section 2, 24 cm.

SMEAR SLIDE SUMMARY (%):

	1, 80 D	2, 5 M	2, 80 D	3, 80 D	4, 80 D	5, 80 D	6, 80 D
COMPOSITION:							
Quartz	—	2	—	—	Tr	—	Tr
Mica	3	6	4	1	3	2	8
Clay	5	30	5	3	2	4	4
Volcanic glass	1	5	2	—	—	—	—
Accessory minerals:							
Pyrite	Tr	Tr	—	—	—	—	Tr
Foraminifers	8	4	8	8	9	8	6
Nannofossils	83	53	81	88	86	86	82

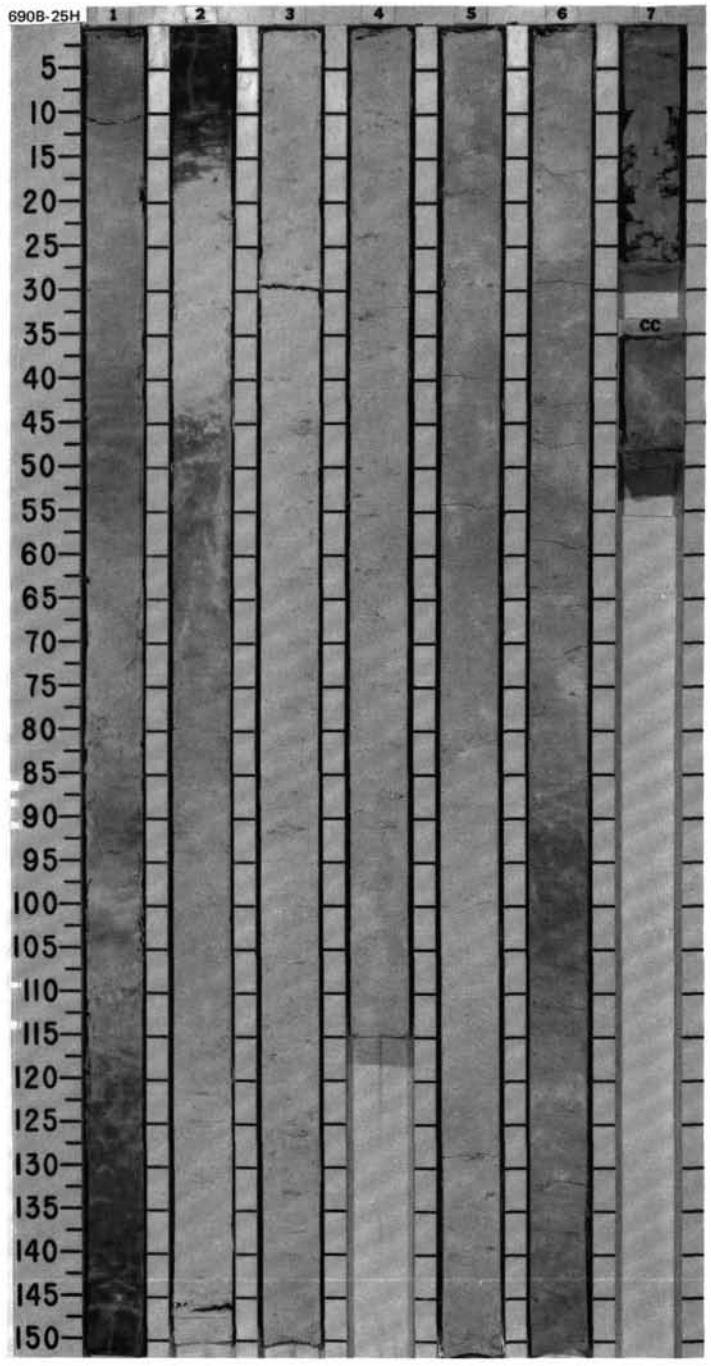

SITE 690 HOLE C CORE 1H CORED INTERVAL 2914.3-2920.4 mbsl; 0-6.1 mbsf

TIME-ROCK UNIT	BIOSTRAT. ZONE/FOSSIL CHARACTER: FORAMINIFERS	NANNOFOSSILS	RADIOLARIANS	DIATOMS	PALYNOMORPHS	PALEOMAGNETICS	PHYS. PROPERTIES	CHEMISTRY	SECTION	METERS	GRAPHIC LITHOLOGY	DRILLING DISTURB.	SED. STRUCTURES	SAMPLES
UPPER PLIOCENE	B	B	A,G	A,G	B				1	0.5				*
			UPPER *Upsilon* Zone	*N. interfrigidaria* F.P *C. eliptopora* / *A. ingens*					1	1.0				
									2					*
									3					*
									4					*
									5					*
									6					*
									CC					

LITHOLOGIC DESCRIPTION

DIATOM-BEARING FORAMINIFERAL OOZE and DIATOM OOZE

Major lithologies: Diatom-bearing foraminifer ooze, very pale brown (10YR 7/3), light gray (10YR 7/2), and very pale brown (10YR 6/3). Diatom ooze, white (2.5Y 8/2, 7.5Y 8/1, 10YR 8/1), light yellowish brown (2.5Y 6/3), light gray (2.5Y 7/2, 10YR 7/2), and very pale brown (10YR 7/3).

Bioturbation is moderate to strong and includes *Planolites*, halo burrows, and vertical burrows. Many gradational color changes are due in part to bioturbation. Scattered throughout are "patches" of white (7.5YR 8/1) diatom ooze. Upper part of core is moderately disturbed by drilling.

SMEAR SLIDE SUMMARY (%):

	1, 50 D	2, 50 D	3, 50 D	4, 50 D	5, 50 D	6, 50 D
COMPOSITION:						
Quartz	Tr	Tr	Tr	Tr	Tr	—
Clay	2	Tr	—	Tr	Tr	—
Foraminifers	76	82	74	Tr	—	2
Diatoms	22	18	26	90	91	86
Radiolarians	Tr	—	Tr	6	9	8
Silicoflagellates	—	—	—	4	Tr	4

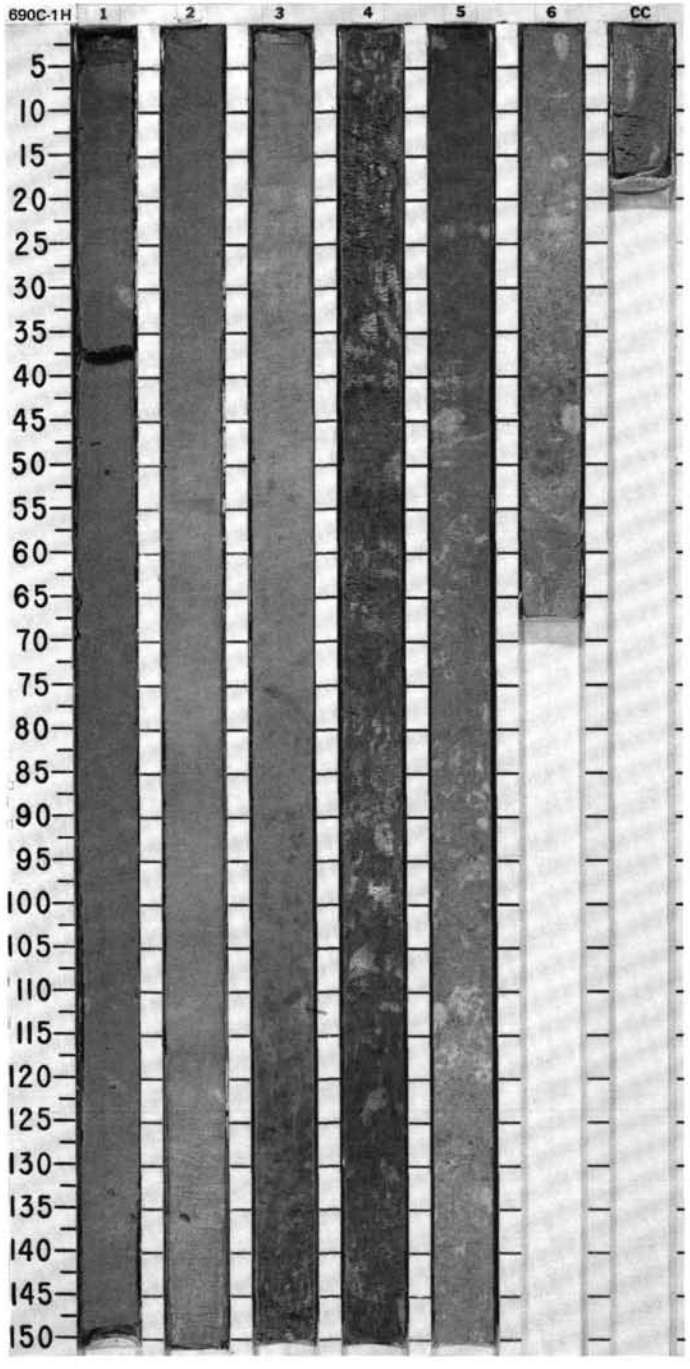

SITE 690 HOLE C CORE 2H CORED INTERVAL 2920.4-2930.1 mbsl; 6. 1-15.8 mbsf

TIME-ROCK UNIT: LOWER PLIOCENE

BIOSTRAT. ZONE/FOSSIL CHARACTER: UPPER *Tau* Zone; *N. angulata*

FORAMINIFERS: B

NANNOFOSSILS: B

RADIOLARIANS: A, G

DIATOMS: A, G

PALYNOMORPHS: B

PALEOMAGNETICS

PHYS. PROPERTIES

CHEMISTRY

SECTION: 1, 2, 3, 4, 5, 6, 7, CC

METERS: 0.5, 1.0

GRAPHIC LITHOLOGY

DRILLING DISTURB.

SED. STRUCTURES

SAMPLES

LITHOLOGIC DESCRIPTION

RADIOLARIAN-BEARING DIATOM OOZE, DIATOM OOZE, SILICOFLAGELLATE- AND RADIOLARIAN-BEARING DIATOM OOZE, and RADIOLARIAN- AND SILICOFLAGELLATE-BEARING DIATOM OOZE

Major lithologies: Radiolarian-bearing diatom ooze, white (10YR 8/2), light gray (10YR 7/1, 7/2), pale yellow (2.5Y 7/3), and very pale brown (10YR 7/3); color changes are gradational. Bioturbation is strong, with color mixing between white, light gray, and very pale brown. Diatom ooze, pure white (10YR 8/0), minor to absent bioturbation. Silicoflagellate- and radiolarian-bearing diatom ooze, very pale brown (10YR 7/3) and grayish brown (10YR 5/2), gradual color change. Radiolarian- and silicoflagellate-bearing diatom ooze, white (2.5Y 8/2) and light gray (2.5Y 8/2); gradational color changes and moderate to strong bioturbation. A color transition at Section 1, 35 cm, is marked by numerous *Planolites*. A color transition at Section 5, 120 cm, is marked by a few halo burrows. Vertical burrows are also present.

Minor lithology: Diatom-bearing foraminifer ooze, very pale brown (10YR 7/3), Section 1, 0–30 cm. Moderately disturbed by coring.

Dropstones are present in Section 1, 92 and 121 cm (both 3 mm long); Section 3, 77 cm (10 mm long), black and subangular; Section 4, 84 cm (5 mm long); and Section 5, 38, 51, and 63 cm (5, 3, and 2 mm long, respectively).

SMEAR SLIDE SUMMARY (%):

	1, 70 D	2, 20 M	2, 70 D	3, 70 D	4, 70 D	5, 70 D	6, 70 D
COMPOSITION:							
Quartz	—	—	—	Tr	Tr	—	Tr
Mica	—	2	—	Tr	—	Tr	—
Clay	Tr	—	2	1	Tr	Tr	—
Volcanic glass	—	—	—	—	—	—	Tr
Accessory minerals	—	—	—	Tr	Tr	—	—
Foraminifers	—	—	Tr	—	—	—	—
Nannofossils	—	—	—	Tr	—	—	—
Diatoms	88	94	82	81	80	74	76
Radiolarians	12	4	16	18	8	18	12
Silicoflagellates	Tr	—	Tr	—	12	8	12

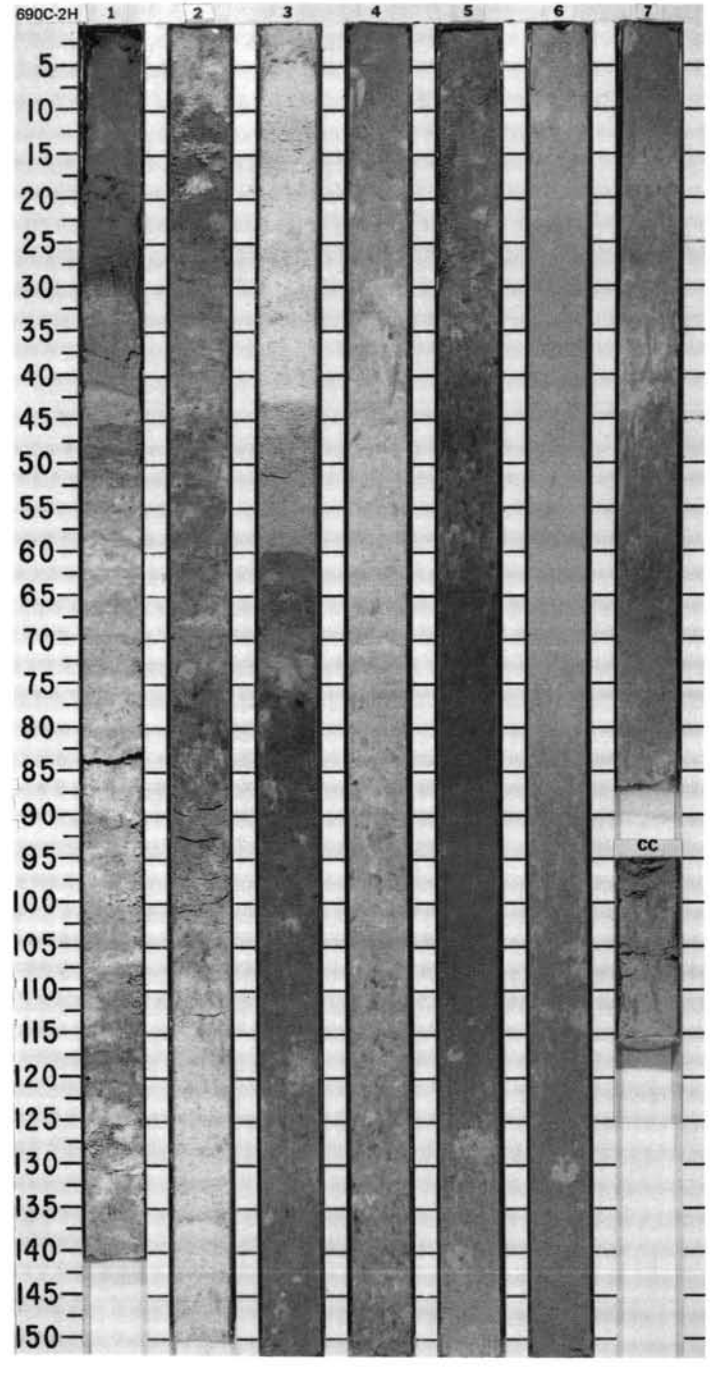

SITE 690 HOLE C CORE 3H CORED INTERVAL 2930.1-2939.8 mbsl; 15.8-25.5 mbsf

TIME-ROCK UNIT	BIOSTRAT. ZONE/ FOSSIL CHARACTER: FORAMINIFERS	NANNOFOSSILS	RADIOLARIANS	DIATOMS	PALYNOMORPHS	PALEOMAGNETICS	PHYS. PROPERTIES	CHEMISTRY	SECTION	METERS	GRAPHIC LITHOLOGY	DRILLING DISTURB.	SED. STRUCTURES	SAMPLES
UPPER MIOCENE / LOWER PLIOCENE	B	B	A,G	A,G	B				1	0.5, 1.0				*
			UPPER *C. spongothorax*	*D. hustedtii*					2					*
				A,G *N. reinholdii*					3					*
									4					*
									5					*
									6					*
									7					*
									CC					

LITHOLOGIC DESCRIPTION

DIATOM OOZE, SILICOFLAGELLATE-DIATOM OOZE, and RADIOLARIAN-BEARING DIATOM OOZE

Major lithologies: Diatom ooze, gray (2.5Y 6/2) to grayish brown (10YR 5/2), minor to moderate bioturbation, in Section 3. Silicoflagellate-bearing diatom ooze, white (10YR 8/2) with light gray vertical burrows and mottling, to gray (2.5Y 6/2). Radiolarian-bearing diatom ooze, grayish brown (10YR 5/2) with light gray to black vertical burrows and mottling; light brown (2.5Y 6/2) and light gray (10YR 7/2) in Sections 4 and 6.

Minor lithology: Nannofossil-bearing diatom ooze, pale brown (10YR 6/3) to light gray (10YR 7/2). Bioturbation slight to moderate, Section 7.

Small dropstones in Section 2, 100, 115, and 125 cm.

SMEAR SLIDE SUMMARY (%):

	1, 50 D	2, 50 D	3, 50 D	4, 50 D	5, 50 D	6, 50 D	7, 50 D
COMPOSITION:							
Quartz	—	2	2	3	3	3	2
Clay	—	2	2	—	—	Tr	3
Volcanic glass	—	Tr	—	—	—	—	—
Accessory minerals:							
Pyrite	Tr	—	—	—	—	—	—
Heavy minerals	—	—	Tr	—	—	—	—
Foraminifers	—	—	Tr	—	—	—	—
Nannofossils	—	—	—	Tr	—	Tr	30
Diatoms	70	84	89	87	87	82	58
Radiolarians	5	7	7	10	10	15	7
Sponge spicules	Tr	—	—	—	—	—	—
Silicoflagellates	25	5	—	Tr	—	—	—

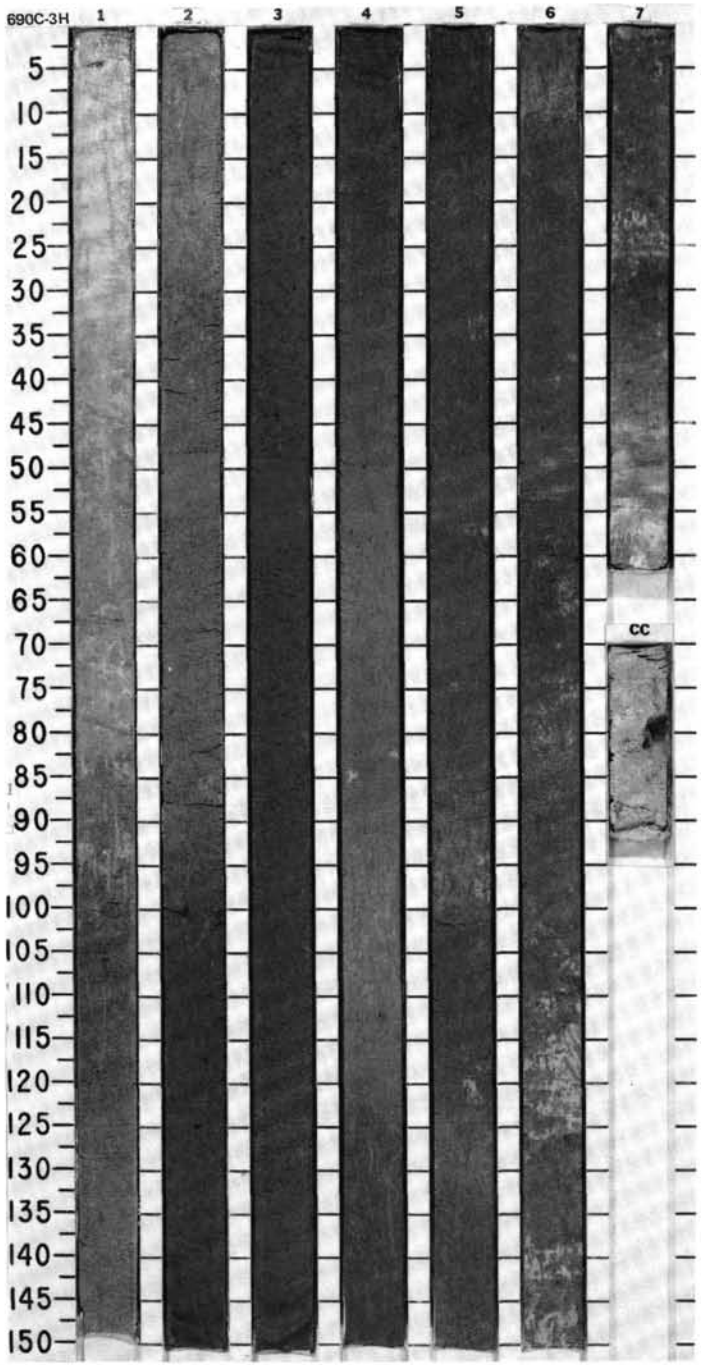

SITE 690 HOLE C CORE 4H CORED INTERVAL 2939.8-2949.5 mbsl; 25.5-35.2 mbsf

TIME-ROCK UNIT	BIOSTRAT. ZONE/ FOSSIL CHARACTER: FORAMINIFERS	NANNOFOSSILS	RADIOLARIANS	DIATOMS	PALYNOMORPHS	PALEOMAGNETICS	PHYS. PROPERTIES	CHEMISTRY	SECTION	METERS	GRAPHIC LITHOLOGY	DRILLING DISTURB.	SED. STRUCTURES	SAMPLES	LITHOLOGIC DESCRIPTION
MIDDLE MIOCENE	B	B	A. tanyacantha	D. hustedtii	B				1	0.5				*	DIATOM-NANNOFOSSIL OOZE, DIATOM-BEARING NANNOFOSSIL OOZE, and DIATOM OOZE
			A, G	C, M						1.0					Major lithologies: Diatom-nannofossil ooze grading down to diatom-bearing nannofossil ooze, white (2.5Y 8/0) and light gray (10YR 7/1, 7/2). Color boundaries gradational. Minor bioturbation. Diatom ooze, light yellowish brown (2.5Y 6/4) and light olive brown (2.5Y 5/4), strongly bioturbated.
														LW	
									2					OC	
														*	
									3					*	
									4					*	
									5					*	
									6					*	
									7					*	
									CC						

SMEAR SLIDE SUMMARY (%):

	1, 50 D	2, 50 D	3, 50 D	4, 50 D	5, 50 D	6, 50 D	7, 10 D
COMPOSITION:							
Quartz	—	Tr	Tr	Tr	Tr	2	2
Volcanic glass	Tr	—	—	—	—	Tr	—
Accessory minerals:							
Opaques	Tr	—	—	—	—	—	Tr
Foraminifers	Tr	—	—	—	—	1	—
Nannofossils	54	85	78	89	78	83	Tr
Diatoms	43	15	20	10	20	15	91
Radiolarians	3	Tr	2	1	2	1	7
Silicoflagellates	Tr	—	—	—	Tr	—	—

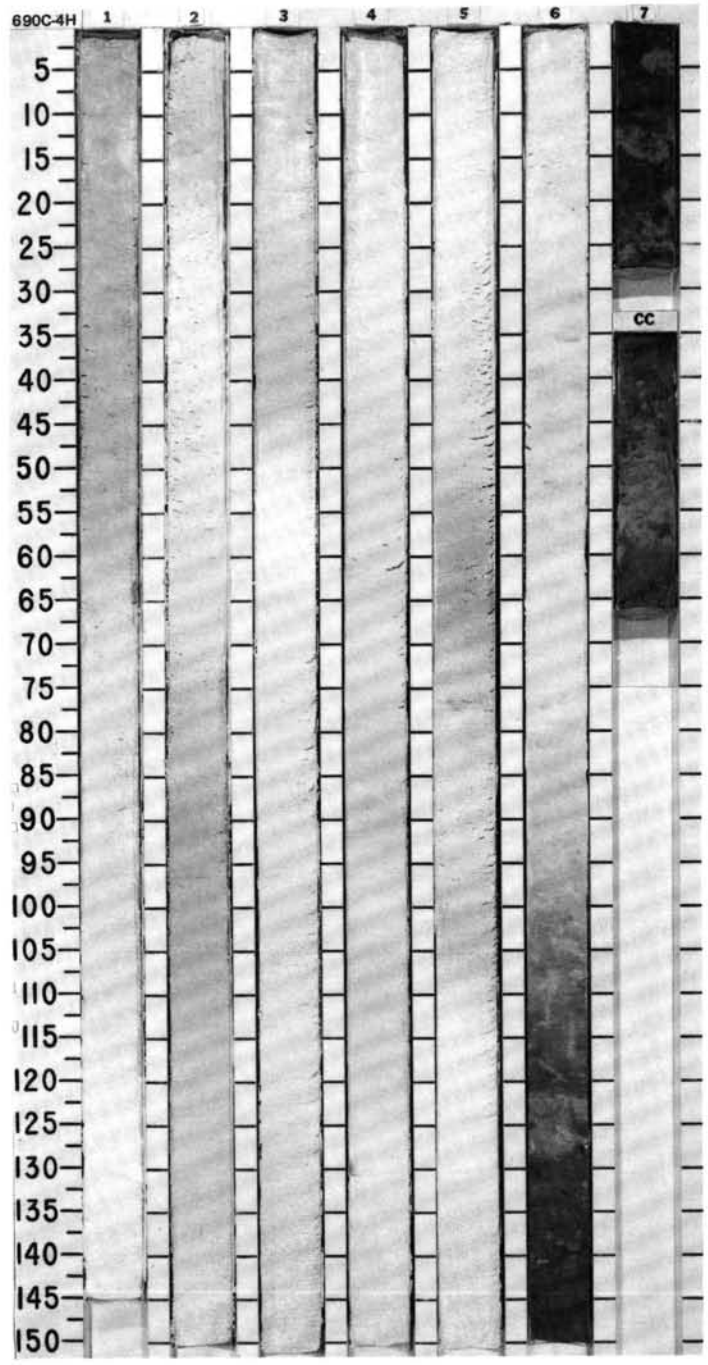

SITE 690 HOLE C CORE 5H CORED INTERVAL 2949.5-2959.2 mbsl; 35.2-44.9 mbsf

TIME-ROCK UNIT: LOWER MIOCENE / MIDDLE MIOCENE

BIOSTRAT. ZONE/FOSSIL CHARACTER: FORAMINIFERS: B; NANNOFOSSILS: B; RADIOLARIANS: A,M; DIATOMS: F,P; PALYNOMORPHS: B

LOWER MIDDLE or LOWER MIOCENE

C. lewisianus - N. grossepuncta

C,M D. hustedtii / D. lauta - N. denticuloides

PALEOMAGNETICS | PHYS. PROPERTIES | CHEMISTRY

SECTION: 1, 2, 3, 4, 5, 6, 7, CC

METERS: 0.5, 1.0

GRAPHIC LITHOLOGY: VOID

DRILLING DISTURB. | SED. STRUCTURES | SAMPLES

LITHOLOGIC DESCRIPTION

DIATOM OOZE, DIATOM-BEARING NANNOFOSSIL OOZE, and RADIOLARIAN- AND MUD-BEARING DIATOM OOZE

Major lithologies: Diatom ooze, homogeneous olive brown (2.5 Y 4/4) with light yellow brown mottles (2.5Y 6/4) in Sections 1 and 2; alternating light olive brown (2.5Y 5/4), light yellowish olive brown (2.5Y 6/4), and olive brown (2.5Y 4/4) in Sections 3 and 4; alternations on the scale of 20–50 cm. Color changes occur over a short interval, but are not sharp. Bioturbation is moderate and includes halo burrows in Section 1 and vertical burrows in Section 4. Diatom-bearing nannofossil ooze, white (10YR 8/1), pale olive, yellow brown (2.5Y 7/4), light olive brown (2.5Y 5/4), and olive brown (2.5Y 4/4), gradually becoming darker from top of Section 6 to bottom of Section 7. Radiolarian- and mud-bearing diatom ooze, olive brown (2.5Y 4/4) at top to light yellow brown (2.5Y 6/4) at bottom of Section 5. Vertical burrow observed below 130 cm.

Minor lithology: Diatom-nannofossil ooze, light yellow brown (2.5Y 6/4), in Section 4, 90–120 cm. Upper boundary is sharp, lower boundary is gradational.

SMEAR SLIDE SUMMARY (%):

COMPOSITION:	1, 50 D	2, 50 D	3, 50 D	4, 50 D	4, 100 M	5, 50 D	6, 50 D
Quartz	5	3	7	5	2	7	—
Clay	—	—	2	2	—	5	Tr
Accessory minerals:							
Heavy minerals	—	—	—	Tr	—	—	—
Foraminifers	—	—	—	—	5	—	Tr
Nannofossils	1	Tr	Tr	Tr	60	—	84
Diatoms	84	90	86	88	30	78	15
Radiolarians	7	7	5	5	3	10	1
Volcanic glass	3	—	—	—	—	—	—

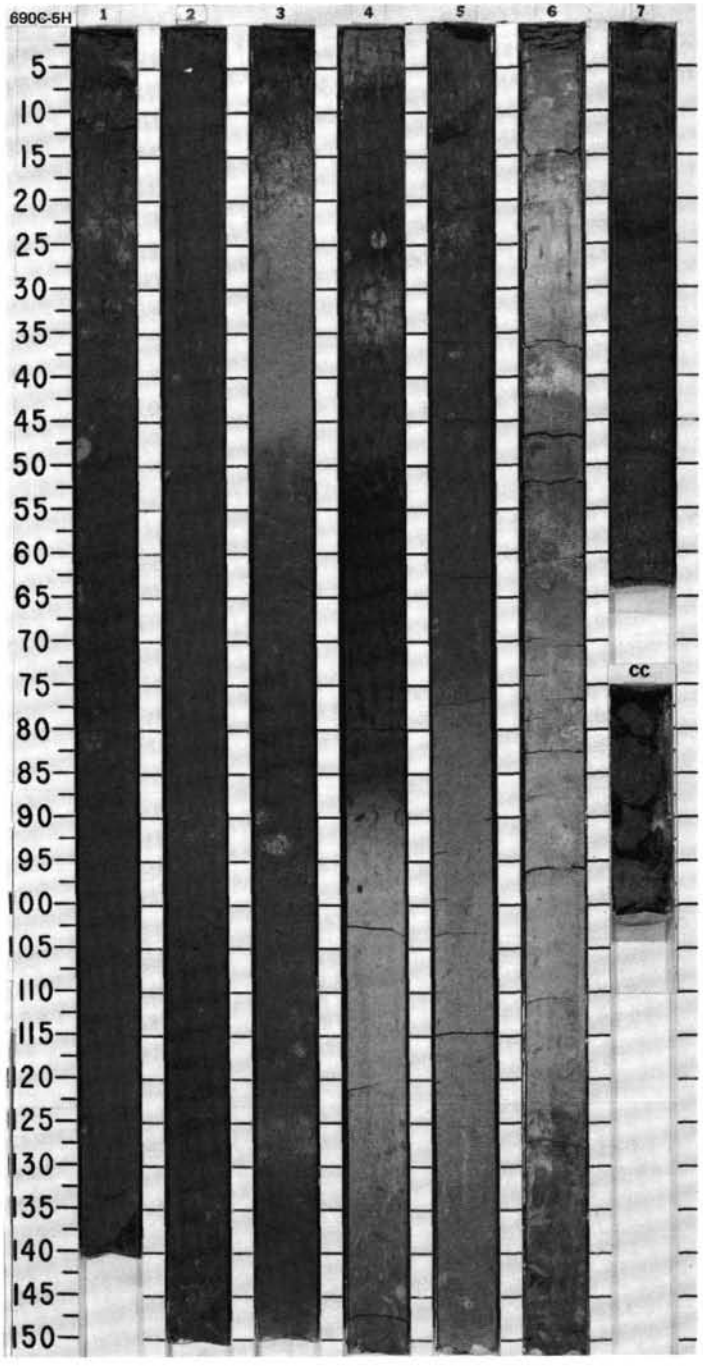

SITE 690 HOLE C CORE 6H CORED INTERVAL 2959.2-2968.9 mbsl; 44.9-54.6 mbsf

TIME-ROCK UNIT	BIOSTRAT. ZONE/ FOSSIL CHARACTER: FORAMINIFERS	NANNOFOSSILS	RADIOLARIANS	DIATOMS	PALYNOMORPHS	PALEOMAGNETICS	PHYS. PROPERTIES	CHEMISTRY	SECTION	METERS	GRAPHIC LITHOLOGY	DRILLING DISTURB.	SED. STRUCTURES	SAMPLES
UPPER OLIGOCENE	A,M	UPPER OLIGOCENE	C,P	OLIGOCENE	F,P	UPPER OLIGOCENE	B				1, 2, 3, 4, 5, 6, 7, CC	0.5, 1.0			*

LITHOLOGIC DESCRIPTION

DIATOM-BEARING NANNOFOSSIL OOZE, MUD-BEARING NANNOFOSSIL-DIATOM OOZE, and MUD- AND DIATOM-BEARING NANNOFOSSIL OOZE

Major lithologies: Diatom-bearing nannofossil ooze, light gray (2.5Y 7/2), light brownish gray (2.5Y 6/2), and grayish brown (10YR 5/2), with white (10YR 8/1) bioturbation mottles. Color transitions occur on the scale of 50 to 100 cm. Mud-bearing nannofossil-diatom ooze, light brown (2.5Y 7/2) and light olive brown (2.5Y 5/4), with light brownish gray (2.5Y 7.2) bioturbation mottles. Gradational color transitions occur on a scale of 60 to 80 cm. Mud- and *diatom-bearing nannofossil ooze, light gray* (2.5Y 7/2), *light brownish gray* (2.5 6/2), grayish brown (2.5Y 5/2), and light olive grayish brown (2.5Y 5/3). Gradational color changes occur on a scale of 30–40 cm.

Core is moderately to strongly disrupted by coring.

SMEAR SLIDE SUMMARY (%):

COMPOSITION:	1, 70 D	2, 70 D	3, 70 D	4, 70 D	5, 70 D	6, 70 D
Quartz	—	1	Tr	3	1	Tr
Mica	—	3	—	Tr	—	—
Clay	—	10	2	7	—	—
Volcanic glass	—	1	—	2	—	—
Accessory minerals:						
Heavy minerals	—	3	1	—	Tr	—
Foraminifers	1	7	1	2	Tr	—
Nannofossils	88	30	73	56	81	82
Diatoms	10	40	20	25	15	15
Radiolarians	1	5	3	5	3	2
Silicoflagellates	—	—	—	Tr	—	Tr

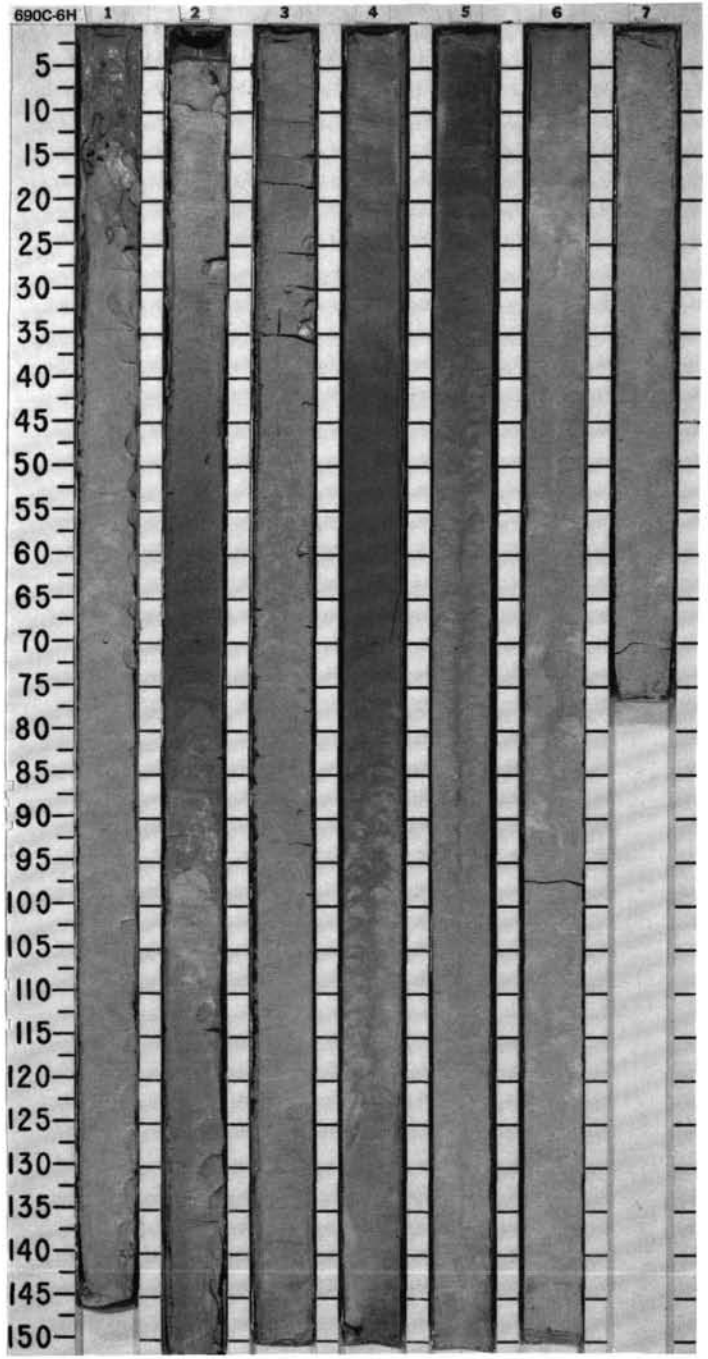

SITE 690 HOLE C CORE 7H CORED INTERVAL 2968.9-2978.6 mbsl; 54.6-64.3 mbsf

TIME-ROCK UNIT	BIOSTRAT. ZONE/ FOSSIL CHARACTER: FORAMINIFERS	NANNOFOSSILS	RADIOLARIANS	DIATOMS	PALYNOMORPHS	PALEOMAGNETICS	PHYS. PROPERTIES	CHEMISTRY	SECTION	METERS	GRAPHIC LITHOLOGY	DRILLING DISTURB.	SED. STRUCTURES	SAMPLES
OLIGOCENE	?		OLIGOCENE	OLIGOCENE					1 2 3 4 5 6 7 CC	0.5 1.0				* * * * *

LITHOLOGIC DESCRIPTION

NANNOFOSSIL OOZE and DIATOM-BEARING NANNOFOSSIL OOZE

Major lithologies: Nannofossil ooze, light gray (2.5Y 7/2), with 10-20-cm-wide white (10YR 8/1) bands. Diatom-bearing nannofossil ooze, light brownish gray (2.5Y 5/2). Transition between lithologies is gradual.

Bioturbation is moderate to strong and includes *Planolites* and halo burrows.

SMEAR SLIDE SUMMARY (%):

	1, 50 D	2, 50 D	3, 50 D	4, 50 D	6, 50 D	7, 30 D
COMPOSITION:						
Quartz	Tr	Tr	Tr	Tr	Tr	Tr
Accessory minerals:						
Heavy minerals	—	—	—	—	—	Tr
Micronodules	—	—	—	—	—	Tr
Foraminifers	—	Tr	Tr	1	—	—
Nannofossils	90	95	95	92	95	83
Diatoms	10	5	5	7	5	15
Radiolarians	Tr	—	—	—	Tr	2
Silicoflagellates	Tr	—	—	—	—	Tr

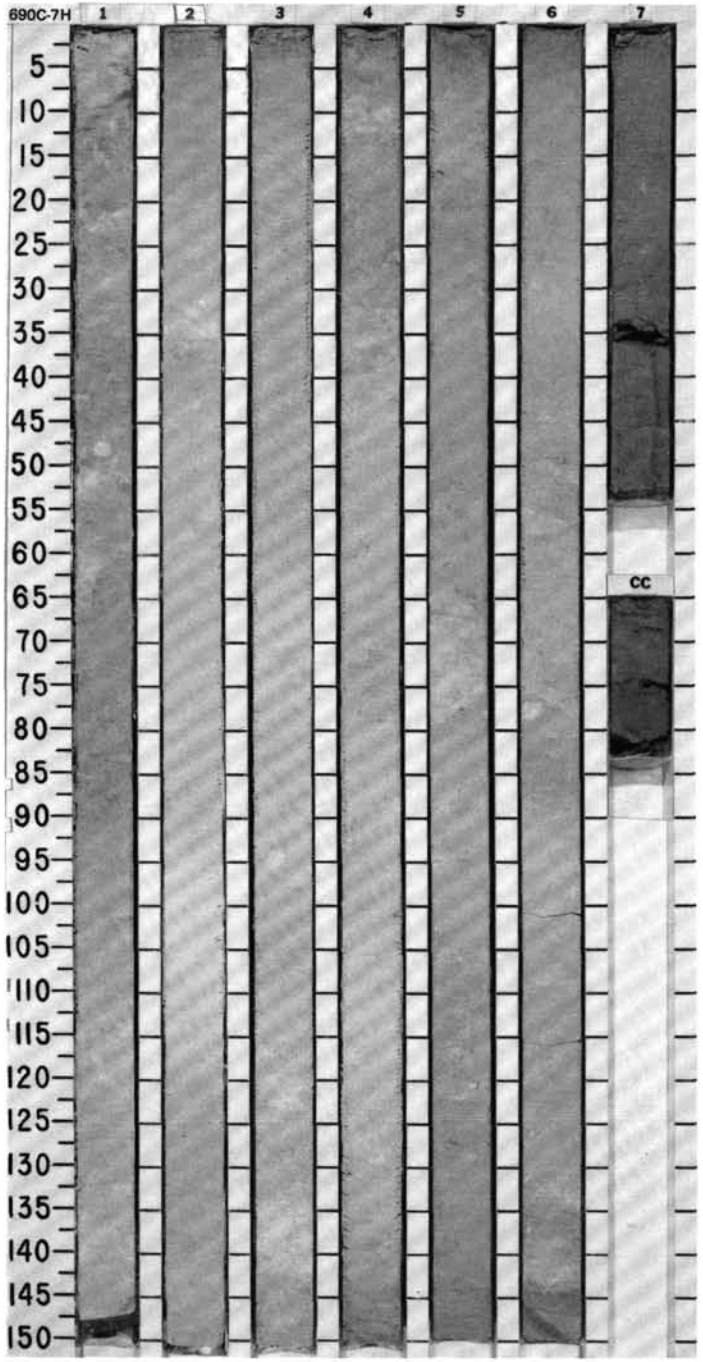

TIME-ROCK UNIT: UPPER OLIGOCENE

BIOSTRAT. ZONE/FOSSIL CHARACTER: FORAMINIFERS: ?; NANNOFOSSILS: OLIGOCENE; RADIOLARIANS: C,P; DIATOMS: UPPER OLIGOCENE; PALYNOMORPHS: F,P; PALEOMAGNETICS: B; PHYS. PROPERTIES: R,M; CHEMISTRY

SECTION: 1, 2, 3, 4, 5, 6, 7, CC

METERS: 0.5, 1.0

GRAPHIC LITHOLOGY

DRILLING DISTURB.

SED. STRUCTURES

SAMPLES

LITHOLOGIC DESCRIPTION

DIATOM-BEARING NANNOFOSSIL OOZE and NANNOFOSSIL OOZE

Major lithologies: Diatom-bearing nannofossil ooze, light brownish yellow (2.5Y 6/4), in Section 1, changing gradually to light gray (2.5Y 7/2). A 10-cm-wide band of light olive brown occurs at the top of Sections 1, 2, and 3. Nannofossil ooze, light gray (10YR 7/2), with minor mm-scale mottling to light brownish gray (2.5Y 6/2).

A dropstone, 3 mm long, occurs in Section 7, 25 cm. Degree of bioturbation varies from minor to moderate, with maximums in Section 2, 40–100 cm, and Section 3, 100–130 cm. Identifiable types include *Planolites*, *Zoophycos*, and halo burrows.

SMEAR SLIDE SUMMARY (%):

	1, 50 D	2, 50 D	3, 50 D	4, 50 D	5, 50 D	6, 50 D
COMPOSITION:						
Quartz	Tr	—	Tr	Tr	Tr	Tr
Volcanic glass	—	—	Tr	—	Tr	—
Accessory minerals:	—	—	—	—	—	—
Foraminifers	—	Tr	—	Tr	Tr	Tr
Nannofossils	78	88	88	84	92	92
Diatoms	20	10	10	15	7	7
Radiolarians	2	2	2	1	1	1
Silicoflagellates	—	—	Tr	—	Tr	—

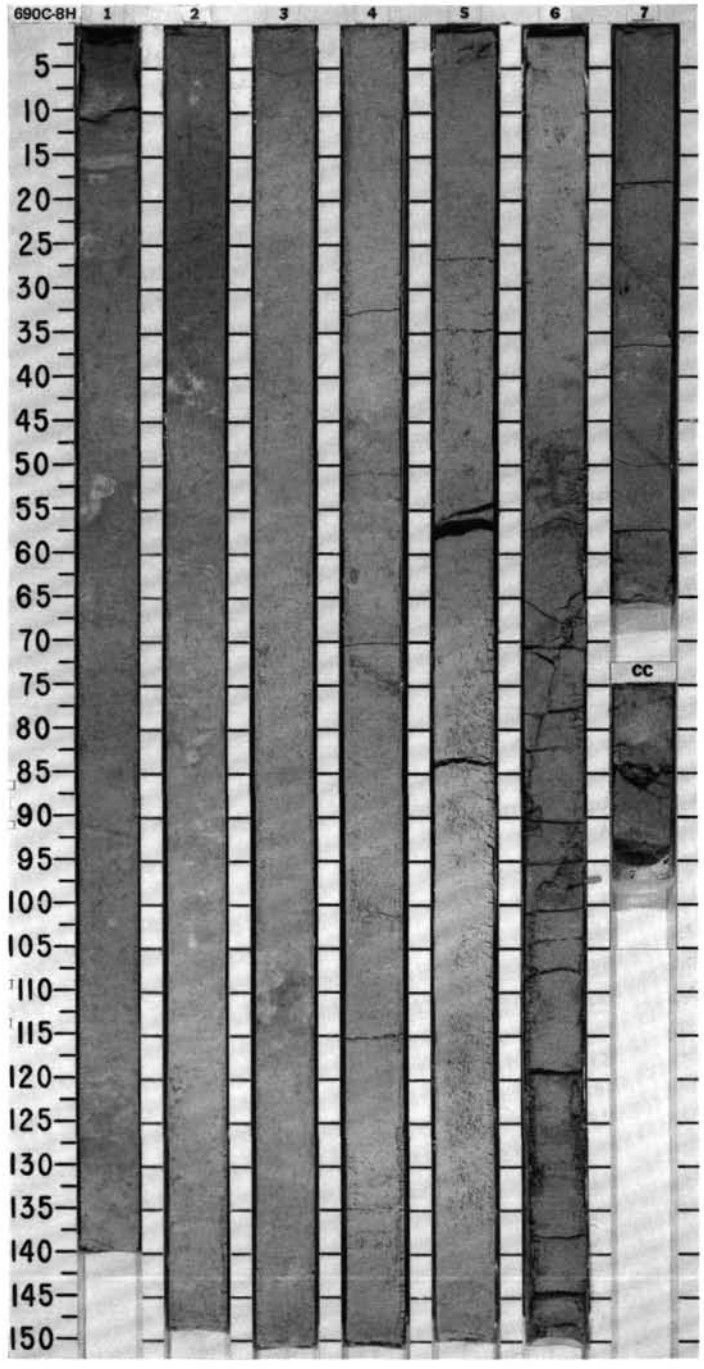

SITE 690 HOLE C CORE 9H CORED INTERVAL 2988.3-2997.9 mbsl; 74.0-83.6 mbsf

TIME-ROCK UNIT	BIOSTRAT. ZONE/ FOSSIL CHARACTER: FORAMINIFERS	NANNOFOSSILS	RADIOLARIANS	DIATOMS	PALYNOMORPHS	PALEOMAGNETICS	PHYS. PROPERTIES	CHEMISTRY	SECTION	METERS	GRAPHIC LITHOLOGY	DRILLING DISTURB.	SED. STRUCTURES	SAMPLES
LOWER OLIGOCENE	LOWER OLIGOCENE A,P		LOWER OLIGOCENE or UPPER EOCENE C,P	OLIGOCENE F,P	B				1	0.5				*
										1.0				
									2					*
									3					*
									4					*
									5					*
									6					*
									7					
									CC					

LITHOLOGIC DESCRIPTION

NANNOFOSSIL OOZE

Major lithology: Nannofossil ooze, light gray (10YR 7/2) and light brownish gray (10YR 6/2). Colors change gradually on a scale of 30–50 cm.

Bioturbation is moderate. Identifiable types include *Planolites*, *Zoophycos*, and halo burrows. Small (< 1 mm) black (10YR 2/1) specks, containing about 30% amorphous organic matter, are present throughout Sections 3–6.

SMEAR SLIDE SUMMARY (%):

	1, 60 D	2, 60 D	3, 60 D	4, 60 D	5, 60 D	6, 60 D
COMPOSITION:						
Quartz	1	Tr	Tr	Tr	Tr	Tr
Mica	—	—	—	—	—	Tr
Volcanic glass	—	Tr	Tr	Tr	—	—
Accessory minerals:						
Heavy minerals	Tr	Tr	Tr	—	—	Tr
Micronodules	Tr	—	Tr	Tr	—	—
Foraminifers	3	5	5	—	Tr	—
Nannofossils	88	88	91	98	98	98
Diatoms	5	7	2	2	1	Tr
Radiolarians	3	Tr	2	Tr	1	2
Sponge spicules	Tr	—	—	Tr	—	—
Silicoflagellates	—	Tr	—	—	—	—

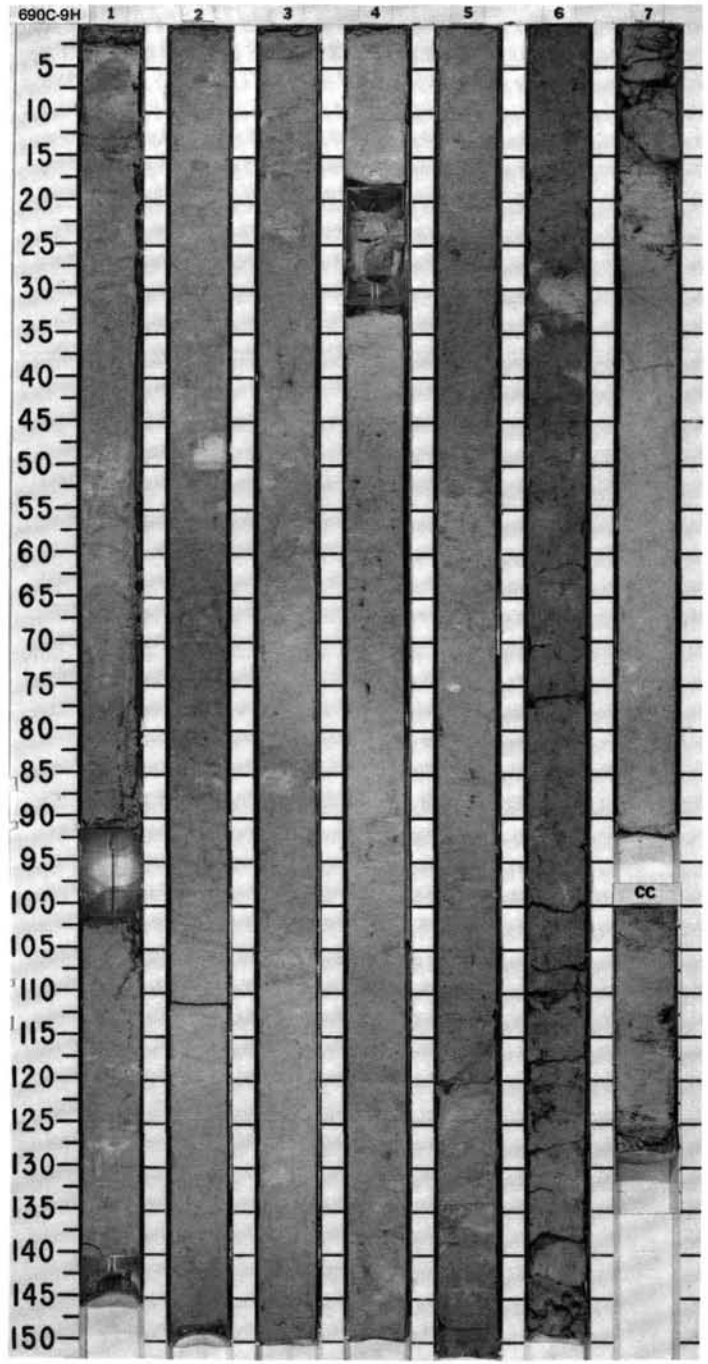

SITE 690 HOLE C CORE 10W CORED INTERVAL 2997.9-3118.5 mbsl; 83.6 - 204.2 mbsf

TIME-ROCK UNIT	BIOSTRAT. ZONE/ FOSSIL CHARACTER: FORAMINIFERS	NANNOFOSSILS	RADIOLARIANS	DIATOMS	PALEOMAGNETICS	PHYS. PROPERTIES	CHEMISTRY	SECTION	METERS	GRAPHIC LITHOLOGY	DRILLING DISTURB.	SED. STRUCTURES	SAMPLES	LITHOLOGIC DESCRIPTION
								1	0.5 1.0	WASH				WASH CORE Sediment recovered in this interval was collected over 120.6 m of hole. It was not described.
								2						
								3						
								4						
								5						
								6						
								CC						

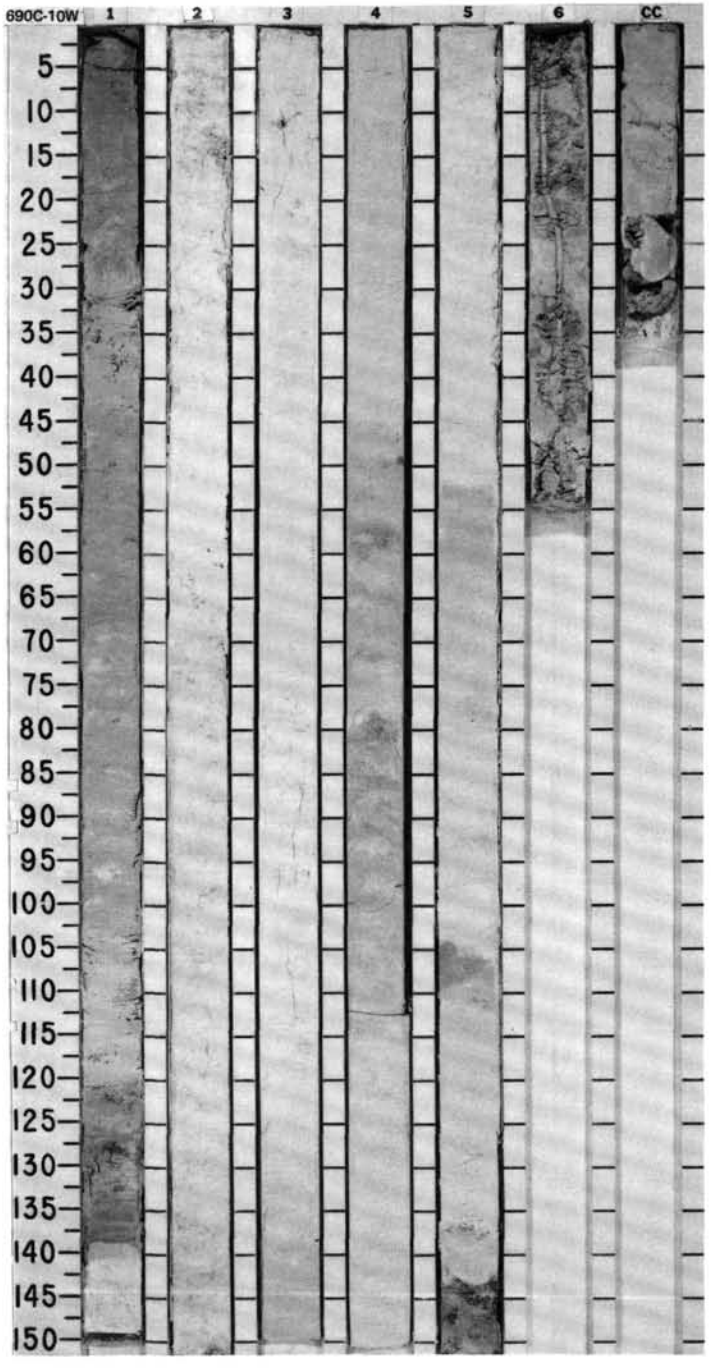

SITE 690 HOLE C CORE 11X CORED INTERVAL 3118.5-3128.2 mbsl; 204.2-213.9 mbsf

TIME-ROCK UNIT	BIOSTRAT. ZONE/ FOSSIL CHARACTER: FORAMINIFERS	NANNOFOSSILS	RADIOLARIANS	DIATOMS	PALYNOMORPHS	PALEOMAGNETICS	PHYS. PROPERTIES	CHEMISTRY	SECTION	METERS	GRAPHIC LITHOLOGY	DRILLING DISTURB.	SED. STRUCTURES	SAMPLES
UPPER PALEOCENE	A, G	A, G		B	B			71.74% ●	1	0.5				*
LOWER? - UPPER PALEOCENE		CP4 (or CP5 ?)							1	1.0				
									2					*
									3					*
									4					IW OG
									CC					*

LITHOLOGIC DESCRIPTION

NANNOFOSSIL OOZE and NANNOFOSSIL CHALK

Major lithologies: Nannofossil ooze and nannofossil chalk, white (7.5YR 8/0), pinkish white (7.5YR 8/2), pink (7.5YR 8/4), light gray (7.5YR 7/2), and reddish yellow (7.5YR 7/6). Color changes consist of gradational changes which commonly occur as light to dark cycles. The cycles vary from 30 to 60 cm in length.

Bioturbation is absent to moderate and includes *Planolites* and *Zoophycos*.

This is the first core after washing. Section 1 is highly disturbed. Coring disturbance also made it impossible to quantitatively determine the relative percentages of ooze and chalk.

SMEAR SLIDE SUMMARY (%):

	1, 50 D	2, 50 D	3, 50 D	4, 50 D
COMPOSITION:				
Quartz	—	Tr	Tr	—
Mica	2	6	2	4
Clay	4	—	—	—
Accessory minerals:				
Heavy minerals	—	—	Tr	Tr
Foraminifers	4	4	8	4
Nannofossils	90	86	86	92
Radiolarians	Tr	4	4	Tr

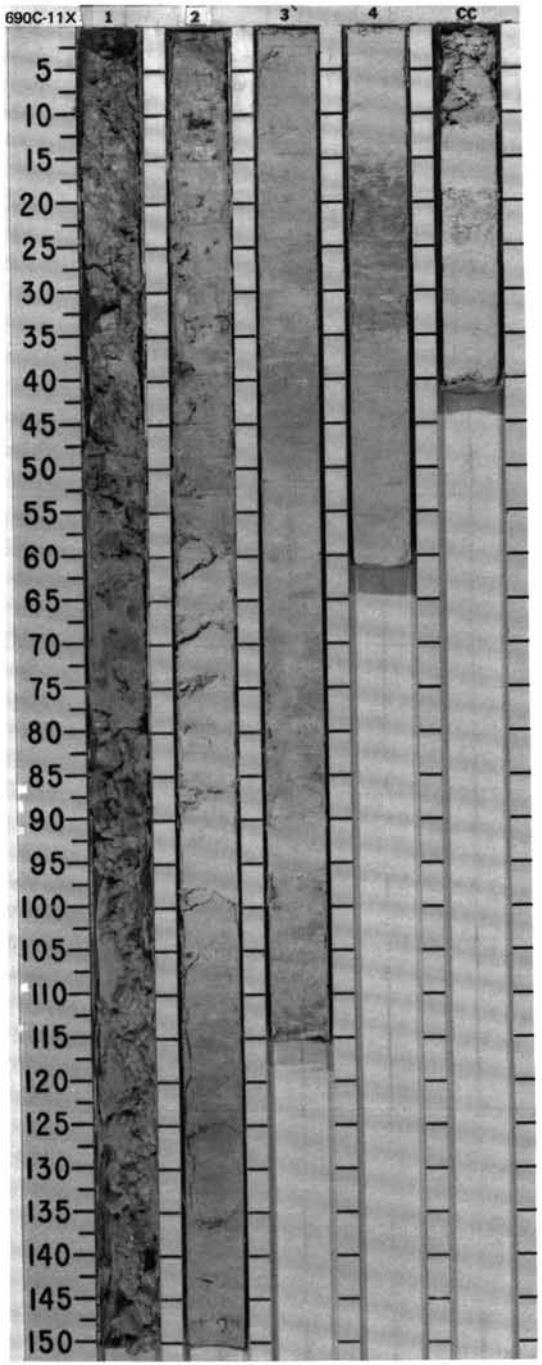

SITE 690 HOLE C CORE 12X CORED INTERVAL 3128.2-3137.9 mbsl; 213.9-223.6 mbsf

TIME-ROCK UNIT	BIOSTRAT. ZONE/ FOSSIL CHARACTER: FORAMINIFERS	NANNOFOSSILS	RADIOLARIANS	DIATOMS	PALEOMAGNETICS	PHYS. PROPERTIES	CHEMISTRY	SECTION	METERS	GRAPHIC LITHOLOGY	DRILLING DISTURB.	SED. STRUCTURES	SAMPLES
LOWER PALEOCENE	A/G P3 *	A, G Below CP4		B B				1 2 3 CC	0.5 1.0				* * * *

LITHOLOGIC DESCRIPTION

NANNOFOSSIL OOZE and NANNOFOSSIL CHALK

Major lithology: Nannofossil ooze and nannofossil chalk, white (10YR 8/1, 8/2; 7.5YR 8/0, 8/1), pinkish white (7.5YR 8/2), pink (7.5YR 8/4), and reddish yellow (7.5YR 6/8). Core severely disturbed by drilling. In the 113-690B hole the core barrel became stuck in this interval. It was not possible to determine the relative percentages of ooze and chalk.

SMEAR SLIDE SUMMARY (%):

	1, 50 D	2, 50 D	3, 50 D	4, 50 D
COMPOSITION:				
Quartz	Tr	—	4	—
Mica	2	2	2	2
Clay	2	2	3	2
Volcanic glass	—	Tr	1	—
Accessory minerals:				
Pyrite	—	—	Tr	—
Foraminifers	6	8	8	8
Nannofossils	90	88	82	88
Radiolarians	Tr	—	—	—

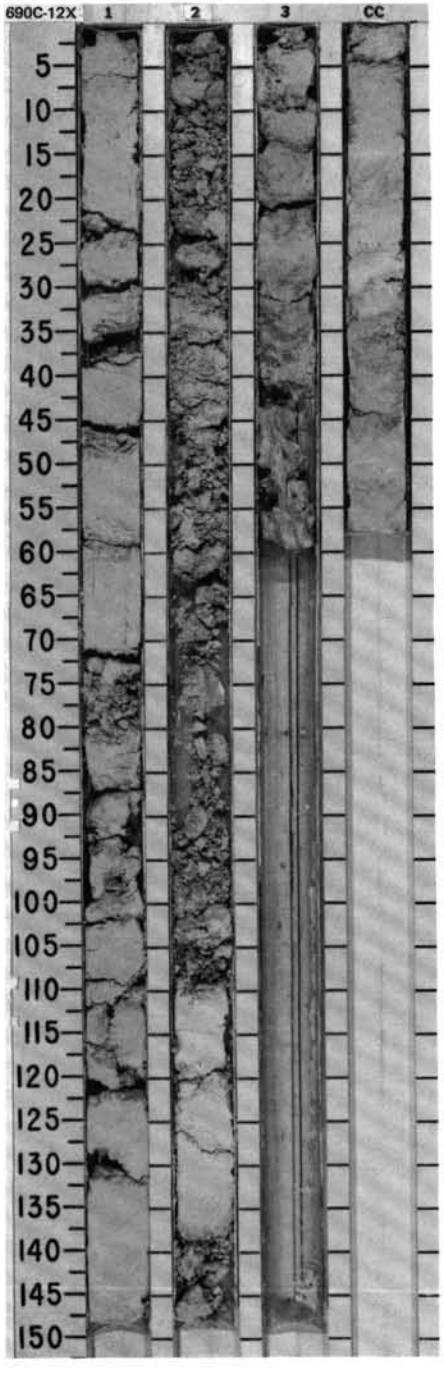

SITE 690 HOLE C CORE 13X CORED INTERVAL 3137.9-3147.5 mbsl; 223.6-233.2 mbsf

TIME-ROCK UNIT	BIOSTRAT. ZONE/ FOSSIL CHARACTER: FORAMINIFERS	NANNOFOSSILS	RADIOLARIANS	DIATOMS	PALYNOMORPHS	PALEOMAGNETICS	PHYS. PROPERTIES	CHEMISTRY	SECTION	METERS	GRAPHIC LITHOLOGY	DRILLING DISTURB.	SED. STRUCTURES	SAMPLES
LOWER PALEOCENE	A,G P1b	A,G		B	B			•	1	0.5				*
	A,G									1.0				
									2					*
									3					*
														*
									4					*
									5					*
									6					*
									CC					
	A,G	A,G												

	FORAMINIFERS	NANNOFOSSILS
P/C	P2 *	CP3-CP2

LITHOLOGIC DESCRIPTION

MUD-BEARING NANNOFOSSIL OOZE and MUD-BEARING NANNOFOSSIL CHALK

Major lithology: Mud-bearing nannofossil ooze and mud-bearing nannofossil chalk, homogeneous pinkish white (7.5YR 8/2) throughout except for a light gray (10YR 7/1) layer in Section 3, 108–120 cm. Sediments vary between ooze and chalk and are moderately disturbed by drilling and cutting. Chalky layers approximately 5 cm wide occur every 15–20 cm, but coring disturbance may have affected this stratigraphy.

Minor lithology: Ash, light gray (10YR 7/1), in Section 3, 108–120 cm. Ash is strongly bioturbated. It correlates with ash layer at 113-689B-23X-4.

SMEAR SLIDE SUMMARY (%):

	1, 80 D	2, 80 D	3, 80 D	3, 118 M	4, 80 D	5, 80 D	6, 80 D
COMPOSITION:							
Quartz	Tr	—	—	2	1	2	1
Mica	2	5	3	4	3	4	2
Clay	10	12	12	15	14	12	12
Volcanic glass	2	2	3	3	2	2	1
Accessory minerals	—	—	—	2	—	—	—
Pyrite	—	—	Tr	—	—	—	—
Foraminifers	5	2	1	2	4	Tr	3
Nannofossils	78	75	81	72	72	77	81
Sponge spicules	—	—	Tr	Tr	—	—	—
Calcispheres	3	4	4	1	4	3	Tr

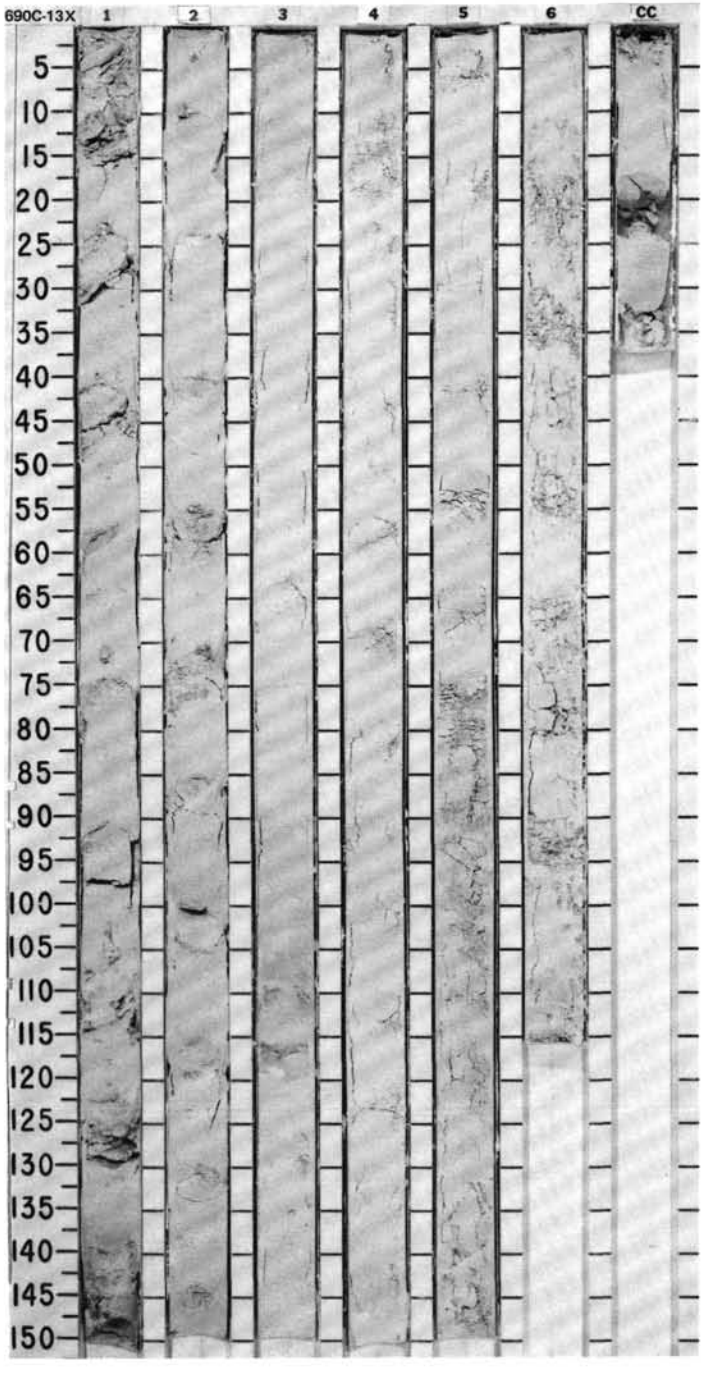

SITE 690 HOLE C CORE 14X CORED INTERVAL 3147.5-3157.2 mbsl; 233.2-242.9 mbsf

TIME-ROCK UNIT	FORAMINIFERS	NANNOFOSSILS	RADIOLARIANS	DIATOMS	PALYNOMORPHS	PALEOMAGNETICS	PHYS. PROPERTIES	CHEMISTRY	SECTION	METERS	GRAPHIC LITHOLOGY	DRILLING DISTURB.	SED. STRUCTURES	SAMPLES
LOWER PALEOCENE	P1b	CP16		B	B			88.7%	1 2 3 4 5 CC	0.5 1.0				IW OG

LITHOLOGIC DESCRIPTION

MUD- AND CALCISPHERE-BEARING NANNOFOSSIL CHALK, CALCISPHERE- AND MUD-BEARING NANNOFOSSIL CHALK, FORAMINIFER-BEARING CALCISPHERE-NANNOFOSSIL CHALK, CALCISPHERE-BEARING NANNOFOSSIL CHALK, and CALCISPHERE-NANNOFOSSIL CHALK (ALL WITH SOME OOZE)

Major lithologies: Mud- and calcisphere-bearing nannofossil chalk (ooze) and calcisphere- and mud-bearing nannofossil chalk (ooze), homogeneously-colored pinkish white (7.5YR 8/2); chalk layers 4–6 cm thick, heavily biscuited and partly rotated. Section 1, bioturbation and drilling disturbance moderate. Section 5, drilling disturbance more severe; amount of bioturbation cannot be determined. Foraminifer-bearing calcisphere-nannofossil chalk (ooze), pinkish white (7.5YR 8/2) throughout Section 2. Calcisphere-bearing nannofossil chalk (ooze), pinkish white (7.5YR 8/2), slight to moderate bioturbation, drilling disturbance moderate; chalk biscuits partly rotated. Calcisphere-nannofossil chalk (ooze), pinkish white (7.5YR 8/2), moderately fractured by drilling in the lower section, slight bioturbation. Chalk layers 5 cm thick, highly rotated *throughout, moderate drilling disturbance, slight bioturbation.*

SMEAR SLIDE SUMMARY (%):

	1, 50 D	2, 50 D	3, 50 D	4, 50 D	5, 50 D
COMPOSITION:					
Quartz	2	Tr	—	Tr	—
Mica	4	2	2	2	2
Clay	12	5	—	6	14
Volcanic glass	—	5	2	Tr	6
Accessory minerals	Tr	—	Tr	—	—
Zeolites	—	3	—	—	—
Foraminifers	8	15	6	8	8
Nannofossils	58	35	60	68	58
Calcispheres	16	35	30	16	12

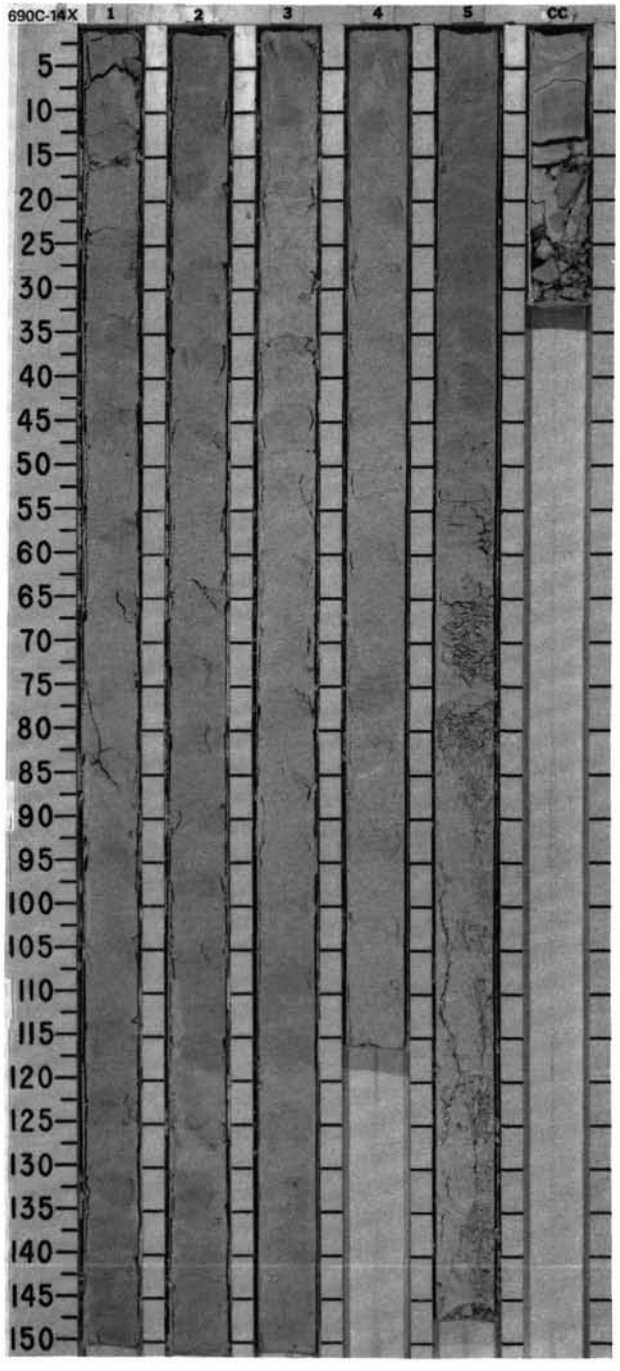

SITE 690 HOLE C CORE 15X CORED INTERVAL 3157.2-3166.8 mbsl; 242.9-252.5 mbsf

TIME-ROCK UNIT	BIOSTRAT. ZONE/ FOSSIL CHARACTER: FORAMINIFERS	NANNOFOSSILS	RADIOLARIANS	DIATOMS	PALEOMAGNETICS	PHYS. PROPERTIES	CHEMISTRY	SECTION	METERS	GRAPHIC LITHOLOGY	DRILLING DISTURB.	SED. STRUCTURES	SAMPLES
UPPER MAESTRICHTIAN / Danian	A.G / A.M	A.G / A.M		B				1, 2, 3, 4, 5, 6, 7, CC	0.5, 1.0				*

A. mayorensis — *Planorotalites eoqubina* Zone A,G — CP1b A,G — *Nephrolithus* — CP1a

LITHOLOGIC DESCRIPTION

FORAMINIFER- AND MUD-BEARING NANNOFOSSIL CHALK and FORAMINIFER-BEARING MUDDY NANNOFOSSIL CHALK

Major lithologies: Foraminifer- and mud-bearing nannofossil chalk, alternatively white (2.5Y 8/0) and pinkish white (2.5Y 8/2) in Section 1, then pinkish white (2.5Y 8/2) grading to pale brown (10YR 7/4) in Section 3. Foraminifer-bearing muddy nannofossil chalk, white (10YR 8/2) to pale brown (10YR 8/3, 7/4).

Minor to strong bioturbation, principally by *Chondrites*, *Planolites*, and *Zoophycos*.

Core contains a strongly bioturbated, very pale brown layer (10YR 7/4) from Section 3, about 115 cm, to Section 4, 50 cm. This layer is associated with the Cretaceous/Tertiary boundary. The material is zeolite-rich but contains only a few percent ash. In Section 3, at approximately 40 and 120 cm, are greenish specks that may be ash-rich.

SMEAR SLIDE SUMMARY (%):

	1, 130 D	2, 50 D	3, 50 D	4, 70 D	5, 30 D	6, 30 D	7, 30 D
COMPOSITION:							
Quartz	Tr	Tr	—	Tr	—	—	—
Mica	3	2	4	2	2	2	8
Clay	4	4	2	6	6	4	4
Volcanic glass	3	3	6	8	12	8	6
Accessory minerals:							
Heavy minerals	Tr	Tr	Tr	—	—	Tr	—
Zeolites	8	6	8	18	14	12	12
Foraminifers	14	12	18	12	10	26	18
Nannofossils	56	65	56	54	56	42	52
Calcispheres	12	8	6	—	Tr	6	Tr

SITE 690 HOLE C CORE 16X CORED INTERVAL 3166.8-3176.1 mbsl; 252.5-261.8 mbsf

TIME-ROCK UNIT	BIOSTRAT. ZONE/ FOSSIL CHARACTER: FORAMINIFERS	NANNOFOSSILS	RADIOLARIANS	DIATOMS	PALYNOMORPHS	PALEOMAGNETICS	PHYS. PROPERTIES	CHEMISTRY	SECTION	METERS	GRAPHIC LITHOLOGY	DRILLING DISTURB.	SED. STRUCTURES	SAMPLES
UPPER MAESTRICHTIAN	A, G	A, G		B	B				1	0.5 / 1.0				*
	A. mayorensis Zone	*Nephrolithus* Zone							2					*
									3					*
									4					*
									CC					

LITHOLOGIC DESCRIPTION

FORAMINIFER-BEARING MUDDY NANNOFOSSIL CHALK (OOZE)

Major lithology: Foraminifer-bearing muddy nannofossil chalk (ooze), white (10YR 8/0, 8/1, 8/2) to light gray (10YR 7/2) and pale brown (10YR 7/3). Minor to strong bioturbation by diffuse burrows and *Planolites*. Convolute bedding in Section 1, 25 and 45 cm, and Section 3, 15 cm. Slump fold in Section 1, 60 cm. Parallel laminae in Section 1, 70, 85, and 135 cm; Section 2, 15, 25, 60, 70, 85, and 110 cm; and CC, 20 cm. Graded bedding in Section 2, 80 and 90 cm. Lenticular bedding in Section 4, 15 cm.

SMEAR SLIDE SUMMARY (%):

	1, 65 D	2, 65 D	3, 65 D	4, 65 D
COMPOSITION:				
Quartz	1	Tr	1	—
Mica	15	15	20	15
Clay	15	25	20	15
Volcanic glass	Tr	—	—	—
Accessory minerals:				
Heavy minerals	Tr	1	—	Tr
Zeolites	7	5	3	Tr
Foraminifers	15	15	10	10
Nannofossils	45	37	46	57
Calcispheres	2	2	Tr	3

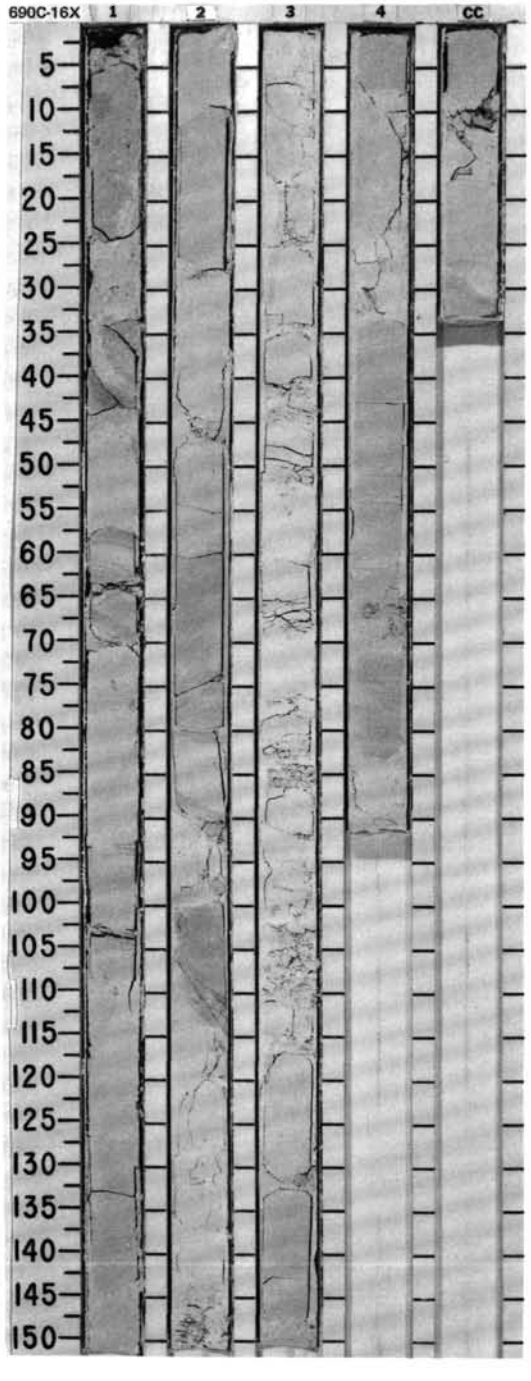

SITE 690 HOLE C CORE 17X CORED INTERVAL 3176.1-3185.7 mbsl; 261.8-271.4 mbsf

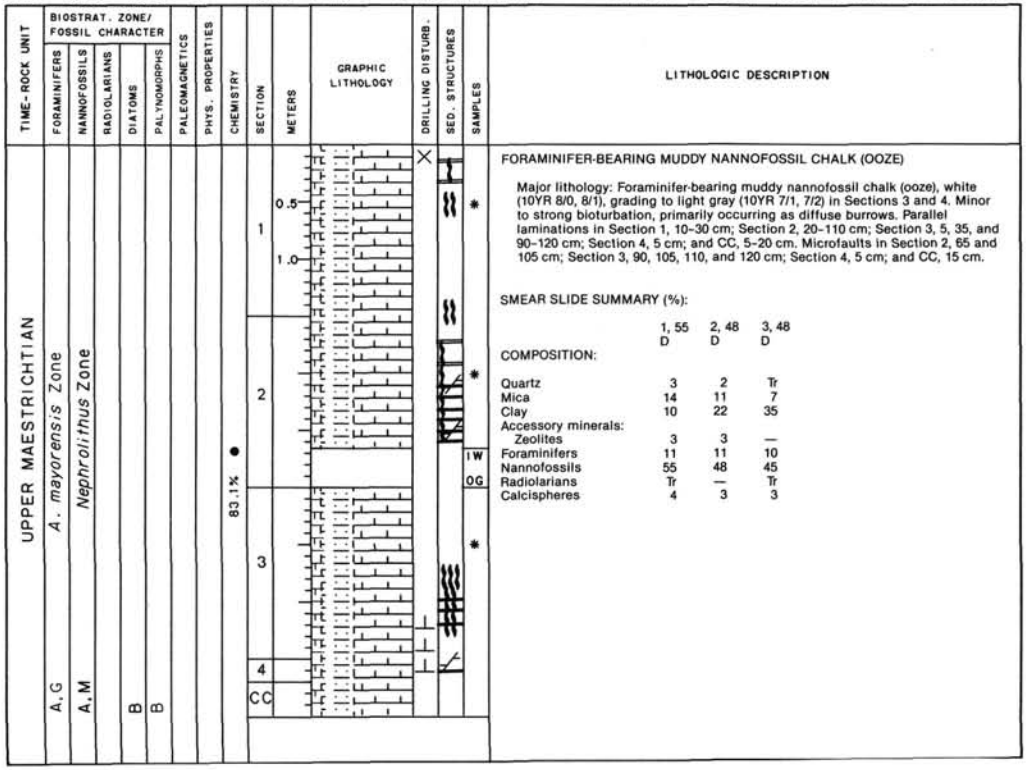

FORAMINIFER-BEARING MUDDY NANNOFOSSIL CHALK (OOZE)

Major lithology: Foraminifer-bearing muddy nannofossil chalk (ooze), white (10YR 8/0, 8/1), grading to light gray (10YR 7/1, 7/2) in Sections 3 and 4. Minor to strong bioturbation, primarily occurring as diffuse burrows. Parallel laminations in Section 1, 10–30 cm; Section 2, 20–110 cm; Section 3, 5, 35, and 90–120 cm; Section 4, 5 cm; and CC, 5–20 cm. Microfaults in Section 2, 65 and 105 cm; Section 3, 90, 105, 110, and 120 cm; Section 4, 5 cm; and CC, 15 cm.

SMEAR SLIDE SUMMARY (%):

	1, 55 D	2, 48 D	3, 48 D
COMPOSITION:			
Quartz	3	2	Tr
Mica	14	11	7
Clay	10	22	35
Accessory minerals:			
Zeolites	3	3	—
Foraminifers	11	11	10
Nannofossils	55	48	45
Radiolarians	Tr	—	Tr
Calcispheres	4	3	3

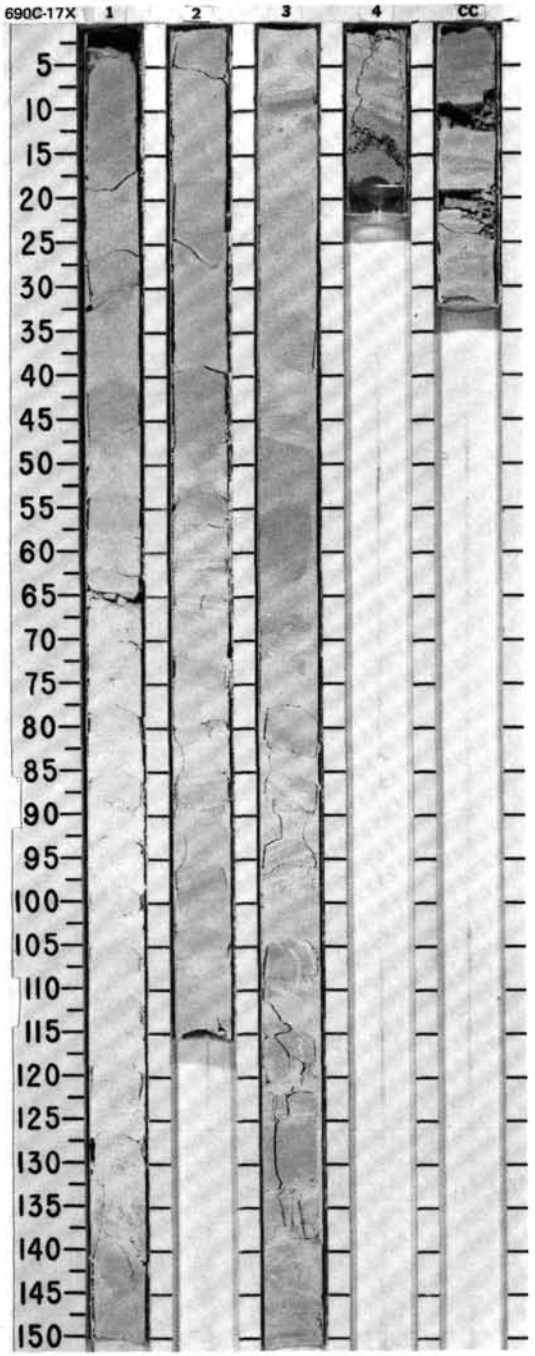

SITE 690 HOLE C CORE 18X CORED INTERVAL 3185.7-3195.4 mbsl; 271.4-281.1 mbsf

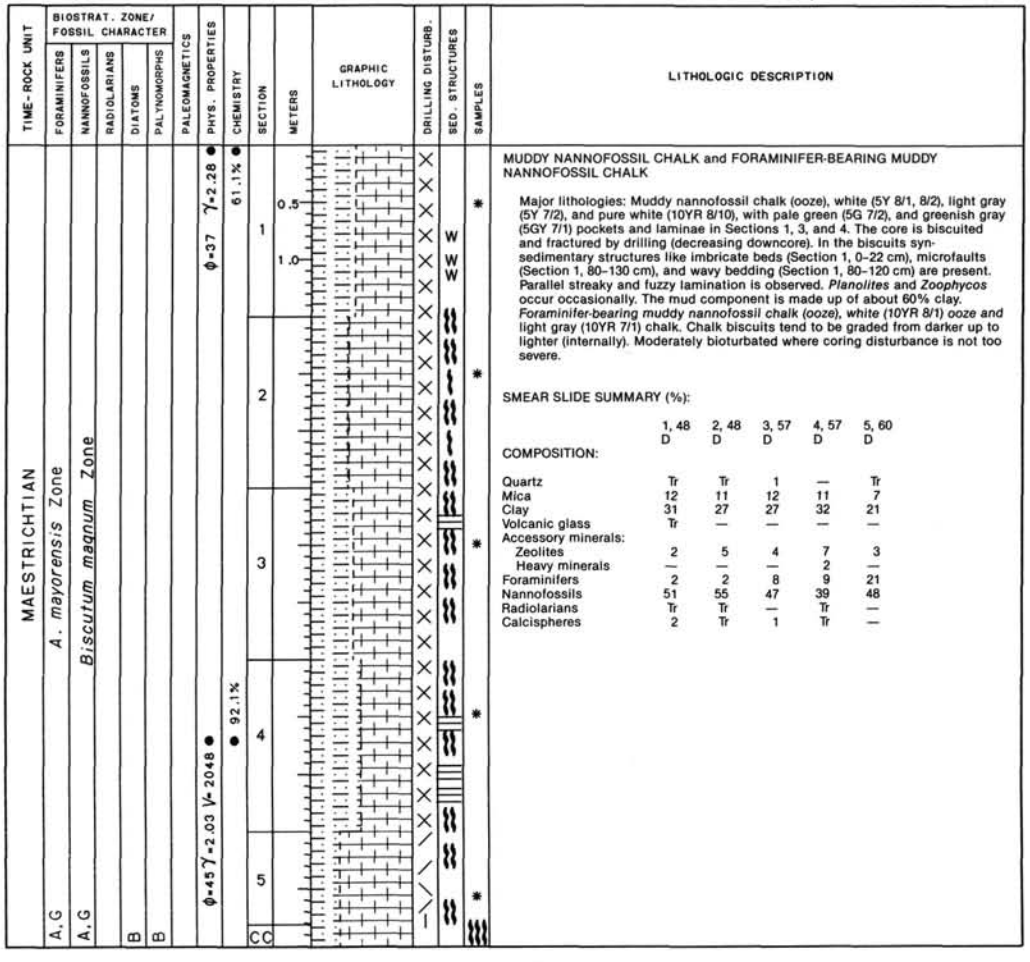

LITHOLOGIC DESCRIPTION

MUDDY NANNOFOSSIL CHALK and FORAMINIFER-BEARING MUDDY NANNOFOSSIL CHALK

Major lithologies: Muddy nannofossil chalk (ooze), white (5Y 8/1, 8/2), light gray (5Y 7/2), and pure white (10YR 8/10), with pale green (5G 7/2), and greenish gray (5GY 7/1) pockets and laminae in Sections 1, 3, and 4. The core is biscuited and fractured by drilling (decreasing downcore). In the biscuits syn-sedimentary structures like imbricate beds (Section 1, 0–22 cm), microfaults (Section 1, 80–130 cm), and wavy bedding (Section 1, 80–120 cm) are present. Parallel streaky and fuzzy lamination is observed. *Planolites* and *Zoophycos* occur occasionally. The mud component is made up of about 60% clay. *Foraminifer-bearing muddy nannofossil chalk (ooze), white (10YR 8/1) ooze and* light gray (10YR 7/1) chalk. Chalk biscuits tend to be graded from darker up to lighter (internally). Moderately bioturbated where coring disturbance is not too severe.

SMEAR SLIDE SUMMARY (%):

	1, 48 D	2, 48 D	3, 57 D	4, 57 D	5, 60 D
COMPOSITION:					
Quartz	Tr	Tr	1	—	Tr
Mica	12	11	12	11	7
Clay	31	27	27	32	21
Volcanic glass	Tr	—	—	—	—
Accessory minerals:					
Zeolites	2	5	4	7	3
Heavy minerals	—	—	—	2	—
Foraminifers	2	2	8	9	21
Nannofossils	51	55	47	39	48
Radiolarians	Tr	Tr	—	Tr	—
Calcispheres	2	Tr	1	Tr	—

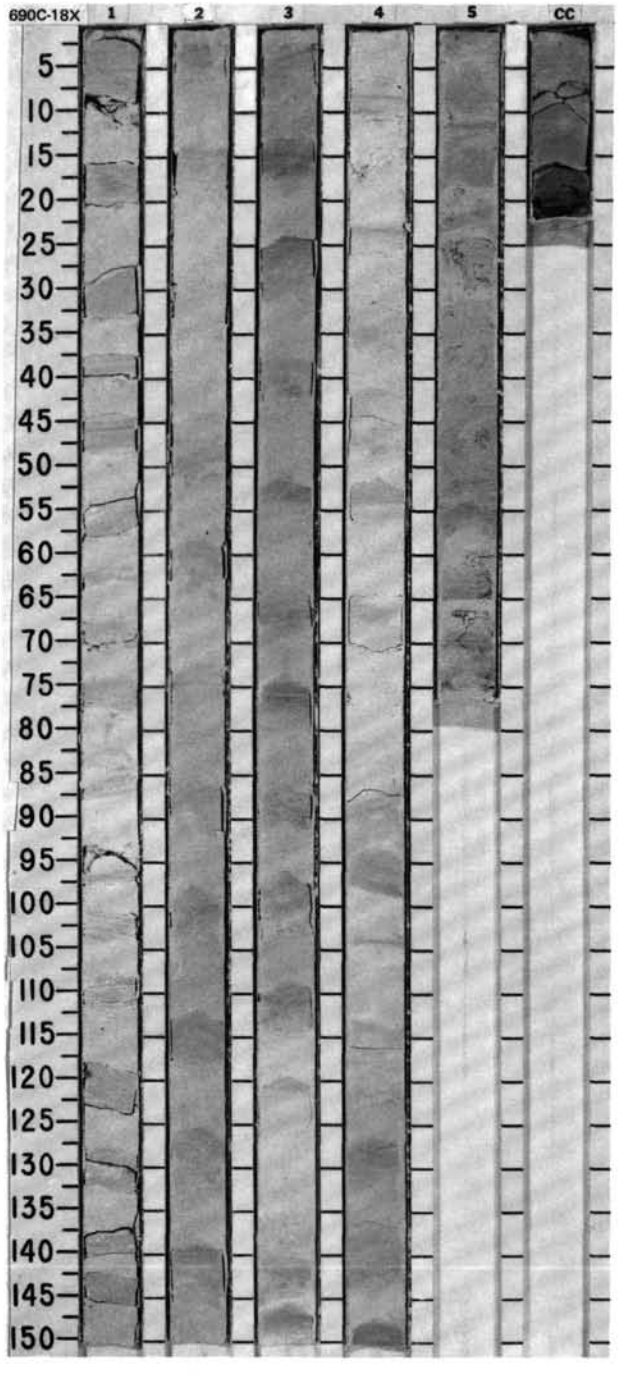

SITE 690 HOLE C CORE 19X CORED INTERVAL 3195.4-3205.1 mbsl; 281.1-290.8 mbsf

TIME-ROCK UNIT	BIOSTRAT. ZONE/FOSSIL CHARACTER: FORAMINIFERS	NANNOFOSSILS	RADIOLARIANS	DIATOMS	PALYNOMORPHS	PALEOMAGNETICS	PHYS. PROPERTIES	CHEMISTRY	SECTION	METERS	GRAPHIC LITHOLOGY	DRILLING DISTURB.	SED. STRUCTURES	SAMPLES
MIDDLE MAESTRICHTIAN	A, G	A, G		B	B	Φ=47 γ=2.01 V=1973	Φ=46 γ=1.98 V=1937	76.1% 74.3%	1 2 3 4 5 6 7 CC	0.5 1.0				*

LITHOLOGIC DESCRIPTION

CALCAREOUS CLAYSTONE

Major lithologies: Calcareous claystone, light olive gray (5Y 6/2) in Sections 2 and 3; light gray (5Y 7/2, 7.5YR 7/0) in Sections 4 and 5; and greenish gray (5GY 6/1) and gray (5Y 6/1) in Sections 6 and 7. Greenish gray laminae (5GY 6/1) at Section 2, 145 cm, and Section 3, 30 and 36 cm. The entire core contains biscuits. *Zoophycos* is present throughout and appears darker than background. In Section 1 *Chondrites* and *Planolites* are observed. There is a generally increasing concentration of clay downcore. Nannofossils and foraminifers occur in roughly equal proportions.

SMEAR SLIDE SUMMARY (%):

	1, 70 D	2, 60 D	3, 50 D	4, 52 D	5, 60 D	6, 50 D
COMPOSITION:						
Quartz	—	1	Tr	—	—	Tr
Mica	7	5	2	1	3	2
Clay	52	69	73	84	85	88
Volcanic glass	1	—	—	—	—	—
Calcite/dolomite	5	—	—	—	—	—
Foraminifers	15	15	15	10	2	2
Nannofossils	20	10	10	5	10	8
Bioclasts	Tr	—	—	—	—	—
Silt	16	15	15	10	2	3
Clay	82	85	85	90	98	97

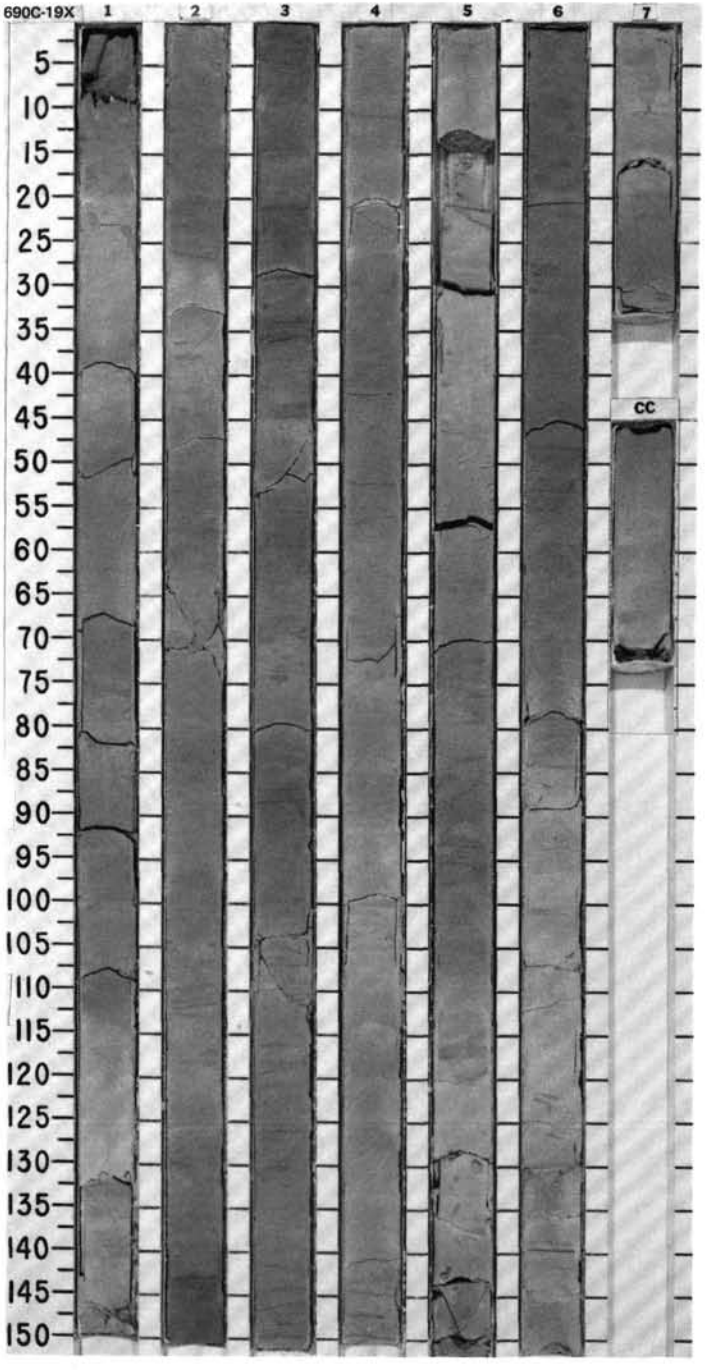

SITE 690 HOLE C CORE 20X CORED INTERVAL 3205.1-3214.7 mbsl; 290.8-300.4 mbsf

TIME-ROCK UNIT	BIOSTRAT. ZONE/ FOSSIL CHARACTER: FORAMINIFERS	NANNOFOSSILS	RADIOLARIANS	DIATOMS	PALYNOMORPHS	PALEOMAGNETICS	PHYS. PROPERTIES	CHEMISTRY	SECTION	METERS	GRAPHIC LITHOLOGY	DRILLING DISTURB.	SED. STRUCTURES	SAMPLES
UPPER CAMPANIAN - LOWEST MAESTRICHTIAN	A, M	A, M		B	B		ϕ=56 γ=2.02 V=1918 ●	56.2% ●	1	0.5				*
	Maestrichtian	*Biscutum coronum*								1.0				
									2					*
								● 64.7%	3					*
									4					*
													IW	
									5				OG	
														*
									6					*
									7					
									CC					

LITHOLOGIC DESCRIPTION

CALCAREOUS CLAYSTONE and CLAYEY CHALK

Major lithologies: Calcareous claystone, alternating on the scale of 50–100 cm, gray (5Y 5/1) and greenish gray (5GY 5/1), with some light gray (5Y 6/1) intervals. Sections 2, 3, and 4 contain abundant, small *Chondrites*. *Zoophycos* is observed in some of the biscuits with decreasing abundance downcore. The calcareous component holds equal proportions of foraminifers and nannofossils. The calcareous component reaches a minimum in Section 3. Clayey chalk, greenish gray (5GY 5/1) and gray (5Y 5/1), is highly fractured by drilling. Individual pieces contain *Zoophycos* and *Chondrites*. Foraminifers and foraminifer fragments dominate the calcareous fraction.

SMEAR SLIDE SUMMARY (%):

	1, 37 D	2, 50 D	3, 52 D	4, 48 D	5, 45 D	6, 38 D
COMPOSITION:						
Quartz	3	1	Tr	3	2	4
Mica	7	5	10	4	8	3
Clay	48	46	69	50	40	37
Volcanic glass	36	—	—	Tr	—	—
Accessory minerals:						
Heavy minerals	2	1	—	—	1	—
Opaques	Tr	—	1	2	—	Tr
Zeolites	—	2	—	—	—	2
Foraminifers	20	25	5	23	30	30
Nannofossils	20	20	15	18	19	24
Sand	—	—	Tr	—	—	—
Silt	—	—	10	—	—	—
Clay	—	—	90	—	—	—

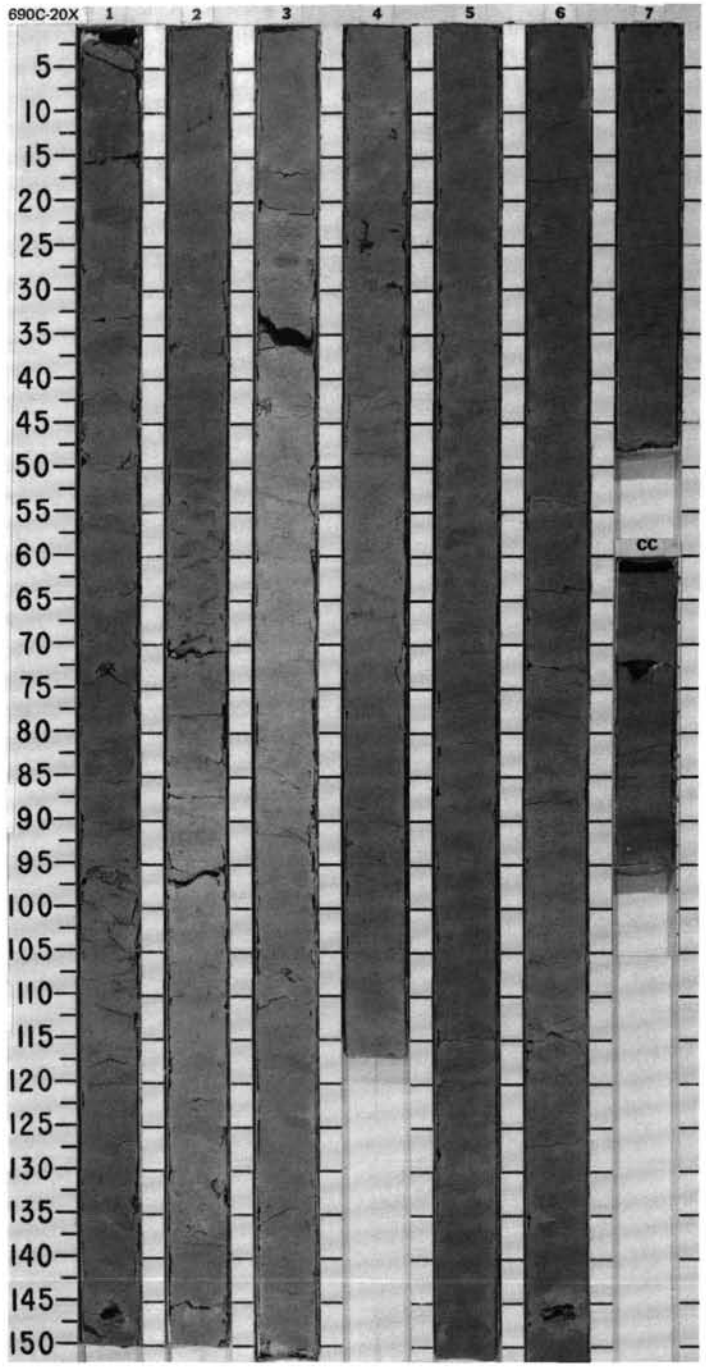

SITE 690 HOLE C CORE 21X CORED INTERVAL 3214.7-3224.4 mbsl; 300.4-310.1 mbsf

TIME-ROCK UNIT	BIOSTRAT. ZONE/ FOSSIL CHARACTER: FORAMINIFERS	NANNOFOSSILS	RADIOLARIANS	DIATOMS	PALYNOMORPHS	PALEOMAGNETICS	PHYS. PROPERTIES	CHEMISTRY	SECTION	METERS	GRAPHIC LITHOLOGY	DRILLING DISTURB.	SED. STRUCTURES	SAMPLES
UPPER CAMPANIAN - LOWEST MAESTRICHTIAN	A, M	A, M	R, P	B	B				1	0.5		X		*
	Maestrichtian	*Biscutum coronum*								1.0				
									2					*
									3					*
									4					*
									5					
									CC					

LITHOLOGIC DESCRIPTION

MUDDY CHALK

Major lithology: Muddy chalk, gray (5Y 6/1), light gray (5Y 7/1), and greenish gray (5GY 6/1), turning rapidly into light brownish gray (2.5Y 6/2) at Section 4, 13 cm. At 90–110 cm, in the bottom of Section 4, *Zoophycos* structures contain small "blebs" of light olive brown material containing more clay and volcanic glass than average lithology. Degree of biscuiting decreases from top to bottom; Section 1 is moderately disturbed. In the lower half of Section 2, Section 3, and the top of Section 4, the biscuits contain abundant *Zoophycos*. *Chondrites* observed at Section 3, 80–100 cm. The mud component is mainly composed of volcanic glass (~60%).

SMEAR SLIDE SUMMARY (%):

	1, 50 D	2, 50 D	3, 50 D	4, 50 D	4, 128 M
COMPOSITION:					
Quartz	5	10	5	2	5
Mica	2	15	1	6	3
Clay	8	5	16	13	25
Volcanic glass	25	15	20	20	25
Accessory minerals:					
Opaque	5	5	5	4	2
Foraminifers	30	35	38	30	25
Nannofossils	25	15	15	25	15

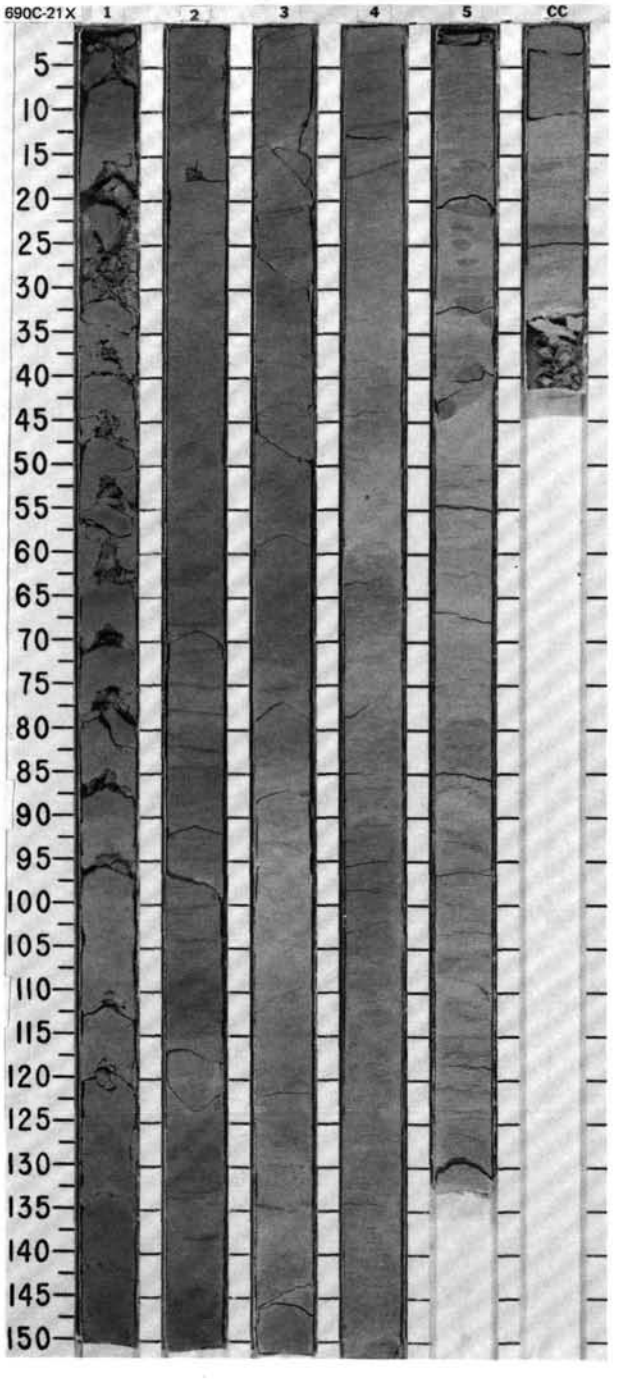

SITE 690 HOLE C CORE 22X CORED INTERVAL 310.1-319.7 mbsl; 3224.1-3233.7 mbsf

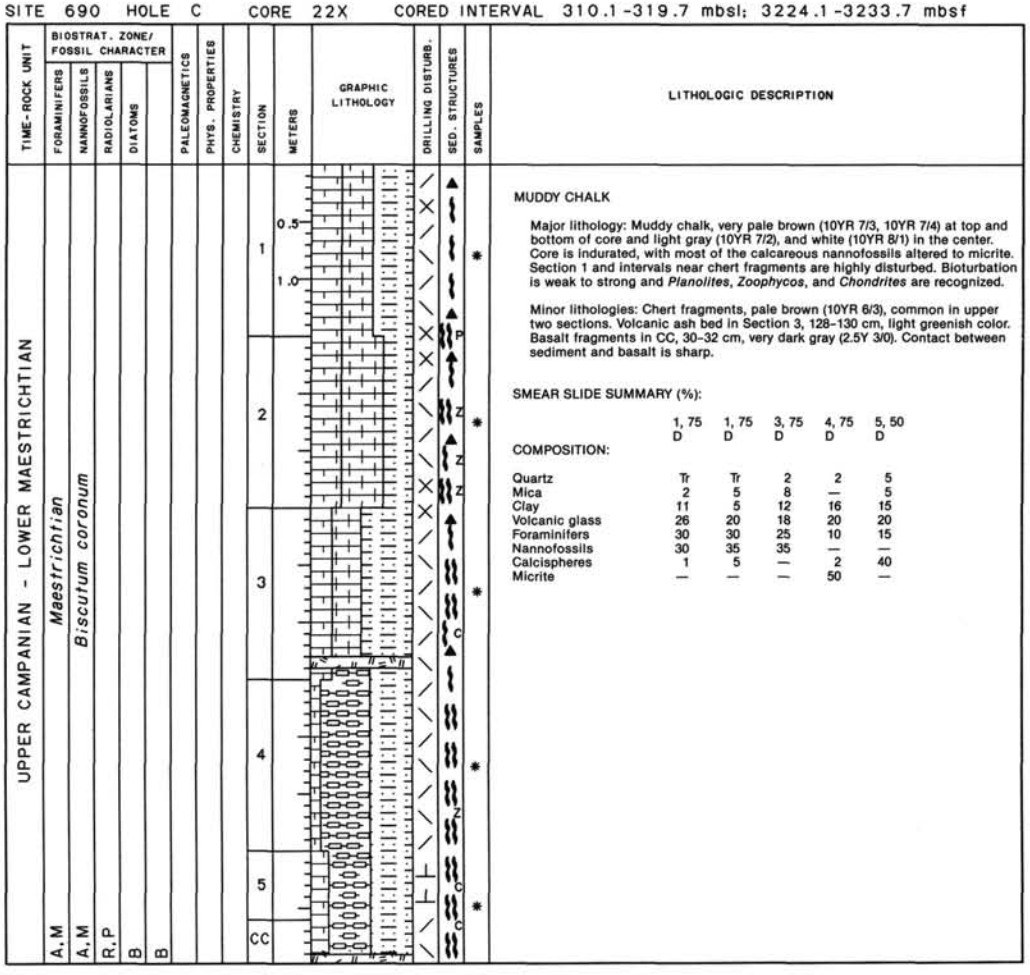

LITHOLOGIC DESCRIPTION

MUDDY CHALK

Major lithology: Muddy chalk, very pale brown (10YR 7/3, 10YR 7/4) at top and bottom of core and light gray (10YR 7/2), and white (10YR 8/1) in the center. Core is indurated, with most of the calcareous nannofossils altered to micrite. Section 1 and intervals near chert fragments are highly disturbed. Bioturbation is weak to strong and *Planolites*, *Zoophycos*, and *Chondrites* are recognized.

Minor lithologies: Chert fragments, pale brown (10YR 6/3), common in upper two sections. Volcanic ash bed in Section 3, 128–130 cm, light greenish color. Basalt fragments in CC, 30–32 cm, very dark gray (2.5Y 3/0). Contact between sediment and basalt is sharp.

SMEAR SLIDE SUMMARY (%):

	1, 75 D	1, 75 D	3, 75 D	4, 75 D	5, 50 D
COMPOSITION:					
Quartz	Tr	Tr	2	2	5
Mica	2	5	8	—	5
Clay	11	5	12	16	15
Volcanic glass	26	20	18	20	20
Foraminifers	30	30	25	10	15
Nannofossils	30	35	35	—	—
Calcispheres	1	5	—	2	40
Micrite	—	—	—	50	—

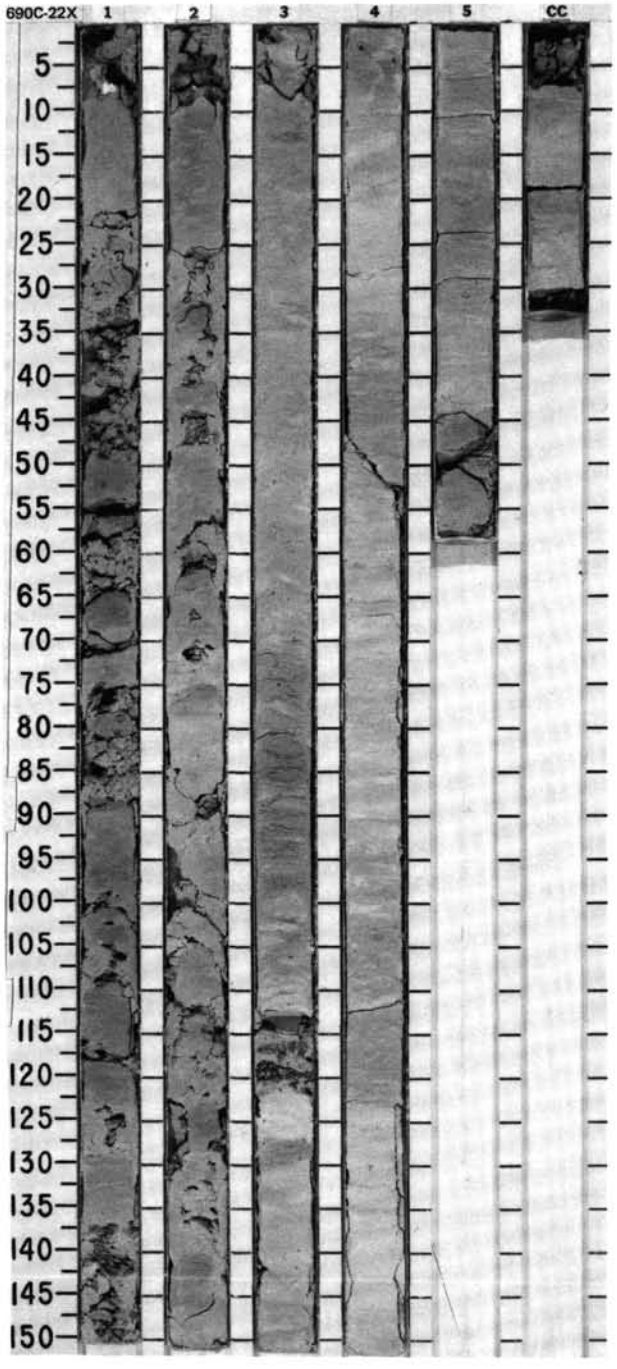

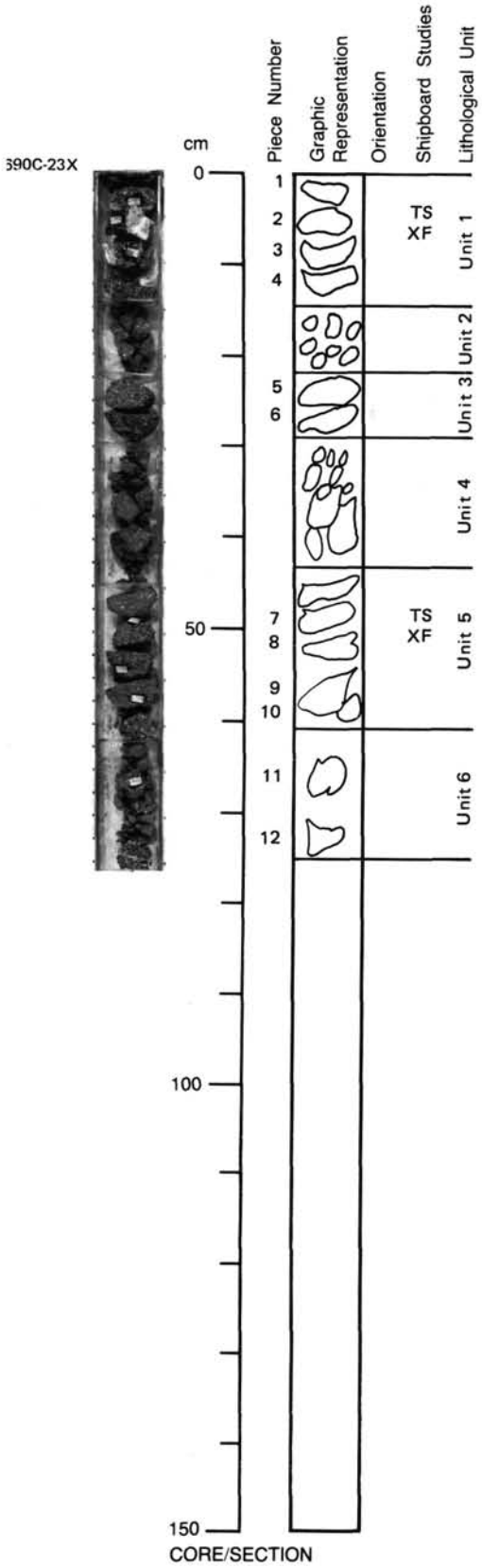

113–690C–23X–1

UNIT 1: PHYRIC PYROXENE-OLIVINE BASALT; AMYGDALOIDAL, HYPOCRYSTALLINE FINE-GRAIN MATRIX

Pieces 1–4

COLOR: Dark gray.
PHENOCRYSTS: Homogenous distribution.
Olivine – 1–2 mm, ~3%, anhedral to euhedral.
Pyroxene – 1 mm, <1%.
AMYGDULES: 10%, calcite filled, round, elongate, white.
VEINS: < 1–5 mm wide.
ALTERATION: Weathering, clayey sediment layer intercalated with basalt. Some chlorite, carbonate.

UNIT 2: SEDIMENT INTERCALATED WITH BASALT; CRUMBLY, MUDDY, FRIABLE PIECES, MOTTLED

PHENOCRYSTS: <1%, varied distribution.
Olivine – 1–2 mm, <1%, anhedral to euhedral.
AMYGDULES: Mostly empty, eroded.
VEINS: 1 small, <1 mm.
ALTERATION: Weathering.

UNIT 3: PHYRIC PYROXENE-OLIVINE AMYGDALOIDAL BASALT

Pieces 5 and 6

GLASS: Some vesicles are glassy; chloritized shards; hypocrystalline fine-grain matrix.
COLOR: Dark gray.
PHENOCRYSTS: <10%.
Olivine – 1–2 mm, 3–5%.
Pyroxene – <1%.
AMYGDULES: 10%, calcite filled, white.
VEINS: Few calcite veins.
ALTERATION: Chloritized shards (5), carbonate.

UNIT 4: SEDIMENT; INTERCALATED WITH BASALT; VERY FEW BASALT FRAGMENTS; 90% CRUMBLY SEDIMENT

COLOR: Dark gray, mottled.
Silt-sized particles with amygdaloidal basalt.

UNIT 5: SPARSELY PHYRIC PYROXENE-OLIVINE BASALT (AMYGDALOIDAL)

Pieces 7–10

GRAIN SIZE: Microcrystalline to fine grained.
GLASS: None; altered shard fragments and weathering.
COLOR: Dark gray.
PHENOCRYSTS: Olivine, 5%, anhedral to euhedral.
AMYGDULES: 10%, 5% infilled with calcite, 5% with zeolites (3–7 mm).
VEIN: Sparse, ~calcite.
ALTERATION: Green chlorite (minor), some weathering, carbonate.

UNIT 6: SPARSELY PHYRIC PYROXENE-OLIVINE BASALT (AMYGDALOIDAL)

Piece 11 and 12

GRAIN SIZE: Microcrystalline to fine grained.
GLASS: None, devitrified shards (minor), chloritized.
PHENOCRYSTS:
Olivine – 2–3%, 1–2 mm, anhedral to euhedral.
Pyroxene – <1%, 1 mm.
AMYGDULES: 1–3 mm, round; 10%, 5% calcite, 5% zeolite, white.
VEINS: Moderate to 2 mm; calcite.
ALTERATION: Chlorite, some weathering, carbonate.

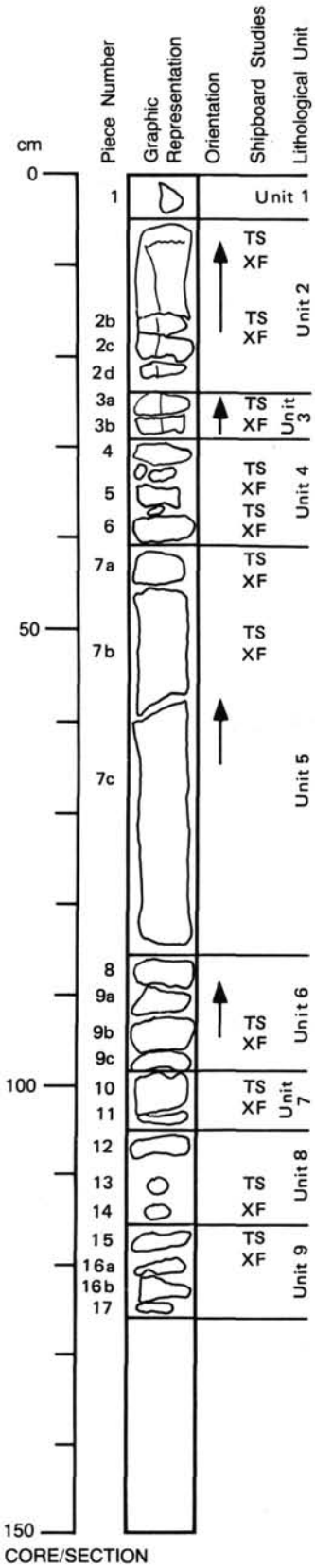

113–690C–24X–1

UNIT 1: MODERATELY PHYRIC PLAGIOCLASE-PYROXENE-OLIVINE BASALT; MATRIX APHANITIC, ROCK: AMYGDALOIDAL GLASS; SOME ADJACENT TO CAVITIES OF AMYGDULES

Piece 1

COLOR: Dark gray.
PHENOCRYSTS:
Pyroxene – 1–5%, ~1 mm, subhedral.
Olivine – 2–3%, 1–2 mm, anhedral to euhedral.
AMYGDULES: 1–2 mm, infilled with calcite and zeolite (white color). Some are chloritized at rim.
VEINS: None.
ALTERATION: Chlorite, carbonate.

UNIT 2: MODERATELY PHYRIC PYROXENE-OLIVINE-BASALT, APHANITIC MATRIX, AMYGDALOIDAL ROCK

Piece 2

GLASS: Small patches, dispersed, chloritized shards.
COLOR: Dark gray.
PHENOCRYSTS:
Pyroxene – 1 mm, subhedral.
Olivine – 3–4%.
AMYGDULES: <1–2 mm, 10%, 5% quartz, 5% blue and white zeolite.
VEINS: 1 prominent vein 2 mm wide crosscuts all pieces in unit (calcite).
ALTERATION: Chlorite, carbonate.

UNIT 3: MODERATELY PHYRIC PYROXENE-OLIVINE BASALT, APHANITIC MATRIX, AMYGDALOIDAL ROCK

Piece 3

COLOR: Dark gray.
GLASS: Patches and developed shards (<1%).
PHENOCRYSTS:
Pyroxene – 1–2%.
Olivine – 2–3%.
AMYGDULES: 10%, zeolite (blue and white) 7%, calcite 3%, chlorite <1%.
VEINS: Carbonate vein continues from Unit 2, chlorite veinlet is alteration on carbonate vein selvages.
ALTERATION: Carbonate, chlorite.

UNIT 4: PHYRIC PYROXENE-OLIVINE BASALT

Piece 4–6

COLOR: Dark gray.
PHENOCRYSTS:
Pyroxene – 1–2 mm.
Olivine – 2 mm, 3–4%.
Plagioclase – 2 mm (only a few).
AMYGDULES: Infilled with blue-white zeolite and calcite (~10%), slightly larger than previous ones.
VEIN: Carbonate veins connect carbonate-filled vesicles.
ALTERATION: Carbonate, chlorite.

UNIT 5: PHYRIC PYROXENE-OLIVINE BASALT, APHANITIC GROUNDMASS, AMYGDALOIDAL ROCK

Piece 7

COLOR: Dark gray.
PHENOCRYSTS:
Pyroxene – 2 mm.
Olivine – 1–2 mm.
Plagioclase – 2 mm (only few recognizable).
GLASS: Shards chloritized, patches of glass.
AMYGDULES: Increase in size to 5–6 mm, variety of infilling: calcite, blue-white, hematite needles, scapolite(?), chlorite, 15%.
VEIN: Intricate network; calcite appears to crosscut zeolite amygdules.
ALTERATION: Carbonate, chlorite, iron oxide stains in amygdules.

113–690C–24X–1

UNIT 6: MODERATELY PHYRIC PYROXENE-OLIVINE BASALT; GLASSY, APHANITIC MATRIX; AMYGDALOIDAL ROCK

Pieces 8 and 9

COLOR: Dark gray.
GLASS: In matrix and as chloritized shards.
PHENOCRYSTS:
Olivine – 2–3%, subhedral, euhedral.
Pyroxene – 1–2%.
Plagioclase – Few.
AMYGDULES: Increase slightly in size and become less densely scattered. Infilling of vesicles: blue-white zeolite, calcite, scapolite(?), chlorite, hematite needles.
VEINS: Decrease in number.
ALTERATION: Carbonate, chlorite, iron oxide stains (minor).

UNIT 7: PHYRIC PYROXENE-OLIVINE BASALT, LESS GLASSY, AMYGDALOIDAL, APHANITIC

Pieces 10 and 11

COLOR: Dark gray.
PHENOCRYSTS:
Olivine – 8%.
Pyroxene – 5–6%.
Plagioclase – Few corroded grains, 2 mm.
AMYGDULES: Infilled mostly with calcite, lesser zeolite.
VEINS: Very few, narrow.
ALTERATION: Chlorite, calcite, iron stain.

UNIT 8: PHYRIC PYROXENE-OLIVINE BASALT, LESS GLASSY, AMYGDALOIDAL, APHANITIC

Pieces 12–14

COLOR: Dark gray.
PHENOCRYSTS:
Olivine – 2 mm, 5%.
Pyroxene – 1–2 mm, 5$%.
AMYGDULES: Same number as in Unit 7, but 60% zeolite, 40% calcite. Chlorite decreases in amygdules.
VEINS: Absent.
ALTERATION: Carbonate, minor chlorite.

UNIT 9: SPARSELY PHYRIC OLIVINE-PYROXENE BASALT; APHANITIC, LESS GLASSY, AMYGDALOIDAL

Pieces 15–17

COLOR: Dark gray.
PHENOCRYSTS:
Olivine – 7–8%, euhedral-subhedral.
Pyroxene – 5%, subhedral-euhedral.
AMYGDULES: Zeolite (white-blue) increases at the expense of calcite. Amygdule percentage same as in Unit 8.
Interesting: Cu stain in one zeolite (turquoise).
VEIN: Wide 2 mm vein + hairline veins crosscut the rock (calcite).
ALTERATION: Carbonate, iron oxide (yellow limonite?), Cu stain in one zeolite.